frontiers | Research Topics

Focus on malignant pleural mesothelioma immunology and immunotherapy

Edited by
Chiara Porta, Christophe Blanquart
and Didier Jean

Published in
Frontiers in Immunology
Frontiers in Oncology

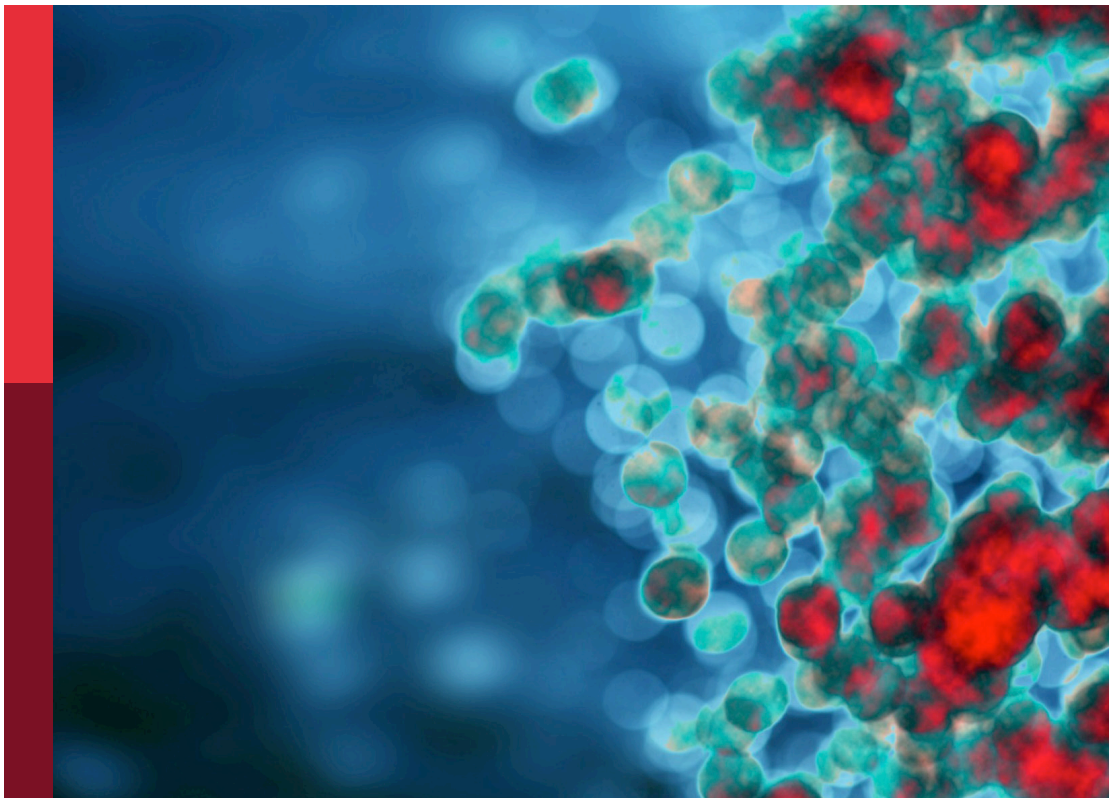

ISSN 1664-8714
ISBN 978-2-8325-3172-3
DOI 10.3389/978-2-8325-3172-3

About Frontiers

Frontiers is more than just an open access publisher of scholarly articles: it is a pioneering approach to the world of academia, radically improving the way scholarly research is managed. The grand vision of Frontiers is a world where all people have an equal opportunity to seek, share and generate knowledge. Frontiers provides immediate and permanent online open access to all its publications, but this alone is not enough to realize our grand goals.

Frontiers journal series

The Frontiers journal series is a multi-tier and interdisciplinary set of open-access, online journals, promising a paradigm shift from the current review, selection and dissemination processes in academic publishing. All Frontiers journals are driven by researchers for researchers; therefore, they constitute a service to the scholarly community. At the same time, the *Frontiers journal series* operates on a revolutionary invention, the tiered publishing system, initially addressing specific communities of scholars, and gradually climbing up to broader public understanding, thus serving the interests of the lay society, too.

Dedication to quality

Each Frontiers article is a landmark of the highest quality, thanks to genuinely collaborative interactions between authors and review editors, who include some of the world's best academicians. Research must be certified by peers before entering a stream of knowledge that may eventually reach the public - and shape society; therefore, Frontiers only applies the most rigorous and unbiased reviews. Frontiers revolutionizes research publishing by freely delivering the most outstanding research, evaluated with no bias from both the academic and social point of view. By applying the most advanced information technologies, Frontiers is catapulting scholarly publishing into a new generation.

What are Frontiers Research Topics?

Frontiers Research Topics are very popular trademarks of the *Frontiers journals series*: they are collections of at least ten articles, all centered on a particular subject. With their unique mix of varied contributions from Original Research to Review Articles, Frontiers Research Topics unify the most influential researchers, the latest key findings and historical advances in a hot research area.

Find out more on how to host your own Frontiers Research Topic or contribute to one as an author by contacting the Frontiers editorial office: frontiersin.org/about/contact

Focus on malignant pleural mesothelioma immunology and immunotherapy

Topic editors

Chiara Porta — University of Eastern Piedmont, Italy

Christophe Blanquart — Centre National de la Recherche Scientifique (CNRS), France

Didier Jean — Institut National de la Santé et de la Recherche Médicale (INSERM), France

Citation

Porta, C., Blanquart, C., Jean, D., eds. (2023). *Focus on malignant pleural mesothelioma immunology and immunotherapy*. Lausanne: Frontiers Media SA. doi: 10.3389/978-2-8325-3172-3

Table of contents

frontiers | Frontiers in Immunology

TYPE Editorial
PUBLISHED 24 July 2023
DOI 10.3389/fimmu.2023.1251384

OPEN ACCESS

EDITED AND REVIEWED BY
Barbara Rolfe,
The University of Queensland, Australia

*CORRESPONDENCE
Chiara Porta
chiara.porta@uniupo.it

RECEIVED 01 July 2023
ACCEPTED 11 July 2023
PUBLISHED 24 July 2023

CITATION
Porta C, Jean D and Blanquart C (2023) Editorial: Focus on malignant pleural mesothelioma immunology and immunotherapy.
Front. Immunol. 14:1251384.
doi: 10.3389/fimmu.2023.1251384

Editorial: Focus on malignant pleural mesothelioma immunology and immunotherapy

Chiara Porta[1,2]*, Didier Jean[3] and Christophe Blanquart[4,5]

[1]Department of Pharmaceutical Sciences, University of Eastern Piedmont, Novara, Italy, [2]Center for Translational Research on Autoimmune & Allergic Diseases (CAAD), University of Eastern Piedmont, Novara, Italy, [3]Centre de Recherche des Cordeliers, INSERM, Université Paris Cité, Sorbonne Université, Functional Genomics of Solid Tumors Laboratory, Paris, France, [4]Centre National de la Recherche Scientifique (CNRS), Paris, France, [5]Institut National de la Santé et de la Recherche Médicale (INSERM) U1232 Centre de Recherche en Cancérologie et Immunologie Nantes Angers (CRCINA), Nantes, France

KEYWORDS

mesothelioma, immune checkpoint inhibitors, predictive biomarkers, tumor microenvironment, eosinophils, microbiota, osteopontin, oncolytic vaccinia virus

Editorial on the Research Topic
Focus on malignant pleural mesothelioma immunology and immunotherapy

Malignant pleural mesothelioma (MPM) is a rare and aggressive thoracic cancer that derives from the mesothelial cells of the pleura and is causally associated with exposure to asbestos. Because of the poor specificity of the clinical symptoms, when it is diagnosed, malignant cells, which are extremely resistant to therapies, have already spread throughout the pleural layers, leading to a poor outcome. Although the recent approval of the combination immunotherapy with anti-CTLA-4 and anti-PD-1 represents a breakthrough for MPM, many patients are still refractory or relapsed after a few months of therapy. Therefore, there is an urgent need of reliable biomarkers to improve patient selection for immune checkpoint blockades (ICBs), as well as of new therapeutic strategies to boost anti-tumor immunity. Recent insights into these unmet medical needs are discussed in this Research Topic. Specifically, Perrino et al. review the clinical efficacy and the most promising predictive biomarkers of response to ICBs in MPM. In addition to widely recognized determinants - such as PD-L1 expression and tumor mutational burden (TMB) - and specific prognostic factors for MPM (i.e. histological subtype), they discuss new elements, which definitively warrant to be further investigated and prospectively validated. Particularly, it is worth noting that in spite of the low TMB, MPM cells usually show multiple chromosomal rearrangements, which can lead to the expression of neo-antigens, thereby predicting response to ICBs.

Besides histological classification in epithelioid, sarcomatoid and biphasic MPM, a growing number of studies have pointed out a striking molecular heterogeneity, which suggests the existence of a range of molecular phenotypes associated with different responsiveness to ICBs and outcome. Based on these premises, the studies of Yang et al. and Liu et al. generate in-silico classification systems for MPM, which could be exploitable

to guide immunotherapy strategies, provided that those results will be validated in prospective studies and larger cohorts. Specifically, Yang et al. provide a machine learning-based 12-gene classifier to separate MPM in two immune-related subtypes. That one associated with a better response to ICBs is the immune activated subtype, which harbors an IFN-γ dominant immune phenotype, a consistent TCR and BCR diversity and the highest lymphocyte infiltration. Conversely, Liu et al. elaborate a classification system based on the expression of damage-associated molecular patterns (DAMPs). In this regard, the "inflammatory DAMPs subtype", which is characterized by the enrichment of proinflammatory cytokine signaling, is also associated with better outcome.

Alongside the analysis of tumor microenvironment (TME) composition, liquid biopsy is emerging as an interesting research area for predictive biomarkers of response to ICBs. Eosinophils can support local anti-tumor response by producing cytotoxic molecules, but they can also secrete cytokines promoting suppressive macrophages, which are both the major component of the MPM microenvironment and limit for ICB success. Willems et al. demonstrate a correlation between a baseline absolute eosinophil count (AEC) of ≥220/μL and a worse outcome of MPM patients undergoing chemo- or immunotherapy. Thus, further prospective studies are warranted to validate blood AEC as a potential predictive biomarker for both therapies.

Microbiome is a key environmental determinant of ICB efficacy for different types of cancers, but it is still a largely underexplored facet of MPM. Through the analysis of TCGA data on 86 MPM patients, Pentimalli et al. identify 107 genera signatures that are significantly associated with patient's survival, thereby suggesting intratumor microbiota both as a novel potential prognostic indicator for MPM and an actionable target for the development of new strategies to improve the efficacy of immunotherapy. Up to date, clinical trials conducted with MPM patients have provided promising results with the combination of ICBs with stereotactic body radiation and chemo-therapy. Along this line, the study of Chang et al. aims to determine the ideal dosing and scheduling of combined treatment with radiotherapy and ICBs. They observe that irradiation of MPM cell lines modulates the expression of immune markers and cytokines that are important for antitumor responses. Consequently, *in vivo* studies should be pursued to gather the mechanisms underlying the synergy between radiotherapy and ICBs. In this regard, it is crucial that preclinical models of mesothelioma improve the accuracy in predicting the response of the human counterpart. For this purpose, Stern et al. characterize the immunobiology of a biphasic mesothelioma model based on intra-peritoneal growth of AB12 cells in immunocompetent mice. Immunologic, transcriptomic, and survival analyses show that intermediate- and advanced-tumors match with human immune active and immunosuppressed MPM, respectively. Therefore, new therapeutics - such as the anti-CTLA-4 + anti-PD-1 + cisplatin triple therapy - showing efficacy at advanced phases, when anti-tumor immune response has decayed, are the most promising candidates to improve outcome in MPM patients.

Additionally, it is important that the research of novel targets and approaches be carried on, in order to increase the number and the efficacy of the therapeutic options for MPM. In this perspective, Digifico et al. find that the protein osteopontin (OPN) is more expressed in human MPM tumors than in normal pleural tissues and is a key promoter of tumor cell proliferation. Accordingly, either the silencing of *OPN* gene in MPM cells or the blocking of its major receptor CD44 by a specific antibody significantly reduce tumor growth *in vivo* in an orthotopic model of MPM. Intriguingly, Chintala et al. performed a phase I clinical trial to evaluate intrapleural administration of oncolytic vaccinia virus, a promising approach for the treatment of solid tumors, in a small cohort of patients with MPM and metastatic disease. Besides being safe and feasible, the study highlights that the genetically engineered vaccinia virus can infect tumor cells and generate immune responses, leading to a decrease in tumor cell density. These results foster further investigation of immunomodulatory effects of oncolytic virus treatment, and their potential clinical implications for combination therapy with ICBs, chemo- or radio- therapy.

Finally, we would like to thank all the authors who have contributed to this Research Topic and the reviewers for their outstanding efforts. We hope that the insights discussed in this Research Topic are not only inspirational for those who are already working in the fields of mesothelioma and immuno oncology, but also captivating and useful for those who are not deeply involved in this Research Topic.

Author contributions

All authors listed have made a substantial, direct and intellectual contribution to the work, and approved it for publication.

Acknowledgments

We thank the institutes where we work, specifically University of Eastern Piedmont, Novara, Italy; Institut National de la Santé et de la Recherche Médicale (INSERM), Paris, France and Centre National de la Recherche Scientifique (CNRS), Paris, France. CP thanks Marcello Arsura, Abeschool, Novara, Italy for the course of scientific English writing.

Conflict of interest

The authors declare that the research was conducted in the absence of any commercial or financial relationships that could be construed as a potential conflict of interest.

Publisher's note

frontiers | Frontiers in Oncology

TYPE Original Research
PUBLISHED 27 September 2022
DOI 10.3389/fonc.2022.995651

OPEN ACCESS

EDITED BY
Didier Jean,
Institut National de la Santé et de la Recherche Médicale (INSERM), France

REVIEWED BY
Mattia Riefolo,
University of Bologna, Italy
Lise Mangiante,
Stanford University, United States
Edward Hollox,
University of Leicester, United Kingdom

*CORRESPONDENCE
Kaidi Yang
lampirl@163.com
Fang Li
13601261747@139.com

SPECIALTY SECTION
This article was submitted to Cancer Immunity and Immunotherapy, a section of the journal Frontiers in Oncology

RECEIVED 16 July 2022
ACCEPTED 14 September 2022
PUBLISHED 27 September 2022

CITATION
Yang K, Yang T, Yang T, Yuan Y and Li F (2022) Unraveling tumor microenvironment heterogeneity in malignant pleural mesothelioma identifies biologically distinct immune subtypes enabling prognosis determination. *Front. Oncol.* 12:995651. doi: 10.3389/fonc.2022.995651

Unraveling tumor microenvironment heterogeneity in malignant pleural mesothelioma identifies biologically distinct immune subtypes enabling prognosis determination

Kaidi Yang[1*], Tongxin Yang[1], Tao Yang[1], Ye Yuan[2] and Fang Li[1*]

[1]Department of Oncology, Hainan Hospital of Chinese People's Liberation Army General Hospital, Sanya, China, [2]Institute of Pathology and Southwest Cancer Center, Southwest Hospital, Third Military Medical University (Army Medical University), Chongqing, China

Background: Malignant pleural mesothelioma (MPM) is a rare and intractable disease exhibiting a remarkable intratumoral heterogeneity and dismal prognosis. Although immunotherapy has reshaped the therapeutic strategies for MPM, patients react with discrepant responsiveness.

Methods: Herein, we recruited 333 MPM patients from 5 various cohorts and developed an *in-silico* classification system using unsupervised Non-negative Matrix Factorization and Nearest Template Prediction algorithms. The genomic alterations, immune signatures, and patient outcomes were systemically analyzed across the external TCGA-MESO samples. Machine learning-based integrated methodology was applied to identify a gene classifier for clinical application.

Results: The gene expression profiling-based classification algorithm identified immune-related subtypes for MPMs. In comparison with the non-immune subtype, we validated the existence of abundant immunocytes in the immune subtype. Immune-suppressed MPMs were enriched with stroma fraction, myeloid components, and immunosuppressive tumor-associated macrophages (TAMs) as well exhibited increased TGF-β signature that informs worse clinical outcomes and reduced efficacy of anti-PD-1 treatment. The immune-activated MPMs harbored the highest lymphocyte infiltration, growing TCR and BCR diversity, and presented the pan-cancer immune phenotype of IFN-γ dominant, which confers these tumors with better drug response when undergoing immune checkpoint inhibitor (ICI) treatment. Genetically, BAP1 mutation was most commonly found in patients of immune-activated MPMs and was associated with a favorable outcome in a subtype-

specific pattern. Finally, a robust 12-gene classifier was generated to classify MPMs with high accuracy, holding promise value in predicting patient survival.

Conclusions: We demonstrate that the novel classification system can be exploited to guide the identification of diverse immune subtypes, providing critical biological insights into the mechanisms driving tumor heterogeneity and responsible for cancer-related patient prognoses.

KEYWORDS

malignant pleural mesothelioma, immune subtypes, immunotherapy, prognosis, machine learning-based gene classifier

Introduction

Malignant pleural mesothelioma (MPM) is a rare and lethal cancer arising from the linings of the lungs, known as the pleura (1). Due to its insidious onset and high local invasiveness, this cancer is often diagnosed at an advanced stage, rendering it incurable (2).

For a long time, platinum-based chemotherapy combined with pemetrexed has been the state-of-the-art treatment for advanced MPM (3). Drug development for this lethal cancer has been slowly pushed over the last two decades until the recent advances in immune checkpoint inhibition (4, 5). Immune checkpoint inhibitors (ICIs) targeting PD-1 and CTLA4 have shown encouraging clinical activity with good tolerability in untreated, histologically confirmed unresectable MPMs relative to standard first-line chemotherapy. Nonetheless, the median life expectancy is only one and a half years, even with 4-months extended survival benefits (6). The varying clinical responses to ICIs and no credible biomarkers available emphasize a more personalized regimen for MPMs (7).

Overexpression of PD-L1 has been confirmed as a predictor of response to anti-PD1 therapy in multiple solid tumors, whereas efficacy by PD-L1 status demonstrated no improvements in survival benefits for MPM patients (7, 8). Emerging evidence indicated the intra-tumoral CD8+ T cell infiltration, TGF-β signaling, and Treg content were associated with curative responses and outcomes (9–11), while for MPM, limited research was available. MPM develops in a heterogeneous immune microenvironment that dynamically interacts with mesothelioma tumor cells to sustain cancer growth and progression (12–14). We hypothesized that a deep dissection of the immunological profiles within MPMs would provide a framework for an in-depth understanding of the immune-genomic mechanisms responsible for cancer-related prognosis and maximize response to immune-based therapies. Lee et al. recently profiled the intratumoral cellular networks within 12 MPMs using CyTOF and defined two immunologic subtypes showing predictive value for ICI response (15). However so far, there is no extensive cohort-based immunological classification system for MPMs, and a robust gene classifier specific for predicting prognosis and subtyping is still lacking.

In this work, we enrolled 333 MPM patients from five independent cohorts as a large-sample MPM cohort, and 87 MPM patients came from TCGA dataset. Several unsupervised classification methods, particularly the non-negative matrix factorization (NMF) and nearest template prediction (NTP) algorithms, were applied to distinguish distinct immunological phenotypes and reveal the intratumoral heterogeneity of MPMs. The predictive, reliable multi-gene classifier holds the value in immune subtyping and prognostic determination and can be used to guide immunotherapy strategies.

Methods

Malignant pleural mesothelioma patient cohort

We enrolled the gene expression profiles and clinical information of MPM datasets from Gene Expression Omnibus (GEO) with the accession numbers GSE29354 (16), GSE2549 (17), GSE163722 (18), and GSE51024 (19). The expression files of the MTAB-6877 dataset (20) were provided in ArrayExpress (https://www.ebi.ac.uk/arrayexpress/). The *ComBat* method came from *sva* package (R version 3.38.0) was used to remove batch effects across different microarray platforms. As shown in Figure S1A, the deviations of mean gene expression were removed and the five datasets were thus comparable to each other. Subsequently, a large MPM dataset including 333 qualified expression profiles was set as a training cohort, while the RNA-seq v2 level-3 dataset of TCGA-MESO (Mesothelioma, from UCSC-Xena) was used for external validation. Detailed information on these datasets is shown in Supplementary Table S1. To validate the finding in proteomic level, we performed

extensive analysis of the Reverse Phase Protein Array (RPPA) data from TCGA cohort on 63 human MPMs characterized with a set of 219 protein features.

NMF classification

After reserving high-variance gene features ranked in the top half of total samples, we performed subtype classification with the mRNA expression profiles using the NMF algorithm packed into the *NMF* package (R version 0.24.0). We plotted the rank-changing trend diagram of the cophenetic coefficient and determined the point that dropped the most along with the rank-changing as the best rank (number of classification). To functionally annotate each subclass/module, the gene signatures were extracted using the *extractfeatures* function and subsequently used for gene over-representation (ORA) analysis utilizing the *clusterProfiler* package (R version 4.5.0). MPMs conferred with the highest immune module score were denoted as an immune-related subtype. Then, the top 200 exemplar genes in the immune module were identified as the classifier genes to dichotomize samples into the immune and non-immune subtypes, further optimized by the multidimensional scaling random forest (MDS-RF) algorithm. To sub-classify immune MPMs, a 26-immune signature scoring file was generated from the *IOBR* package (R version 0.99.0) as an input into the NTP module (GenePattern platform, https://cloud.genepattern.org). The molecular similarity between the two MPM cohorts was estimated using Subclass Mapping (GenePattern).

Immune signature analysis

To delineate the tumor microenvironment (TME) contexture, the *IOBR* package (https://github.com/IOBR/IOBR) integrating eight published methodologies was used for computing the single-sample gene set enrichment (ssGSEA) score (21). Identifying TME signatures associated with ICI response was performed using the *iobr_cor_plot* function. Immune-related indices, previously defined by TCGA pan-cancer programs, were incorporated into comparisons across different subtypes. Also, Thorsson's pan-cancer immune phenotyping (22) was used for feature comparisons and subtype correlations. Immune-related indices, including Stroma fraction, Leukocyte fraction, TCR richness, and so on, were obtained from supplementary material of Thorsson's research. Of note, the index has been adjusted for tumor purity as demonstrated. Tumor immune proportions were computed by CIBERSORT, which ran with mRNA profiles as input and produced absolute abundances of 22 immune components. To predict the immunotherapy response of MPM patients, we imported the tumor pre-treatment expression profiles into TIDE (http://tide.dfci.harvard.edu), which computed the response scores based on signatures of T-cell dysfunction and exclusion, the two primary mechanisms of tumor immune evasion (23). The cohort of human MPMs that received anti-PD-1 immunotherapy (GSE99070) was considered for investigating of association between immune subtypes and immunotherapy response.

Pathway activity analysis

The dataset of pathway activity comprising 1387 constituent pathways was downloaded from UCSC-Xena browser (http://xena.ucsc.edu/). Pathway analysis was conducted using the PARADIGM algorithm (24), and the top expressed pathways were generated through differential expression analysis.

Genomic mutation analysis

The mutation annotation format (MAF) file with aggregated somatic mutation annotation of TCGA MPM cases was deposited in the TCGA portal. For summarization, analyses, and visualization of somatic genomic alterations, various functions were provided by the *maftools* package (R version 2.7.40). The *mafCompare* function was applied to compare two groups to identify and visualize differentially mutated genes. The *clinicalenrichment* function was used for groupwise comparisons, thus identifying enriched mutations or copy number variations (CNVs) for each subtype. We ran MutSigCV1.41 using the recommended default parameters on GenePattern to identify the driven mutations highly relevant to MPMs (q-value < 0.10).

Subtype classifier identification

First, we prefiltered genes by different feature selection algorithms, including *Chi2-algorithm*, *Fast correlation-based filter*, and *Information gain* using the *Biocomb* package (R version 0.4). This set of gene candidates was supplemented with gene features computed by machine-learning models of *Randomforest* (RF), *XGBoost*, and *Brutal*. Genes nominated by multiple algorithms were ranked by the frequency of being selected by the six methods. It resulted in a panel of 94 genes selected by at least four algorithms. (Supplementary Table 2) Then, we used the *findCorrelation* function packed in the *Caret*

package 6.0-92 to remove highly correlated features. If two features have a high correlation, the function looks at each feature through pair-wise correlations and removes the feature with the mean absolute correlation over 0.8. After removing features showing high correlation, we adopted a stepwise selection strategy to determine the optimal size of the gene panel. Specifically, starting from the top-ranked gene (ordered by count and index of mean decrease accuracy), gene panels with incremental sizes (adding one gene at a time) were evaluated for their ability to correctly classify each case by RF with a cross-validation approach of LOOCV (leave-one-out cross-validation). To identify the best feature combination to improve classification accuracy, especially for distinguishing immune-activated from immune-suppressed subtype, we adopted the approach similar to the multiple algorithms-based feature selection method above, followed by removing features with high pair-wise correlations. The two comparisons (immune versus non-immune, immune-activated versus immune-suppressed) respectively generate seven and nine genes through the *recursive feature elimination* (RFE) algorithms using *rfeControl* functions (from *Caret* package 6.0-92), which was assisted by machine learning methods of RF-LOOCV or RF-CV. The optimal features computed from two classification systems were combined into a 16-gene panel for the following filtering step. All the models metrics of gene features filtering and selection process were stored in Supplementary Table 3. Then, we apportion the data into training and test sets, with 70-30 splits, and fit the models on the training sets. By evaluating the performance of different machine learning models (Linear discriminant analysis, Naive Bayes, Bagged trees, and RF with LOOCV or CV) on testing sets, we identified the best machine-learning model (with the highest prediction accuracy) when undergoing the RFE process, which generated the optimal gene features. The selected gene classifier was evaluated for its predictive efficiency in the external TCGA-MESO dataset.

Statistical analysis

When the dependent variable was continuous but not normally distributed for two independent groups, the Mann-Whitney U test was used for comparisons. In comparison, normally distributed data were compared between two groups *via* the Student t-test. We performed a Shapiro test to check whether the considered data is normally distributed data or not by the *stats* package (R version 4.0.4). Kaplan-Meier plot and Log-rank test were used to estimate the survival curve and compare the difference in survival curves between different groups. The Chi-square test illustrated the correlations between newly defined subtypes and proposed molecular subtypes. The forest plot was used to visualize the prognostic impact of individual variables of the multivariate Cox regression model using the *forestmodel* package (R version 0.6.2). All analyses were performed by Graphpad Prism 8.0 or R version 4.0.2, and a two-sided *p*-value less than 0.05 was considered statistically significant.

Results

Identification of immune-associated subtype for an integrated large-sample MPM cohort

A total of 333 MPMs patients from five independent cohorts were enrolled, along with their clinical information and microarray-based expression profiles. After correcting batch effects, an integrated large-sample MPM cohort were established for subsequent analysis. To obtain a robust classification system and distinct molecular patterns, we applied the NMF algorithm to reduce data dimensionality by decomposing it into several smaller non-negative factors with physical interpretation for subclass discovery. As cophenetic correlation coefficients from k = 2 to k = 10, we determined k=4 as the parameter that yielded the most robust clustering (Figures S1B, C). Among the four subclasses, we defined the one characterized with high immune enrichment scores as an immune-associated subtype, whereas the other three subclasses were respectively termed as Cell cycle-, Epithelial/Interferon (IFN) response-, and Extracellular matrix (ECM)-related subtypes according to the results of ORA analysis (Figure 1A and Figure S2). The top 200 weighted genes in the immune module/subclass were defined as exemplar genes that reflect the core features of immune components in MPM (Figure S1D). To simplify the subtyping process for fast-recognition of immune related subtypes, we performed consensus clustering analysis using the exemplar genes, which classified MPM patients into immune and non-immune subclasses (Figure 1B). Next, this classification was further modified by the MDS-RF algorithm (Figure 1C). The sorting result of multiple methods for the 333 MPM patients was shown in Figure 1D and Supplementary Table 4. We presented that simplifying the classification process using the top 200 weighted genes matched with the genome-wide expression profiling-based NMF algorithm for identifying immune-related subtypes for MPMs.

Sub-classification and dissection of MPM immune microenvironment

Recent studies on the immunological microenvironment revealed three representative phenotypes with general applicability, including inflamed, excluded, and desert subtypes (25). To further dissect the immunological heterogeneity for

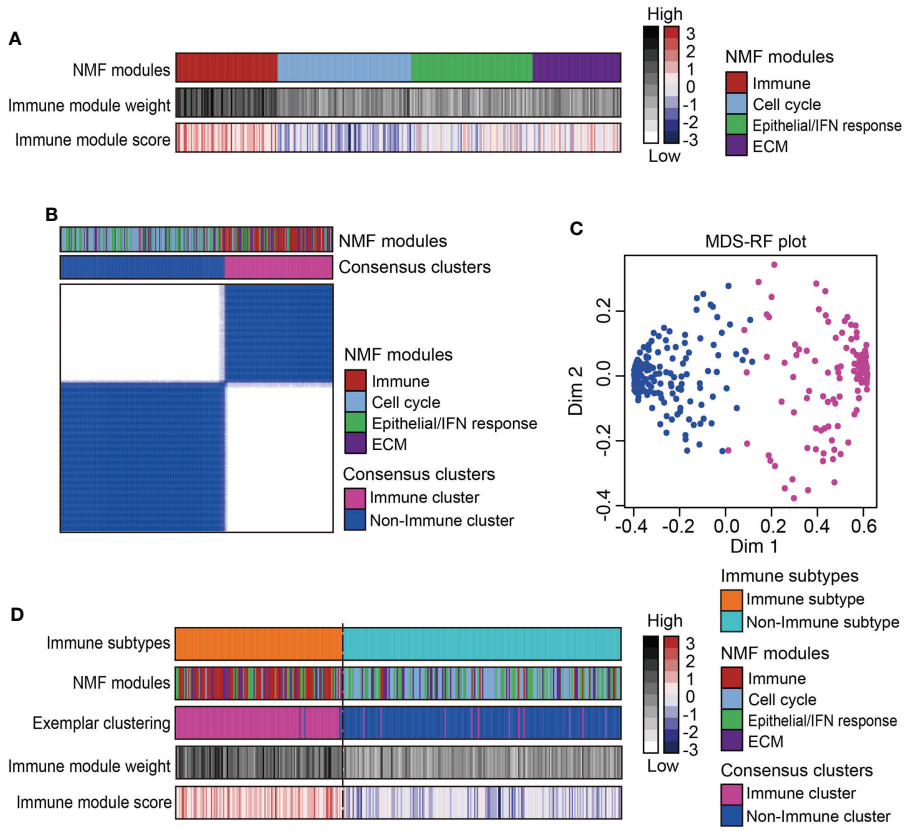

FIGURE 1
Identification of immune subtype for an integrated large-sample MPM cohort. **(A)** Non-negative matrix factorization (NMF) algorithms identified four functional expression modules to classify the microarray-based expression profiles of 333 MPM samples. One expression module showed the highest immune enrichment score and NMF module weight was marked red and recognized as an immune-associated subtype. IFN, Interferon; ECM, Extracellular matrix. **(B)** Consensus clustering based on the top 200 exemplar genes expression identified two subclasses with one subclass presenting enrichment of immune-related NMF module. **(C)** The multidimensional scaling random forest (MDS-RF) refined the classification and divided whole MPM samples into immune and non-immune subtypes. **(D)** Heatmap shows the final classification results along with various NMF modules, exemplar clustering subtypes, immune module weight, and immune enrichment score.

MPMs, scorings of 26 immune-related signatures were collected to subdivide the immune-related MPMs into two subsets using the NTP algorithm. One subset of 55 patients (16.5%, 55/333) showed increased enrichment of immunocytes, cytolytic activity (CYT) score, ooand IFN related signatures as compared with other MPMs and hence, was termed an immune-activated subtype (Figure 2A). Other indices like Wnt/β-catenin signaling, TGF-β signaling, and the extracellular matrix (ECM) have been shown to play an essential role in establishing immunological tolerance (9, 26, 27). Likewise, the myeloid components, including tumor-associated macrophages (TAMs) and myeloid-derived suppressor cells (MDSCs), act as central regulators of immune suppression and can secrete multiple soluble cytokines and chemokines to deactivate the process of immune activation (28). For these reasons, we defined the sub-classified subtype with high stroma infiltration and immune-suppressive components as immune-suppressed MPMs (21.0%, 70/333) (Figure 2A). The redefined three subtypes (immune-activated, immune-suppressed and non-immune) were relatively well distributed in different enrolled MPM cohorts (Supplementary Table 5). Histologically, consistent with previous finding (20), sarcomatoid MPMs was enriched in immune-activated MPMs relative to other subtypes (27.3% *versus* 3.9%, 12.1%). By contrast, greater proportions of epithelioid and biphasic tumors were respectively present in non-immune and immune-suppressed MPMs (Figure S3A). Next, we performed survival analysis and observed that immune-suppressed MPM patients displayed shortened survival relative to immune-activated or non-immune MPM patients (Figure 2B), indicating the prognostic significance of the immunological subtyping. The immune-related signature was a good indicator of patient survival (29). Our multivariate analysis by the Cox proportional hazards model on prognoses of patients indicated that the Th2 cells, MDSC, and Pan-F-TBRs (Pan fibroblast TGF-β response signature) informed poor outcome (Figure S3B). To investigate whether the immunological

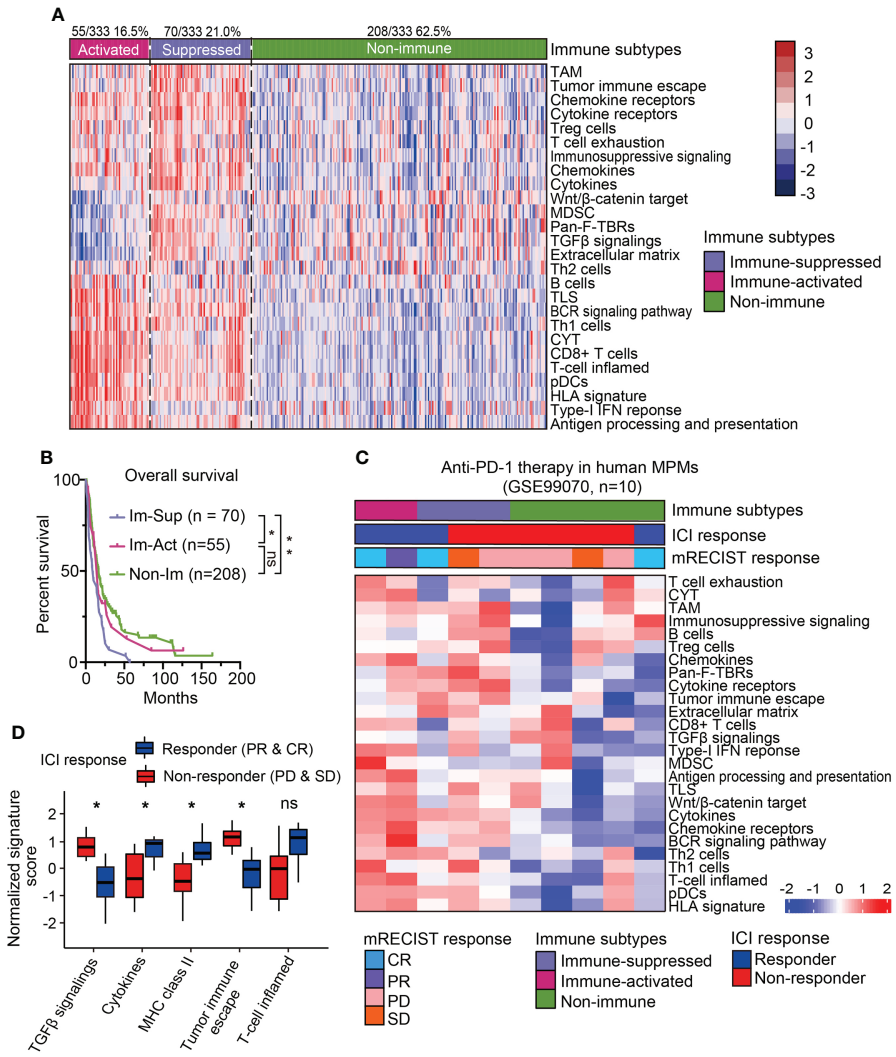

FIGURE 2
Sub-classification and dissection of MPM immune microenvironment. **(A)** The immune subtype was further subdivided into immune-activated (70/125, 21.0%) and immune-suppressed (55/333, 16.5%) MPMs, using nearest template prediction (NTP) analysis with signatures covering 26 immune- and TME-related signatures. TAM, Tumor-associated macrophage; MDSC, Myeloid-derived suppressor cell; TLS, Tertiary lymphoid structure; CYT, Cytolytic activity. pDCs, Plasmacytoid dendritic cell; Pan-F-TBRs, Pan fibroblast TGF-β response signature. **(B)** Kaplan-Meier survival analyses of overall survival in the integrated MPM cohort with different immunological subtypes. **, $p < 0.01$; *, $p < 0.05$; n.s., Not significant. **(C)** The heatmap showing the expressions of 26 immune- and TME-related signatures in the pretreatment human MPM cohort upon the anti-PD-1 treatment. The dataset was classified using the same approach as previously shown in Figure 2A. Top column shows the corresponding immune subtype and mRECIST response of each case. ICI, Immune checkpoint inhibitor. **(D)** The normalized signature score of immune characteristics in anti-PD-1 response and non-response subgroups. CR, Complete response; PR, Partial response; PD, Progression disease; SD, Stable disease.

subtyping can predict the treatment response of ICIs, the pretreatment human MPMs (n=10) upon the immunotherapy of anti-PD-1 were classified using the same approach (GSE99070, Figure 2C). Intriguingly, although with only two patients, immune-activated MPM patients show partial or complete response to the treatment. By comparison, most of the immune-suppressed and non-immune patients (2/3, 4/5) were shown to be unresponsive when undergoing such therapy (Figure 2C), highlighting the relevance of our immunological subtyping to the therapeutic effects of ICI. Relative to the non-response subgroup, the ICI response subgroup showed prominent expressions of pathways regulating T-cell inflamed, cytokines, and MHC class-II, along with decreased enrichments of TGF-β signaling and tumor immune escape (Figure 2D). Immune-activated MPMs were enriched with these signatures and also highly expressed multiple immune checkpoint genes (Figure 2A and Figure S4A), demonstrating that ICI therapy is poised for clinical evaluation for them.

Validation of the novel immune-subtyping in external TCGA-MPM cohort

To see whether the above classification system can be reappeared, we explored the expression profiles from the TCGA-MESO dataset containing 87 patients and performed the same classification procedures (Figures S5A, B). The classification results showed that 54.0% (47/87) of patients were immune-related MPMs characterized with distinct immune phenotypes. Among them, 24 patients (27.6%) were defined as immune-activated MPMs, and other 23 patients (26.4%) were regarded as immune-suppressed MPMs, enriched with TAMs, Treg cells, MDSCs and, tumor immune escape signatures, indicating that immune characteristics can reappear in the validation cohort (Figure 3A). Subtypes of the TCGA dataset showed high consistency with corresponding subtypes of the large-sample MPM cohort through subclass correlation analysis (Figure S5C), suggesting a good reproducibility of the three-subgroup-clustering system for identifying MPM immunological signatures. Kaplan-Meier survival analyses confirmed that immune-activated MPMs exhibited the most favourable outcome relative to the other two subtypes (Figure 3B). By associating our immune subtyping with Thorsson's pan-cancer immune phenotyping (22), we found that approximately 50% of immune-activated MPMs pertained to the IFN-γ-dominant (C2) phenotype. In contrast, the wound healing (C1) phenotype occupied the most parts (47.8%, 45%) for the other two subtypes. C6 phenotype, defined as TGF-β dominant, showed the largest proportion in immune-suppressed MPMs compared with other subtypes (21.7% *versus* 10%, 8.3%) (Figure 3C), supporting the previous findings of TGF-β's role in immunosuppression (30). Further profiling of the immune milieu demonstrated that three MPM subtypes manifested distinct immune-related signatures. Immune-activated MPMs harbor the lowest genomic alteration fraction and homologous recombination defects (HRDs), reflecting their ability to repair DNA damage and maintain genomic stability. The much more hypervariable and diverse TCR and BCR, and highest lymphocyte infiltration score informed increased probability of immune responsiveness to ICIs (Figure 3D), consistent with the findings of ICI response estimated by TIDE (Figure 3A). By contrast, immune-suppressed subtype MPMs displayed the highest stroma and leukocyte fractions (Figure 3D). Microsatellite instability (MSI) status and tumor mutation burden (TMB) has been widely recognized as biomarkers predicting the therapeutic efficacy of ICIs (31–33). As the ICI therapeutic effects estimated by TIDE (Figure 3A), the decreased MSI scores in immune-suppressed MPMs also informs poor ICI efficacy (Figure S5D). In comparison, as we observed, there was no significant difference in TMB levels across the three groups (Figure S5D).

Then, we investigated the oncogenic pathways mediating the distinct phenotype of each subtype. Interestingly, immune-activated MPMs displayed the most intense T cell-mediated antitumor response, with high scorings of the T-cell receptor, JAK-STAT, and interferon-γ. Stromal-enriched immune-suppressed MPMs were associated with high activities of MAPK, TNFα-NF-κB, and IL-7 signalings, while non-immune MPMs were characterized by abundant intracellular signals of N-cadherin, FGF, EphA2, EGFR, and hypoxia (Figure S6A).

Genomic landscape of the three MPM immune subtypes

Gene- or pathway-level somatic mutations were shown to affect the immune microenvironment. With the implementation of well-established statistical and computational methods in the *maftools* package, we presented the genomic landscape of mutational alterations and copy number variations across the three immunological subtypes. It is illustrated that the three immunological subtypes displayed distinct genomic characteristics (Figure 4A and Figures S7A, B). Of note, immune-suppressed MPMs had the highest genomic alteration rate of *SETDB1* and *NF2* (18%, 45%) relative to immune-activated (0%, 25%) and non-immune (2%, 28%) MPMs (Figures 4A, B). *BAP1* alteration was most commonly found in patients with immune-activated MPMs (Figure 4A) and was specifically associated with a favorable outcome for these patients (Figure 4D and Figure S7C), indicating subtype-specific prognostic value. *MTAP* loss is a reliable surrogate for *CDKN2A* (p16) homozygous deletion in mesothelioma diagnosis (34, 35). These two highly specific markers for malignancy lesions of mesothelioma have lower copy number deletion rates in immune-activated MPMs than other MPMs (Figure 4C and Figure S7A). *LATS2* mutation or inactivation is a positive regulator of mesothelioma proliferation *via* constitutively activating YAP and Hippo signaling pathways (36). Herein, we demonstrated that *LATS2* genomic alteration was an indicator of adverse prognosis for both immune-activated and immune-suppressed MPMs (Figure 4D), while the same finding was not observed in non-immune MPMs (Figure S7D). To support the findings at the proteomic level, we determined the phosphorylation levels of the residues serine 127 (S127) of YAP, together with a common *CDKN2A* encoding tumor suppressor, p16 (INK4A) (37), across the three subtypes using TCGA-RPPA dataset. As expected, immune-activated MPMs exhibited compromised phospho-YAP (S127) levels and upregulated p16 (INK4A) levels relative to non-immune MPMs with statistical significance, which would be a partial interpretation of the optimistic outcomes (Figure S7E).

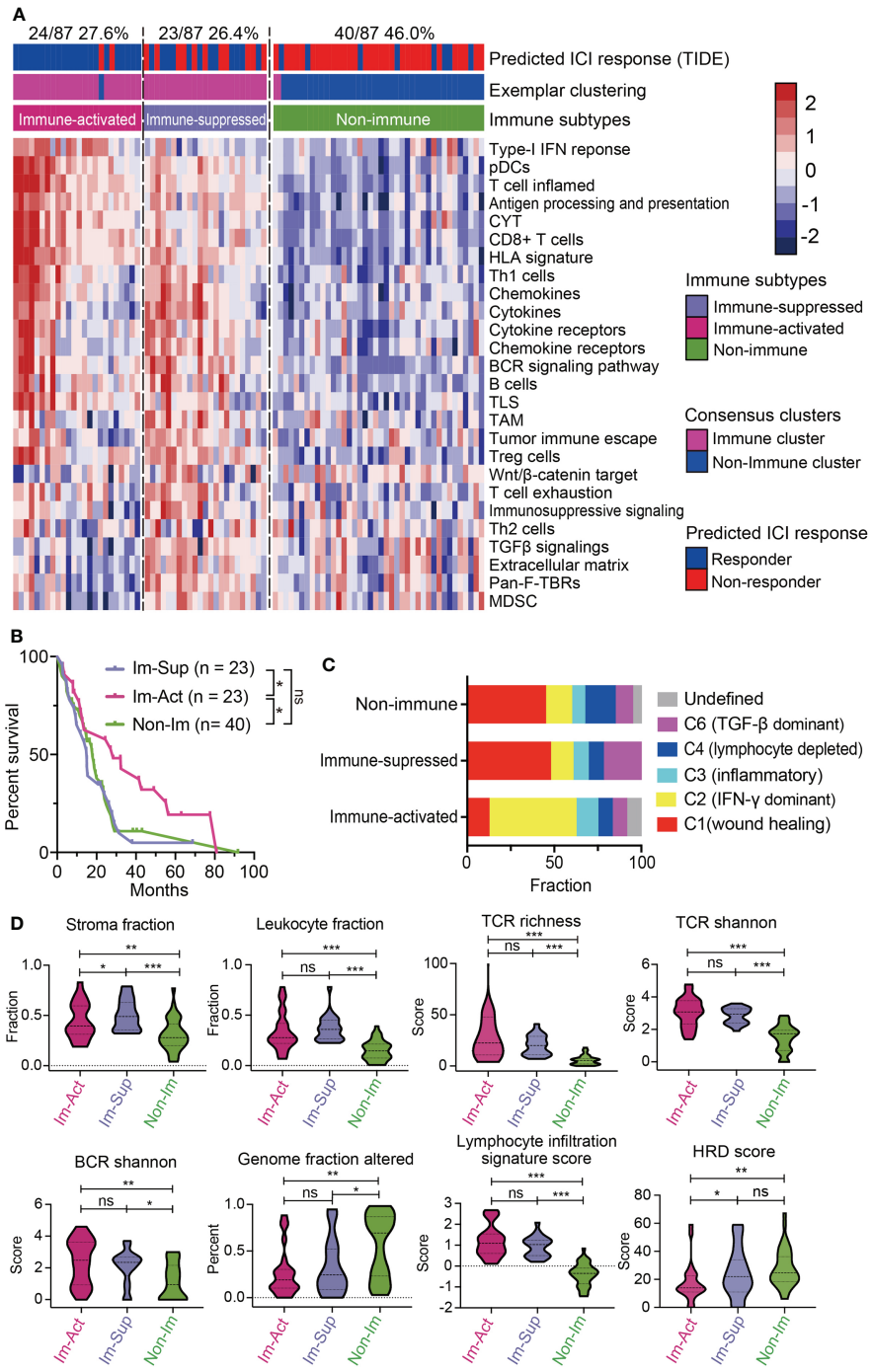

FIGURE 3
Validation of the novel immune-subtyping in external MPM cohort. **(A)** The TCGA-MPM cases were subdivided into non-immune (40/87, 46.0%), immune-suppressed (23/87, 26.4%), and immune-activated (24/87, 27.6%) MPMs using methods of consensus clustering, MDS-RF modification, and NTP division with signatures covering 26 immune- and TME-related signatures which were shown in the heatmap. Top column shows the predicted ICI response estimated by IOBR and corresponding immune subtype of each case. **(B)** Kaplan-Meier survival analyses of overall survival in MPMs with different immunological subtypes using TCGA RNA-seq cohort. **, $p < 0.01$; *, $p < 0.05$; n.s., Not significant. **(C)** Percentage column plots showing the distribution of predicted Thorsson's pan-cancer immune phenotyping across the three immune subtypes. ***, $p > 0.001$; **, $p > 0.01$; *, $p > 0.05$; n.s., Not significant. **(D)** Scoring or fraction of immune cell components and indices in different immune subtypes.

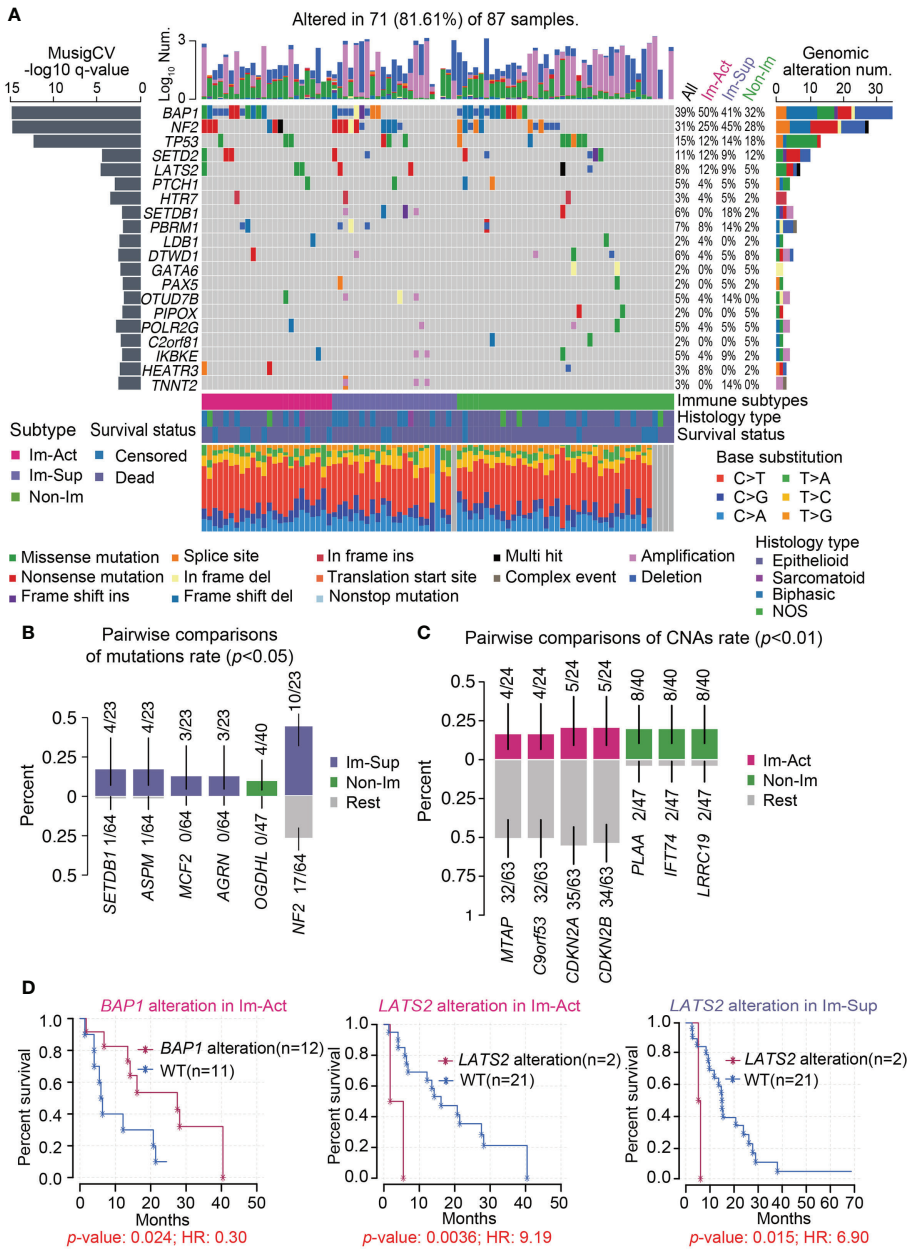

FIGURE 4
Genomic landscape of the three MPM immune subtypes. **(A)** Oncoplot representation of the distribution of genomic alterations (mutations and copy number variations) in driven genes identified by Mutsig across the three MPM immune subtypes, with the significance of mutations (Log10 transformation of MutSig q-value) shown at the left panel. Genomic alterations frequency of all MPM samples stratified by immunological subtypes were listed on the right side of the Oncoplot. The top column illustrates the overall counts of genomic alterations per sample with Log10 transformation, and the column at the bottom presents the mutation spectrum of base substitutions. NOS, Not otherwise specified. Del, Deletion. **(B, C)** Identification of significantly enriched mutations **(B)**, $p < 0.05$) or CNAs (copy number alterations) **(C)**, $p < 0.01$) of genes for each subtype by pairwise comparisons. The upper and bottom columns indicate the alteration rate in enriched subtype and the other subtypes respectively. **(D)** Kaplan-Meier curves of the overall survival in the corresponding subtype of MPM patients stratified by *BAP1* or *LATS2* genomic alteration status. WT, Wild-type.

Development and validation of robust classifiers for distinguishing three subtypes of MPMs

To simplify a biomarker set classifying MPMs for molecular diagnosis and clinical practice, we set out to develop a robust panel of classifier genes with the application of machine-learning algorithms. The workflow is shown in Figure 5A. To identify non-redundant and uncorrelated marker genes, we assembled multiple variable feature-selection algorithms to select the most informative features and ranked the candidates in order of feature importance (Supplementary Table 2, see Materials and Methods for details). To determine the optimal gene panel size, we iteratively trained the RF-LOOCV model by adding one gene in one run. We noticed that classifier performance was almost no more improved for panels larger than 20 genes (Figure S8A). Although the average overall accuracy of classification reaches a maximum around 0.850, the capability of this model for distinguishing immune-activated MPMs from immune-suppressed MPMs is still far from satisfactory (Figure S8A). Therefore, we adopted a two-step feature selection process accompanied by an RFE algorithm to obtain the optimum gene combinations for improving the separating capacity of two comparisons, including immune *v.s.* non-immune and immune-suppressed *v.s.* immune-activated (Figure S8B). Using the combined 16-gene panel as an input for multiple machine learning training procedures, we identified the RF plus cross-validation (CV) algorithm as the best one in terms of classification accuracy. In this setting, a 12-gene classifier showed the highest discriminant performance (93.6%) with RFE process on the training set and was thus identified as the best optimal set (Figure 5B). The efficiency of this 12-gene classifier was confirmed using a testing set and external TCGA dataset with accuracies of 90.9% and 79.4% (Figure 5D). More importantly, using the 12-gene classifier, each immune subtype can be efficiently diagnosed with no bias (Figure 5C). The summarization of the feature selection process was shown in Supplementary Table 3. The classification accuracy was no longer improved by increasing the panel size that incorporated additional clinical covariates, including histology, tumor stage, lymph node stage, metastasis stage, *etc.* (Figure S8C).

Intriguingly, the predicted immune-activated MPMs showed a better prognosis than the predicted non-immune MPMs (Figure 5E), demonstrating that the 12-gene classifier is a good predictor of survival. Multivariate Cox regression analysis confirmed that the 12-gene classifier was a promising and independent biomarker set for predicting patient survival (Figure S9A). To assess the expression patterns of 12 genes, we correlated their expression levels with immune cell infiltrates estimated by CIBERSORT. Hence, two gene categories were identified with distinct expression patterns: genes within category one (*GZMA, APOBEC3G, BTN3A2, TRAT1, HCK, BIN2*, and *SLAMF8*) showed a positive relationship with the abundance of various types of T cells, while category two (*TNC, TNFAIP6, HAS2, SH2B3*, and *ITGA4*) was associated with myeloid components (Figure S10A).

Discussion

The recently published result of Checkmate743 has established the position of dual-target immunotherapy in first-line treatment for MPMs (6). This new therapy pattern raises demands for predicting patients capable of benefiting from ICIs. TMB and PD-L1 are two well-recognized biomarkers for predicting the efficiency of immunotherapy with a wide application (38, 39). Although KEYNOTE-158 has confirmed the clinical efficacy of Keytrude in tumors harboring a TMB≥10 across multiple solid tumors including mesothelioma (40), our analyses revealed a deficiency of TMB with an average expression around 0.5 (Figure S5D). By contrast, expression of PD-L1 ranged from 22 to 42% in MPM patients with a variety of assessment methods (41–43). High PD-L1 expression seemed to be correlated with adverse clinical outcomes for MPMs (43). However, the optimal cutoff score used for predicting prognosis or ICI response remains to be determined. Moreover, there is no consensus regarding PD-L1's predictive value in recognizing potential beneficial patients upon immunotherapy. As a single biomarker, TMB or PD-L1 is insufficient to cover all the intrinsic and environmental factors driving immune heterogeneity of MPMs, and thus has its limitation in being applied to clinical practice.

From this, we speculate that proposing a subtyping system for MPM can promote our understanding of TME heterogeneity and is critical for improving the efficacy of current immunotherapeutic strategies. Previously, classical classification patterns were defined to stratify the immune microenvironment of solid tumors into four types based on the presence or absence of tumor-infiltrating lymphocytes (TILs) and PD-L1 expression, including Type I cancers (PD-L1$^+$ TILs$^+$), Type II cancers (PD-L1$^-$ TILs$^-$), Type III cancers (PD-L1$^+$ TILs$^-$), Type IV cancers (PD-L1$^-$TILs$^+$) (44). Correlating this stratification system with our classification identified immune-activated MPMs as Type I cancers, which were more likely to benefit from anti-PD1/anti-PD-L1 therapy. Similar to previous findings (45), PD-L1 showed greater expression in immune-activated MPMs accompanied by infiltration of cytotoxic T-cells (Figure S4A). For the explanations, the persistent involvement of T cells in tumor immunity was balanced by PD-L1 engagement, which is induced by IFN-γ as an adaptive mechanism and thus exactly appropriate for anti-PD1/PD-L1 therapy (46).

Meanwhile, we observed patients within immune-suppressed MPMs contained substantial myeloid components

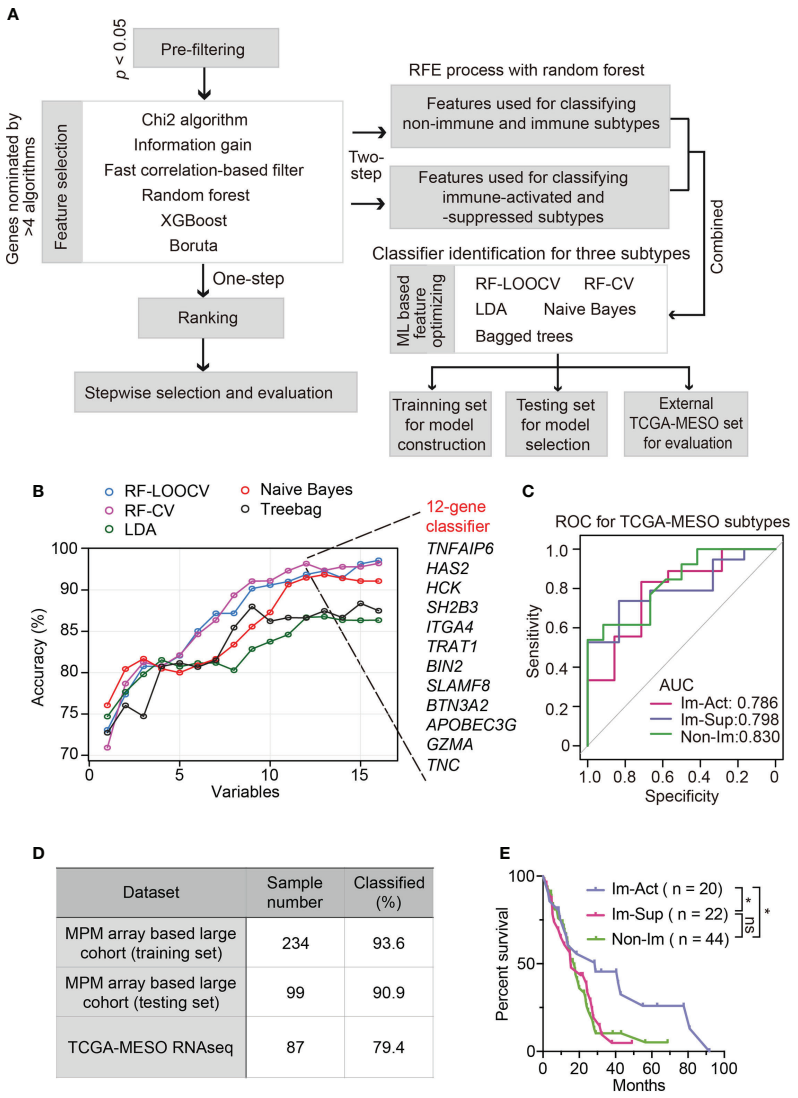

Dataset	Sample number	Classified (%)
MPM array based large cohort (training set)	234	93.6
MPM array based large cohort (testing set)	99	90.9
TCGA-MESO RNAseq	87	79.4

FIGURE 5
Development and validation of robust classifiers for distinguishing three subtypes of MPMs. **(A)** The workflow of a multi-step procedure for identifying classifiers to distinguish three immune subtypes of MPMs. LDA, Linear discriminant analysis; CV, Cross-validation; LOOCV, Leave-one-out cross-validation; ML, Machine learning. **(B)** Line graphs illustrate the variation trend of classification accuracy computed by multiple feature selection algorithms plus stepwise recursive feature elimination (RFE) process. The x-axis suggested a different number of variable combinations. **(C)** Receiver operating characteristic (ROC) curves of the 12-gene classifier for classifying each immune subtype separately. The scores of the area under curve (AUC) are presented in the plot. **(D)** Percentage of correctly classified samples using the 12-gene classifier in different MPM datasets. **(E)** Kaplan-Meier analysis of overall survival of TCGA MPM patients based on classification predicted by the 12-gene classifier. *, $p < 0.05$; n.s., Not significant.

(MDSCs, TAMs) and Tregs responsible for mediating immune tolerance. To take control of this predicted Type IV cancers-associated MPMs, we deemed that simple using combination regiments containing antibodies against PD-L1, CTLA-4, and other immune checkpoints may not be enough considering the immune-suppressive status. TAMs can suppress T cell activity *via* upregulating checkpoint molecules, indirectly crosstalk with Tregs, and secreting immunosuppressive cytokines (47), which eventually results in ICI treatment failure. Thus, immune-suppressed MPMs may benefit from inhibiting the CSF1/CSF1R pathway, a key participant in the proliferation, differentiation, and recruitment of macrophages (48). The efficacy of the CSF1/CSF1R antibody, Cabiralizumab, combined with nivolumab in advanced solid tumors, is currently being investigated in a phase 2 trial (NCT02526017).

The remaining non-immune MPMs accounted for a large part and held the characteristics of Type II (PD-L1 negative with no TIL indicating immune ignorance) or Type III cancers (PD-L1

positive with no TIL indicating intrinsic induction). For these "cold" tumors, enhancing the immunogenicity of tumor cells to attract more T cell infiltration should be prioritized. To achieve it, developing therapies to induce exposure to tumor antigens would be a primary measure to take. As an ideal way to cause immunogenic cell death and liberate neo-antigens, radiotherapy has been combined with immunotherapy to enhance CD8 T-cell responses (49). For the consideration of inducing vascular normalization, anti-angiogenic therapy allows more TILs to access the TME and thus improves the efficiency of ICI through augmenting immune recognition (50). Some treatment guidelines recommended the addition of the anti-angiogenic agent bevacizumab to platinum plus pemetrexed chemotherapy as first-line treatment for selected MPM patients (51, 52). Given the durable survival benefit seen in CheckMate 743, combining nivolumab plus ipilimumab with other therapies, including anti-angiogenic agents, merits further investigation to determine whether tumor response can be enhanced.

Clinical survival is one of our primary concerns for this classification scheme. Our work identified that immune-activated MPM patients exhibited more favourable prognoses relative to immune-suppressed MPM patients in both two cohorts, while conflicting data exist regarding the patient survival of non-immune MPMs. Those seemingly contradictory data might be attributed to different sample properties, including TMN staging, histology, and sample size. For the non-immune MPMs, delineating molecular features using the NMF algorithm (Figure 1A) has summarized three distinct functional modules/subclasses: Cell cycle, Epithelial/IFN response, and ECM subtypes. Further work should investigate these heterogeneous molecular patterns and their associations with immune reprogramming and clinical outcome.

The limitation of the current study is the lack of histology evaluation for each sample. In particular, all the analyses were solely based on bulk transcriptome and cell type deconvolution. The recent finding suggested that some SCLC (small cell lung cancer) cases do contain not low immune cells that were more immunological sequestrated (53). A tumor-immune microenvironment is well-organized and structured from compartmentalized to mixed patterns relating to survival (54). With the advances in the spatial transcriptome, future work should pay more attention to the spatial distribution of immune cells in MPMs, which can help choose appropriate patients to receive the immunotherapy. Besides, the ability of our immune subtypes to predict responses to different immunotherapeutic approaches is worth exploring in clinical trials or real-world studies.

To sum up, we developed a novel and feasible subtype classification system for delineating MPM immune features. We demonstrate that this classification system can be exploited to guide immunotherapy strategies, providing critical biological insights into the mechanisms driving tumor heterogeneity. A machine learning-based 12-gene classifier was exploited to simplify classified procedures, holding promise in clinical translation and prognostic determination.

Data availability statement

The original contributions presented in the study are included in the article/Supplementary Material. Further inquiries can be directed to the corresponding authors.

Author contributions

KY was associated with conceptualization, methodology design, data validation, visualization, writing an original draft, and supervision of the study. TXY and TY conducted data collection and curation. YY took charge of formal analysis. FL performed the investigation, project administration, and conducted writing review & editing. All authors contributed to the article and approved the submitted version.

Acknowledgments

All authors would like to thank the patients and investigators who participated in TCGA and GEO for providing data.

Conflict of interest

The authors declare that the research was conducted in the absence of any commercial or financial relationships that could be construed as a potential conflict of interest.

Publisher's note

Supplementary material

The Supplementary Material for this article can be found online at: https://www.frontiersin.org/articles/10.3389/fonc.2022.995651/full#supplementary-material

References

1. Bueno R. Multimodality treatments in the management of malignant pleural mesothelioma: an update. *Hematol Oncol Clin North Am* (2005) 19:1089–97, vii. doi: 10.1016/j.hoc.2005.09.011

2. Remon J, Reguart N, Corral J, Lianes P. Malignant pleural mesothelioma: new hope in the horizon with novel therapeutic strategies. *Cancer Treat Rev* (2015) 41:27–34. doi: 10.1016/j.ctrv.2014.10.007

3. Christoph DC, Eberhardt WE. Systemic treatment of malignant pleural mesothelioma: new agents in clinical trials raise hope of relevant improvements. *Curr Opin Oncol* (2014) 26:171–81. doi: 10.1097/CCO.0000000000000053

4. Gray SG, Mutti L. Immunotherapy for mesothelioma: a critical review of current clinical trials and future perspectives. *Transl Lung Cancer Res* (2020) 9: S100–19. doi: 10.21037/tlcr.2019.11.23

5. Hotta K, Fujimoto N. Current evidence and future perspectives of immune-checkpoint inhibitors in unresectable malignant pleural mesothelioma. *J Immunother Cancer* (2020) 8:e000461. doi: 10.1136/jitc-2019-000461

6. Baas P, Scherpereel A, Nowak AK, Fujimoto N, Peters S, Tsao AS, et al. First-line nivolumab plus ipilimumab in unresectable malignant pleural mesothelioma (CheckMate 743): a multicentre, randomised, open-label, phase 3 trial. *Lancet* (2021) 397:375–86. doi: 10.1016/S0140-6736(20)32714-8

7. Popat S, Curioni-Fontecedro A, Dafni U, Shah R, O'Brien M, Pope A, et al. A multicentre randomised phase III trial comparing pembrolizumab versus single-agent chemotherapy for advanced pre-treated malignant pleural mesothelioma: the European thoracic oncology platform (ETOP 9-15) PROMISE-meso trial. *Ann Oncol* (2020) 31:1734–45. doi: 10.1016/j.annonc.2020.09.009

8. Fennell DA, Ewings S, Ottensmeier C, Califano R, Hanna GG, Hill K, et al. Nivolumab versus placebo in patients with relapsed malignant mesothelioma (CONFIRM): a multicentre, double-blind, randomised, phase 3 trial. *Lancet Oncol* (2021) 22:1530–40. doi: 10.1016/S1470-2045(21)00471-X

9. Mariathasan S, Turley SJ, Nickles D, Castiglioni A, Yuen K, Wang Y, et al. TGFbeta attenuates tumour response to PD-L1 blockade by contributing to exclusion of T cells. *Nature* (2018) 554:544–8. doi: 10.1038/nature25501

10. Pender A, Titmuss E, Pleasance ED, Fan KY, Pearson H, Brown SD, et al. Genome and transcriptome biomarkers of response to immune checkpoint inhibitors in advanced solid tumors. *Clin Cancer Res* (2021) 27:202–12. doi: 10.1158/1078-0432.CCR-20-1163

11. Kang DH, Chung C, Sun P, Lee DH, Lee SI, Park D, et al. Circulating regulatory T cells predict efficacy and atypical responses in lung cancer patients treated with PD-1/PD-L1 inhibitors. *Cancer Immunol Immunother* (2021) 71:579–88 doi: 10.1007/s00262-021-03018-y

12. Fusco N, Vaira V, Righi I, Sajjadi E, Venetis K, Lopez G, et al. Characterization of the immune microenvironment in malignant pleural mesothelioma reveals prognostic subgroups of patients. *Lung Cancer* (2020) 150:53–61. doi: 10.1016/j.lungcan.2020.09.026

13. Bertino P, Premeaux TA, Fujita T, Haun BK, Marciel MP, Hoffmann FW, et al. Targeting the c-terminus of galectin-9 induces mesothelioma apoptosis and M2 macrophage depletion. *Oncoimmunology* (2019) 8:1601482. doi: 10.1080/2162402X.2019.1601482

14. Pappas AG, Magkouta S, Pateras IS, Skianis I, Moschos C, Vazakidou ME, et al. Versican modulates tumor-associated macrophage properties to stimulate mesothelioma growth. *Oncoimmunology* (2019) 8:e1537427. doi: 10.1080/2162402X.2018.1537427

15. Lee HS, Jang HJ, Choi JM, Zhang J, de Rosen VL, Wheeler TM, et al. Comprehensive immunoproteogenomic analyses of malignant pleural mesothelioma. *JCI Insight* (2018) 3:e98575. doi: 10.1172/jci.insight.98575

16. Bott M, Brevet M, Taylor BS, Shimizu S, Ito T, Wang L, et al. The nuclear deubiquitinase BAP1 is commonly inactivated by somatic mutations and 3p21.1 losses in malignant pleural mesothelioma. *Nat Genet* (2011) 43:668–72. doi: 10.1038/ng.855

17. Gordon GJ, Rockwell GN, Jensen RV, Rheinwald JG, Glickman JN, Aronson JP, et al. Identification of novel candidate oncogenes and tumor suppressors in malignant pleural mesothelioma using large-scale transcriptional profiling. *Am J Pathol* (2005) 166:1827–40. doi: 10.1016/S0002-9440(10)62492-3

18. De Rienzo A, Coleman MH, Yeap BY, Severson DT, Wadowski B, Gustafson CE, et al. Association of RERG expression with female survival advantage in malignant pleural mesothelioma. *Cancers (Basel)* (2021) 13:565. doi: 10.3390/cancers13030565

19. Suraokar MB, Nunez MI, Diao L, Chow CW, Kim D, Behrens C, et al. Expression profiling stratifies mesothelioma tumors and signifies deregulation of spindle checkpoint pathway and microtubule network with therapeutic implications. *Ann Oncol* (2014) 25:1184–92. doi: 10.1093/annonc/mdu127

20. Blum Y, Meiller C, Quetel L, Elarouci N, Ayadi M, Tashtanbaeva D, et al. Dissecting heterogeneity in malignant pleural mesothelioma through histo-molecular gradients for clinical applications. *Nat Commun* (2019) 10:1333. doi: 10.1038/s41467-019-09307-6

21. Zeng D, Ye Z, Shen R, Yu G, Wu J, Xiong Y, et al. IOBR: Multi-omics immuno-oncology biological research to decode tumor microenvironment and signatures. *Front Immunol* (2021) 12:687975. doi: 10.3389/fimmu.2021.687975

22. Thorsson V, Gibbs DL, Brown SD, Wolf D, Bortone DS, Ou Yang TH, et al. The immune landscape of cancer. *Immunity* (2018) 48:812–830 e14. doi: 10.1016/j.immuni.2018.03.023

23. Jiang P, Gu S, Pan D, Fu J, Sahu A, Hu X, et al. Signatures of T cell dysfunction and exclusion predict cancer immunotherapy response. *Nat Med* (2018) 24:1550–8. doi: 10.1038/s41591-018-0136-1

24. Vaske CJ, Benz SC, Sanborn JZ, Earl D, Szeto C, Zhu J, et al. Inference of patient-specific pathway activities from multi-dimensional cancer genomics data using PARADIGM. *Bioinformatics* (2010) 26:i237–45. doi: 10.1093/bioinformatics/btq182

25. Chen DS, Mellman I. Elements of cancer immunity and the cancer-immune set point. *Nature* (2017) 541:321–30. doi: 10.1038/nature21349

26. Spranger S, Bao R, Gajewski TF. Melanoma-intrinsic beta-catenin signalling prevents anti-tumour immunity. *Nature* (2015) 523:231–5. doi: 10.1038/nature14404

27. Peng DH, Rodriguez BL, Diao L, Chen L, Wang J, Byers LA, et al. Collagen promotes anti-PD-1/PD-L1 resistance in cancer through LAIR1-dependent CD8(+) T cell exhaustion. *Nat Commun* (2020) 11:4520. doi: 10.1038/s41467-020-18298-8

28. Groth C, Hu X, Weber R, Fleming V, Altevogt P, Utikal J, et al. Immunosuppression mediated by myeloid-derived suppressor cells (MDSCs) during tumour progression. *Br J Cancer* (2019) 120:16–25. doi: 10.1038/s41416-018-0333-1

29. Patil NS, Nabet BY, Muller S, Koeppen H, Zou W, Giltnane J, et al. Intratumoral plasma cells predict outcomes to PD-L1 blockade in non-small cell lung cancer. *Cancer Cell* (2022) 40:289–300 e4. doi: 10.1016/j.ccell.2022.02.002

30. Yang L, Pang Y, Moses HL. TGF-beta and immune cells: an important regulatory axis in the tumor microenvironment and progression. *Trends Immunol* (2010) 31:220–7. doi: 10.1016/j.it.2010.04.002

31. Goodman AM, Kato S, Bazhenova L, Patel SP, Frampton GM, Miller V, et al. Tumor mutational burden as an independent predictor of response to immunotherapy in diverse cancers. *Mol Cancer Ther* (2017) 16:2598–608. doi: 10.1158/1535-7163.MCT-17-0386

32. Hellmann MD, Callahan MK, Awad MM, Calvo E, Ascierto PA, Atmaca A, et al. Tumor mutational burden and efficacy of nivolumab monotherapy and in combination with ipilimumab in small-cell lung cancer. *Cancer Cell* (2018) 33:853–861 e4. doi: 10.1016/j.ccell.2018.04.001

33. Ganesh K, Stadler ZK, Cercek A, Mendelsohn RB, Shia J, Segal NH, et al. Immunotherapy in colorectal cancer: rationale, challenges and potential. *Nat Rev Gastroenterol Hepatol* (2019) 16:361–75. doi: 10.1038/s41575-019-0126-x

34. Chapel DB, Schulte JJ, Berg K, Churg A, Dacic S, Fitzpatrick C, et al. MTAP immunohistochemistry is an accurate and reproducible surrogate for CDKN2A fluorescence *in situ* hybridization in diagnosis of malignant pleural mesothelioma. *Mod Pathol* (2020) 33:245–54. doi: 10.1038/s41379-019-0310-0

35. Krasinskas AM, Bartlett DL, Cieply K, Dacic S. CDKN2A and MTAP deletions in peritoneal mesotheliomas are correlated with loss of p16 protein expression and poor survival. *Mod Pathol* (2010) 23:531–8. doi: 10.1038/modpathol.2009.186

36. Murakami H, Mizuno T, Taniguchi T, Fujii M, Ishiguro F, Fukui T, et al. LATS2 is a tumor suppressor gene of malignant mesothelioma. *Cancer Res* (2011) 71:873–83. doi: 10.1158/0008-5472.CAN-10-2164

37. Kettunen E, Savukoski S, Salmenkivi K, Bohling T, Vanhala E, Kuosma E, et al. CDKN2A copy number and p16 expression in malignant pleural mesothelioma in relation to asbestos exposure. *BMC Cancer* (2019) 19:507. doi: 10.1186/s12885-019-5652-y

38. Sha D, Jin Z, Budczies J, Kluck K, Stenzinger A, Sinicrope FA. Tumor mutational burden as a predictive biomarker in solid tumors. *Cancer Discovery* (2020) 10:1808–25. doi: 10.1158/2159-8290.CD-20-0522

39. Yarchoan M, Albacker LA, Hopkins AC, Montesion M, Murugesan K, Vithayathil TT, et al. PD-L1 expression and tumor mutational burden are independent biomarkers in most cancers. *JCI Insight* (2019) 4:e126908 doi: 10.1172/jci.insight.126908

40. Marabelle A, Fakih M, Lopez J, Shah M, Shapira-Frommer R, Nakagawa K, et al. Association of tumour mutational burden with outcomes in patients with

advanced solid tumours treated with pembrolizumab: prospective biomarker analysis of the multicohort, open-label, phase 2 KEYNOTE-158 study. *Lancet Oncol* (2020) 21:1353–65. doi: 10.1016/S1470-2045(20)30445-9

41. Chapel DB, Stewart R, Furtado LV, Husain AN, Krausz T, Deftereos G. Tumor PD-L1 expression in malignant pleural and peritoneal mesothelioma by dako PD-L1 22C3 pharmDx and dako PD-L1 28-8 pharmDx assays. *Hum Pathol* (2019) 87:11–7. doi: 10.1016/j.humpath.2019.02.001

42. Matsumura E, Kajino K, Abe M, Ohtsuji N, Saeki H, Hlaing MT, et al. Expression status of PD-L1 and B7-H3 in mesothelioma. *Pathol Int* (2020) 70:999–1008. doi: 10.1111/pin.13028

43. Inaguma S, Lasota J, Wang Z, Czapiewski P, Langfort R, Rys J, et al. Expression of ALCAM (CD166) and PD-L1 (CD274) independently predicts shorter survival in malignant pleural mesothelioma. *Hum Pathol* (2018) 71:1–7. doi: 10.1016/j.humpath.2017.04.032

44. Teng MW, Ngiow SF, Ribas A, Smyth MJ. Classifying cancers based on T-cell infiltration and PD-L1. *Cancer Res* (2015) 75:2139–45. doi: 10.1158/0008-5472.CAN-15-0255

45. Awad MM, Jones RE, Liu H, Lizotte PH, Ivanova EV, Kulkarni M, et al. Cytotoxic T cells in PD-L1-Positive malignant pleural mesotheliomas are counterbalanced by distinct immunosuppressive factors. *Cancer Immunol Res* (2016) 4:1038–48. doi: 10.1158/2326-6066.CIR-16-0171

46. Pardoll DM. The blockade of immune checkpoints in cancer immunotherapy. *Nat Rev Cancer* (2012) 12:252–64. doi: 10.1038/nrc3239

47. Xiang X, Wang J, Lu D, Xu X. Targeting tumor-associated macrophages to synergize tumor immunotherapy. *Signal Transduct Target Ther* (2021) 6:75. doi: 10.1038/s41392-021-00484-9

48. Pyonteck SM, Akkari L, Schuhmacher AJ, Bowman RL, Sevenich L, Quail DF, et al. CSF-1R inhibition alters macrophage polarization and blocks glioma progression. *Nat Med* (2013) 19:1264–72. doi: 10.1038/nm.3337

49. Kalbasi A, June CH, Haas N, Vapiwala N. Radiation and immunotherapy: a synergistic combination. *J Clin Invest* (2013) 123:2756–63. doi: 10.1172/JCI69219

50. Wu X, Giobbie-Hurder A, Liao X, Lawrence D, McDermott D, Zhou J, et al. VEGF neutralization plus CTLA-4 blockade alters soluble and cellular factors associated with enhancing lymphocyte infiltration and humoral recognition in melanoma. *Cancer Immunol Res* (2016) 4:858–68. doi: 10.1158/2326-6066.CIR-16-0084

51. Scherpereel A, Opitz I, Berghmans T, Psallidas I, Glatzer M, Rigau D, et al. ERS/ESTS/EACTS/ESTRO guidelines for the management of malignant pleural mesothelioma. *Eur Respir J* (2020) 55:1900953 doi: 10.1183/13993003.00953-2019

52. Zalcman G, Mazieres J, Margery J, Greillier L, Audigier-Valette C, Moro-Sibilot D, et al. Bevacizumab for newly diagnosed pleural mesothelioma in the mesothelioma avastin cisplatin pemetrexed study (MAPS): a randomised, controlled, open-label, phase 3 trial. *Lancet* (2016) 387:1405–14. doi: 10.1016/S0140-6736(15)01238-6

53. Chan JM, Quintanal-Villalonga A, Gao VR, Xie Y, Allaj V, Chaudhary O, et al. Signatures of plasticity, metastasis, and immunosuppression in an atlas of human small cell lung cancer. *Cancer Cell* (2021) 39:1479–1496 e18. doi: 10.1016/j.ccell.2021.09.008

54. Keren L, Bosse M, Marquez D, Angoshtari R, Jain S, Varma S, et al. A structured tumor-immune microenvironment in triple negative breast cancer revealed by multiplexed ion beam imaging. *Cell* (2018) 174:1373–1387 e19. doi: 10.1016/j.cell.2018.08.039

frontiers | Frontiers in Oncology

TYPE Original Research
PUBLISHED 31 October 2022
DOI 10.3389/fonc.2022.1020493

OPEN ACCESS

EDITED BY
Didier Jean,
Institut National de la Santé et de la Recherche Médicale (INSERM), France

REVIEWED BY
Marc De Perrot,
University Health Network (UHN), Canada
Violetta Borelli,
University of Trieste, Italy

*CORRESPONDENCE
Alistair M. Cook
alistair.cook@uwa.edu.au

SPECIALTY SECTION
This article was submitted to Cancer Immunity and Immunotherapy, a section of the journal Frontiers in Oncology

RECEIVED 16 August 2022
ACCEPTED 03 October 2022
PUBLISHED 31 October 2022

CITATION
Chang F, Keam S, Hoang TS, Creaney J, Gill S, Nowak AK, Ebert M and Cook AM (2022) Immune marker expression of irradiated mesothelioma cell lines. *Front. Oncol.* 12:1020493. doi: 10.3389/fonc.2022.1020493

Immune marker expression of irradiated mesothelioma cell lines

Faith Chang[1,2], Synat Keam[1,3], Tracy Seymour Hoang[1,2], Jenette Creaney[1,2], Suki Gill[4,5], Anna K. Nowak[1,3,6], Martin Ebert[4,5] and Alistair M. Cook[1,2]*

[1]National Centre for Asbestos Related Diseases, Institute for Respiratory Health, Perth, WA, Australia, [2]School of Biomedical Sciences, University of Western Australia, Perth, WA, Australia, [3]Medical School, University of Western Australia, Perth, WA, Australia, [4]School of Physics, Mathematics and Computing, University of Western Australia, Perth, WA, Australia, [5]Department of Radiation Oncology, Sir Charles Gairdner Hospital, Perth, WA, Australia, [6]Department of Medical Oncology, Sir Charles Gairdner Hospital, Perth, WA, Australia

Background: Though immune checkpoint inhibition has recently shown encouraging clinical efficacy in mesothelioma, most patients do not respond. Combining immune checkpoint inhibition with radiotherapy presents an attractive option for improving treatment responses owing to the various immunomodulatory effects of radiation on tumors. However, the ideal dosing and scheduling of combined treatment remains elusive, as it is poorly studied in mesothelioma. The present study characterizes the dose- and time-dependent changes to expression of various immune markers and cytokines important to antitumor responses following irradiation of mesothelioma cell lines.

Methods: Two murine (AB1, AE17) and two human (BYE, JU77) mesothelioma cell lines were treated with titrated gamma-radiation doses (1-8 Gy) and the expression of MHC class-I, MHC class-II and PD-L1 was measured over a series of post-irradiation timepoints (1-72 hours) by flow cytometry. Levels of cytokines IL-1α, IL-1β, IL-6, IL-10, IL-12p70, IL-17A, IL-23, IL-27, MCP-1, IFN-β, IFN-γ, TNF-α, and GM-CSF were measured by multiplex immunoassay in murine cell lines following 8 Gy radiation.

Results: Following irradiation, a dose-dependent upregulation of MHC-I and PD-L1 was observed on three of the four cell lines studied to varying extents. For all cell lines, the increase in marker expression was most pronounced 72 hours after radiation. At this timepoint, increases in levels of cytokines IFN-β, MCP-1 and IL-6 were observed following irradiation with 8 Gy in AB1 but not AE17, reflecting patterns in marker expression.

Conclusions: Overall, this study establishes the dose- and time-dependent changes in immune marker expression of commonly studied mesothelioma

cell lines following radiation and will inform future study into optimal dosing and scheduling of combined radiotherapy and immune checkpoint inhibition for mesothelioma.

KEYWORDS

radiotherapy, immune checkpoint inhibition, MHC, PD-L1, mesothelioma

Introduction

Mesothelioma is an aggressive, incurable cancer in urgent need of more effective therapies. Mesothelioma may develop in any mesothelial surface of the body, but most commonly it arises in the lung pleura following inhalation of asbestos, which acts as a carcinogen (1). The long average latency of 40 years, as well as insidious and non-specific onset of symptoms of this disease, mean that diagnosis usually occurs at an advanced stage where tumor removal is impossible, and treatment options are limited (1). For this reason, mesothelioma remains one of the deadliest cancers, with an untreated median overall survival (mOS) of nine months (2). For several decades, treatment has largely been limited to cytotoxic chemotherapy with cisplatin and pemetrexed, which only slightly improves mOS to twelve months (2). However, immune checkpoint inhibition (ICI) has recently shown encouraging clinical benefit in mesothelioma (3).

Immune checkpoints such as cytotoxic T-lymphocyte-associated protein-4 (CTLA-4), and the programmed death protein-1 (PD-1)/programmed death ligand-1 (PD-L1) signaling axis are co-inhibitory pathways that physiologically prevent inappropriate activation of immune responses, but are often upregulated by cancers to prevent or dampen T-cell activation and thus suppress antitumor activity (4). Inhibition of these checkpoints by ICI can restore or enhance tumor immunogenicity and T-cell activity against cancer (4). The recent phase 3 Checkmate 743 trial found that combined PD-1 and CTLA-4 blockade meaningfully improved survival rates over pemetrexed and platinum chemotherapy in the first-line setting for malignant pleural mesothelioma – leading to approval of this treatment strategy for clinical use (3). However, successful treatment occurred predominantly in the rarer, non-epithelioid mesothelioma subtypes that are often refractory to chemotherapy. The majority of patients either do not respond or acquire resistance to treatment, highlighting the need to find strategies to sensitize a greater proportion of patients to ICI.

The administration of other treatment modalities in conjunction with ICI, such as radiotherapy (RT), may increase both the rate and durability of responses. In mesothelioma, RT is used routinely during surgical resection as well as palliatively to assist in symptoms of pain and dyspnoea (5). Though conventionally exploited for its ability to effect DNA damage and cell death (6), recently RT has been found to produce a host of immunomodulatory effects on tumors through altering the tumor microenvironment (7, 8), initiating immunogenic cell death (9, 10), and altering the surface expression of immune markers, such as major histocompatibility complex (MHC) molecules and PD-L1, on cancer cells (11–14). These effects, as well as the relatively limited systemic toxicities of RT compared to other treatments such as chemotherapy, provide strong rationale for investigating how RT might boost ICI responses (15).

Preclinical studies in some cancers have shown improved efficacy of combined RT and ICI over either treatment alone (16–20), and combined RT and ICI is gradually being translated into the clinical setting (21). At present, however, preclinical studies combining RT and ICI in mesothelioma are limited. In one study using the AB12 murine mesothelioma model, hypo-fractionated RT (5 Gy x 3) followed by anti-CTLA-4 antibody led to abscopal effects, increased T cell infiltration, and increases in immune-related gene expression and cytokine production (22). Another study assessing a similar schedule of 5 Gy x 3 followed by anti-CTLA-4 in the AE17 model of mesothelioma found significantly smaller tumors following combined treatment compared to either treatment alone (23). Though such results are encouraging, more work is needed to assess a larger range of doses and sequences, to gain a more comprehensive understanding of the mechanisms by which combined RT and ICI can augment antitumor immune responses. To our knowledge, the immunomodulatory effects of radiation on mesothelioma cells over time and in the context of carefully titrated doses have not previously been investigated. Such information is essential to inform the design of future preclinical and clinical studies in mesothelioma. The present study therefore aimed to measure the changes to the surface expression of several immune markers relevant to ICI; namely, MHC class-I (MHC-I), MHC class-II (MHC-II) and PD-L1, following irradiation of both murine and human mesothelioma cell lines. In addition, we aimed to characterize the cytokine profile of irradiated cell lines to find potential mechanisms underlying changes to surface expression.

Materials and methods

Cell lines and culture

Murine mesothelioma cell lines AB1 and AE17 were generated as previously described (24). Human mesothelioma cell lines BYE10412 (BYE) and JU77, generated from patient malignant pleural effusions using methods described by Manning et al. (25), were obtained from the National Centre for Asbestos Related Disease (NCARD) biobank. Details of cell lines are summarized in Supplementary Table 1. Cells were cultured in R10, consisting of RPMI 1640 medium (Gibco, Thermo Fisher, MA, USA) supplemented with 20 mM N-2-hydroxyethylpiperazine-N'-2-ethanesulfonic acid (HEPES) (Gibco), 100 U/mL benzylpenicillin, 50 mg/mL gentamicin, 0.05 mM 2-mercaptoethanol (2-ME), and 10% neonatal calf serum (NCS). Cells were maintained in a humidified atmosphere at 37 °C with 5% CO2 and media was replaced twice a week.

IFN-γ stimulation

Murine mesothelioma cell lines were treated with 10 ng/mL recombinant mouse interferon-gamma (IFN-γ) (Cat#200-16, Shenandoah Biotechnology, PA, USA) and incubated for 48 h to induce MHC-I/II and PD-L1 expression. Similarly, human mesothelioma cell lines were subject to a 48 h stimulation with 100 ng/mL recombinant human IFN-γ (Cat#PHC4031, Gibco, Thermo Fisher).

Irradiation

At 80% confluency, cells in culture were harvested and resuspended in R10 at 1×10^6 cells/mL. Cells were irradiated in separate 50 mL tubes by a caesium-137 source at a dose rate of 3.78 Gy/min (Gammacell 3000 SN #0211, Nordion, Ottawa, Canada) at room temperature with doses of 1, 2, 4, 6, and 8 Gy. As the actual radiation dose administered may vary by ± 15% depending on position in the rotating irradiation cannister, tubes were positioned centrally for all irradiations. Immediately after radiation 1×10^6 cells were seeded into separate T175 culture flasks for each timepoint. Cells were then incubated for 1, 6, 24, 48 or 72 h post-irradiation. At the completion of each timepoint, 0.5×10^6 cells were collected per dose and cryopreserved at -80°C until analysis. For cytokine studies, cells were irradiated at 8 Gy and incubated for 72 h, after which cell culture supernatant was collected, centrifuged (300 RCF, three minutes) to remove debris, and stored at -80°C until analysis. All irradiations were conducted in triplicate.

Flow cytometry

Surface expression of MHC-I, MHC-II and PD-L1 was assessed on irradiated cell lines by flow cytometry. Frozen samples were thawed in a 37°C water bath for one minute, then transferred to fresh 15 mL tubes. Cells were washed in 10 mL R10 by centrifugation (300 RCF, three minutes, max brake). Each sample was resuspended in 200 µl R10, transferred to a 96 well plate, and washed by centrifugation (300 RCF, three minutes, max brake). Samples were washed twice with 200 µL/well PBS (300 RCF, three minutes, max brake). Fixable Viability Dye eFluorTM 506 (eF506) diluted 1/1600 in 20 µL PBS was added to the appropriate wells, and samples were incubated for 20 minutes in the dark at room temperature. Samples were then washed twice in 200 µL flow buffer (PBS/2% NCS/5mM EDTA)/well. Samples were stained with 20 µL of appropriate antibody cocktail (Supplementary Table 1) and incubated for a minimum of 30 minutes at room temperature in the dark. Following staining, samples were washed twice (300 RCF, 3 minutes, max brake) with 200 µL/well flow buffer, then resuspended in 50 µL/well 1X BD Stabilizing Fixative diluted in 5mM EDTA before analysis.

Compensation was performed using singly stained UltraComp eBeads (eBioscience, San Diego, CA). Gating was optimized using FMO controls for each marker (gating strategies are presented in Supplementary Figure 2). Where appropriate, IFNγ-stimulated mesothelioma cells (AB1, AE17 and JU77) were used as biological positive controls for each experiment. As MHC-II was not expressed on either murine cell line following IFN-γ, mouse splenocytes were selected as a technical positive staining control for MHC-II antibody.

Samples were acquired using the FACSCantoII (BD Biosciences, NJ, USA) and FACSDiva software (BD Biosciences), and a minimum of 10,000 live events were recorded per sample. Data were analyzed using FlowJo software, version 10.8.0 (Treestar, OR, USA) to generate values for the percentage of cells positive for MHC-I, MHC-II and PD-L1 expression and median fluorescence intensity (MFI). Normalized MFI (nef) was generated by dividing the MFI of each sample with MFI of an unstained control. All radiation doses and timepoints within any individual irradiation experimental repeat were stained and data acquired in the same session.

Multiplex immunoassay

Levels of inflammatory cytokines (IL-1α, IL-1β, IL-6, IL-10, IL-12p70, IL-17A, IL-23, IL-27, MCP-1, IFN-β, IFN-γ, TNF-α, and GM-CSF) were measured in murine mesothelioma cell lines using the LEGENDplex™ 13-plex Mouse Inflammation Panel with Filter Plate (Cat#740150, Biolegend, CA, USA). The assay was performed according to manufacturer's instructions. Standards and samples were assayed in duplicate. Samples

were acquired with the FACSCantoII and FACSDiva software (BD Biosciences). Standard curves and cytokine data were generated using the free cloud-based LEGENDplex™ Data Analysis Software Suite (Biolegend).

Statistical analysis

Data were analyzed and visualized using GraphPad Prism software (version 9.1.2). Immune marker expression was analyzed by two-way analysis of variance (ANOVA), followed by multiple pairwise comparisons with Tukey adjustment. The non-parametric Mann-Whitney U test was used to compare concentrations of a given cytokine in un-irradiated (0 Gy) versus irradiated (8 Gy) samples. Results are presented as mean ± one standard deviation of $n = 3$ independent experimental repeats in all figures. $P < 0.05$ was considered statistically significant.

Results

Basal and IFNγ-induced expression of immune markers

Prior to irradiation, we first assessed our mesothelioma cell lines for surface expression of three markers commonly found on tumor cells, and of particular relevance to cancer immunotherapy: MHC-I, MHC-II and PD-L1. These were present at varying levels of expression at baseline (Figure 1). In proportional terms, AB1 cells expressed high levels of MHC-I (95%) and moderate levels of PD-L1 (21%), whereas the AE17 cell line expressed negligible levels of both markers (2.6% and 1.2% respectively) (Figures 1A, B). Neither murine cell line expressed MHC-II on its surface (<1%). Moreover, when treated with IFN-γ, expression of MHC-I and PD-L1 was substantially upregulated on both murine cell lines, while expression of MHC-II remained unaffected. Similar to AB1, human cell line JU77 constitutively expressed high levels of MHC-I (90%) and PD-L1 (52%) but exhibited no basal expression of MHC-II (Figure 1C). However, when subject to IFN-γ treatment, expression of all markers was substantially upregulated on this cell line. In contrast, BYE cells showed no apparent expression of MHC-I, MHC-II or PD-L1, and IFN-γ did not induce expression of any marker (Figure 1D).

Radiation leads to a dose- and time-dependent upregulation of MHC-I but not MHC-II on mesothelioma cell lines

We previously showed that effects of radiation on cell proliferation and survival saturate at doses of 8 Gy in the mesothelioma cell lines studied (26); therefore, in studying immune marker modulation cells were irradiated with a dose range of 0-8 Gy. No substantial increase in dead cells was observed 72 h after irradiation compared to unirradiated samples.

A dose-dependent upregulation of surface MHC-I on both murine mesothelioma cell lines was observed following irradiation (Figures 2A–D). Effects were observed 72 h post-irradiation and not at earlier timepoints. A 2.5-fold increase in MHC-I MFI was found 72 h after irradiation with 4 Gy in the AB1 cell line ($p = 0.0345$), and this was not significantly different to expression induced by 8 Gy (Figure 2B). In contrast, irradiation with 8 Gy was required to induce MHC-I expression on AE17 (Figures 2C, D), and by 72 h was only slightly higher than unirradiated controls (1.91 ± 1.35% vs 9.15 ± 1.08%, $p = 0.0015$).

We also sought to compare responses to radiation in between murine and human mesothelioma cell lines. Though baseline MHC-I expression on BYE was extremely low, a stark increase in MHC-I expression was observed on this cell line following radiation (Figures 2E, F). Similar to murine cell lines, the effect of radiation was delayed, and observed to the greatest extent 72 h after radiation treatment. Compared to unirradiated controls, the percentage of MHC-I+ cells significantly increased 48 h after irradiation with 6 Gy (2.51 ± 1.80% vs 15.0 ± 2.67%, $p = 0.019$) and 8 Gy (18.6 ± 6.35%, $p = 0.001$). Seventy-two hours post-irradiation, however, cells irradiated with 4 Gy showed increased MHC-I (Figure 2E), and expression was further increased in cells irradiated with 6 Gy (35.0 ± 14.7%, $p < 0.0001$) and 8 Gy (42.9 ± 8.48%, $p < 0.0001$) (Figure 2E). No significant difference was found between 6 Gy and 8 Gy (Figures 2E, F), suggesting radiation-induced expression begins to saturate at 6 Gy. MFI levels showed similar dose- and time-related trends in expression (Figure 2F), with MFI increasing 4-fold after 8 Gy ($p < 0.0001$). In contrast, radiation did not substantially alter MHC-I expression on the JU77 cell line (Figures 2G, H). Also, radiation did not induce MHC-II expression on any mesothelioma cell line, regardless of dose (Supplementary Figure 2).

Radiation leads to upregulation of PD-L1 on mesothelioma cell lines concurrent with MHC-I

Radiation led to increased surface PD-L1 protein expression on AB1, AE17 and BYE cell lines in a dose- and time-related manner, concurrent with patterns in MHC-I expression. Seventy-two hours after radiation of AB1 cells both the percentage of PD-L1$^+$ cells and PD-L1 MFI increased substantially (Figures 3A, B). This increase was apparent at lower doses (1-2 Gy) and radiation-induced upregulation saturated at 4 Gy, with five times as many cells expressing PD-L1 compared to un-irradiated controls (11.5 ± 5.00% vs 67 ± 11.7%, $p < 0.0001$). At the 72 h timepoint, a 3.3-fold increase in PD-L1 MFI was observed after delivery of 4 Gy, which was not

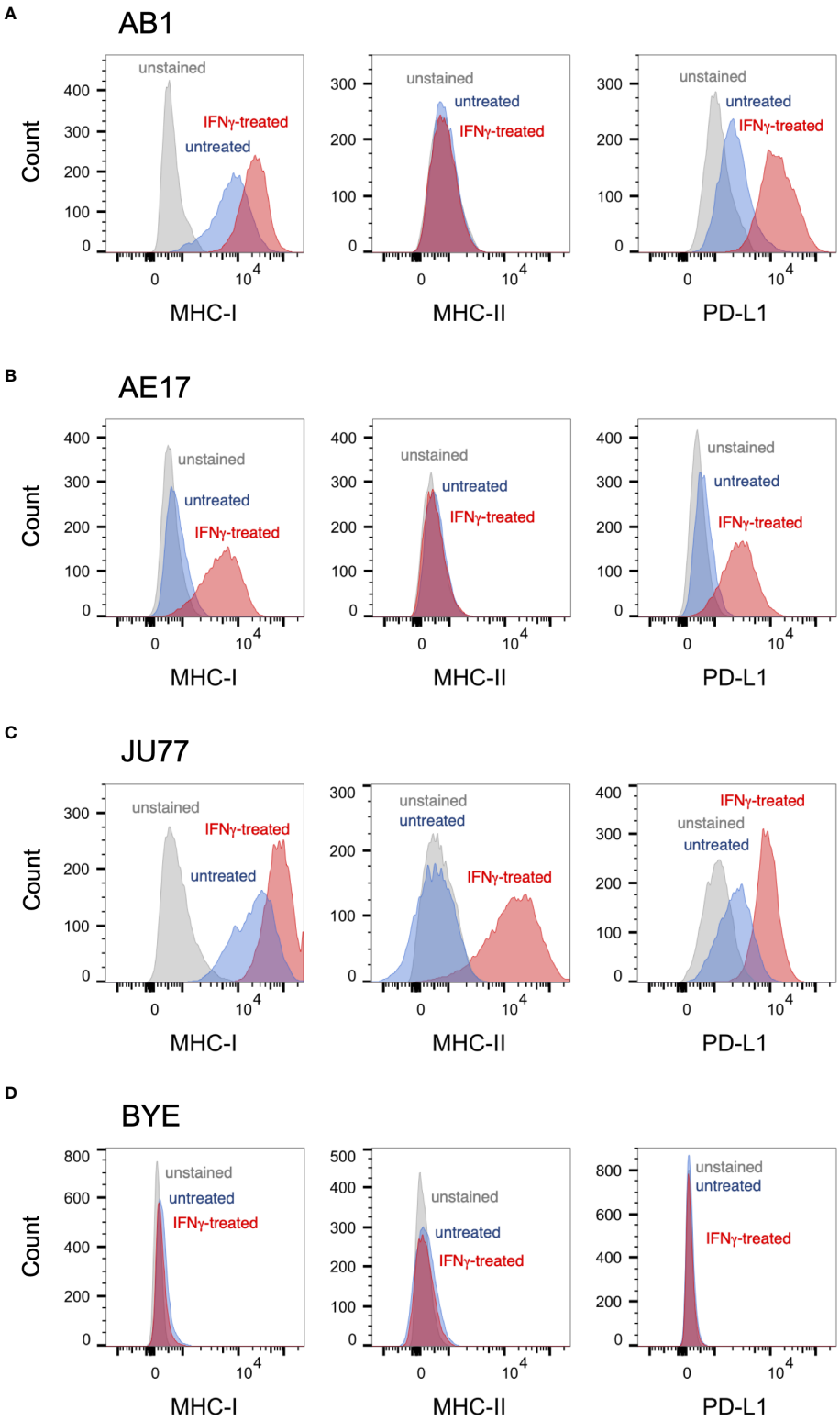

FIGURE 1
Basal expression of immune markers on mesothelioma cell lines measured by flow cytometry. **(A–D)** Representative histograms of surface MHC-I, MHC-II and PD-L1 staining on untreated mesothelioma cells (blue) against unstained controls (grey) and IFNγ-stimulated controls (red) for murine cell lines AB1 **(A)** and AE17 **(B)**, and human cell lines JU77 **(C)** and BYE **(D)**.

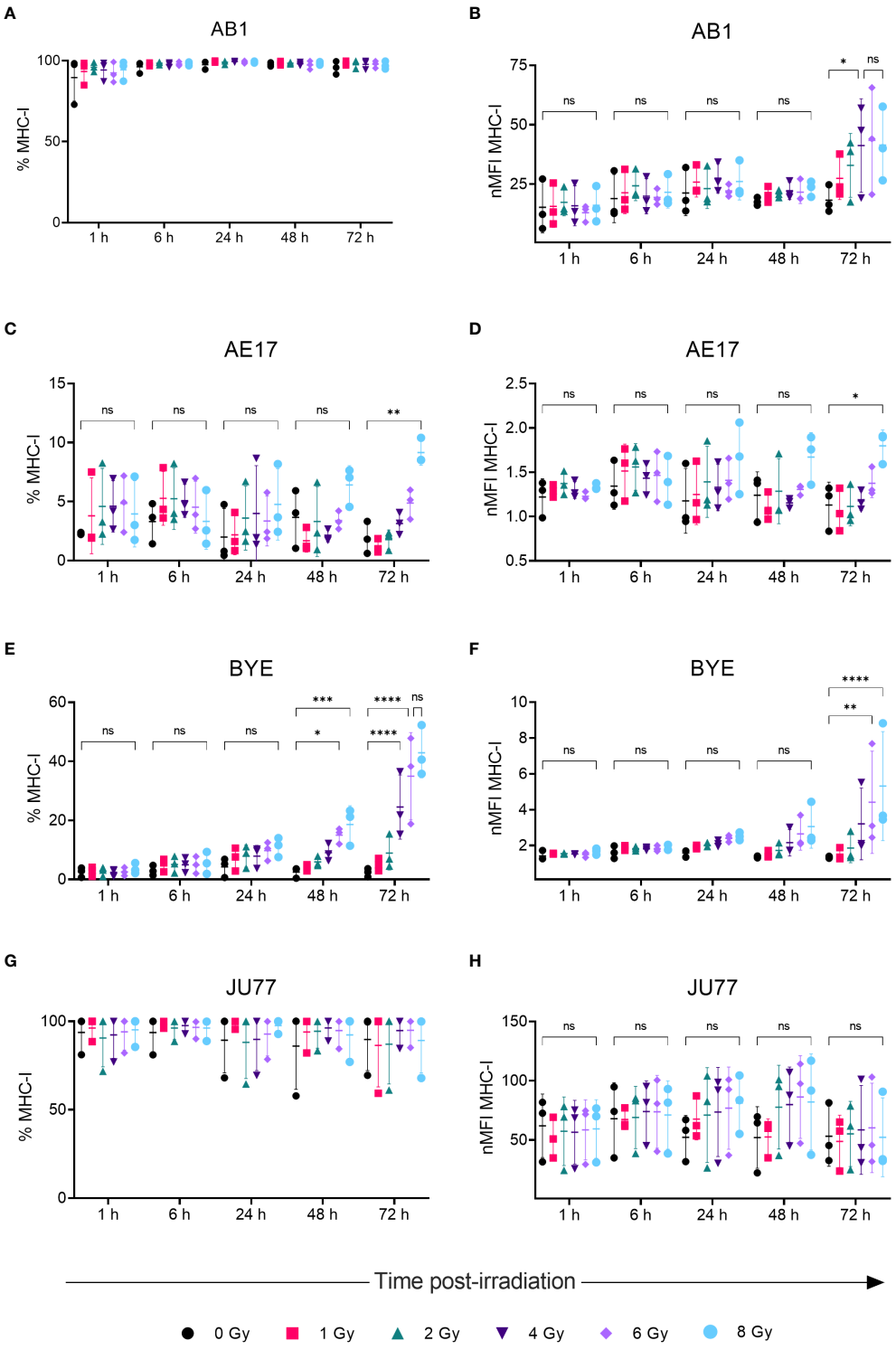

FIGURE 2
Radiation increases MHC-I expression on mesothelioma cells in a dose- and time-dependent manner. **(A–H)** Mesothelioma cells were irradiated with 0-8 Gy and changes to the percentage of MHC-I positive cells and nMFI over time (1, 6, 24, 48 and 72 h) were determined by flow cytometry for AB1 **(A, B)**, AE17 **(C, D)**, BYE **(E, F)** and JU77 **(G, H)** cell lines. Data are presented as mean ± S.D. of $n = 3$ independent experimental repeats. All p-values were determined by two-way ANOVA and multiple pairwise comparison with Tukey adjustment. P-values are represented as follows: *$p < 0.05$, **$p < 0.01$, ***$p < 0.001$, ****$p < 0.0001$. ns, not significant.

significantly different to the 3.9-fold increase in PD-L1 MFI observed after 8 Gy. In contrast, 1-6 Gy did not significantly alter PD-L1 expression on AE17 cells, but expression was higher following 8 Gy radiation compared to un-irradiated samples ($p < 0.05$); again, this occurred only 72 h after treatment and not at earlier timepoints (Figures 3C, D). A similar increase in PD-L1 expression was also observed on human cell line BYE following doses of 6-Gy and above (Figures 3E, F). However, as with MHC-I, radiation did not significantly alter PD-L1 expression on the JU77 cell line (Figures 2G, H).

Inflammatory cytokine profile following radiation differs between murine cell lines

We hypothesized that the radiation-induced changes in immune marker expression in murine cell lines would associate with changes in the profile of secreted inflammatory cytokines detectable in the supernatant. IL-1α, IL-1β, IL-10, IL-12p70, IL-17A, IL-23, IL-27, IFN-γ, TNF-α, and GM-CSF were not detected in the supernatant of either cell line before or after radiation treatment (Table 1). A non-significant increase of IFN-β, MCP-1 and IL-6 was observed following 8 Gy radiation in AB1 (Figures 4A–C). Interestingly, these cytokines were not upregulated in AE17 following the same dose of radiation (Figures 4D–F).

Discussion

ICI has transformed the landscape of cancer treatment, but sensitizing a greater proportion of patients to this therapy remains a serious challenge. RT has exhibited the potential to improve the frequency and durability of ICI responses in cancer. However, the ideal dosing and scheduling of combined RT and ICI to optimize antitumor activity, while avoiding immunosuppressive effects, remains poorly understood for many cancers including mesothelioma (27). Moreover, the radiation-induced immune-related changes at the level of tumor cells for mesothelioma have not previously been established; such information is essential to identifying potential mechanisms of synergy between RT and ICI. The present *in vitro* study therefore characterizes the dose- and time-dependent effects of radiation on expression of selected markers, crucial to immune function, in various mesothelioma cell lines with the aim of identifying an optimal radiation dose to use in future studies. Furthermore, in murine cell lines we study associated changes to inflammatory cytokine release in response to radiation, aiming to gain an understanding of the role that radiation-induced cytokines may play in the immune modulation of tumors.

Firstly, MHC-I on the surface of tumor cells is responsible for presentation of tumor-specific antigen to $CD8^+$ T cells; downregulated levels of MHC-I expression typically correlate with poorer prognosis and treatment response in cancer (28). Consistent with previous studies in breast cancer (10), colon cancer (10, 11), lung cancer (10, 29) and melanoma cell lines (11), radiation increased MHC-I expression in three out of the four mesothelioma cell lines studied, presenting a potential mechanism by which radiation can sensitize tumor cells to $CD8^+$ T cell-mediated killing. As expected, upregulation of MHC-I expression was dose-dependent. For the AB1 cell line, MHC-I MFI increased following 4 Gy radiation. This was not significantly different from 8 Gy and so one might conclude that a dose fraction of 4 Gy would be ideal for use in future preclinical study in this model. On the other hand, the AE17 cell line exhibited minimal basal MHC-I expression and, while 8 Gy significantly increased MHC-I expression, this occurred to a lesser extent than AB1; this may be attributed to inherent differences in radiosensitivity between mouse strains from which these cell lines were established. It is possible that higher doses may result in more pronounced marker upregulation for AE17, but as radiation is often delivered at lower doses per fraction to avoid toxicities associated with higher radiation doses, the clinical relevance and utility of this is uncertain.

Radiation-induced increases in MHC-I were accompanied by similar dose- and time-dependent changes in PD-L1 expression on AB1 and AE17 cell lines. The concurrent upregulation of the suppressive PD-L1 immune checkpoint alongside MHC-I molecules may be an adaptive mechanism to control antitumor activity, as these molecules have opposing effects on immunity. Indeed, this may indicate two different routes of immune escape resulting from selective pressure by the immune system – on the one hand MHC-I downregulation to avoid immune detection in the first place (as seen in AE17), and on the other hand constitutive elevation of PD-L1 to dampen the activity of tumor-specific T cells (as in AB1). Previous preclinical studies in other cancers including hepatocellular carcinoma (30), pancreatic ductal adenocarcinoma (16), head and neck squamous cell carcinoma (18), and non-small cell lung cancer (18, 31) have found that combining anti-PD-1 or anti-PD-L1 therapies with RT improve treatment response by circumventing this adaptive upregulation of PD-L1; such combinations may likewise be assessed in our mesothelioma models. An important factor influencing treatment response found in these studies was the ability of radiation to induce IFN-γ release by T cells to cause MHC-I and PD-L1 upregulation. Notably, IFN-γ treatment markedly increased expression of MHC-I and PD-L1 on both AB1 and AE17, underlining the importance of assessing the effect of radiation on marker expression *in vivo*, which will undoubtedly be impacted by interactions within the wider tumor microenvironment. Moreover, comparing these mesothelioma models *in vivo* will be valuable to understanding variation in responses to combined radio-immunotherapy, and the potential effects of basal and radiation-induced immune marker expression on these responses.

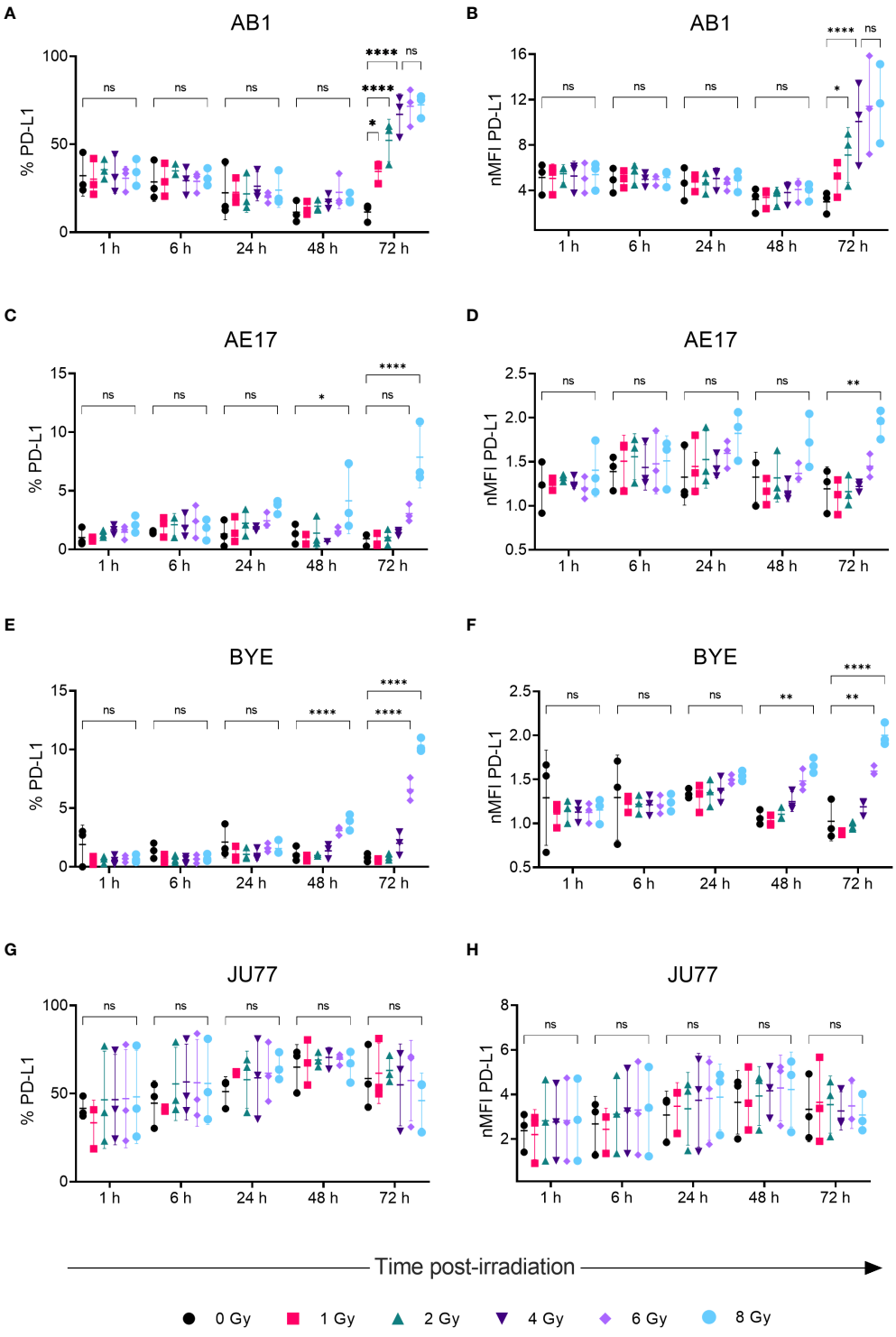

FIGURE 3
Radiation increases PD-LI expression on mesothelioma cells in a dose- and time-dependent manner. **(A–H)** Mesothelioma cells were irradiated with 0-8 Gy and changes to the percentage of PD-LI positive cells and nMFI over time (1, 6, 24, 48 and 72 h) were determined by flow cytometry for AB1 **(A, B)**, AE17 **(C, D)**, BYE **(E, F)** and JU77 **(G, H)** cell lines. Data are presented as mean ± S.D. of *n = 3* independent experimental repeats. All p-values were determined by two-way ANOVA and multiple pairwise comparison with Tukey adjustment. P-values are represented as follows: *$p < 0.05$, **$p < 0.01$, ****$p < 0.0001$. ns, not significant.

TABLE 1 Limit of detection (LOD) of undetected cytokines.

Undetected cytokines	LOD (pg/mL)
IL-23	40.40
IL-1α	0.3662
IFN-γ	3.408
TNF-α	12.60
IL-12p70	4.118
IL-1β	1.141
IL-10	19.29
IL-27	19.35
IL-17A	1.312
GM-CSF	7.643

We also sought to compare murine mesothelioma cell lines to human cell lines. Interestingly, though MHC-I was initially poorly expressed by the BYE cell line, radiation strongly induced MHC-I expression in a dose-dependent manner. MHC-I expression was saturated at 6 Gy, showing that such effects can be achieved in humans with clinically used radiation doses. Interestingly, IFN-γ treatment did not induce MHC-I expression on BYE, suggesting an IFNγ-independent mechanism of upregulation *in vitro* for this cell line. In contrast, both MHC-I and PD-L1 were constitutively expressed by JU77 cells and could be further upregulated by IFN-γ, but expression was unchanged by any dose of radiation administered. It is possible that radiation treatment may have resulted in other immune-related phenotypic or transcriptional changes in this cell line that were beyond the scope of this study.

Optimizing the timing of delivering ICI with respect to RT is essential to improve antitumor immune responses. However, few studies have measured the dynamic changes to marker expression in response to RT; the present study therefore assessed expression at early (1-6 h) and late (24-72 h) stages post-irradiation. Importantly, we show that where modulation of immune markers is observed, this occurs maximally and, in most cases, solely at the 72 h timepoint, regardless of the level of

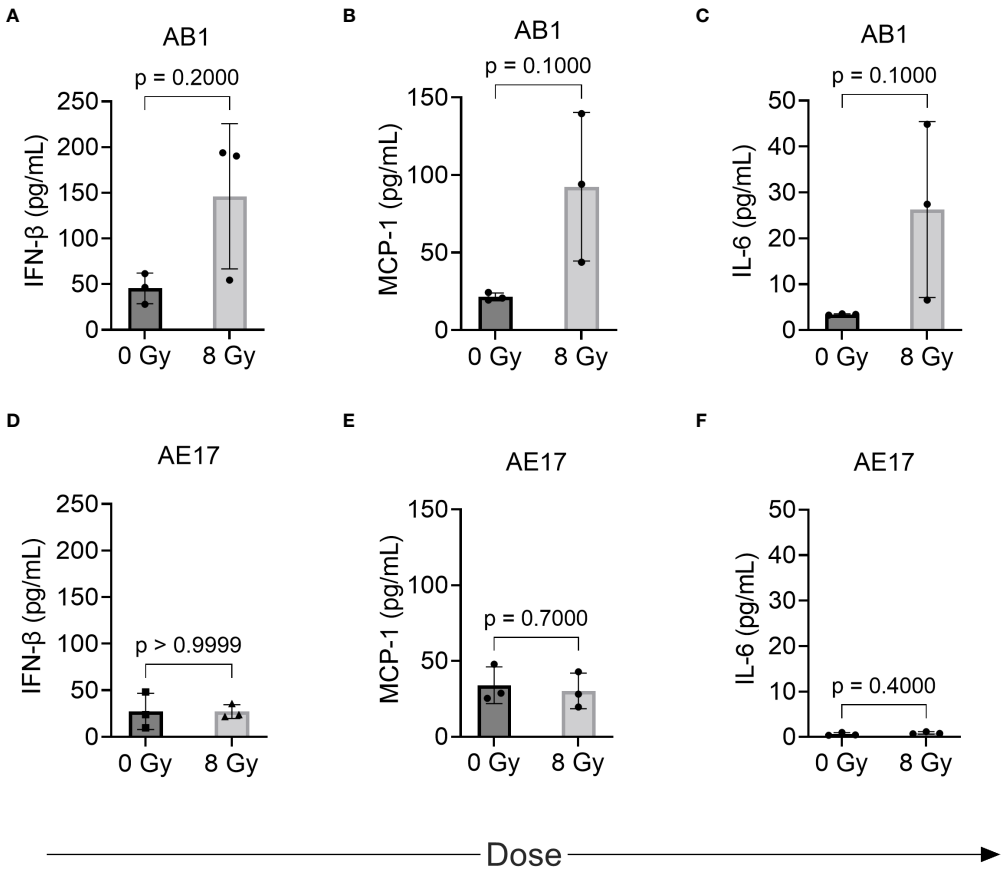

FIGURE 4
The effect of radiation on cytokine production by murine mesothelioma cell lines as measured by multiplex assay. **(A–F)** Concentrations of IFN-β, MCP-1 and IL-6 respectively in AB1 **(A–C)** and AE17 **(D–F)** cell lines, 72 h after irradiation with 8 Gy compared to sham-irradiated (0 Gy) controls. Data are presented as mean ± S.D. of *n = 3* independent experimental repeats. P-values were determined by the non-parametric Mann-Whitney U test.

radiation. This differs from a study in a melanoma cell line, where increased expression of cells irradiated with 10 and 25 Gy was apparent as early as 18 h after radiation; this may have been due to the higher doses administered in this study (12). Our findings may suggest the superior benefit of delivering RT prior to ICI; timing is also likely to be influenced by mechanisms of action of different ICI agents and requires further study. Whether marker expression is sustained beyond 72 h or is transient will also have implications for the relative scheduling of RT and ICI.

We hypothesized that observed increases in MHC-I and PD-L1 would associate with changes in the profile of inflammatory cytokines secreted by our cell lines. Although increased levels of MCP-1, IL-6 and IFN-β in AB1 following irradiation with 8 Gy were observed, this did not reach the set level of significance for this study. Interestingly however, the lack of change to these cytokines in AE17 corresponds with the relatively lower increases in MHC-I and PD-L1 expression observed. The increase in MCP-1 observed in AB1 is consistent with a study in a breast carcinoma cell line, where irradiation with 9 and 23 Gy significantly increased levels of this cytokine. Furthermore, IL-6 (32–35) and IFN-β (29) have previously been shown to increase tumor cell PD-L1 and MHC-I expression respectively in other cancers, and may play a similar role in mesothelioma. IL-17 (36), TNF-α (36), and IL-27 (37) can also upregulate tumor cell PD-L1 expression in various tumor cell lines, however these cytokines were not detected following irradiation of the mesothelioma cell lines in this study. It should also be noted that other cytokines that were not studied here may have the capacity to influence immune response in mesothelioma. One example is IL-15, which works to stimulate the proliferation of CD8+ T cells and natural killer cells, thereby enhancing antitumor responses (38). Administration of IL-15 superagonist and glucocorticoid-induced tumor necrosis factor receptor–related protein (GITR) agonist alongside RT improved control of irradiated AE17 mesothelioma tumor (38). The inflammatory cytokine profile and mechanisms of PD-L1 or MHC-I upregulation may also be of importance to predicting toxicities associated with delivering combined RT and ICI. A recent study of a small group of mesothelioma patients treated with radical hemithoracic RT showed that signaling pathways associated with inflammatory and fibrotic processes were upregulated in patients with no or low-grade toxicity following RT and ICI treatment, compared to those experiencing high grade toxicities (39). Overall, these results warrant further characterization of the role of these cytokines in tumor marker expression and particularly in antitumor immune responses *in vivo*.

One limitation of this study relates to our use of single-dose RT. While fractionated doses of RT are commonly used in the clinic, due to difficulties of studying fractionation *in vitro*, only single doses were administered in this study. Fractionation aims to affect a greater proportion of proliferating tumor cells by delivering multiple low doses at different times, while minimizing toxicity to healthy cells. Future work should establish whether different levels of fractionation result in more pronounced or prolonged antitumor effects compared to single doses. Nevertheless, the studied doses reflect those used in conventional fractionation (2 Gy), as well as hypo-fractionated (> 2 Gy) or hyper-fractionated (< 2 Gy) schedules.

Here, we have characterized changes in a number of crucial molecules involved in the antitumor immune response, following clinically used doses of radiation. Importantly, however, mechanisms of synergy with ICI are undoubtedly facilitated by a host of different immunomodulatory effects, such as recruitment of different immune cell subsets to tumor or remodeling of tumor vasculature, and these will require further characterization *in vivo*. Another avenue for study is the search for biomarkers to predict likelihood of response to RT and ICI, and dynamic changes to tumor or immune cell expression following radiation or ICI may be one such biomarker (27, 40). Overall, the present study lays the essential groundwork to expedite the optimization of radioimmunotherapy combinations for mesothelioma.

Data availability statement

The raw data supporting the conclusions of this article will be made available by the authors, without undue reservation.

Author contributions

FC contributed to study design, performed all experiments, analyzed and interpreted the data and wrote the manuscript. SK and TH assisted in preparing samples and performing experiments. AC developed the concept and design of the study, and supervised writing of the manuscript. ME, SG and AN reviewed the manuscript. All authors contributed to the article and approved the submitted version.

Funding

This research was supported by the Cancer Australia Priority-driven Collaborative Cancer Research Scheme (PdCCRS) (APP1163065) and the National Health and Medical Research Council (NHMRC) Centres of Research Excellence Scheme (APP1197652 and APP1107043). This material is the responsibility of the authors and does not reflect the views of these funding bodies.

Acknowledgments

The authors acknowledge the facilities, and the scientific and technical assistance of the Centre for Microscopy,

Characterization & Analysis, The University of Western Australia, a facility funded by the University, State and Commonwealth Governments. We thank staff managing the NCARD biobank for access to human cell lines in this study. We also thank Dr Tamara Abel, Dr Blake Klyen and Dr Don Heng at the Telethon Kids Institute for training and assistance with the gamma irradiator.

Conflict of interest

The authors declare that the research was conducted in the absence of any commercial or financial relationships that could be construed as a potential conflict of interest.

Publisher's note

Supplementary material

The Supplementary Material for this article can be found online at: https://www.frontiersin.org/articles/10.3389/fonc.2022.1020493/full#supplementary-material

References

1. Australian Institute of Health and Welfare. *Mesothelioma in Australia 2020 [Internet]*. Canberra (ACT): Australian Institute of Health and Welfare (2021). [cited 2022 Aug 16]. 20 p. Report No.: CAN 143. Available at: https://www.aihw.gov.au/reports/cancer/mesothelioma-in-australia-2020/summary.

2. Vogelzang NJ, Rusthoven JJ, Symanowski J, Denham C, Kaukel E, Ruffie P, et al. Phase III study of pemetrexed in combination with cisplatin versus cisplatin alone in patients with malignant pleural mesothelioma. *J Clin Oncol* (2003) 21 (14):2636–44. doi: 10.1200/JCO.2003.11.136

3. Baas P, Scherpereel A, Nowak AK, Fujimoto N, Peters S, Tsao AS, et al. First-line nivolumab plus ipilimumab in unresectable malignant pleural mesothelioma (CheckMate 743): A multicentre, randomised, open-label, phase 3 trial. *Lancet* (2021) 397(10272):375–86. doi: 10.1016/S0140-6736(20)32714-8

4. de Gooijer CJ, Borm FJ, Scherpereel A, Baas P. Immunotherapy in malignant pleural mesothelioma. *Front Oncol* (2020) 10:187. doi: 10.3389/fonc.2020.00187

5. MacRae RM, Ashton M, Lauk O, Wilson W, O'Rourke N, Simone CB2nd, et al. The role of radiation treatment in pleural mesothelioma: Highlights of the 14th international conference of the international mesothelioma interest group. *Lung Cancer* (2019) 132:24–7. doi: 10.1016/j.lungcan.2019.03.023

6. Wang J-S, Wang H-J, Qian H-L. Biological effects of radiation on cancer cells. *Mil Med Res* (2018) 5(1):20. doi: 10.1186/s40779-018-0167-4

7. Honeychurch J, Colton M, Illidge TM, Cheadle EJ. Reprogramming the tumour microenvironment by radiotherapy: Implications for radiotherapy and immunotherapy combinations. *Radiat Oncol (Lond Engl)* (2020) 15(1):1–254. doi: 10.1186/s13014-020-01678-1

8. Philippou Y, Sjoberg HT, Murphy E, Alyacoubi S, Jones KI, Gordon-Weeks AN, et al. Impacts of combining anti-PD-L1 immunotherapy and radiotherapy on the tumour immune microenvironment in a murine prostate cancer model. *Br J Cancer* (2020) 123(7):1089–100. doi: 10.1038/s41416-020-0956-x

9. Keam S, Gill S, Ebert MA, Nowak AK, Cook AM. Enhancing the efficacy of immunotherapy using radiotherapy. *Clin Transl Immunol* (2020) 9(9):e1169. doi: 10.1002/cti2.1169

10. Gameiro SR, Jammeh ML, Wattenberg MM, Tsang KY, Ferrone S, Hodge JW. Radiation-induced immunogenic modulation of tumor enhances antigen processing and calreticulin exposure, resulting in enhanced T-cell killing. *Oncotarget* (2013) 5(2):403–16. doi: 10.18632/oncotarget.1719

11. Garnett CT, Palena C, Chakraborty M, Tsang KY, Schlom J, Hodge JW. Sublethal irradiation of human tumor cells modulates phenotype resulting in enhanced killing by cytotoxic T lymphocytes. *Cancer Res* (2004) 64(21):7985–94. doi: 10.1158/0008-5472.CAN-04-1525

12. Reits EA, Hodge JW, Herberts CA, Groothuis TA, Chakraborty M, Wansley EK, et al. Radiation modulates the peptide repertoire, enhances MHC class I expression, and induces successful antitumor immunotherapy. *J Exp Med* (2006) 203(5):1259–71. doi: 10.1084/jem.20052494

13. Derer A, Spiljar M, Bäumler M, Hecht M, Fietkau R, Frey B, et al. Chemoradiation increases PD-L1 expression in certain melanoma and glioblastoma cells. *Front Immunol* (2016) 7:610. doi: 10.3389/fimmu.2016.00610

14. Mori Y, Sato H, Kumazawa T, Mayang Permata TB, Yoshimoto Y, Murata K, et al. Analysis of radiotherapy-induced alteration of CD8+ T cells and PD-L1 expression in patients with uterine cervical squamous cell carcinoma. *Oncol Lett* (2021) 21(6):446–. doi: 10.3892/ol.2021.12707

15. Alley EW, Katz SI, Cengel KA, Simone CB. Immunotherapy and radiation therapy for malignant pleural mesothelioma. *Trans Lung Cancer Res* (2017) 6 (2):212–9. doi: 10.21037/tlcr.2017.04.01

16. Azad A, Yin Lim S, D'Costa Z, Jones K, Diana A, Sansom OJ, et al. PD-L1 blockade enhances response of pancreatic ductal adenocarcinoma to radiotherapy. *EMBO Mol Med* (2017) 9(2):167–80. doi: 10.15252/emmm.201606674

17. Gong X, Li X, Jiang T, Xie H, Zhu Z, Zhou F, et al. Combined radiotherapy and anti-PD-L1 antibody synergistically enhances antitumor effect in non-small cell lung cancer. *J Thorac Oncol* (2017) 12(7):1085–97. doi: 10.1016/j.jtho.2017.04.014

18. Oweida A, Lennon S, Calame D, Korpela S, Bhatia S, Sharma J, et al. Ionizing radiation sensitizes tumors to PD-L1 immune checkpoint blockade in orthotopic murine head and neck squamous cell carcinoma. *Oncoimmunology* (2017) 6(10):e1356153–e. doi: 10.1080/2162402X.2017.1356153

19. Deng L, Liang H, Burnette B, Beckett M, Darga T, Weichselbaum RR, et al. Irradiation and anti-PD-L1 treatment synergistically promote antitumor immunity in mice. *J Clin Invest* (2014) 124(2):687–95. doi: 10.1172/JCI67313

20. Dovedi SJ, Adlard AL, Lipowska-Bhalla G, McKenna C, Jones S, Cheadle EJ, et al. Acquired resistance to fractionated radiotherapy can be overcome by concurrent PD-L1 blockade. *Cancer Res* (2014) 74(19):5458–68. doi: 10.1158/0008-5472.CAN-14-1258

21. Gill S, Nowak AK, Bowyer S, Endersby R, Ebert MA, Cook A. Clinical evidence for synergy between immunotherapy and radiotherapy (SITAR). *J Med Imaging Radiat Oncol* (2022) 66(6):881–95. doi: 10.1111/1754-9485.13441

22. Wu L, Wu MO, de la Maza L, Yun Z, Yu J, Zhao Y, et al. Targeting the inhibitory receptor CTLA-4 on T cells increased abscopal effects in murine mesothelioma model. *Oncotarget* (2015) 6(14):12468–80. doi: 10.18632/oncotarget.3487

23. De La Maza L, Wu M, Wu L, Yun H, Zhao Y, Cattral M, et al. *In situ* vaccination after accelerated hypofractionated radiation and surgery in a mesothelioma mouse model. *Clin Cancer Res* (2017) 23(18):5502–13. doi: 10.1158/1078-0432.CCR-17-0438

24. Davis MR, Manning LS, Whitaker D, Garlepp MJ, Robinson BW. Establishment of a murine model of malignant mesothelioma. *Int J Cancer* (1992) 52(6):881–6. doi: 10.1002/ijc.2910520609

25. Manning LS, Whitaker D, Murch AR, Garlepp MJ, Davis MR, Musk AW, et al. Establishment and characterization of five human malignant mesothelioma cell lines derived from pleural effusions. *Int J Cancer* (1991) 47(2):285–90. doi: 10.1002/ijc.2910470219

26. Keam S, MacKinnon KM, D'Alonzo RA, Gill S, Ebert MA, Nowak AK, et al. Effects of photon radiation on DNA damage, cell proliferation, cell survival and

apoptosis of murine and human mesothelioma cell lines. *Adv Radiat Oncol* (2022) 7(6):101013. doi: 10.1016/j.adro.2022.101013

27. Demaria S, Guha C, Schoenfeld J, Morris Z, Monjazeb A, Sikora A, et al. Radiation dose and fraction in immunotherapy: One-size regimen does not fit all settings, so how does one choose? *J Immunother Cancer* (2021) 9(4):e002038. doi: 10.1136/jitc-2020-002038

28. Garrido F, Aptsiauri N, Doorduijn EM, Garcia Lora AM, van Hall T. The urgent need to recover MHC class I in cancers for effective immunotherapy. *Curr Opin Immunol* (2016) 39:44–51. doi: 10.1016/j.coi.2015.12.007

29. Wan S, Pestka S, Jubin RG, Lyu YL, Tsai YC, Liu LF. Chemotherapeutics and radiation stimulate MHC class I expression through elevated interferon-beta signaling in breast cancer cells. *PLoS One* (2012) 7(3):e32542. doi: 10.1371/journal.pone.0032542

30. Kim KJ, Kim JH, Lee SJ, Lee EJ, Shin EC, Seong J. Radiation improves antitumor effect of immune checkpoint inhibitor in murine hepatocellular carcinoma model. *Oncotarget* (2017) 8(25):41242–55. doi: 10.18632/oncotarget.17168

31. Kamdem DT, Steel JC, Wise-Draper T, Kassing WM, Hashemi Sadraei N, Mierzwa ML, et al. Combined radiation and PD-L1 blockade improved tumor control in mouse head and neck squamous cell carcinoma (HNSCC). *Int J Radiat Oncol Biol Phys* (2016) 94(4):928–. doi: 10.1016/j.ijrobp.2015.12.185

32. Chan L-C, Li C-W, Xia W, Hsu J-M, Lee H-H, Cha J-H, et al. IL-6/JAK1 pathway drives PD-L1 Y112 phosphorylation to promote cancer immune evasion. *J Clin Invest* (2019) 129(8):3324–38. doi: 10.1172/JCI126022

33. Chen M-F, Chen P-T, Chen W-C, Lu M-S, Lin P-Y, Lee KD. The role of PD-L1 in the radiation response and prognosis for esophageal squamous cell carcinoma related to IL-6 and T-cell immunosuppression. *Oncotarget* (2016) 7(7):7913–24. doi: 10.18632/oncotarget.6861

34. Shen MJ, Xu LJ, Yang L, Tsai Y, Keng PC, Chen Y, et al. Radiation alters PD-L1/NKG2D ligand levels in lung cancer cells and leads to immune escape from NK cell cytotoxicity *via* IL-6- MEK/Erk signaling pathway. *Oncotarget* (2017) 8 (46):80506–20. doi: 10.18632/oncotarget.19193

35. Chen S, Crabill GA, Pritchard TS, McMiller TL, Wei P, Pardoll DM, et al. Mechanisms regulating PD-L1 expression on tumor and immune cells. *J Immunother Cancer* (2019) 7(1):305. doi: 10.1186/s40425-019-0770-2

36. Wang X, Yang L, Huang F, Zhang Q, Liu S, Ma L, et al. Inflammatory cytokines IL-17 and TNF-α up-regulate PD-L1 expression in human prostate and colon cancer cells. *Immunol Lett* (2017) 184:7–14. doi: 10.1016/j.imlet.2017.02.006

37. Carbotti G, Dozin B, Martini S, Giordano C, Scordamaglia F, Croce M, et al. IL-27 mediates PD-L1 expression and release by human mesothelioma cells. *Cancers (Basel)* (2021) 13(16):4011. doi: 10.3390/cancers13164011

38. Murakami J, Wu L, Kohno M, Chan M-L, Zhao Y, Yun Z, et al. Triple-modality therapy maximizes antitumor immune responses in a mouse model of mesothelioma. *Sci Transl Med* (2021) 13(589):eabd9882. doi: 10.1126/scitranslmed.abd9882

39. Crovella S, Revelant A, Muraro E, Moura RR, Brandão L, Trovò M, et al. Biological pathways associated with the development of pulmonary toxicities in mesothelioma patients treated with radical hemithoracic radiation therapy: A preliminary study. *Front Oncol* (2021) 11:784081. doi: 10.3389/fonc.2021.784081

40. Fujimoto D, Uehara K, Sato Y, Sakanoue I, Ito M, Teraoka S, et al. Alteration of PD-L1 expression and its prognostic impact after concurrent chemoradiation therapy in non-small cell lung cancer patients. *Sci Rep* (2017) 7(1):11373. doi: 10.1038/s41598-017-11949-9

frontiers | Frontiers in Immunology

TYPE Original Research
PUBLISHED 04 January 2023
DOI 10.3389/fimmu.2022.1026185

OPEN ACCESS

EDITED BY
Barbara Rolfe,
The University of Queensland,
Australia

REVIEWED BY
Connie Jackaman,
Curtin University, Australia
Stefan Eugen Sonderegger,
Australian Institute for Bioengineering and Nanotechnology, University of Queensland, Australia

*CORRESPONDENCE
Ori Wald
ori.wald@mail.huji.ac.il
Didier Jean
didier.jean@inserm.fr

†PRESENT ADDRESS
Stefano Caruso,
Université Paris Est Créteil, Inserm, Institut Mondor de Recherche Biomédicale (IMRB), U955, Team 18, Créteil, France

SPECIALTY SECTION
This article was submitted to Cancer Immunity and Immunotherapy, a section of the journal Frontiers in Immunology

RECEIVED 23 August 2022
ACCEPTED 31 October 2022
PUBLISHED 04 January 2023

CITATION
Stern E, Caruso S, Meiller C, Mishalian I, Hirsch TZ, Bayard Q, Tadmor CT, Wald H, Jean D and Wald O (2023) Deep dive into the immune response against murine mesothelioma permits design of novel anti-mesothelioma therapeutics. *Front. Immunol.* 13:1026185. doi: 10.3389/fimmu.2022.1026185

Deep dive into the immune response against murine mesothelioma permits design of novel anti-mesothelioma therapeutics

Esther Stern[1], Stefano Caruso[2†], Clément Meiller[2], Inbal Mishalian[1], Theo Z. Hirsch[2], Quentin Bayard[2], Carmit T. Tadmor[1,3], Hanna Wald[1], Didier Jean[2*] and Ori Wald[1,4*]

[1]Gene Therapy Institute, Hadassah Hebrew University Medical Center and Faculty of Medicine, Hebrew University of Jerusalem, Jerusalem, Israel, [2]Centre de Recherche des Cordeliers, Inserm, Sorbonne Université, Université Paris Cité, team Functional Genomics of Solid Tumors, Paris, France, [3]Tel Aviv University, Tel Aviv, Israel, [4]Department of Cardiothoracic Surgery, Hadassah Hebrew University Medical Center and Faculty of Medicine, Hebrew University of Jerusalem, Jerusalem, Israel

Given the need to improve the efficacy of standard-of-care immunotherapy (anti-CTLA-4 + anti-PD-1) in human malignant pleural mesothelioma (hMPM), we thoroughly characterized the immunobiology of the AB12 murine mesothelioma (MM) model, aiming to increase its accuracy in predicting the response of hMPM to immunotherapy and in designing novel anti-hMPM treatments. Specifically, we used immunologic, transcriptomic and survival analyses, to synchronize the MM tumor growth phases and immune evolution with the histo-molecular and immunological characteristics of hMPM while also determining the anti-MM efficacy of standard-of-care anti-hMPM immunotherapy as a benchmark that novel therapeutics should meet. We report that early-, intermediate- and advanced- AB12 tumors are characterized by a bell-shaped anti-tumor response that peaks in intermediate tumors and decays in advanced tumors. We further show that intermediate- and advanced- tumors match with immune active ("hot") and immune inactive ("cold") hMPM respectively, and that they respond to immunotherapy in a manner that corresponds well with its performance in real-life settings. Finally, we show that in advanced tumors, addition of cisplatin to anti CTLA-4 + anti PD-1 can extend mice survival and invigorate the decaying anti-tumor response. Therefore, we highlight this triple combination as a worthy candidate to improve clinical outcomes in hMPM.

KEYWORDS

immunotherapy, lung neoplasms, thoracic cancer, animal models, immunomodulation

Introduction

Human malignant pleural mesothelioma (hMPM) is a highly aggressive cancer for which immunotherapy with nivolumab + ipilimumab (anti PD-1 + anti CTLA-4, respectively) is the standard-of-care. Unfortunately, therapy response rates do not peak above 40% and median survival periods do not exceed 18 months (1, 2). Therefore, combinations of anti-hMPM immunotherapy with or without other treatments that will show benefit over and above the standard-of-care are highly desired (3).

To test and design new anti-hMPM therapies, asbestos-induced syngeneic murine mesothelioma (MM) cell lines were developed (4–7). However, only minority of treatment protocols designed using these preclinical cell line based MM tumor models showed sufficient clinical benefit to be broadly adopted (5). A key question is how to better utilize such MM tumor models to properly select effective therapeutics.

MM tumor models are appealing for immunotherapy research because they mimic the histological spectrum of hMPM and because they provoke an anti-tumor response that is responsive to immunotherapy within a week from implantation (8). Illustrating their utility, previous research using these models has highlighted impressive anti-MM effects of various combinations of checkpoint therapies together with chemotherapy or radiotherapy or surgery (9). For example, Fear et al. showed that combination of anti CTLA-4 together with anti OX-40 was synergistic in enhancing complete MM tumor regression (6). Similarly, Wu et al. and De La maza et al. respectively showed that administration of anti CTLA-4 between intervals of chemotherapy (8) or after radiotherapy and surgery (10) offered effective multimodal anti-MM therapeutics, successfully boosting the anti-tumor response.

And yet, the majority of studies in MM tumor models suffer from common limitations that preclude linear deduction of their findings to the clinic. First, in many studies, therapeutic interventions were tested relatively early following tumor implantation when the tumor has not yet imprinted its immunosuppressive effects in the tumor microenvironment (TME) nor remotely in the host (11, 12). This may yield an underestimation of loss of treatment efficacy in advanced disease phases which is almost always the state of hMPM at the time of diagnosis (13, 14). Second, so far, studies have not longitudinally compared the TME of MM tumors relative to that of hMPM, nor tested treatment efficacy across tumor growth phases that represent distinct immune activation states. Thus, optimal anti-MM effects were possibly detected under conditions that do not properly mimic hMPM. Third, studies did not routinely compare the efficacy of new immunotherapeutic combinations relative to that of the standard-of-care, which could result in selection of suboptimal candidates for translation to the clinic (6).

To address these issues, we herein report on a systematic investigational approach that we applied in the AB12 MM tumor model in order to improve its preclinical predictive capacity. First, specific AB12 tumor growth phases were determined to assure that what is tested are well-established tumors. Second, the immune response in the TME and at remote immune sites was characterized in each of the tumor growth phases to identify specific phases that are predominated by immune activation, immune transition and immune suppression. Third, the efficacy of standard-of-care anti-hMPM immunotherapy was determined in all tumor growth phases to serve as a preclinical benchmark for evaluation of new interventions. In parallel, in steps one and two, the histo-molecular and immunological characteristics of AB12 tumors were respectively compared to hMPM in order to permit synchronization of experimental conditions in the model with its counterpart human disease.

Of the wide variety of MM cell lines that are available for research (7, 15, 16) we selected to implement our investigational approach using the biphasic murine AB12 cell line for three reasons: (i) biphasic MPM is the most common histo-molecular subtype of hMPM, representing 50% of all human disease (17); (ii) previous studies have shown that AB12 cells are highly immunogenic in the manner in which they elicit an anti-tumor immune response (8, 10); and (iii) this study is focused on immunotherapy which nowadays is becoming the standard-of-care treatment for non-epithelioid hMPM (1, 18). We further selected to use young female mice in our experiments, despite the fact that hMPM is mainly diagnosed in elderly males and despite that fact the efficacy of immunotherapy is partly age dependent (19) because past research demonstrates striking histological similarities between biphasic hMPM and AB12 tumors that were transplanted in young female mice (4). This coupled with the fact that the vast majority of studies that examine the immune response associated with MM tumors have been performed in young female mice (5, 6, 8, 16, 20–24) will allow other researchers to more easily align past and future research with our findings.

Abbreviations: ANOVA, Analysis of variance; BM- Bone marrow; CTLA4, Cytotoxic T lymphocyte antigen-4; ELISA, Enzyme-Linked Immunosorbent Assay; E-score, epithelioid-component proportion; FC, Fold-Change; FPKM, Fragments Per kilobase of transcript per Million reads mapped; hMPM, Human MPM; IFN, Interferon; IFNg, IFN-gamma; IV, Intravenous; KEGG, Kyoto Encyclopedia of Genes and Genomes; LAG-3, Lymphocyte-activation gene 3; MCP-counter, Microenvironment cell population counter; MM, Murine mesothelioma; mMCP-counter, Mouse MCP –counter; MPM, Malignant pleural mesothelioma; OX40, Tumor necrosis factor receptor superfamily, member 4, also known OX40; NK, Natural killer; PB, Peripheral blood; PD, Programmed death-ligand 1; RIN, RNA integrity number; RNA-Seq, RNA sequencing; ROC, receiver operating characteristic curve; RT-PCR, Reverse transcription polymerase chain reaction; S-score, sarcomatoid-component proportion; TIM-3, T-cell immunoglobulin domain and mucin domain 3; TIS, Tumor immune subtypes; TME, Tumor microenvironment.

Overall, in light of the surge of novel immunotherapeutic drugs that are anticipated to be approved in the near future (25), our study delineates a more standardized and systematic approach aiming to guide the utilization of MM models in preclinical studies.

Methods

Study design

This study was designed, using immunologic, transcriptomic and survival analyses, to explore a three-step approach that permits synchronization of tumor growth phases and of immune response in the MM model (both in tumor and in remote immune sites) with that of histo-molecular and immunological characteristics of hMPM while also determining in the MM model the efficacy of current standard-of-care anti-hMPM immunotherapy as a benchmark that novel therapeutics should meet.

Mice

BALB/c mice were purchased from Envigo. 8-week-old female mice were used for all studies.

Cell lines

The AB12 cell line was kindly provided by prof. Zvi Friedlander's lab at Hadassah. AB12 cells were grown in DMEM culture medium (Gibco) supplemented with 10% fetal bovine serum (FBS) (Biological industries), 2 mM l-glutamine, penicillin (100 U/ml), streptomycin (100 ug/ml), neomycin (100 ug/ml) and sodium pyruvate (2mm) (BI). Cells were grown in a 37°C and 5% CO2 environment and were harvested when 70% confluent.

Preparation of cell suspensions for flow-cytometry analysis

Peripheral blood (PB) was collected in tubes containing heparin. Spleens were harvested and passed through a 70-mm cell strainer to generate single cell suspension. Bone marrow (BM) cells were extracted from two femur bones by flushing with 1ml of cold PBS, using a 25G needle. Next, the PB, spleen and BM cell suspensions were treated with an erythrocyte lysis solution (155 mM NH_4Cl, 10 mM $KHCO_3$, 0.1 mM Na_2EDTA, pH: 7.4). The cells were then washed and stained as described below.

Isolation of tumor infiltrating cells

Fresh tissue was cut into 1 mm^3 pieces and digested with 1.5mg/mL collagenase type IV (Worthington Biochemical) and 0.05 mg/mL DNase I (Sigma-Aldrich) at 37°C for 20 minutes. The dissociated tissues were filtered through a 70μm cell strainer and washed with DMEM culture medium (Gibco) supplemented with 10% FBS and centrifuged.

Flow-cytometry

Staining was performed for 30 minutes at 4°C in PBS. All antibodies were purchased from Biolegend and were used in 1:50-1:100 dilutions. The complete list of antibodies is shown in Supplementary Table 1. The compensation control was performed using single color staining. Unstained controls and Fluorescence minus one (FMO) control were utilized to establish baseline gate settings for each respective antibody-fluorophore combination used in individual experiments. Stained cells were analyzed with CytoFLEX Cytometer (Beckman Coulter). Data analysis was performed using the Cytexpert software (Beckman Coulter).

Tumor experiments

AB12 cells (1×10^5) were injected to the peritoneum of BALB/c mice (at least 7 mice per group). To determine survival, mice were routinely monitored and when they developed significant ascites or their general condition deteriorated, they were euthanized. Tumor tissue was collected from the peritoneal cavity immediately after the mice were anesthetized. The percentage of necrotic area out of entire tumor area was determined in hematoxylin and eosin stained tumor section based on morphology using the ImageJ software.

CTLA-4, PD-1, LAG-3 and TIM-3 blockade and cisplatin treatment

200μg of anti CTLA-4 (clone 9D9), anti PD-1 (clone RPMI-14) anti LAG-3 (clone C9B7W) or anti TIM-3 (RMT3-23) blocking antibodies (BioXcell) were injected to the peritoneum of tumor-bearing mice at the indicated time points. The treatment protocol for all antibodies, unless otherwise stated in text, consisted of four injections: two injections per week for two weeks. 5mg/kg of cisplatin (Pharmachemie B.V.) was injected intravenously to tumor-bearing mice at the indicated time points. The treatment protocol consisted of two injections: one injection per week for two weeks.

RNA isolation

Total RNA from tumor and spleen tissues was isolated using TRIzol reagent (Ambion) according to the manufacturer's

protocol, followed by Direct-zol (Zimo). The concentration and the quality were evaluated using a NanoDrop 2000c (Thermo scientific) and the RNA integrity number (RIN) was determined using Agilent Bioanalyzer (TapeStation RNA 2200) for RNA sequencing.

Quantitative real-time RT-PCR

cDNA was synthesized from 1-2µg total RNA using Biosciences qScript cDNA Synthesis Kit (Quanta). Quantitative PCR (qPCR) was performed using the CFX384, C1000 touch thermal cycler (Bio-Rad), and a SYBR Green PCR Kit (Quanta). The fold expression and statistical significance were calculated using the $2^{-\Delta\Delta Ct}$ method. All experiments were performed in triplicate. Primers were purchased from IDT-syntezza. The primer sequences are listed in Supplementary Table 2.

Co-culture and ELISA assay

For co-culture assays, mice were injected with AB12 cells, at the indicated time points prior to the experiment. Spleens from these mice were collected and splenocytes were isolated as described above. The number of viable splenocytes in each sample was determined by trypan blue staining. 24 hours prior to the experiment, 3×10^4 AB12 cells per well were plated in flat-bottom, 24-well plates (Corning). Next, the medium was changed to fresh medium and splenocytes were added in 1:20 ratio. For cisplatin pretreatment, AB12 cells were plated 48 hours prior to the experiment and 24 hours later, the medium was changed to fresh medium either supplemented or not with 5µg/mL cisplatin. On the experiment day, the medium was replaced again by fresh non-cisplatin containing medium and splenocytes were added in 1:20 ratio. In both experiments, 24 hours following the co-culturing of tumor cell and splenocytes, the medium was collected for ELISA assay. IFN-gamma (IFNg) levels in culture medium were quantified using ELISA (DuoSet Mouse IFN-gamma immunoassay, R&D Systems) according to the manufacturer's instructions.

RNA sequencing

RNA-Seq was performed on AB12 tumors from at least 3 independent mice per group at the indicated time points. Libraries were prepared using the KAPA RNA HyperPrep kit (Roche), according to the manufacturer instructions. Paired-end 75 or 100 base massively parallel sequencing was then carried out on an Illumina NextSeq500 or NovaSeq6000, respectively. FASTQ files were aligned to the mouse reference genome GRCm38/mm10 using TopHat2 (v2.0.14). Uniquely mapped reads were kept and BAM files were indexed and sorted using Sambamba (v0.6.5). We used HTSeq to obtain the number of reads associated with each gene in the Gencode vM21 transcriptome indexes. The Bioconductor DESeq2 package was used to import raw HTSeq counts for each sample into R statistical software and to apply variance stabilizing transformation to the raw count matrix to obtain an expression matrix without variance-mean dependence (DESeq2-normalized counts). FPKM scores (number of fragments per kilobase of exon per millions of mapped reads) were calculated by normalizing the count matrix for the library size and the coding length of each gene. We removed 21,883 unexpressed genes (i.e., detected in less than 5% of samples) and an additional 4,102 genes with a significant batch effect (area under the ROC curve > 0.95 between one sequencing project and others).

Human-mouse transcriptomic integrative analysis

A total of 306 samples from 3 different RNA-sequencing datasets were used for the comparative transcriptomic analysis, including 295 hMPM (from 2 different datasets: 209 and 86 hMPM from the Bueno and TCGA series, respectively) (26, 27) and 11 mouse AB12 samples. First, common genes that are 1:1 orthologs in human and mouse were selected using the list of mouse-human 1:1 orthologous genes from MGI (http://www.informatics.jax.org). Then, we filtered out most of the genes by keeping only the 2000 mouse-human 1:1 orthologous genes with the highest variance in human datasets. Finally, we standardized gene expression in each dataset to have mean 0 and standard deviation 1 per gene just before the three datasets were integrated. Unsupervised hierarchical clustering of the integrated data was performed using cosine distance and Ward's linkage method on the 2000 most variant orthologous genes with ComplexHeatmap package in R statistical software. Histologic and molecular subtypes of hMPM were retrieved from Bueno et al. and Hjmeljak et al. (26, 27) and the histo-molecular scores were retrieved from Blum et al. (17).

Pathway enrichment analysis

Differentially expressed protein coding genes between groups were determined using the DESeq2 package in R. Only genes with an adjusted *p*-value below 0.05 and a fold-change higher than 2 were considered. The hypergeometric test was used on overexpressed and underexpressed genes separately to identify enriched mouse Molecular Signatures Database gene sets (MSigDB v7.2.1 obtained using msigdb in R) in the list of differentially expressed genes. Over-representation analyses were performed using the Hallmark, KEGG, Reactome and

GeneOntology databases. The over-represented signal pathways over-represented in several of the databases were grouped into families and sub-families, which are highlighted in Supplementary Table 3.

Molecular classification and histo-molecular score predictions

Expression data from RNA sequencing (FPKM scores) were used to predict Thorsson subgroups (28). In particular, an ensemble classifier based on XGBoost was implemented to classify tumor samples into one of six immune subtypes using the "ImmuneSubtypeClassifier" package in R. Histo-molecular scores in human tumor samples were previously predicted (17). Only samples with a cumulated E.score and S.score higher than 50% were taken into account to ensure sufficient tumor content for correct estimation.

Tumor microenvironment cell content

The human microenvironment cell population counter (MCP-counter) or mouse dedicated (mMCP-counter) methods were used to compute scores of infiltration for different immune and stromal cell populations from DESeq2-normalized RNA-seq data. MCP-counter scores were calculated using the MCP-counter method (29) previously validated in hMPM tumor samples (17) and adapted to RNAseq data using genes filtered on hMPM cell lines (30) whereas mMCP-counter scores were obtained using the mMCPcounter package in R (31). The list of specific genes used for each population is available in Supplementary Table 4. Infiltrations were determined using the scores of MCP-counter for hMPM and mMCP-counter for AB12 tumors and matching of the cell populations between the two predictive tools. A total of 295 human tumor samples from two different series of RNAseq were combined in the integrated analysis with public datasets, including the 209 samples from Bueno et al. (26) and 86 samples from TCGA (27). Then, we standardized gene expression separately to have a mean of 0 and a standard deviation of 1 per gene in each dataset. Statistical analysis and data visualization were performed using R software. Unsupervised hierarchical clustering was performed using cosine distance and Ward's linkage method.

Statistics

Statistical analysis was done using the GraphPad Prism software or R statistical software. Statistical significance was calculated using unpaired Student's t-test for pairwise comparisons. For multiple comparisons, a one-way ANOVA test was performed, and pairwise significance was determined by Tukey's multiple comparisons test. Statistical differences between survival curves were calculated by log-rank test. Values of $p < 0.05$ were considered statistically significant.

Study approval

The Animal Care and Use Committee of the Hebrew University approved all experiments.

Results

PART 1. Determining the AB12 tumor growth phases and comparison to hMPM.

Determining the AB12 tumor growth phases

To define the AB12 tumor growth phases, we measured the survival of tumor bearing mice and we longitudinally sampled the tumor appearance across time (days 3, 6, 10 and 14). As shown in Figure 1A, mice survived between 20 to 30 days following tumor implantation. We found that day 6 (d6) was the earliest time point at which peritoneal tumor nodules were visible to the naked eye and collectable. As shown in Figures 1B, C, the histological appearance of the tumors was notable for small nodular implants on d6, for large and viable tumors on day 10 (d10), and for even larger tumors with multiple necrotic foci on day 14 (d14) (tumor diameter range: 2 to 4, 5 to 10, and > 12 mm, respectively). Based on these observations and given that the architectural patterns of the tumor developed in a gradual fashion, we defined the tumor growth phases as follows: days 0 to 3 (when no tumor implants are visible): "implantation phase"; days 4 to 7: "early-phase"; days 8 to 12: "intermediate-phase"; and days 13 and on: "advanced phase" (Figure 1D).

Comparison of AB12 tumors to hMPM

To compare the transcriptomic profile of AB12 tumors to that of hMPM, we performed unsupervised clustering of d6 (n=3), d10 (n=5) and d14 (n=3) AB12 tumors together with a cohort of 295 hMPM samples (Supplementary Table 5). As shown in Figure 1E, the series split into three main transcriptomic clusters, termed C1 to C3. Further, AB12 tumors— in all of their growth phases— belonged to cluster C3. Comparison of the distribution of the histologic and molecular subtypes in human tumor samples (26, 27) as well as the E.score and the S.score of the histo-molecular gradients (17) (Figure 1E, Supplementary Figure 1A) showed that tumors in clusters C1, C2 and C3 are sarcomatoid, epithelioid and biphasic, respectively, representing 23%, 24% and 52% of hMPM samples in the cohort.

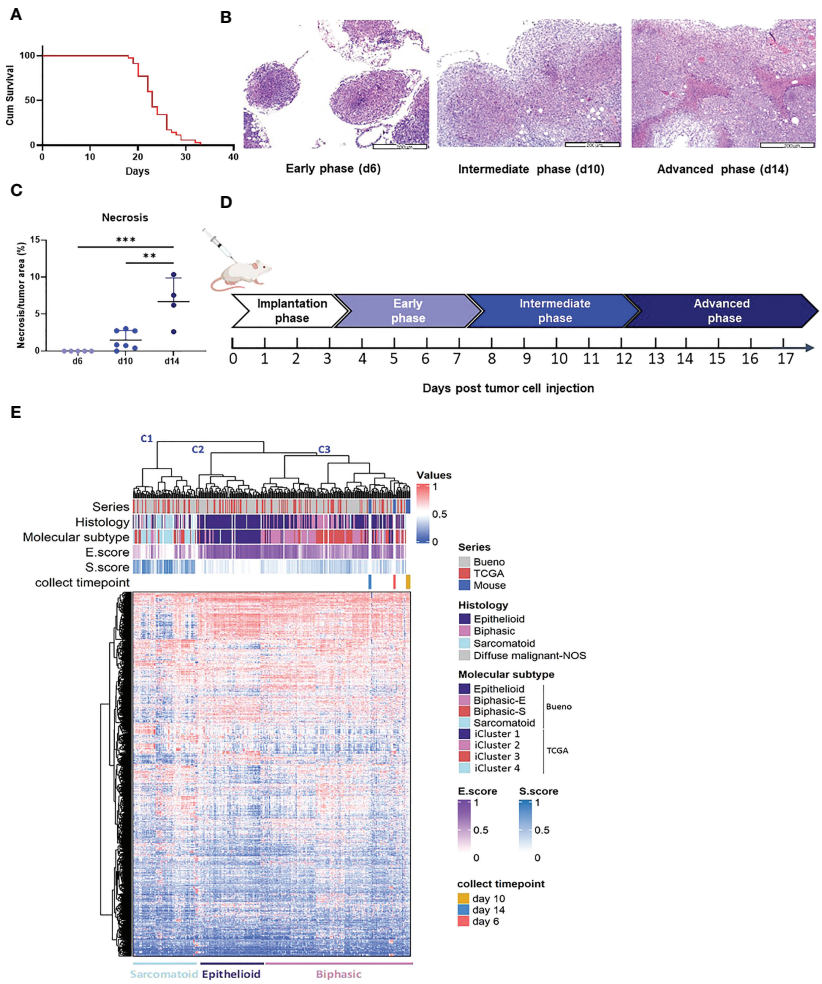

FIGURE 1
AB12 tumors characterization. **(A)** Kaplan-Meier survival curve of mice injected with AB12 cells. n=28. Cum: cumulative. **(B)** Histological features of early, intermediate and advanced phase AB12 tumors. Representative hematoxylin and eosin staining of tumors. Original magnification X10. **(C)** Evaluation of the necrosis area in AB12 tumors. The percentage of necrotic area out of the entire tumor area in d6, d10 and d14 tumors is shown. Values of the *post hoc* Tukey test are indicated at the top of the dot plots. **: $p \leq 0.01$; ***: $p \leq 0.001$. **(D)** Schematic axis of tumor development. **(E)** Integration based on transcriptomic data of AB12 tumors in hMPM tumors. Unsupervised clustering of d6, d10 and d14 AB12 tumors with 295 hMPM tumor samples was performed based on transcriptomic data obtained by RNA-Seq. The series of each tumor sample, the histologic and molecular subtypes, the histo-molecular gradients (E.score and S.score) and the collect timepoint of AB12 tumors are indicated by a color code or a color gradient at the top of the heatmap. Clusters C1 to C3 are indicated at the top as well as the deduced histologic subtypes at the bottom.

PART 2. Characterizing the tumor phase dependent immune response that AB12 cells provoke and alignment with immune states in hMPM

Characterizing the immune response that AB12 cells provoke in the TME

To probe the immune response in the TME of AB12 tumors, we used pathway enrichment analysis and the mMCP-counter immune and stromal cell populations predictive tool (29, 30). We found that dysregulated pathways between the tumor growth phases were mainly related to the immune system (Supplementary Table 3). In particular, early-phase tumors were notable for relative enrichment in pathways associated with type I and type II interferon (IFN) responses whereas intermediate-phase tumors were notable for enrichment in pathways associated with T cell activation and signaling as well as pathways associated with natural killer (NK) immunity and cytotoxicity (Figure 2A, Supplementary Figure 1B). In line with the latter findings, the mMCP-counter tool showed that intermediate-phase tumors, relative to both early- and advanced-phase tumors, were enriched with T cells and CD8 T cells infiltration, with a higher fold-change for CD8 T cells between d6 and d10 (Figure 2B, Supplementary Figure 1C,

10.3389/fimmu.2022.1026185

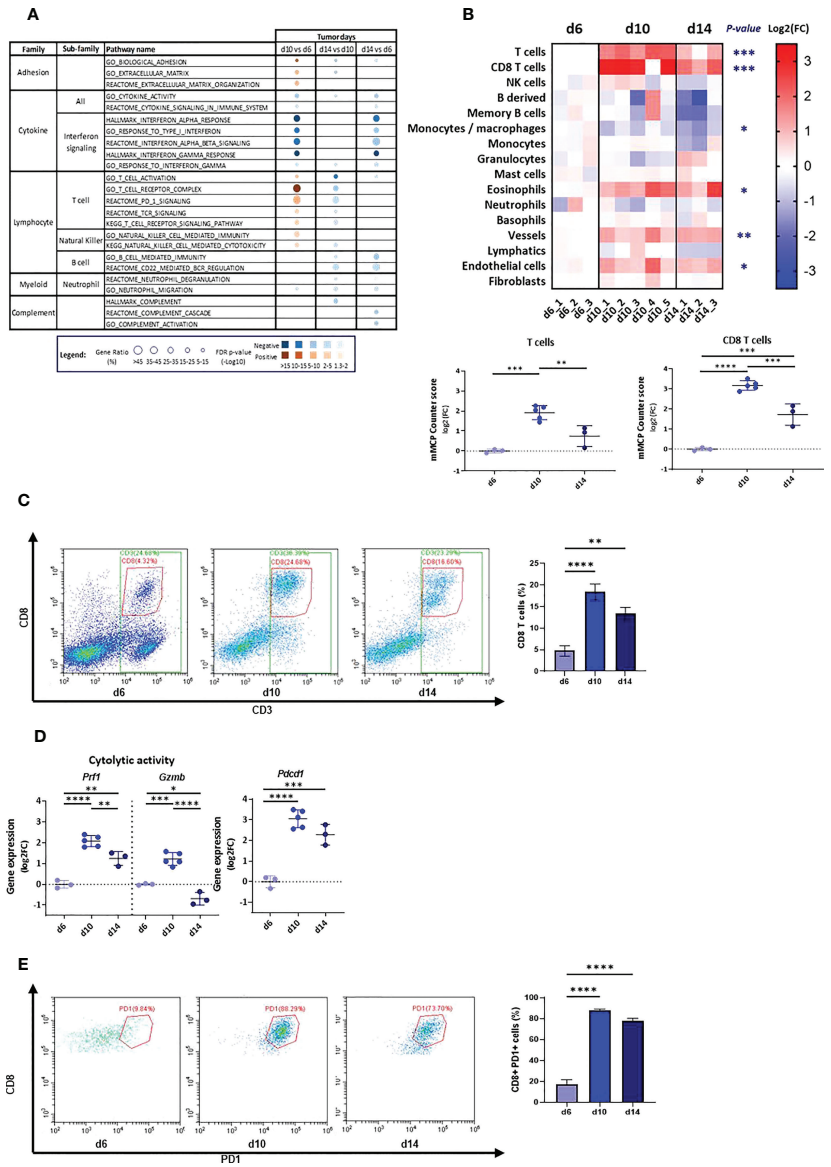

FIGURE 2
Tumor microenvironment in d6, d10 and d14 AB12 tumors. **(A)** Dysregulated signal pathways between tumors identified by over-representation analysis. The families and sub-families of the major over-represented signal pathways are shown in the figure for each comparison indicated at the top of the figure. Over-representation of each pathway, based on underexpressed and overexpressed genes, in blue and brown, respectively, is indicated as a circle, whose size is proportional to the gene ratio and the color gradient represents the FDR *p*-values. **(B)** Differential infiltration of immune and stromal cell populations between tumors. In the upper part, the fold-changes (FC) in mMCP-counter scores of each cell population are represented as a heatmap. The collect timepoints and the names of the AB12 tumor samples are indicated above and below the heatmap, respectively. The significant *p*-values of the ANOVA test are indicated at the left of the heatmap if the FC is higher than 2 in d10 or d14 compared to d6. In the lower part, the dot plots show the FC of T cell and CD8 T cell populations. The FC are relative to the mean scores obtained in d6 tumors. **(C)** T cell infiltration of AB12 tumors identified by flow cytometry. Single cell tumor suspensions, stained with anti CD45, anti CD3 and anti CD8 antibodies, were analyzed using flow cytometry. Representative FACS dot plots show the percentage of CD3+, CD8+ and CD3+ CD8-, corresponding to CD3+ CD4+ cells, out of CD45+ cells in the tumors. On the right, the bars show the average percentage of CD3+ PD8+ cells out of CD45+ cells in the tumors (n=3 per time point). **(D)** Differential expression of T cells cytolytic and activation genes between d6, d10 and d14 AB12 tumors. The dot plots show the FC relative to the mean of the d6 tumor gene expressions of *Prf1* (perforin-1), *Gzmb* (granzyme B) and *Pdcd1* (PD-1) genes, based on RNA-Seq data. **(E)** PD-1 expression on tumor infiltrating CD8 T cells identified by flow cytometry. Single cell tumor suspensions, stained with anti CD45, anti CD3, anti CD8 and anti PD-1 antibodies, were analyzed by flow cytometry. Representative FACS dot plots show the percentage of CD8+ PD-1+ cells out of CD3+ cells in the tumors. On the right, the bars show the average percentage of CD8+ PD-1+ cells out of CD3+ cells in the tumors (n=3 per time point). The *p*-values of the *post hoc* Tukey test are indicated at the top of the dot plots and of the histogram (B, D and E). FC: Fold-Change. *$p \leq 0.05$; **$p \leq 0.01$; ***$p \leq 0.001$; ****$p \leq 0.0001$.

Supplementary Table 4). Further, flow cytometry confirmed these findings and indicated that the increased infiltration of T cells is due to CD8 T cells (Figure 2C, Supplementary Figure 1D). Notably, gene expression analysis and flow cytometry demonstrated that the cytolytic and activation genes of T cells – perforin-1 (*Prf1*), granzyme B (*Gzmb*) and PD-1 (*Pdcd1*) – all peaked in expression in the TME of intermediate-phase tumors (Figures 2D, E).

Characterizing the immune response that AB12 cells provoke at remote immune sites

To characterize the immune response that AB12 tumors provoke at remote immune sites, we first determined the changes in immune content of the spleen, peripheral blood (PB) and bone marrow (BM) between our baseline at d6 and that at d10, d14 and d20. Supplementary Figure 2A shows the gating strategy to evaluate the presence of each immune cell population. We found that in the spleen, the number of CD8 T cells increased between d6 to d14 ($p < 0.05$), whereas that of CD4 T cells was relatively stable. Consequently, the CD8/CD4 ratio in the spleen tended to tilt more towards CD8 on d10, d14 and d20 than on d6 (Figure 3A). We also found that the numbers of F4/80 positive monocytes and of neutrophils in the spleen sharply rose from d6 to d20 ($p < 0.001$ and $p < 0.01$, respectively) and that in contrast, the number of B cells significantly declined ($p < 0.01$). The number of NK cells in the spleen rose on d14 ($p < 0.0001$) and returned to baseline on d20 (Figure 3A). Notably, the changes in immune content of the spleen were overall mirrored in the PB. To illustrate, the number of CD8 T cells in the PB peaked on d10 ($p < 0.001$) and d14 ($p < 0.01$) while the number of CD4 T cells was relatively stable and consequently, the CD8/CD4 ratio in the PB tilted towards CD8 at these time points ($p < 0.01$ for both time points) before decreasing at d20 ($p < 0.01$, Figure 3B). Further, as illustrated in Figure 3B, the number of neutrophils ($p < 0.05$) in the PB rose from d6 to d14 whereas the number of B cells constantly decreased ($p < 0.01$). Evaluation of the immune content of the BM showed that this organ was also influenced by the tumor. In particular, like the spleen, the BM showed a rise in content of neutrophils and F4/80 positive monocytes, as well as a sharp decrease in content of B cells (Supplementary Figure 2B).

Comparison of the type and kinetics of the immune response that AB12 cells provoke in the spleen relative to that in TME

To compare the immune response in the spleen relative to that in the TME, we measured in the spleen the expression levels of key genes that we found characterized the immune response

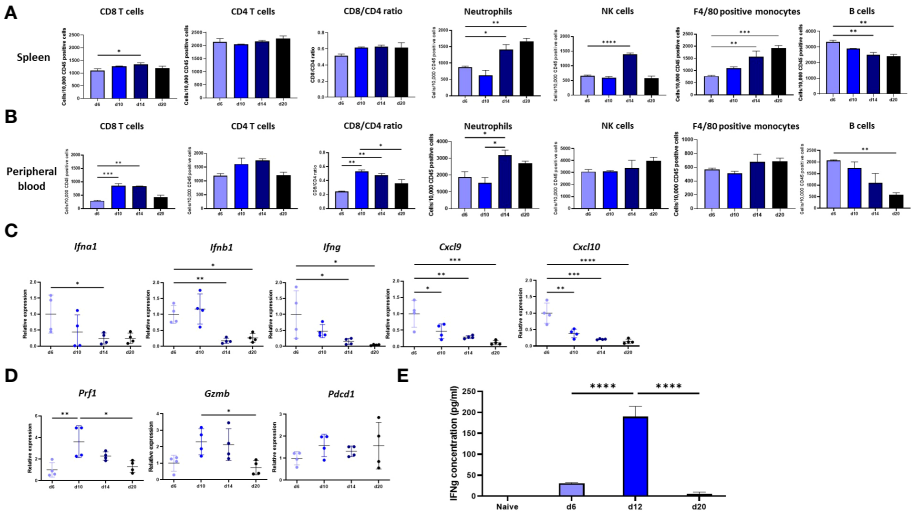

FIGURE 3
Immune response at remote immune sites. **(A, B)**. Changes in the immune content of the spleen and peripheral blood (PB) of tumor bearing mice between d6, d10, d14 and d20. The numbers, determined by flow cytometry, of CD8 and CD4 T cells, NK cells, neutrophils, F4/80 positive monocytes and B cells out of 10,000 CD45+ cells in the spleen **(A)** or peripheral blood **(B)** of tumor bearing mice are shown (n≥6). The CD8/CD4 ratio at both sites is shown as well **(C)** Tumor phase dependent expression in the spleen of genes that mark the anti-tumor response in the TME. The changes relative to d6 tumor mean expression of the *IFNa*, *IFNb1*, *IFNg*, *Cxcl9* and *Cxcl10* genes in the spleen of tumor bearing mice between d6, d10, d14 and d20 are shown (n=4). **(D)** Tumor phase dependent expression of cytolytic and activation genes in the spleen. The changes relative to d6 tumor mean expression of the *Prf1*, *Gzmb* and *Pdcd1* genes in the spleen of tumor bearing mice between d6, d10, d14 and d20 are shown (n=4). **(E)** Responsiveness of splenocytes derived from tumor bearing mice to AB12 cells *in vitro*. AB12 cells were co-cultured with splenocytes derived either from d6, d12 and d20 tumor bearing mice or from naïve mice and 24 hours later, the levels of IFNg protein in the medium were measured by ELISA (n=3). The *p*-values of the *post hoc* Tukey test are indicated at the top of the dot plots and the histogram (A to E). *$p \leq 0.05$; **$p \leq 0.01$; ***$p \leq 0.001$; ****$p \leq 0.0001$.

changes in the TME across time. As shown in Figure 3C, the expression of type I and type II IFNs (and the chemokines CXCL9 and CXCL10 that type II IFN regulates) were at their peak at d6, a finding that echoes well with the enhanced representation of interferon-related pathways in the TME of early-phase tumors. Furthermore, as shown in Figure 3D, the expression of perforin-1, granzyme B and to a lesser extent of PD-1 were at their peak on d10, findings that dovetail with the expression patterns found in the TME.

Next, to evaluate the kinetics of the immune response in spleen, we tested *in vitro* whether splenocytes derived from tumor bearing mice respond against AB12 cells in a tumor phase dependent manner. Specifically, we measured the production of IFNg in a co-culture of splenocytes and AB12 cells. As shown in Figure 3E, we found that splenocytes of mice with intermediate-phase tumors produced the maximal amounts of IFNg whereas splenocytes of mice with either early- or advanced-phase tumors produced minimal amounts of IFNg (both $p < 0.0001$). Notably, splenocytes of naïve mice did not produce IFNg.

Testing the kinetics of the immune response that AB12 cells provoke in the TME and spleen *via* the prism of the response to immune checkpoint inhibitors

Given that anti CTLA-4 has previously been shown to be highly effective against AB12 tumors we selected using this agent to test whether AB12 tumor respond to immunotherapy in a tumor growth phase dependent manner (8, 20).

First, we evaluated how early treatment with anti CTLA-4 (injection on d6 and d10) affected the anti-tumor response by comparing d14 tumors, spleen, and PB from treated mice to d10 and d14 tumors, spleen, and PB from untreated mice. We found that pathways associated with T cells, B cells, neutrophils and NK cells activation, which are all negatively regulated between d10 to d14 in untreated tumors (Figure 2A), were all positively regulated in treated d14 tumors relative to untreated d14 tumors (Figure 4A, Supplementary Figure 3A, Supplementary Table 3). Moreover, pathways that are associated with immune mediators and complement were also positively regulated in treated tumors (Figure 4A). Notably, treated d14 tumors did not differ from untreated d10 tumors in their pathway activation pattern (Supplementary Figure 3A, Supplementary Table 3). In line with these findings, we found that the infiltration of T cells and CD8 T cells, determined by mMCP Counter, in treated d14 tumors was similar to their content in untreated d10 tumors but higher than their content in untreated d14 tumors (Figure 4B, Supplementary Figure 3B, Supplementary Table 4). In addition, we found that the expression levels of perforin-1, granzyme B and PD-1 in treated d14 tumors were similar to those observed in untreated d10 tumors, but higher than those observed in untreated d14 tumors (Figure 4C).

Concerning the spleen and PB, we found that relative to untreated d14 samples, early treatment with anti CTLA-4 induced an elevation in d14 of the number of CD8 T cells with a shift in CD8/CD4 ratio as well as a reduction in the number of neutrophils and a trend for reduction in numbers of F4/80 positive monocytes (Figure 4D). The effect of anti CTLA-4 on the number of NK cells and B cells were less consistent as were its effects on the BM (Supplementary Figure 3C). The expression levels of perforin-1, granzyme B and to a lesser extent of PD-1 were elevated in d14 in the spleens of treated vs. untreated mice (Figure 4E).

Second, we compared how early treatment and late treatment (injection on d14 and d18) with anti CTLA-4 affected the production of IFNg in the *in vitro* AB12 cells and splenocyte co-culture system described above. We found that early treatment with anti CTLA-4 increased the potential of splenocytes to produce IFNg ($p < 0.0001$) while late treatment with anti CTLA-4 failed to do so (Figure 4F).

Comparison of the immune response that AB12 cells provoke in the TME to immune states in hMPM

To compare the TME of AB12 tumors in each of the tumor growth phases with immune activation states in hMPM, we first used immune content-based unsupervised clustering of human tumors, which allow to separate immune active ("hot") and immune inactive ("cold") hMPM as previously described (30) together with murine tumors (Supplementary Table 4). As shown in Figure 5A, we found that early- and advanced-phase tumors clustered with "cold" hMPM whereas intermediate-phase tumors as well as advanced-phase tumors that were collected from mice that received early treatment with anti CTLA-4 clustered with "hot" hMPM. Next, to determine which hMPM immune subtype the TME of AB12 tumors mimics, we used the Thorsson immune classification of human tumors, which represents the complete immune landscape of human cancer, as a comparative platform (28). Specifically, we determined the tumor immune subtypes (TIS) of all hMPM and all AB12 tumors in our cohort based on the six TIS defined by Thorsson et al. (Supplementary Table 5) (28) As shown in Figure 5B, TIS.2 (IFNg predominant) was the most common (32%) TIS among hMPM. Furthermore, all AB12 tumors were TIS.2.

PART 3. Determining the efficacy of standard-of-care anti-hMPM immunotherapy in the model and testing new therapeutic combinations against this benchmark

Determining the therapeutic efficacy of standard-of-care anti-MPM immunotherapy in the model

To determine the efficacy of anti CTLA-4 and anti PD-1 in the model either as single or combination therapy, we used survival assay. As shown in Figures 6A, B, we found that the

10.3389/fimmu.2022.1026185

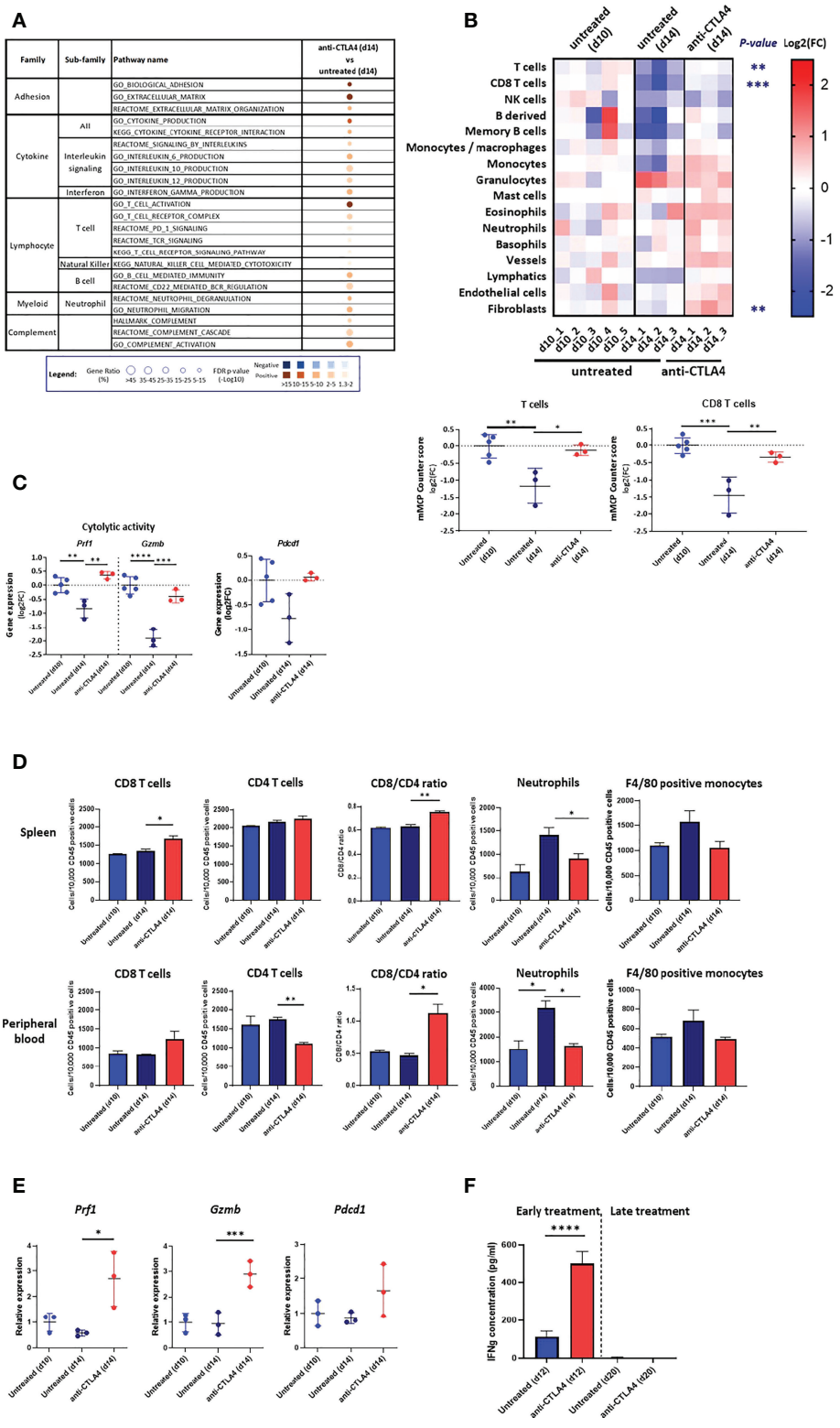

FIGURE 4 (Continued)

FIGURE 4 (Continued)
Response to anti CTLA-4 immune checkpoint inhibitor. **(A)** Dysregulated signal pathways in anti CTLA-4 treated AB12 tumors identified by over-representation analysis. Signal pathways representation in AB12 tumors either treated on d6/d10 with anti-CTLA4 (early treatment) or untreated and collected on d14 has been compared. The families and sub-families of the major over-represented signal pathways are shown in the figure. Over-representation of each pathway, based on underexpressed and overexpressed genes, in blue and brown, respectively, is indicated as a circle, whose size is proportional to the gene ratio and the color gradient represents the FDR p-values. **(B)** Differential infiltration of immune and stromal cell populations. In the upper part, the fold-changes (FC) in mMCP-counter scores of each cell population are represented as a heatmap. The collect timepoints and the treatment, and the names of the tumor samples are indicated above and below the heatmap, respectively. The significant *p*-values of the ANOVA test, comparing untreated and anti CTLA-4 treated tumors, are indicated at the left of the heatmap if the FC is higher than 2. In the lower part, the dot plots show the FC for T cell and CD8 T cell populations. The FC are relative to the mean scores obtained in untreated AB12 tumors and collected on d=10. **(C)** Gene expression of cytolytic and activation genes. The dot plots show the FC relative to the mean of d10 tumors of *Prf1* (perforin-1), *Gzmb* (granzyme B) and *Pdcd1* (PD-1) gene expression, based on RNA-Seq data, between anti CTLA-4 treated and untreated tumors. **(D)** Immune content of the spleen and peripheral blood (PB). The numbers, determined by flow cytometry, of CD8 and CD4 T cells, neutrophils and F4/80 positive monocytes out of 10,000 CD45+ cells in the spleen and PB of either untreated d10 and d14 tumor-bearing mice or anti CTLA-4 treated d14 tumor-bearing mice are shown (n>6). The CD8/CD4 ratio at both sites is shown as well. **(E)** Expression of T cells cytolytic and activation genes in the spleen. The relative change in mean expression of the *Prf1*, *Gzmb* and *Pdcd1* genes in the spleens either untreated d10 and d14 tumor-bearing mice or anti CTLA-4 treated d14 tumor-bearing mice are shown (n=3). **(F)** Responsiveness of splenocytes derived from anti CTLA-4 treated mice to AB12 cells *in vitro*. Tumor-bearing mice were either treated early (on d6/d10) or late (on d14/d18) with two injections of anti CTLA-4 and splenocytes were derived from these mice on d12 and d20, respectively, as well as splenocytes from untreated mice. The levels of IFNg protein secreted in the medium were measured by ELISA in splenocytes co-cultured with AB12 cells (n≥4). The *p*-values of the *post hoc* Tukey test and of the unpaired T test are indicated at the top of the dot plots (B to E) and at the top of the histogram **(F)**, respectively. FC: Fold-Change. *$p \leq 0.05$; **$p \leq 0.01$; ***$p \leq 0.001$; ****$p \leq 0.0001$.

efficacy of anti CTLA-4 linearly decreased as the tumor progressed whereas the efficacy of anti PD-1 peaked in d9. Furthermore, we found that anti CTLA-4 showed high cure rates but only in d3 and d6 tumors. In contrast, anti PD-1 showed only moderate cure rates but its maximal potency was in d9 tumors. Based on these observations, we next tested the combination of anti CTLA-4 + anti PD-1 in intermediate phase tumors (d9). We found that the combination was highly effective relative to single agent therapy, raising the cure rates of anti CTLA-4 or anti PD-1 from 28.6%, 35.7% respectively to 78.6% for the combination, and extending the median survival period from 17 and 29 days, respectively, to higher than 57 days for the combination (Figure 6C upper left panel, Supplementary Figure 4A). Furthermore, we highlighted that anti CTLA-4 + anti PD-1 maintained its efficacy in late-intermediate tumor (d12) but not in advanced tumors (d14).

Testing new therapeutic combinations against the standard-of-care efficacy bar

Having determined the efficacy of anti CTLA-4 + anti PD-1 as a preclinical benchmark in the model, we turned to evaluate the relative performance of other combination therapies. First,

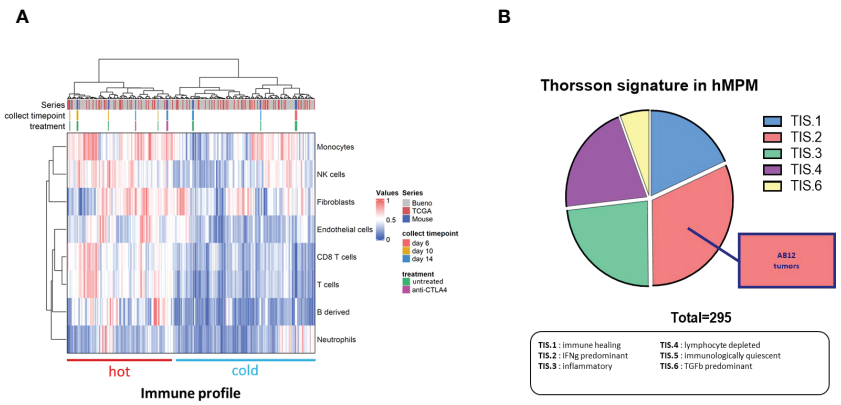

FIGURE 5
Immune features of AB12 tumors in comparison to hMPM. **(A)** Integration based on immune and stromal cells infiltrations of AB12 tumors in hMPM tumors. Unsupervised clustering of untreated and anti CTLA-4 treated AB12 tumors with 295 hMPM tumor samples was performed based on the infiltrations of immune and stromal cell populations. The series of each tumor sample, the collect timepoint and the treatment of AB12 tumors are indicated by a color code at the top of the heatmap. At the bottom of the heatmap, clusters were divided into tumors with a "hot" and "cold" immune profiles based on immune cells infiltration. **(B)** Thorsson immune classification. Thorsson immune subtypes (TIS) were determined in the 295 hMPM and in AB12 tumor samples using TIS transcriptomic signatures. Tumor samples were classified in one of the TIS based on the highest signature score. The pie chart shows the distribution of the 6 TIS in hMPM tumor samples. AB12 tumors were all classified as TIS2.

10.3389/fimmu.2022.1026185

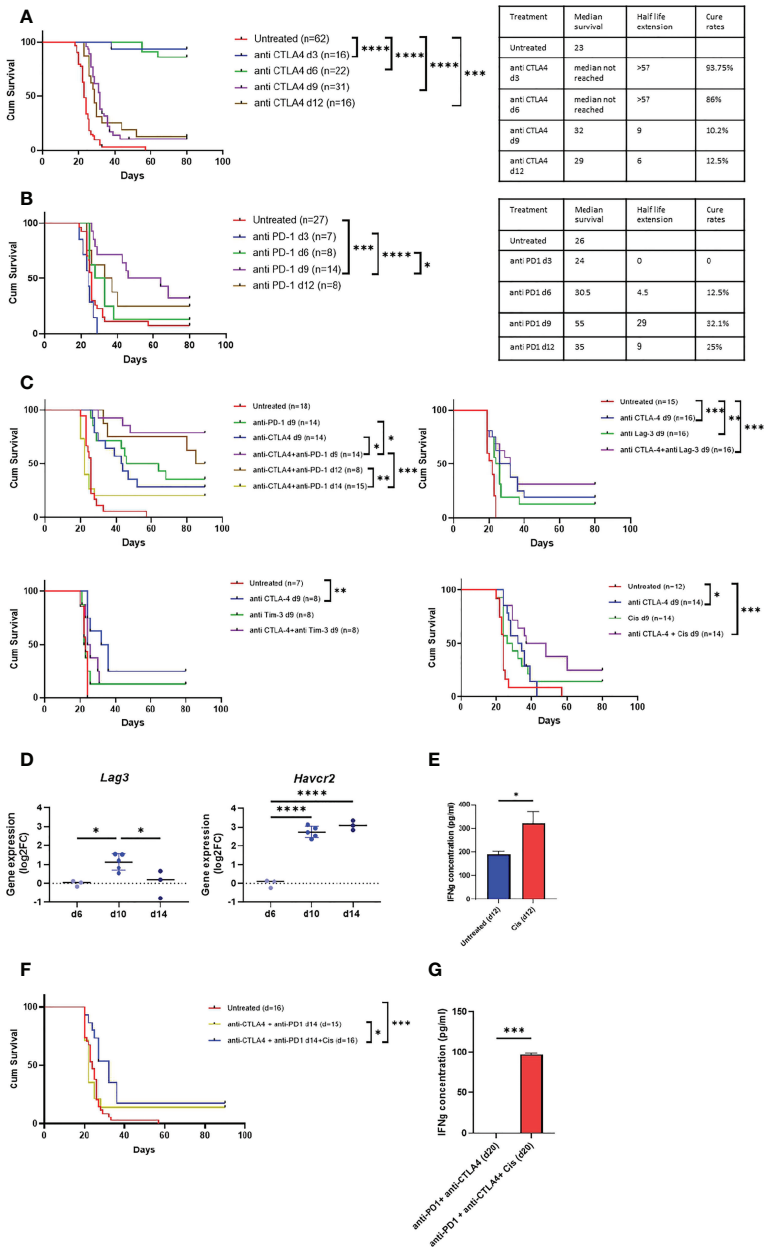

Treatment	Median survival	Half life extension	Cure rates
Untreated	23		
anti CTLA4 d3	median not reached	>57	93.75%
anti CTLA4 d6	median not reached	>57	86%
anti CTLA4 d9	32	9	10.2%
anti CTLA4 d12	29	6	12.5%

Treatment	Median survival	Half life extension	Cure rates
Untreated	26		
anti PD1 d3	24	0	0
anti PD1 d6	30.5	4.5	12.5%
anti PD1 d9	55	29	32.1%
anti PD1 d12	35	9	25%

FIGURE 6
Anti MPM immunotherapy in AB12 tumor model. A-B. Tumor phase dependent efficacy of single agent immunotherapy. The Kaplan-Meier survival curves show the response of AB12 tumors to treatment with either anti CTLA-4 **(A)** or anti PD-1 **(B)** when initiated on d3, d6, d9 or d12. The tables show the median survival, the half-life extension period and the cure rates for each treatment and time point. **(C)** Differential expression *Havcr2* and *Lag3* genes between d6, d10 and d14 AB12 tumors. The dot plots show the fold-changes (FC) of gene expression relative to the mean of d6 tumors of *Havcr2* (TIM-3) and *Lag3* (LAG-3) genes, based on RNA-Seq data. The *p*-values of the *post hoc* Tukey test are indicated at the top of the dot plots. **(D)** Responsiveness of splenocytes to cisplatin treated AB12 cells *in vitro*. AB12 cells were either treated or not with cisplatin. The levels of IFNg protein in the medium were measured by ELISA in tumor cells co-cultured with splenocytes. (n=3). **(E)** Efficacy of combination immunotherapy against AB12 tumors. The Kaplan-Meier survival curves show the response of AB12 tumors to treatment with several combinations of immunotherapy. The responses to anti CTLA-4 + anti PD-1 initiated on d9, or d12 or d14 (upper left), anti CTLA-4 + anti LAG-3 initiated on d9 (upper right), anti CTLA-4 + anti TIM-3 initiated on d9 (lower left), anti CTLA-4 + cisplatin initiated on d9 (lower right) are shown. **(F)** Efficacy of anti CTLA-4 + anti PD-1 + cisplatin against advanced AB12 tumors. The Kaplan-Meier survival curves show the response of AB12 tumors to treatment with either anti CTLA-4 + anti PD-1 or anti CTLA-4 + anti PD-1 + cisplatin initiated on d14. **(G)** Responsiveness of splenocytes derived from anti CTLA-4 + anti PD-1 + cisplatin treated mice to AB12 cells *in vitro*. Splenocytes were derived on d20 from tumor-bearing mice that were treated on d14 with either anti CTLA-4 + PD-1 or anti CTLA-4 + PD-1 + cisplatin. The levels of IFNg protein were measured by ELISA in the medium of tumor cells co-cultured with splenocytes. (n=3). The *p*-values of the unpaired T test are indicated at the top of the histogram (**D, G**). The differences between survival curves were calculated by the log-rank test (**A, B, E**, **F**). FC: Fold-Change; cis: cisplatin. *$p \leq 0.05$; **$p \leq 0.01$; ***$p \leq 0.001$; ****$p \leq 0.0001$.

given that anti CTLA-4 showed very high cure rates in early-phase tumors, we sought to explore whether certain combinations could jumpstart its positive effect also at later time points. Specifically, we tested anti CTLA-4 in combination with either anti LAG-3 or anti TIM-3 or cisplatin. We selected anti LAG-3 and anti TIM-3 because drugs that target them are in advanced clinical development (25) and as shown in Figure 6D, their expression levels sharply rise in intermediate-phase tumors in comparison to early-phase tumors. In addition, we selected cisplatin because it is widely used to treat MPM patients (32) and because in our *in vitro* co-culture system, we found that pretreatment of AB12 cells with cisplatin stimulated the production of IFNg by anti-tumor splenocytes (Figure 6E).

As shown in Figure 6C, in intermediate-phase tumors, combination of anti CTLA-4 with anti LAG-3 or with anti TIM-3 or with cisplatin was ineffective relative to the efficacy of anti CTLA-4 + anti PD-1. However, comparing the efficacy of the combination relative to the efficacy of its separate components, we found that anti CTLA-4 + cisplatin had a marginally significant (p = 0.057) synergistic effect relative to either anti CTLA-4 or cisplatin alone. In contrast, anti CTLA-4 + anti LAG-3 showed a minor though insignificant synergism while anti CTLA-4 + anti TIM-3 had no synergism at all (Figure 6C).

Based on these observations and on publications showing that in humans anti LAG-3 and cisplatin synergize with anti PD-1 (33, 34), we next tested whether the addition of either of these drugs to the anti CTLA-4 + anti PD-1 combination could improve outcomes in advanced-phase tumors. We found that cisplatin improved the efficacy of standard-of-care in advanced-phase tumors (Figure 6F). Moreover, this triple therapy also restored the potential of splenocytes from mice with advanced-phase tumors to produce IFNg *in vitro* upon co-culture with AB12 cells (Figure 6G). In contrast, improved efficacy relative to benchmark was not found in the CTLA-4 + anti PD-1 + anti LAG-3 combination (Supplementary Figure 5A).

Discussion

Preclinical models of MM using syngeneic cell lines are used to test and design new anti-hMPM therapeutics (21). However, disparities that exist between MMs and hMPM as well as insufficient characterization of the immunology of MM may result in inaccurate design of preclinical investigations and in premature translation of preclinical findings to the clinics (35). In the current work, comprehensive characterization of the immunobiology of AB12 tumors relative to hMPM as well as calibration of its responsiveness to standard-of-care anti-hMPM immunotherapy generated a systematic three-step approach to improve the utility of the AB12 model as an indicative preclinical tool.

In the first step, we determine the AB12 tumor growth phases showing that based on size and appearance, intermediate- and advanced-phase tumors may be considered as well-established tumors which we suggest are more likely to represent hMPM. Next, based on transcriptomic analysis, we show that in line with their histologic classification (4), AB12 tumors mimic the most common histo-molecular subtype of hMPM: Biphasic (17). In addition, we show that AB12 tumors also represent the most common hMPM immunological subtype: TIS.2 (28). Thus, given that AB12 tumors represents the most prevalent type of hMPM, supports focusing empirical interest on this MM model.

In the second step, we characterize the growth phase-dependent immunobiology of AB12 tumors in the TME and at remote immune sites. With respect to the TME, we show that type I and type II IFN pathways dominate the early-phase of tumor growth. Furthermore, we show that CD8 T cell activation pathways, cytotoxicity genes and immune cell infiltration indices dominate the intermediate-phase of tumor growth while they all decay in advanced tumors. Accordingly, we find that intermediate-phase tumors match "hot" hMPM and that advanced-phase tumors match "cold" hMPM. Based on these findings, and as anticipated by previous works on the role of CD8 T cells in anti-MM responses (8), we can conclude that AB12 cells induce in the TME a bell-shaped, CD8 T cell predominant anti-tumor response that peaks in intermediate-phase tumors. With respect to remote immune organs, we show that AB12 tumors gradually remodel the cellular composition of the spleen, PB and BM, thus indicating that tumor growth has systemic immune effects. In particular, when focusing on the expression of IFNs and cytotoxic genes in the spleen, we demonstrate that the evolution of the anti-tumor response in the spleen and TME has concordant kinetics. This, together with results showing peak production of IFNg by intermediate-phase splenocytes and the potential to enhance IFNg production only by early treatment with anti CTLA-4, substantiates the recognition that immune activation prevails during the early-phase of tumor growth and that profound immune suppression prevails during the advanced-phase of tumor growth.

Together, steps one and two of our approach lay the foundation to evaluate the tumor phase-dependent response to immunotherapy and its efficacy compared to outcomes described in hMPM immunotherapy clinical trials. We approach this in step three, where we show that anti CTLA-4 is highly effective but only in early-phase tumors and that in contrast anti PD-1 is only moderately effective but that it is most potent in intermediate-phase tumors. In addition, we show that standard-of-care combination immunotherapy is superior to single agent therapy in intermediate-phase tumors, and yet, its efficacy declines in advanced-phase tumors. Together, these findings dovetail with clinical trials in hMPM showing that anti CTLA-4 failed to achieve clinical benefit, that anti PD-1 provided marginal clinical benefit with short durations of responses (34), and that CTLA-4 + anti PD-1 provided better results than single agent therapy (1). The overall correspondence

between the performance of immunotherapy in the model and in hMPM suggests that the efficacy of standard-of-care in the model can serve as preclinical benchmark that future therapeutics should meet to be considered good candidates for translation to the clinics. Illustrating this principle are our findings on the efficacy of CTLA-4 + anti PD-1 + cisplatin triple therapy relative to benchmark, thereby advocating for its testing in biphasic MPM patients.

From a broader practical perspective, our findings suggest that when testing immunotherapy in the AB12 model, three types of immune effects can be detected depending on time of drug administration. The first immune effect relates to interventions that show efficacy mainly during the *early tumor growth phase*. These interventions should be regarded as ones that are capable of boosting the generation of the anti-tumor response but not necessarily as interventions that can delay the onset of immune suppression or invigorate the anti-tumor response once it has decayed. We predict that such interventions are unlikely to achieve clinical benefit in real-life settings, given that hMPM slowly develop under a strong immunological pressure and because hMPM is often diagnosed in advanced disease stages (13, 14). The second immune effect relates to interventions that show efficacy mainly during the *intermediate phase of tumor growth*, when the anti-tumor response is in its peak. These should be considered as interventions that have the potential to prolong or maintain an existing anti-tumor response. We contemplate that such interventions are most likely to achieve clinical benefit in real-life settings in immune active ("hot") tumors. The third immune effect relates to interventions that show efficacy also during the *advanced phase of tumor growth*, when the anti-tumor response decays. These should be considered as interventions that have the potential to invigorate an anti-tumor response that has already at least partially been shut down. We propose that such therapies are the most promising with respect to their potential to show clinical benefit in patients with advanced hMPM.

Looking forward from a clinical perspective, our findings that show successful boost in efficacy resulting from the addition of cisplatin to the standard-of care suggests that a promising direction for future research is to explore other potential chemotherapies or targeted therapies to yield even more optimal efficacy. For example, carboplatin offers one potential target given that in the recent checkmate 816 study, it showed greater synergism with anti PD-1 than did cisplatin, in inducing complete response in non-small cell lung cancer patients (33). As another potential target, researchers might explore epigenetic modulators given the synergism that histone deacetylase inhibitors achieved in combination with immunotherapy in non-small cell lung cancer as reported in clinical trials (36). From a preclinical perspective the link between the capacity of AB12 stimulated splenocytes to produce IFNg *in vitro* and the outcomes of *in vivo* survival assays, suggests that a promising direction would be to explore using the AB12 and splenocyte co-culture system as an efficient screen to detect survival enhancing therapeutics prior to *in vivo* testing.

Last but not least, our model focused on biphasic hMPM using the AB12 cell line, however, other murine MM cell lines such as the AB1 (7) and AE17 (22) cells that mimic other histological subtypes of hMPM, also exist. Indeed, using AB1 (6, 24, 37, 38) and AE17 (21, 24) cells as well as AB12 cells (6, 8, 21), past research made significant progress in developing new combination treatments to fight the entire histological spectrum of hMPM subtypes. However, we think that if murine tumor models such as AB1 and AE17 would be assessed and characterized using our approach, the likelihood of successfully translating treatments proposed based on these models to the clinic would increase. To elaborate, promising leads to combining specific chemotherapies and repurposed non-chemotherapeutic drugs with immunotherapy have been made (8, 38). For example, with respect to chemotherapy, using the AB1 cell line, Nowak et al. and Lesterhuis et al. have shown that gemcitabine is not detrimental to antitumor immunity and that it may thus be useful in combination with immunotherapy in general and with anti CTLA-4 in particular (23, 39). In addition, more recently, using both the AB1 cell line and the AE17 cell line Principe et al. have shown that 5-fluorouracil and cisplatin have additive effects when combined with anti CTLA-4 and anti PD-1 (24). With respect to identification of drugs that can be repurposed and combined with immunotherapy, Lesterhuis et al. used network analysis of immunotherapy responsive and irresponsive AB1 tumors to show that hub genes and pathways that are associated with response to immunotherapy can be identified and that drugs that augment or inhibit these hub genes can be effective in combination with immunotherapy. Proof of concept was demonstrated using the nitric oxide generator isosorbide dinitrate to enhance Nitric oxide synthase 2 (NOS2) activity and the small-molecule VX680 to inhibit Aurora Kinase B (AURKB) (38). And yet, these studies were all performed using subcutaneously transplanted MM tumors, presumably to ease follow-up on tumor growth and on response to therapy (6, 8, 20, 22, 24, 38). Furthermore, treatment in these studies was initiated no later than day 12 (in most experiments no later than day 10) and its efficacy was not tested in a tumor growth phase dependent manner. As such, these studies might have tested their interventions in an improper microenvironment or prior to induction of systemic immune suppression by the tumor. Given these considerations, we propose that it may be fruitful for future research to retest these promising leads under orthotopic tumor implantation conditions and using the three-step investigational approach that we applied as a benchmark for calibration of the model and for evaluation of treatment efficacy.

Conclusions

Our study delineates a systematic approach that improves the capacity of the AB12 model to serve as a screening tool to test and design novel anti biphasic hMPM therapies. We suggest that the

efficacy of new therapeutics should be compared to the efficacy of standard-of-care in intermediate- and advanced-phase tumors as these phases more accurately represent hMPM. Therapeutics showing efficacy in advanced-phase tumors are the ones that should be translated to the clinics given their potential to invigorate the anti-tumor immune response even once it has decayed. One such promising combination is the anti CTLA-4 + anti PD-1 + cisplatin triple therapy.

Data availability statement

The datasets supporting the conclusions of this article are included within the article and its supplementary materials. Raw RNA-seq data are available in Gene Expression Omnibus (GEO) repository under the GSE197542 series number.

Ethics statement

The animal study was reviewed and approved by Animal Care and Use Committee of the Hebrew University.

Author contributions

OW, ES and DJ are responsible for the study concept and design. ES, IM, HW performed the experiments. TH, QB and SC developed the bioinformatics tools and the pipeline analysis. ES, OW, SC, CM, and DJ performed the analysis and interpretation of data. OW and DJ were major contributors in writing the manuscript. CT assisted in review and editing of manuscript. OW and DJ are responsible for the study supervision. All authors read and approved the final manuscript.

Funding

This research was supported by the Israeli Science Foundation (grant no. 1728/20) and Inserm, and by a generous donation by Hadassah France.

Conflict of interest

The authors declare that the research was conducted in the absence of any commercial or financial relationships that could be construed as a potential conflict of interest.

Publisher's note

Supplementary material

The Supplementary Material for this article can be found online at: https://www.frontiersin.org/articles/10.3389/fimmu.2022.1026185/full#supplementary-material

SUPPLEMENTARY FIGURE 1
Tumor microenvironment in AB12 tumors. Supplementary Figure 1A. Comparison of the histologic and molecular subtypes, and the histo-molecular gradients (E.score and S.score) of hMPM tumor samples between the clusters C1 to C3 of the heatmap of . Histograms at the top show the distribution of histologic subtypes and molecular subtypes of hMPM in the TCGA and Bueno series (26, 27). Enrichment of biphasic-like related subtypes is observed in cluster C3 and Chi-square contingency tests highlight significant differential distribution of subtypes between the three clusters ($p < 0.0001$). Box plots at the bottom show the values of the E.score and S.score retrieved from Blum et al. (17). Intermediate values are observed in cluster C3 compared to the two other clusters. The ANOVA tests highlight significant differences between the 3 cluster ($p < 0.0001$) and the p-values of the *post hoc* Tukey test are indicated at the top of the box plots. Supplementary Figure 1B. Changes in signal pathways related to alpha and gamma interferon responses and, T cell activation and signaling between d6 to d10 and d14 AB12 tumors. The volcanoplots show the differential mRNA expression between AB12 tumors collected at different timepoints of all the genes included in the pathways: Hallmark_interferon_alpha_response, Hallmark_interferon_gamma_response, GO_T_cell_activation and GO_T_cell_receptor_complex. The collect timepoints are indicated at the top left and right of the volcanoplots. The fold-change (FC) and the adjusted p-values for each gene were retrieved from RNA-Seq data analyzed by DESeq2 package. Supplementary Figure 1C. Differential infiltration of immune and stromal cell populations between d6 to d10 and d14 AB12 tumors. The dot plots show the FC relative to the mean of the d6 tumor mMCP counter scores for each of the immune and stromal cell populations between d6, d10 and d14 tumors. Only cell populations showing a significant differential mMCP-Counter scores by ANOVA tests between d6 to d10 or d14 (, left panel) are presented. The p-values of the *post hoc* Tukey test are indicated at the top of the dot plots. Supplementary Figure 1D. Gating strategy for AB12 tumor derived cells. Forward and side scatter detector voltage settings were selected based on the position of CD45 + or +CD3 T cell staining. For the detection of T cells, cells of interest were gated for CD45+ and these were split into CD3+ CD8+ and CD3+ CD8- cells. Subpopulation percentages are calculated out of the total number of CD45+ cells. For the detection of CD8 + PD1+ T cells, cells of interest were gated for CD3+ and then for the PD1 +CD8+ subpopulation. Subpopulation percentages of CD8+ PD1+ cells were calculated out of the total number of CD3+ cells.

SUPPLEMENTARY FIGURE 2
Immune response at remote immune sites. Supplementary Figure 2A. Gating strategy for spleen, PB and BM derived cells. Forward and side scatter detector voltage settings were selected based on the position of CD45+ cell staining. The gating strategy was anchored on FITC-CD45+ and the percentages of all subpopulations were calculated out of the total number of CD45+ cells. For the detection of T cells, cells of interest were gated for CD45+ and these were split into CD3+ CD8+ and CD3+ CD4+ cells. For the detection of neutrophils, cells of interest were gated for CD45+ and next for CD11b+ and these were split into Ly6G+, Ly6C^{high}+ and Ly6C^{low}+ cells. For the detection of F4/80 positive monocytes, cells of interest were gated for CD45+ and then were gated for CD11b+ F4/80 + cells. For the detection of NK cells, cells of interest were gated for CD45 + and then were gated for CD3- CD49B+ cells. For the detection of B cells, cells of interest were gated for CD45+ and then were gated for

CD19+ cells. Supplementary Figure 2B. Changes in the immune content of the bone marrow (BM) of tumor bearing mice between d6, d10, d14 and d20. The numbers, determined by flow cytometry, of CD8 and CD4 T cells, Ly6G+ myeloid cells, NK cells, F4/80 positive monocytes and B cells out of 10,000 CD45+ cells in the BM of tumor bearing mice are shown (n≥6). The CD8/CD4 ratio in the BM is shown as well. Notably in the BM, in contrast to the spleen and PB we determined the numbers of Ly6G+ myeloid cells and not neutrophils since that the used antibody panel permits only making this definition with respect to BM derived cells.

SUPPLEMENTARY FIGURE 3

Response to anti CTLA-4 immune checkpoint inhibitor. Supplementary Figure 3A. Changes in signal pathways related to T cell activation and signaling in anti CTLA-4 treated AB12 tumors. The volcanoplots show the differential mRNA expression between anti-CTLA4 treated and untreated AB12 tumors of all the genes included in the pathways: GO_T_cell_activation and GO_T_cell_receptor_complex. The treatment and the collect timepoints are indicated at the top left and right of the volcanoplots. The fold-change (FC) and the adjusted p-values for each gene were retrieved from RNA-Seq data analysed by DESeq2 package. Supplementary Figure 3B. Differential infiltration of fibroblast cell population in anti CTLA-4 treated AB12 tumors. The dot plots show the fold change (FC) of mMCP-counter scores relative to the mean of the untreated d10 tumors for the population of fibroblasts between untreated d10, untreated d14 and treated d14 tumors. Differences in mean fibroblast mMCP-counter scores between treated and untreated tumors were evaluated by ANOVA test, and the p-values of the *post hoc* Tukey test are indicated at the top of the dot plots. *: $P \leq 0.05$; **: $P \leq 0.01$; ***: $P \leq 0.001$; ****: $P \leq 0.0001$. Supplementary Figure 3C. Immune content of the bone marrow (BM), spleen and peripheral blood (PB) of anti CTLA-4 treated mice. The numbers, determined by flow cytometry, of CD8 and CD4 T cells, Ly6G+ myeloid cells, NK cells and F4/80 positive monocytes out of 10,000 CD45+ cells in the BM of untreated d10 and d14 or anti CTLA-4 treated d14 tumor bearing mice are shown. The CD8/CD4 ratio in the BM is shown as well. The numbers, determined by flow cytometry, NK cells and B cells out of 10,000 CD45+ cells in the spleen and PB of untreated d10 and d14 or anti CTLA-4 treated d14 tumor bearing mice are shown. n>6. Notably in the BM, in contrast to the spleen and PB we determine the numbers of Ly6G+ myeloid cells and not neutrophils since that the antibody panel that we used permits only making this definition with respect to BM derived cells.

SUPPLEMENTARY FIGURE 4

Summary of the response of tumor bearing mice to immunotherapy. The tables show the median survival, the half-life extension period and the cure rates of tumor bearing mice in response to immunotherapy. The half-life extension period is calculated as the difference in days between the median survival period of untreated mice to the median survival period of mice in the treatment group. Cure rates were determined based on the percentage of mice in each treatment group that survived for more than 80 days. The immunotherapy treatment is listed at the top of each table.

SUPPLEMENTARY FIGURE 5

Efficacy of anti CTLA-4 + anti PD-1 + LAG-3 against advanced AB12 tumors. The Kaplan-Meir survival curves show the response of AB12 tumors to treatment (two injections per week for a total of two weeks) with either anti CTLA-4 + anti PD-1 or anti CTLA-4 + anti PD-1 + LAG-3 when initiated on d14 (n = 8).

SUPPLEMENTARY TABLE 1

Flow cytometry data. Table S1.1 List of antibodies for flow cytometry. Table S1.2 Panel of antibodies. Table S1.3 Compensation matrix.

SUPPLEMENTARY TABLE 2

List of primers.

SUPPLEMENTARY TABLE 3

Signal pathways enrichment analysis in AB12 tumors. Table S3.1 Differentially expressed genes between untreated mice. Table S3.2 Pathways dysregulated between untreated mice. Table S3.3 Differentially expressed genes between anti CTLA4 treated mice and untreated mice. Table S3.4 Pathways dysregulated between anti CTLA4 treated mice and untreated mice. Pathways are grouped into families and sub-families and the ones over-represented, based on underexpressed and overexpressed genes, are highlighted in blue and brown, respectively.

SUPPLEMENTARY TABLE 4

Infiltration of immune and stromal cell populations in Tumor microenvironment. Table S4.1 List of biomarkers used in mMCP Counter. Table S4.2 mMCP Counter normalized scores for mouse tumor samples. Table S4.3 List of biomarkers used in MCP Counter. Table S4.4 MCP Counter normalized scores for Human tumor samples.

SUPPLEMENTARY TABLE 5

Annotations of Human tumor samples.

References

1. Baas P, Scherpereel A, Nowak AK, Fujimoto N, Peters S, Tsao AS, et al. First-line nivolumab plus ipilimumab in unresectable malignant pleural mesothelioma (CheckMate 743): a multicentre, randomised, open-label, phase 3 trial. *Lancet* (2021) 397(10272):375–86. doi: 10.1016/S0140-6736(20)32714-8

2. Scherpereel A, Mazieres J, Greillier L, Lantuejoul S, Dô P, Bylicki O, et al. Nivolumab or nivolumab plus ipilimumab in patients with relapsed malignant pleural mesothelioma (IFCT-1501 MAPS2): a multicentre, open-label, randomised, non-comparative, phase 2 trial. *Lancet Oncol* (2019) 20(2):239–53. doi: 10.1016/S1470-2045(18)30765-4

3. Aldea M, Benitez JC, Chaput N, Besse B. New immunotherapy combinations enter the battlefield of malignant mesothelioma. *Cancer Discovery* (2021) 11 (11):2674–6. doi: 10.1158/2159-8290.CD-21-1046

4. Mezzapelle R, Rrapaj E, Gatti E, Ceriotti C, Marchis FD, Preti A, et al. Human malignant mesothelioma is recapitulated in immunocompetent BALB/c mice injected with murine AB cells. *Sci Rep* (2016) 6:22850. doi: 10.1038/srep22850

5. Robinson BW, Redwood AJ, Creaney J. How our continuing studies of the pre-clinical inbred mouse models of mesothelioma have influenced the development of new therapies. *Front Pharmacol* (2022) 13:858557. doi: 10.3389/fphar.2022.858557

6. Fear VS, Tilsed C, Chee J, Forbes CA, Casey T, Solin J, et al. Combination immune checkpoint blockade as an effective therapy for mesothelioma. *Oncoimmunology* (2018) 7(10):e1494111. doi: 10.1080/2162402X.2018.1494111

7. Davis MR, Manning LS, Whitaker D, Garlepp MJ, Robinson BW. Establishment of a murine model of malignant mesothelioma. *Int J Canc* (1992) 52(6):881–6. doi: 10.1002/ijc.2910520609

8. Wu L, Yun Z, Tagawa T, Rey-McIntyre K, de Perrot M. CTLA-4 blockade expands infiltrating T cells and inhibits cancer cell repopulation during the intervals of chemotherapy in murine mesothelioma. *Mol Cancer Ther* (2012) 11 (8):1809–19. doi: 10.1158/1535-7163.MCT-11-1014

9. Wu L, de Perrot M. Radio-immunotherapy and chemo-immunotherapy as a novel treatment paradigm in malignant pleural mesothelioma. *Transl Lung Cancer Res* (2017) 6(3):325–34. doi: 10.21037/tlcr.2017.06.03

10. De La Maza L, Wu M, Wu L, Yun H, Zhao Y, Cattral M, et al. *In situ* vaccination after accelerated hypofractionated radiation and surgery in a mesothelioma mouse model. *Clin Cancer Res* (2017) 23(18):5502–13. doi: 10.1158/1078-0432.CCR-17-0438

11. Leach DR, Krummel MF, Allison JP. Enhancement of antitumor immunity by CTLA-4 blockade. *Science* (1996) 271(5256):1734–6. doi: 10.1126/science.271.5256.1734

12. Ireson CR, Alavijeh MS, Palmer AM, Fowler ER, Jones HJ. The role of mouse tumour models in the discovery and development of anticancer drugs. *Br J Canc* (2019) 121(2):101–8. doi: 10.1038/s41416-019-0495-5

13. Asciak R, George V, Rahman NM. Update on biology and management of mesothelioma. *Eur Respir Rev* (2021) 30(159):1–13. doi: 10.1183/16000617.0226-2020

14. Wald O, Sugarbaker DJ. New concepts in the treatment of malignant pleural mesothelioma. *Annu Rev Med* (2018) 69:365–77. doi: 10.1146/annurev-med-041316-085813

15. Sneddon S, Patch AM, Dick IM, Kazakoff S, Pearson JV, Waddell N, et al. Whole exome sequencing of an asbestos-induced wild-type murine model of malignant mesothelioma. *BMC Canc* (2017) 17(1):396. doi: 10.1186/s12885-017-3382-6

16. Blanquart C, Jaurand MC, Jean D. The biology of malignant mesothelioma and the relevance of preclinical models. *Front Oncol* (2020) 10:388. doi: 10.3389/fonc.2020.00388

17. Blum Y, Meiller C, Quetel L, Elarouci N, Ayadi M, Tashtanbaeva D, et al. Dissecting heterogeneity in malignant pleural mesothelioma through histo-molecular gradients for clinical applications. *Nat Commun* (2019) 10(1):1333. doi: 10.1038/S41467-019-09307-6

18. Rijavec E, Biello F, Barletta G, Dellepiane C, Genova C. Novel approaches for the treatment of unresectable malignant pleural mesothelioma: A focus on immunotherapy and target therapy (Review). *Mol Clin Oncol* (2022) 16(4):89. doi: 10.3892/mco.2022.2522

19. Sceneay J, Goreczny GJ, Wilson K, Morrow S, DeCristo MJ, Ubellacker JM, et al. Interferon signaling is diminished with age and is associated with immune checkpoint blockade efficacy in triple-negative breast cancer. *Cancer Discovery* (2019) 9(9):1208–27. doi: 10.1158/2159-8290.CD-18-1454

20. Wu L, Wu MO, De la Maza L, Yun Z, Yu J, Zhao Y, et al. Targeting the inhibitory receptor CTLA-4 on T cells increased abscopal effects in murine mesothelioma model. *Oncotarget* (2015) 6(14):12468–80. doi: 10.18632/oncotarget.3487

21. Murakami J, Wu L, Kohno M, Chan ML, Zhao Y, Yun Zb, et al. Triple-modality therapy maximizes antitumor immune responses in a mouse model of mesothelioma. *Sci Transl Med* (2021) 13(589):eabd9882. doi: 10.1126/scitranslmed.abd9882

22. Jackaman C, Bundell CS, Kinnear BF, Smith AM, Filion P, van Hagen D, et al. IL-2 intratumoral immunotherapy enhances CD8+ T cells that mediate destruction of tumor cells and tumor-associated vasculature: a novel mechanism for IL-2. *J Immunol* (2003) 171(10):5051–63. doi: 10.4049/jimmunol.171.10.5051

23. Nowak AK, Robinson BW, Lake RA. Gemcitabine exerts a selective effect on the humoral immune response: implications for combination chemo-immunotherapy. *Cancer Res* (2002) 62(8):2353–8.

24. Principe N, Aston WJ, Hope DE, Tilsed CM, Fisher SA, Boon L, et al. Comprehensive testing of chemotherapy and immune checkpoint blockade in preclinical cancer models identifies additive combinations. *Front Immunol* (2022) 13:872295. doi: 10.3389/fimmu.2022.872295

25. Marin-Acevedo JA, Kimbrough EO, Lou Y. Next generation of immune checkpoint inhibitors and beyond. *J Hematol Oncol* (2021) 14(1):1–29. doi: 10.1186/S13045-021-01056-8

26. Bueno R, Stawiski EW, Goldstein LD, Durinck S, De Rienzo A, Modrusan Z, et al. Comprehensive genomic analysis of malignant pleural mesothelioma identifies recurrent mutations, gene fusions and splicing alterations. *Nat Genet* (2016) 48(4):407–16. doi: 10.1038/ng.3520

27. Hmeljak J, Sanchez-Vega F, Hoadley KA, Shih J, Stewart C, Heiman D, et al. Integrative molecular characterization of malignant pleural mesothelioma. *Cancer Discovery* (2018) 8(12):1548–65. doi: 10.1158/2159-8290.CD-18-0804

28. Thorsson V, Gibbs DL, Brown SD, Wolf D, Bortone DS, Ou Yang TH, et al. The immune landscape of cancer. *Immunity* (2019) 51(2):411–2. doi: 10.1016/j.immuni.2019.08.004

29. Becht E, Giraldo NA, Lacroix L, Buttard B, Elarouci N, Petitprez F, et al. Estimating the population abundance of tissue-infiltrating immune and stromal cell populations using gene expression. *Genome Biol* (2016) 17(1):218. doi: 10.1186/S13059-016-1070-5

30. Meiller C, Montagne F, Hirsch TZ, Caruso S, de Wolf J, Bayard Q, et al. Multi-site tumor sampling highlights molecular intra-tumor heterogeneity in malignant pleural mesothelioma. *Genome Med* (2021) 13(1):113. doi: 10.1186/S13073-021-00931-W

31. Petitprez F, Levy S, Sun CM, Meylan M, Linhard C, Becht E, et al. The murine microenvironment cell population counter method to estimate abundance of tissue-infiltrating immune and stromal cell populations in murine samples using gene expression. *Genome Med* (2020) 12(1):1–15. doi: 10.1186/S13073-020-00783-W

32. de Gooijer CJ, Borm FJ, Scherpereel A, Baas P. Immunotherapy in malignant pleural mesothelioma. *Front Oncol* (2020) 10:187. doi: 10.3389/fonc.2020.00187

33. Forde PM, Spicer J, Lu S, Provencio M, Mitsudomi T, Awad MM, et al. Neoadjuvant nivolumab plus chemotherapy in resectable lung cancer. *N Engl J Med* (2022) 386(21):1973–85. doi: 10.1056/NEJMoa2202170

34. Tawbi HA, Schadendorf D, Lipson EJ, Ascierto PA, Matamala L, Castillo Gutiérrez E, et al. Relatlimab and nivolumab versus nivolumab in untreated advanced melanoma. *N Engl J Med* (2022) 386(1):24–34. doi: 10.1056/NEJMoa2109970

35. Testa JR, Berns A. Preclinical models of malignant mesothelioma. *Front Oncol* (2020) 10:101. doi: 10.3389/fonc.2020.00101

36. Kommalapati A, Tanvetyanon T. Epigenetic modulation of immunotherapy cofactors to enhance tumor response in lung cancer. *Hum Vaccin Immunother.* (2021) 17(1):51–4. doi: 10.1080/21645515.2020.1764273

37. Nowak AK, Lake RA, Marzo AL, Scott B, Heath WR, Collins EJ, et al. Induction of tumor cell apoptosis *in vivo* increases tumor antigen cross-presentation, cross-priming rather than cross-tolerizing host tumor-specific CD8 T cells. *J Immunol* (2003) 170(10):4905–13. doi: 10.4049/jimmunol.170.10.4905

38. Lesterhuis WJ, Rinaldi C, Jones A, Rozali EN, Dick IM, Khong A, et al. Network analysis of immunotherapy-induced regressing tumours identifies novel synergistic drug combinations. *Sci Rep* (2015) 5:12298. doi: 10.1038/srep12298

39. Lesterhuis WJ, Salmons J, Nowak AK, Rozali EN, Khong A, Dick IM, et al. Synergistic effect of CTLA-4 blockade and cancer chemotherapy in the induction of anti-tumor immunity. *PloS One* (2013) 8(4):e61895. doi: 10.1371/journal.pone.0061895

frontiers | Frontiers in Immunology

TYPE Review
PUBLISHED 27 January 2023
DOI 10.3389/fimmu.2023.1121557

OPEN ACCESS

EDITED BY
Chiara Porta,
University of Eastern Piedmont, Italy

REVIEWED BY
Evelien Smits,
University of Antwerp, Belgium
Dan Merrick,
University of Colorado Anschutz Medical Campus, United States

*CORRESPONDENCE
Paolo Andrea Zucali
paolo.zucali@hunimed.eu

SPECIALTY SECTION
This article was submitted to Cancer Immunity and Immunotherapy, a section of the journal Frontiers in Immunology

RECEIVED 11 December 2022
ACCEPTED 16 January 2023
PUBLISHED 27 January 2023

CITATION
Perrino M, De Vincenzo F, Cordua N, Borea F, Aliprandi M, Santoro A and Zucali PA (2023) Immunotherapy with immune checkpoint inhibitors and predictive biomarkers in malignant mesothelioma: Work still in progress. *Front. Immunol.* 14:1121557. doi: 10.3389/fimmu.2023.1121557

Immunotherapy with immune checkpoint inhibitors and predictive biomarkers in malignant mesothelioma: Work still in progress

Matteo Perrino[1], Fabio De Vincenzo[1], Nadia Cordua[1], Federica Borea[1,2], Marta Aliprandi[1,2], Armando Santoro[1,2] and Paolo Andrea Zucali[1,2]*

[1]Department of Oncology, Istituto di Ricovero e Cura a Carattere Scientifico (IRCCS) Humanitas Research Hospital, Milan, Italy, [2]Department of Biomedical Sciences, Humanitas University, Milan, Italy

Malignant mesothelioma (MM) is a rare and aggressive neoplasm, usually associated with a poor prognosis (5 years survival rate <10%). For unresectable disease, platinum and pemetrexed chemotherapy has been the only standard of care in first line for more than two decades, while no standard treatments have been approved in subsequent lines. Recently, immunotherapy has revolutionized the therapeutic landscape of MM. In fact, the combination of ipilimumab plus nivolumab has been approved in first line setting. Moreover, immune checkpoint inhibitors (ICIs) showed promising results also in second-third line setting after platinum-based chemotherapy. Unfortunately, approximately 20% of patients are primary refractory to ICIs and there is an urgent need for reliable biomarkers to improve patient's selection. Several biological and molecular features have been studied for this goal. In particular, histological subtype (recognized as prognostic factor for MM and predictive factor for chemotherapy response), programmed death ligand 1 (PD-L1) expression, and tumor mutational burden (widely hypothesized as predictive biomarkers for ICIs in several solid tumors) have been evaluated, but with unconclusive results. On the other hand, the deep analysis of tumor infiltrating microenvironment and the improvement in genomic profiling techniques has led to a better knowledge of several mechanisms underlying the MM biology and a greater or poorer immune activation. Consequentially, several potential biomarkers predictive of response to immunotherapy in patients with MM have been identified, also if all these elements need to be further investigated and prospectively validated.

In this paper, the main evidences about clinical efficacy of ICIs in MM and the literature data about the most promising predictive biomarkers to immunotherapy are reviewed.

KEYWORDS

immunotherapy, immune checkpoint inhibitors, biomarkers, predictive of response, malignant mesothelioma

Introduction

Malignant mesothelioma (MM) is a rare and aggressive neoplasm originating from the mesothelial lining of the pleural cavity (1). Its annual incidence is globally increasing and it is closely related to asbestos exposure (accounting 80% of cases), with a long latency of almost 40 years between exposure and the disease onset. In general, the prognosis of MM is poor, with a median survival not exceeding 14 months and with a 5 years survival rate less than 10%. In Europe, according to the differences in terms of asbestos exposure, MM is more frequent in males (1.7/1000) than in females (0.4/1000). At diagnosis, median age is 70 years old in western countries. According to the World Health Organization (WHO) 2021 classification, MM is categorized in three main histological subtypes: epithelioid (50-70% of cases), characterized by a better prognosis, sarcomatoid (10-20% of cases), more aggressive and typically chemo-resistent, and biphasic, with features of both the previous (2–4).

The therapeutic landscape of mesothelioma is changing. In first line setting, platinum and pemetrexed chemotherapy has been the standard of care for unresectable disease since 2004 and no other treatments have been approved in the second- and third-line setting (1, 5). However, the immunotherapy revolution has improved the survival outcomes of patients with a broad range of cancers, including mesothelioma. In fact, the combination of ipilimumab plus nivolumab was recently approved by the US Food and Drug Administration (FDA) and the European Medicines Agency (EMA) based on the results of the randomized phase III CheckMate 743 trial (6). In this study, nivolumab plus ipilimumab significantly improved overall survival (OS) versus platinum-pemetrexed chemotherapy in unresectable chemo-naive MM patients. The 3-year updates of efficacy and safety analyses showed, after a minimum follow-up of 35.5 months, that immunotherapy with ipilimumab plus nivolumab continued to provide OS benefit over chemotherapy (HR 0.75) and 28% of patients had an ongoing response at 3 years in the immunotherapy arm (7). In second line setting, nivolumab achieved a statistically significant improvement of both progression-free survival (PFS) and OS compared to placebo in pre-treated MM patients in the randomized, phase III, CONFIRM trial (8). Lastly, several ongoing phase III trials should provide robust evidence for any benefits from combining immunotherapy with chemotherapy in the first-line setting (1).

Despite these exciting results, approximately 20% of patients are primary refractory to immunotherapy (6). Unfortunately, in clinical setting there is not yet the availability of predictive biomarkers able to guide the selection of patients really benefiting from immunotherapy. Moreover, compared with other malignancies, progress in MM biomarker research is limited.

In this paper, the main evidences about clinical efficacy of immuno-checkpoint inhibitors (ICIs) in patients with MM and the literature data regarding the biomarkers potentially predictive of response to immunotherapy are reviewed.

Immune checkpoint inhibitors in malignant mesothelioma

Tumor-infiltrating lymphocytes (TILs), macrophages, and natural killer (NK) cells usually infiltrate the tumor tissue of mesothelioma. Epithelioid mesothelioma presents an increased stromal infiltration by TILs and helper-1-polarized T cells, whereas sarcomatoid mesothelioma is infiltrated by TILs with a high CD8+ population and a low CD4+ population and presents an increased expression of immune checkpoint programmed death ligand-1 (PD-L1). Moreover, an immunosuppressive environment is promoted through M2 polarized macrophages and regulatory T (Treg) cells. Starting from this scenario, an effort for the identification of therapies modulating the immune system, including dendritic cell (DC) therapy, chimeric antigen receptor (CAR) T-cell therapy, cancer vaccines, and checkpoint inhibitors, is ongoing. In the last decade, monoclonal antibodies directed against cytotoxic T lymphocyte antigen 4 (CTLA4) or programmed cell death (PD-1) or its ligand PD-L1 have received regulatory approval across the globe, alone or in combination with chemotherapy for the treatment of tumors, including thoracic cancer such as mesothelioma. In mesothelioma, the main evidence regards front-line and salvage settings, while neoadjuvant/adjuvant and multimodality treatment trials are still ongoing. The main results of ICIs are presented below and summarized in Table 1.

Immune checkpoint inhibitors as salvage therapy

The CTLA4 inhibitor tremelimumab was the first immune checkpoint inhibitor assessed in mesothelioma. In the phase II MESO-TREM 2008 study, tremelimumab administered at the dose of 15 mg/kg every 90 days in relapsed disease setting, showed a low but durable activity with an overall response rate (ORR) of 7% (2 of 29 patients) lasting up to 18 months (9). A more intensive schedule of intravenous tremelimumab (10 mg/kg 4-weekly for seven doses, then every 12 weeks until treatment discontinuation) was compared to placebo in the randomized, double blind, phase 2b DETERMINE study. The study enrolled 571 patients, with previously treated MM, randomized 2:1 to tremelimumab or placebo arm. The median age was 66 years and 83% of patients presented epithelioid histology. The primary endpoint of the study was not reached: no statistically significant difference in terms of OS was observed between the two arms, with median OS of 7.7 months in the tremelimumab arm and 7.3 months in the placebo arm (HR 0.92, p 0.41). The ORR observed was only 4.5% and patients with sarcomatoid subtype seemed to benefit better from the CTLA4 inhibitor than patients with epithelioid subtype (10). Therefore, tremelimumab as monotherapy is not indicated for second/third-line therapy in MM.

Pembrolizumab was the first PD-1 inhibitor studied in patients with MM. KEYNOTE-28 was a single arm, phase 1b, multicohort basket trial that treated patients with PD-L1 positive (defined as ≥1% expression in the tumor cells) tumors (11). Thirty-five patients with pleural mesothelioma, who had failed to standard therapy, received pembrolizumab 10 mg/kg every two weeks up to 2 years. The median age was 65 years and 72% of patients had epithelioid histology. Primary endpoints were safety, tolerability and ORR. Five patients (20%) achieved objective response whereas 13 patients (52%) had stable disease with a median duration of response of 12 months. There was no treatment related mortality and there were no discontinuations of therapy attributable to treatment related adverse events.

10.3389/fimmu.2023.1121557

TABLE 1 Main trials of ICIs in malignant mesothelioma.

Name study	Phase	N pts	Drugs	Line	ORR (%)	mPFS (months)	mOS (months)
Monotherapy							
MESO-TREM (2008) (9)	II	29	Tremelimumab	2	7.0	6.2	10.7
DETERMINE (2017) (10)	IIb	571	Tremelimumab *vs* placebo (R2:1)	2-3	4.5 *vs* 1.1	2.8 *vs* 2.7	7.7 *vs* 7.3
KEYNOTE-028 (2017) (11)	Ib	35	Pembrolizumab	2-5	20.0	5.4	18.0
KEYNOTE-158 (2021) (12)	II	118	Pembrolizumab	2-5	8.0	2.1	10.0
PROMISE-MESO (2020) (13)	III	144	Pembrolizumab *vs* CHT	2	22.0 *vs* 6.0 (P = 0.004)	2.5 *vs* 3.4 (P = 0.76)	10.7 *vs* 12.4 (P = 0.85)
NIVO MES (2018) (14)	II	34	Nivolumab	2-3	24.0	2.6	11.8
MERIT (2019) (15)	II	34	Nivolumab	2-3	29.0	6.1	17.3
CONFIRM (2021) (8)	III	332	Nivolumab *vs* placebo (R2:1)	2	11.0 *vs* 1.0 (p=0.00086)	3.0 *vs* 1.8 (p=0.0012)	10.2 *vs* 6.9 (p=0.0090)
JAVELIN (2019) (16)	Ib	53	Avelumab	2-5	9.0	4.1	10.7
Combination therapy							
NIBIT-MESO 1 (2018) (17)	II	40	Tremelimumab + Durvalumab	2-3	28.0	5.7	16.6
INITIATE (2019) (18)	II	34	Nivolumab + Ipilimumab	2-5	29.0	6.2	NR
MAPS2 (2019) (19)	II	125	Nivolumab +/− Ipilimumab	2-5	Nivo arm 19.0 Ipi-Nivo arm 28.0	Nivo arm 4.0 Ipi-Nivo arm 5.6	Nivo arm 11.9 Ipi-Nivo arm 15.9
CHECKMATE 743 (2021) (6)	III	605	Nivolumab + Ipilimumab *vs* CHT	1	40 *vs* 44	6.8 *vs* 7.2	18.1 *vs* 14.1 (p=0.0020)
DREAM (2020) (20)	II	54	Durvalumab + CDDP + pemetrexed	1	48	6.9	NR
PrE0505 (2020) (21)	II	55	Durvalumab + CDDP + pemetrexed	1	56.4	6.7	20.4

PTS, patients; ORR, overall response rate; mPFS, median progression free survival. mOS, median overall survival; CHT, chemotherapy.

In the single arm, open label, phase 2 KEYNOTE-158 trial, 118 patients with previously treated mesothelioma, received pembrolizumab 200 mg every 21 days for up to 35 cycles. Primary endpoint was ORR. Ten out of 118 patients (8%) had an objective response. Median duration of response was 14.3 months and 60% of objective response were ongoing at 12 months. Stratifying for PD-L1 expression, objective responses were observed in six out of 77 patients (8%) with PD-L1 positive tumor (median duration of response: 17.7 months) and in four out of 31 patients (13%) with PD-L1 negative tumor (median duration of response: 10.2 months). Median OS and the median PFS were 10 months (95% CI 7.6–13.4) and 2.1 months (95% CI 2.1–3.9), respectively. In conclusion, pembrolizumab showed durable anti-tumor activity in patients with advanced MM, regardless of PD-L1 status (12). In the phase 3 PROMISE-MESO trial, a total of 144 patients who had progressed after previous platinum-based chemotherapy and regardless of PD-L1 expression, were randomized 1:1 to pembrolizumab 200 mg every three weeks or physician's choice of chemotherapy gemcitabine at 1000 mg/m2 (days 1 and 8) every 3 weeks or vinorelbine at 30 mg/m2 IV (days 1 and 8) until progression. The primary endpoint was PFS. The median age was 70 years, with almost 90% having epithelioid histology. Although ORR with pembrolizumab was 22% compared to 6% with chemotherapy, the study did not show a statistically significant improvement in median PFS or in median OS even stratifying by PD-L1 expression status. Median PFS was 2.5 months in the pembrolizumab group versus 3.4 months in the chemotherapy group (HR 1.06; p=0.76). Median OS was 10.7 months in the pembrolizumab arm versus 12.4 months in the chemotherapy arm (HR 1.12; p=0.59) (13).

Nivolumab has been evaluated as monotherapy in two phase 2 trials. The Dutch study NivoMes was a single-center, single arm study of 34 patients enrolled to receive nivolumab (3 mg/kg) every two weeks for up to 12 months. The primary endpoint was disease control

rate (DCR) assessed at 12 weeks ≥40%. The study met its primary endpoint with DCR at 12 weeks of 47%. The median PFS and median OS were 2.6 months and 11.8 months, respectively. Half of the patients with stable disease (n=4), achieved disease stability for more than 6 months. The safety profile included one treatment-related death from pneumonitis. Responses by PD-L1 status showed that PD-L1 expression did not correlate with survival outcomes (14). The MERIT trial was an open label, single arm, phase 2 study of 34 patients enrolled to receive nivolumab 240 mg every two weeks until progression disease or unacceptable toxicity. The primary endpoint was ORR. Ten out of 34 patients (29%) achieved an objective response. The median PFS and OS were 6.1 months and 17.3 months, respectively. In this trial, PD-L1 expression (≥1% *vs* <1%) had an impact in terms of ORR (40% versus 8%), PFS (7.2 months versus 2.9 months), and OS (17.3 months versus 11.6 months) even if not statistically significant. Based on these results, the Japanese MERIT trial was the world's first study to obtain regulatory approval for a checkpoint inhibitor in August 2018 (15). The phase 3 CONFIRM trial demonstrated that nivolumab improves PFS and OS over placebo in 332 patients randomized 2:1 to nivolumab at dose of 240 mg IV every 14 days or placebo until disease progression or a maximum of 12 months (8). Of note, 57% of patients were treated in the 3rd line setting. The co-primary endpoints PFS and OS were met: Nivolumab achieved a statistically significant improvement in terms of both mPFS (HR: 0.67; p=0.0012) and mOS (HR: 0.69; p=0.0090). If the PD-L1 expression (≥1%) was not predictive for either PFS or OS, a statistically significant improvement in terms of PFS and OS was reported in the subgroup analysis in patients with epithelioid histology but not in non-epithelioid patients. These data justify using an anti-PD-1 inhibitor in MM patients after failure with platinum-pemetrexed-based chemotherapy.

The safety and efficacy of avelumab have been investigated in the large, multicohort phase 1b JAVELIN study. Fifty-three patients with pretreated mesothelioma received avelumab 10 mg/kg every two weeks until progression disease or unacceptable toxicity. The confirmed ORR was 9% (5 patients: 95% CI, 3.1%-20.7%), with complete response in 1 patient and partial response in 4 patients. The median PFS and OS were 4.1 months and 10.7 months, respectively. According to PD-L1 tumor expression (positive PD-L1≥5% versus negative PD-L1<5%), a higher ORR (14.3% versus 8.0%) and a longer PFS (17.1 weeks versus 7.4 weeks) were observed in the PD-L1-positive group (16).

Trials investigating combinations of ICIs targeting either PD-1 or PD-L1 with anti-CTLA4 antibodies in a salvage setting emerged almost in parallel with those testing ICIs as monotherapy.

The combination of the anti-CTLA-4 tremelimumab (1 mg/kg) and the anti-PD-L1 durvalumab (20 mg/kg) administered every 4 weeks for up to 4 doses followed by maintenance durvalumab alone was evaluated in the open-label, single-arm, phase 2 NIBIT-MESO-1 trial. In total, 40 patients with MM (28 pre-treated and 12 treatment-naïve patients) were enrolled. The primary endpoint of this study (immune-related ORR ≥25%) was met: the ORR was 28% in all populations and 33% in the treatment naïve patients. The median duration of response was 16.1 months, but the tumor PD-L1 expression was not associated with better ORR or longer survival outcomes. Despite positive results, the small sample size of this trial does not justify the use of these drugs in clinical practice (17).

The single-arm phase 2 INITIATE trial studied nivolumab (240 mg every 2 weeks) combined with ipilimumab (1 mg/kg every 6 weeks up to 4 doses) in 34 patients with MM relapsed after platinum-based therapy (18). The primary endpoint was met because a 12-weeks DCR of 67% was observed. Response to therapy resulted higher in patients with PD-L1 expression (≥1%) compared with patients with negative tumors (47% versus 16%).

The MAPS2 trial, a non-comparative, randomized phase II study, enrolled 125 MM patients to receive Nivolumab alone (3 mg/kg every 2 weeks) or combined with ipilimumab (1 mg/kg every 6 weeks) after platinum-based chemotherapy (19). The primary endpoint of this trial was the DCR at 12 weeks (at least 40% of patients with disease control) and it was reached in both arms (nivolumab arm: 44%; nivolumab-ipilimumab arm: 50%). The combination nivolumab/ipilimumab showed a higher ORR (28% versus 19%), a longer mPFS (5.6 months versus 4.0 months) and mOS (15.9 months versus 11.9 months), and a higher grade 3-4 treatment-related adverse events (AEs) incidence (26% versus 14%) compared to nivolumab alone. In the exploratory analysis, PD-L1 expression (≥1%) resulted correlated with higher ORR, but not with 12-week DCR. Despite the lack of FDA approval due to the absence of randomized comparisons with other treatments, the National Comprehensive Cancer Network Clinical (NCCN) Practice Guidelines in Oncology recommend nivolumab with or without ipilimumab as a preferred treatment option (Category 2A) in second-line or later settings.

In summary, the results of the phase II MAPS2 and MERIT trials and the results of the randomized phase III CONFIRM trial support using an anti-PD-1 inhibitor (in particular nivolumab) as monotherapy in patients progressing during or after platinum-pemetrexed-based chemotherapy, representing a new therapeutic horizon in second-line setting for MM.

Immune checkpoint inhibitors in first line setting

The CheckMate-743 trial is the first phase III study demonstrating an OS improvement achieved by immunotherapy with the combination nivolumab/ipilimumab compared to standard platinum-pemetrexed chemotherapy in first-line setting in patients with unresectable MM (6). Overall, 605 patients not selected for PD-L1 expression were randomized to receive ipilimumab (1 mg/kg every 6 weeks) and nivolumab (3 mg/kg every 2 weeks) for up to 2 years versus standard platinum-pemetrexed therapy. The primary endpoint OS was met. In fact, patients treated with immunotherapy achieved a statistically significant longer OS (18.1 months versus 14.1 months; HR: 0.74; p=0.0020). Moreover, a statistically significant advantage in OS was described despite histology (mOS 18.7 months in epithelioid histology and 18.1 months in non-epithelioid one), with a greater benefit versus chemotherapy in PD-L1 (≥1%) tumor positive expression (mOS 18.0 versus 13.3 months, HR 0.69) or in non-epithelioid tumors (mOS 18.1 versus 8.8 months, HR 0.46). The ORR resulted comparable (immunotherapy arm: 40%; chemotherapy arm: 43%) whereas the duration of response (DOR) was longer in the immunotherapy arm (median 11.0 months versus 6.7 months). Both arms achieved similar mPFS (immunotherapy arm: 6.8 months;

chemotherapy arm: 7.2 months; HR 1.00) whereas the incidence of grade 3-4 treatment-related AEs resulted comparable (immunotherapy arm: 30%; chemotherapy arm: 32%). Therefore, the combination ipilimumab/nivolumab was approved as first-line therapy for patients with unresectable MM either by FDA and by EMA. The 3-year updates of efficacy and safety analyses confirmed the advantage of immunotherapy with ipilimumab/nivolumab compared to chemotherapy in terms of OS (HR 0.75) (7). Of note, 28% of patients in the immunotherapy arm had an ongoing response at 3 years.

With the aim to increase the efficacy of immunotherapy in patients with mesothelioma, ICIs were also evaluated in combination with chemotherapy, tyrosine kinase inhibitors (TKIs) and other therapeutic strategies.

The single-arm, phase II DREAM trial studied the efficacy of chemo-immunotherapy by administering durvalumab (1125 mg), cisplatin (75 mg/m2), and pemetrexed (500 mg/m2) every 3 weeks for up to 6 cycles and then durvalumab as maintenance therapy up to 12 months (20). The 6-week PFS in the intention to treat population was the primary endpoint of this study. A total of 54 MM patients unselected for PD-L1 expression were enrolled. After a median follow-up of 28.2 months, 57% of patients were progression-free and alive at 6 months. The mPFS was 6.9 months, and the ORR was 48%. The PD-L1 expression did not correlate with treatment outcomes.

The single-arm, phase II PrE0505 trial is evaluating first-line immunotherapy with durvalumab and platinum-based chemotherapy and then durvalumab alone as maintenance treatment (21). The primary endpoint was the OS compared to historical control with cisplatin-pemetrexed chemotherapy. A total of 55 MM patients were enrolled. The primary endpoint of this study was met: the combination of chemotherapy with durvalumab achieved a median OS of 20.4 months compared to 12.1 months with historical control and the estimated 12-months OS rate was 70.4%. The mPFS was 6.7 months whereas the ORR was 56.4%. The genomic and immune cell repertoire analyses showed that: a higher immunogenic mutations burden coupled with a higher immune cell repertoire resulted related to a favorable clinical outcome; a higher degree of genomic instability was present in responding patients with epithelioid mesothelioma; patients carrying germline alterations in cancer-predisposing genes, such as those involved in DNA repair, resulted more likely to be long-term survivors. Therefore, a phase III study (the PrE0506/DREAM3R trial) is now enrolling patients with unresectable and treatment-naïve MPM to compare standard platinum-based chemotherapy ± durvalumab (NCT04334759).

The phase II-III IND.227 trial is comparing cisplatin-pemetrexed ± pembrolizumab in unresectable mesothelioma patients (NCT02784171). The Beat-meso trial, a randomized phase III study, is comparing the triplet therapy of carboplatin, pemetrexed, and bevacizumab versus the quadruple therapy of carboplatin, pemetrexed, bevacizumab, and atezolizumab in 320 mesothelioma patients (NCT03762018). Considering the detailed biomarker studies planned in these trials, their results should probably guide patient selection for different therapeutic strategies.

In conclusion, the immunotherapy revolution has improved the survival outcomes of patients with a broad range of cancers, mesothelioma included. In fact, starting from the data of the randomized Checkmate-743 phase III trial, the combination ipilimumab/nivolumab gained FDA and EMA approval as first-line therapy for unselected patients with unresectable MM, giving for the first time after two decades a new option of care instead of (or in addition to) platinum-pemetrexed based chemotherapy.

Predictive biomarkers

In order to personalize the treatments and avoid unnecessary toxicity, the main issue about the use of ICIs in MM is the needing for biological or molecular features usable as reliable biomarkers to predict which patients are more likely responders to immunotherapy. Table 2 shows the main predictive biomarkers under evaluation in MM.

Histology

Histological subtype in MPM has been widely recognized as a prognostic factor, with non-epithelioid histology considered as a predictor of poor survival in two main prognostic scores (EORTC and CALGB) (22, 23). In fact, a longer median survival has been seen in epithelioid tumors compared with non-epithelioid ones. Moreover, a better response to platinum and pemetrexed chemotherapy has been observed for epithelioid tumors (24, 25). On the other hand, it is not clear if histology can be used as an item predictive of immunotherapy response. Due to the small sample size and the low percentage of patients with non-epithelioid tumors, in several phase I and II trials testing ICIs, data about response according to histology was not reported or was too small to draw definitive conclusions (11, 18, 19).

Cedres et al. evaluated, in a retrospective cohort of 189 patients, systemic therapy outcomes according to histology (26). The study was focused on chemotherapy, confirming better results in terms of OS and PFS in epithelioid than in non-epithelioid tumors in first line setting (26.7 *vs* 15.0 months for OS, p<0.001, respectively; 4.8 *vs* 3.6 months for PFS, p=0.03, respectively). Moreover, an analysis of 27 patients receiving immunotherapy in second or subsequent lines showed a statistically significant difference in OS in favour of epithelioid histology compared with non-epithelioid one (28.3 *vs* 13.8 months, p=0.01), while no statistically significant difference was observed for PFS (2.7 months in epithelioid subtype *vs* 3 months in non-epithelioid one, p=0.43).

In a similar way, in the PROMISE-meso trial, considering the pembrolizumab arm, non-epithelioid histology showed poorer PFS and OS than the epithelioid histology (HR 1.76 and 1.54, respectively), although these data were not statistically significant (95% CI 0.58–5.33 and 0.49–4.83, respectively), probably for the small sample size (on 73 patients receiving immunotherapy, only 7 (9.6%) had a non-epithelioid histology) (13).

Moreover, in the CONFIRM trial, evaluating nivolumab versus placebo in pre-treated patients, a subgroup analysis reported a significant improvement for PFS and OS with nivolumab in epithelioid group (for PFS HR=0.64 (95% CI 0.50–0.83) and for OS HR=0.67 (95% CI 0.50–0.91)) but not in non-epithelioid one (for PFS HR=0.77 (95% CI 0.37–1.60) and for OS HR=0.79 (95% CI 0·35–1·80)) (8).

TABLE 2 Main predictive biomarkers under evaluation in MM.

	Rationale	Limits
Histology	• Known prognostic role for MPM: non-epithelioid histology considered as a predictor of poor survival (22, 23). • Evidence of better response to platinum and pemetrexed chemotherapy in epithelioid tumors (24, 25).	• Data about response according to histology are mostly not reported or too small to draw definitive conclusions (6, 8, 11, 13, 18, 19, 26). • Variable percentage of epithelioid differentiation in biphasic form, without a clear threshold value (27).
PD-L1 espression	• Known prognostic role for MPM: higher levels of expression apparently associated to poorer outcomes (28, 29). * Widely used as predictive biomarker for ICIs in particular in NSCLC.	• Conflicting data about correlation between higher levels and better responses to ICIs (6, 8, 13). • Availability of several immunohistochemistry assays (30). • No clear cut off value for defining PD-L1 positivity in mesothelioma (16, 30, 31). • Dynamic feature in disease history (32, 33).
TMB	• A greater value may lead to a higher immunogenic neoantigen exposure and, consequently, to a stronger immune activation and a greater benefit from ICIs (34). • Tumors related with carcinogenic exposure (like asbestos for mesothelioma) usually have a high TMB (35, 36). • A predictive value for ICIs response was observed in NSCLC and melanoma (37, 38).	• Availability of different sequencing assays (39–41). • No clear depth of sequencing to be performed (39–41). • Low average value (despite what was expected) (35, 36).
Genomic biomarker	• A better knowledge of the mechanisms underlying the MPM biology by genomic profiling techniques can help identifying patients more likely to be ICIs responders. • Specific genomic alterations can explain an higher neoantigens formation and/or the mechanisms underlying a greater or poorer immune activation (7, 40–54)	• Limited data about potentially useful specific genomic alterations. • Needing of time, funds and specially trained personnel to perform genomic sequencing techniques. • Not enough data to hypothesize an application in clinical practice outside of clinical trials.
TME	• The only biomarker to evaluate the immune cells infiltrating the tumor microenvironment rather than the tumor cells alone (35, 46). • Probable correlation between TME characteristics, survival and better or poorer immune activation when ICIs are administered (7, 35, 46, 49, 55–79)	• No commercially-available standardized gene panels to evaluate tumor immune microenvironment. • Not enough data to hypothesize an application in clinical practice outside of clinical trials.
Other immune checkpoint molecules	• LAG-3, is a receptor expressed on activated T cells and suppress their activation and expansion (80, 81). • TIM-3 is express on immune cells (CD8 and CD4 T cells, NKs, macrophages, DCs), it inhibits Th1 response and stimulates Tregs activation. Low levels of TIM-3 seem to correlate with improved OS in MPM patients treated with anti-CTLA4 (49, 80–82). • VISTA inhibits T cells proliferation and activation; it seems to be highly expressed in MPM rather than in other solid tumors (47, 49).	• Limited and early data, currently not sufficient to hypothesize an application in clinical practice.

MPM, Malignant Pleural Mesothelioma; PD-L1, Programmed death-ligand 1; ICIs, Immune Checkpoint Inhibitors; NSCLC, non-small cell lung cancer; TMB, Tumor Mutational Burden; TME, Tumor Microenvironment; LAG-3, Lymphocyte Activation Gene-3; TIM-3, T-cell immunoglobulin and mucin containing protein 3; VISTA, V-domain Ig suppressor of T cell activation; CTLA4, Cytotoxic T-Lymphocyte Antigen 4; NKs, Natural Killers; DCs, Dendritic Cells; Th1, T Helper 1; Tregs, T Regulatory Cells.

It is also interesting to consider that, in non-epithelioid mesothelioma, biphasic form can display a variable percentage of epithelioid differentiation and Vigneswaran et al. found this percentage as an independent predictor of survival (27).

Important data about the role of histology has been reported in CheckMate-743 study. This large phase III trial compared the combination of ipilimumab and nivolumab versus chemotherapy with cisplatin and pemetrexed with OS as primary endpoint in all patient. A stratification by histology (epithelioid versus non-epithelioid) was pre-planned. Among 303 patients receiving immunotherapy, histology was epithelioid in 229 patients (76%) and non-epithelioid in 74 patients (24%). Immunotherapy showed a greater benefit over chemotherapy in non-epithelioid histology than epithelioid. In particular, a median OS of 18.1 months in immunotherapy arm and 8.8 months in chemotherapy arm (HR 0.46, 95% CI 0.31–0.68) were observed for non-epithelioid histology compared to 18.7 months and 16.5 months for epithelioid histology (HR 0.86, 95% CI 0.69–1.08), respectively (6). Although the greater OS benefit in non-epithelioid group seems to be mostly related to a poor performance of chemotherapy and the trial was not specifically designed to identify a difference according to the histological subtype, also considering the consistent sample size, these findings could suggest histology as a potential biomarker in therapeutic choice, with non-epithelioid tumors having a particular benefit from immunotherapy rather than chemotherapy.

Programmed death-ligand

Human PD-1 is a membrane protein belonging to the CD28 family and normally expressed by immune cells (T and B cells, macrophages and dendritic cells). It is involved, by interacting with its ligand PD-L1, in negative regulation of immunity. PD-1 can be also expressed in TILs and, on the other hand, tumor cells can express PD-L1 in different percentage, contributing to the inhibition of CD4+ and CD8+ T-cell activation and to the apoptosis of antigen-specific T-cell clones (83, 84).

The PD-L1 expression, evaluated by immunohistochemistry, seems to have a negative prognostic role in several solid tumors (85–87). Around 20-50% of MPM express PD-L1 (considering

positivity of cells =>1%) and a higher level of PD-L1 expression is apparently associated to poorer outcomes and most likely observed in sarcomatoid tumors (28, 29).

However, the predictive role of PD-L1 for ICIs response in mesothelioma is not clear. In fact, since the first phase 1 and 2 studies, conflicting results have been found about a higher response rate in PD-L1 positive tumors treated with ICIs compared with negative ones.

For example, in phase 1b KEYNOTE-028 trial, enrolling only PD-L1-positive pretreated patients with MPM (with positivity defined as immunohistochemistry expression in at least 1% of tumor cells) to receive pembrolizumab, promising results in terms of durability and efficacy of response were observed (11). These data seemed to be confirmed in a phase 2 single-arm trial testing pembrolizumab in previously treated patients not selected for PD-L1 expression, showing a greater ORR in PD-L1 positive than in negative patients (26-31% *vs* 7% respectively) (88). However, no statistically significant difference in terms of response was observed in patients with MPM expressing PD-L1 compared to patients with MPM negative for PD-L1 expression in the KEYNOTE-158 trial (12). Also in the NivoMes trial, nivolumab showed no differences in terms of DCR, PFS and OS by stratifying patients enrolled according to PD-L1 status (14). On the contrary, in the MERIT trial, testing nivolumab in a similar pretreated population, an interesting trend (not statistically significant) in favor of PD-L1 positivity compared to PD-L1 negativity was reported in terms of ORR (40% (95% CI 21.9–61.3) *vs* 8% (95% CI 1.5–35.4); PFS (7.2 months *vs* 2.9 months; p=0.4490), and OS (17.3 months *vs* 11.6 months; p=0.2021) (15, 89). Similarly, in the INITIATE trial evaluating nivolumab and ipilimumab, a *post-hoc* analysis about the disease response at 12 weeks and the duration of response for more than 6 months according to PD-L1 status suggested a greater benefit in PD-L1 positive tumors compared to negative ones (RR at 12 weeks 47% *vs* 16% (p 0.018) and DOR > 6 months 73% *vs* 32% (p=0.037), respectively) (18). The MAPS2 trial, testing nivolumab and nivolumab plus ipilimumab in a non-comparative design, reported an advantage in terms of ORR but not in terms of 12-week DCR for patients with PD-L1 positive tumors (19).

Similarly, the predictive value of PD-L1 in terms of response to ICIs therapy remain controversial also in the larger phase 3 trials.

In particular, in the CONFIRM and PROMISE-Meso trials, PD-L1 expression ≥1% was not related to either PFS or OS (8, 13), while in the CheckMate-743 trial the PD-L1 positivity seemed to predict better outcomes with nivolumab plus ipilimumab over chemotherapy (6). Nevertheless, it should be noted that in this last trial the difference observed in terms of survival benefit was related to a poorer efficacy of chemotherapy in PD-L1 positive patients compared to negative ones (median OS 15.4 months and 16.6 months, respectively), while median OS with nivolumab plus ipilimumab was similar in the two groups (PD-L1 ≥1% group: 18 months; PD-L1 <1% group: 17.3 months). Moreover, in the CheckMate-743 trial, the PD-L1 status was not a stratification factor, so this datum is purely descriptive and a potential imbalance in positive and negative group could not be excluded, precluding firm conclusions (7).

Several confounding factors complicate the evaluations about the role of PD-L1 expression as a predictive biomarker.

First of all, the use of different immunohistochemistry assays and its application on tumor cells only (tumor proportion score, TPS) or both on tumor and infiltrate immune cells (combined positive score, CPS) can lead to different positivity scores and to not comparable findings between various studies (30). The majority of trials evaluating ICIs activity in MM have evaluated the PD-L1 expression only on tumor cells. However, the role of the tumor immune microenvironment in the biology of MM is known. In particular, the abundance of the tumor-associated macrophages (TAMs), which are the key inflammatory cells with a potent immunosuppressive activity, suggests a potential key role of the myelomoncytic cells in the immunosuppression in MM and in the activity of PD-1 targeting antibodies. Therefore, the valuation of PD-L1 expression not only on tumor cells but also on the tumor microenvironment cells could be more informative about prediction of response to ICIs. Nonetheless, no association with PD-L1 status (measured by both TPS and CPS) was observed for PFS and OS in the DREAM trial (20). Moreover, also if a threshold of 1% is usually been used, a clear cut off for defining PD-L1 positivity in mesothelioma has not been identified yet. In phase 1b JAVELIN trial, it was tried to evaluate avelumab anti-tumor activity according to two different cut-off values for defining PD-L1 positivity on tumor cells (≥1% and ≥5%): a similar benefit for both the threshold values in ORR, PFS and OS was observed, without better results by increasing the threshold value (16). Continuing on this topic, it is not even clear whether the peritoneal mesothelioma should be distinguished from the pleural form: the former is rarer than the latter, but it seems to express higher PD-L1 levels so has not been established if a different threshold for PD-L1 expression should be used and the very small number of cases makes this assessment difficult (30, 31). Furthermore, PD-L1 expression seems to be a dynamic feature in disease history, so an evaluation at diagnosis may not be consistent with PD-L1 status after one or more lines of treatments (32, 33).

Another open issue is the role of PD-L1 expression when ICIs are combined with other drugs, in particular with chemotherapy. For example, no association with PD-L1 status (measured by both TPS and CPS) was observed for PFS and OS in the DREAM trial (20). Results of larger ongoing phase 3 trials testing chemoimmunotherapy (DREAM3R, IND227-IFCT1901 and BEAT-meso) will probably help to clarify this issue (NCT04334759, NCT02784171, NCT03762018).

On the basis of data from these studies, the predictive value of response of PD-L1 to ICIs in patients with MM still remains weak and uncertain. However, the feeling is that tumors with a higher positivity for PD-L1 present a higher probability to benefit from immunotherapy. In example, in patients with epithelioid MM, who achieved apparently similar outcomes on combination ICIs and chemotherapy, the PD-L1 expression could be a useful marker to discern treatment selection. Certainly, a deeper study of biological characteristics of these responsive patients with a tumoral PD-L1 positivity and the identification of a standardized method to define the positivity of PD-L1 in MM (type of assay, type of cells to evaluate, threshold of positivity) may help us to better clarify the predictive value of PD-L1.

Tumor mutational burden

The TMB is defined by the number of mutations per megabase of sequenced tumor DNA and it is considered a potential predictive

biomarker of response to ICIs also in MM (90). In fact, a greater number of somatic mutations identified in tumor cells may lead to a higher immunogenic neoantigen exposure and, consequently, to a stronger immune activation which could benefit from therapy with ICIs (34). Currently, there are different sequencing assays for TMB evaluation and the depth of sequencing to be performed is not yet established. As for PD-L1, the lack of standardization of the method for determining the TMB complicates any comparison between different trials and cancer types. However, a predictive value of TMB for ICIs response was observed in patients with non-small cell lung cancer (NSCLC) and melanoma (37, 38). On June 2020, the FDA approved the use of pembrolizumab for advanced solid tumors, previously treated or without any valid alternative treatment option, with a mutational burden of at least 10 mutations per megabase, determined by an FDA-approved test (91).

Mesotheliomas usually appear to have a low average TMB of around 2 mutations per megabase, which is an unexpected finding, because tumors related with carcinogenic exposure (like asbestos for mesothelioma) usually have a high TMB, as seen in particular in NSCLC and melanoma (35, 36).

In the KEYNOTE-158 trial, a prospective exploratory analysis was planned to investigate the relation between tissue-TMB (evaluated by using the FoundationOne CDx assay) and clinical outcomes with pembrolizumab monotherapy in ten different solid tumor types, including mesothelioma (cohort H). 790 patients with evaluable tissue-TMB scores were included in the analysis and 102 of them had TMB-high status (threshold defined at ≥10 mutations per megabase). Across all tumors, an advantage in ORR was found in TMB-high group compared to non-TMB-high one (29% *vs* 6% respectively). However, considering mesothelioma cohort, on 85 evaluable cases only 1 was TMB-high and a disease response was reported in 9 of 84 TMB-low patients; notably, the same median tissue-TMB score was observed both in responders and non-responders to pembrolizumab (1.26 mutations per megabase) (92).

An exploratory analysis regarding TMB was performed also in Checkmate-743 trial. The TMB evalutation was feasible in 53% of patients treated with nivolumab plus ipilimumab and in 45% of patients treated with chemotherapy arm, with the evidence of a median low value (1.75 mut/Mb). However, in this analysis, a higher mutational burden was not correlated to a higher OS in either the immunotherapy or chemotherapy arm.

Based on the results available to date, TMB seems not particularly promising to predict ICIs efficacy in mesothelioma. Moreover, it should be considered that, for its evaluation, next-generation sequencing is traditionally used to identify single nucleotide variation and this technique seems not able to identify the complex chromosomal rearrangements with neo-antigenic potential observed in mesothelioma (39–41).

Genomic biomarkers

Despite the low TMB of MPM and the lack of predictivity of PD-L1 to immunotherapy response, several analyses of the genomic landscape of MM suggested interesting signs to understand the basis for a response to ICIs. Chromosomal rearrangements such as insertions, deletions, and chromosomal translocations are frequently found in MM. Mansfield et al. observed wide inter- and intra-chromosomal rearrangements in the form of chromo-anagenesis, such as chromoplexy or chromothripsis, in 86% of MM samples analyzed (40). Chromothripsis is a pattern of different chromosomal rearrangements resulting from multiple double-strand breaks and reassembly of a long segment or an entire chromosome (42). Chromothripsis has been associated with a worse prognosis in MM patients (40). However, this structural chromosomal variant, also called tumor junction burden, is associated with potential neoantigens formation that facilitates intra-tumural expansion of T-cell clones, suggesting that chromothripsis could have a role in the response to immunotherapy (40). Kosari et al., studied the relationship between tumor junction burden and OS in MM patients treated with nivolumab or nivolumab plus ipilimumab relapsed after first line chemotherapy. Even if tumor junction burden didn't directly demonstrate a predictive role, its strong correlation with "antigen presentation and antigen processing" (APP) gene signatures predicted longer OS. In particular, considering that the impact of tumor junction burdens seemed to be modulated by APP, Kosari and collegues hypothesized that the neo-antingenic potential of chromosomal rearrangements was dependent on the capability of cancer cells to present neoantigens to the immune system. Therefore, to test whether there was an interaction between APP gene sets and tumor junction burdens that affected outcomes, they selected 12 APP gene sets from the Gene Ontology Biological Processes data set in the Molecular Signature Database and calculated their enrichment scores. Using these scores to test for interactions between APP gene sets and junction burdens on survival they found significant interactions with six APP gene sets. With these six APP gene sets, the HRs representing associations between tumor junction burdens and OS favored patients with high APP scores (all HRs < 1) more so than patients with low APP scores (all HRs > 1). Moreover, patients with a low APP gene expression and a high tumor junction burden showed a worse prognosis compared to patients with high APP score and high tumor junction burden when treated with ICIs (42). This is in line with the concept that ICIs need neoantigens presentation on cancer cells to activate cytotoxic T-cell antitumor response (42). Therefore, if prospectively confirmed, this interaction signature between the tumor junction burdens and APP gene sets could represent a potential biomarker for immunotherapies patients' selection in clinical practice.

In general, MM is driven by commonly occurring somatic copy-number alterations at the genomic level. These alterations involve loss of a small number of tumor suppressor genes such as BRCA1-associated protein 1 (BAP1) (located in 3p21) and CDKN2A (located in 9p21), meanwhile oncogenic gain-of-function alterations are rare. The genomic structural variants, characterizing these genes loss of function, are often in the form of chromothripsis (43–47).

BAP1 (BRCA1-associated protein 1 carboxy-terminal hydrolase) is a tumor suppressor gene that modulates gene expression regulating histone H2A activity. It is also implicated in the regulation of apoptosis and DNA replication and repair (48, 49). BAP1 is the most common mutated gene in MM, with its alterations (somatic mutations and deletions) found in ~55% of cases (44–48). In particular, BAP1 mutations are characteristic of epithelioid MM more than of other subtypes (49). BAP1 alterations are found both in the germline and the somatic setting. The heterozygous germline

alterations have an autosomal dominant hereditary pattern and people inheriting these alterations have a higher risk of developing MM (especially after asbestos exposure), melanoma, clear-cell renal cell carcinoma and cholangiocarcinoma (43, 44, 49). Forde et al. in the PrE0505 trial, testing the efficacy of durvalumab plus chemotherapy in MM first line setting, demonstrated that BAP1 germline mutations were associated with a significantly prolonged survival after chemo-immunotherapy. Moreover, other MPM associated germline loss-of-function mutations (MLH1, MLH3, BRCA1, BRCA2 and BLM), in particular those associated with DNA damage repair mechanisms, have been linked to a longer OS (p=0.05 in all MMs analysed and p=0.032 in epithelioid MMs) (44). A possible explanation for this phenomenon is that the tumor immune microenvironment in BAP1 muted gene is more inflammatory. In fact, Forde et al. demonstrated that BAP1 null MM had an increased CD8+ T cell infiltration and higher levels of granzyme B transcripts, indicating an active cytotoxic tumor immune microenvironment (TIME), suggesting that MMs with BAP1 loss may be more responsive to immunotherapy (35, 44). Hmeljak et al. demonstrated that BAP1 loss of function mutations are associated with an upregulation of IRF8. IRF is a transcription factor that regulates interferon signalling and dendritic cells differentiation (particularly CD103+), the latter importantly involved cytotoxic T cells' stimulation in the tumor immune microenvironment (TIME). This finding supports BAP1's role in influencing the TIME (47).

One of the most frequent copy-number mutation in MM is 9p21 deletion, which contains CDK2NA and MTAP (its adjacent gene). This alteration is associated with worse prognosis and with primary resistance to immune checkpoint therapy (45, 46, 50). Han et al., in pan-cancer analysis of The Cancer Genome Atlas (TCGA) data of eight ICIs trials, demonstrated that 9p21 deletion is associated with a "cold" tumor microenvironment characterized by diminished T, B, and NK cells' infiltration, reduced immune cell activation, lower PD-L1 expression levels and a stronger immunosuppressive signalling (50). Considering that almost 50% of the TCGA MM samples presents 9p21 loss, this mechanism represents an important explanation of ICIs' resistance in MPM (35). Moreover, in an extensive genome analysis of MPM, Nastase et al. (45) revealed that CDKN2A loss on 9p21.3 was frequently associated with the deletion of the near located Type I Interferon (IFN) genes (found delated in 52% of samples). IFNs induce a pro-inflammatory status in the tumor microenvironment. In melanoma, IFN loss of function has been related to a reduced response to CTLA4 inhibition. Even if Nastase et al. did not found a statistically significant difference in OS in patients with CDKN2A and IFN type I co-deletion, this genomic alteration may have a role in MPM cells immune escape.

Zhang et al., using an exome sequencing approach of MM samples, identified 5 genomic clusters, characterized by a temporally ordered tumorigenesis and bearing a prognostic value (48). These evolutionary clusters ranged from low (cluster 1) to high (cluster 5) complexity. The phylogenetic evolution analysis showed that loss of BAP1/−3p21, FBXW7/-chr4 and 9p21.3 were always early clonal events in MM tumorigenesis, demonstrated by their presence in nearly all subclones. Instead, Hippo pathway inactivation, caused by NF2/−22q events, are mainly late events occurring only in some subclones. The loss of Hippo pathway activity is found in advanced, more aggressive MPMs and is associated with chemoresistance, suggesting its role as critical bottleneck in the tumoral evolution. The MMs' clonal neoantigen architecture modulates the immune surveillance, and so it has the potential to be a biomarker of response to ICIs. Interestingly, evolutionary cluster C5 has the highest degree of repeated early clonal alterations (and so of neoantigen burden), the worst OS, the highest CD8 T lymphocyte infiltration, and, at the same time, has the inferior Treg cell infiltration rate. Of note, in Zhang et al.'s MEDUSA cohort, C5 was found only in the epithelioid subtype, thus demonstrating a subset of patients with a worse survival in epithelioid MPMs. For these reasons cluster C5 could be a potential predictor of response to immunotherapies (48).

In the PrE0505 trial Forde et al., considering that DNA breaks are common in MM, assessed chromosomal instability quantifying copy number breakpoints in the samples' genome. The authors identified these alterations more frequently in epithelioid MPM of patients with an OS of 12 or more months (p=0.053). This supports the hypothesis that DNA breaks, and their potential of neoantigen formation, are a positive prognostic biomarker in MPM and a possible predictor of response to ICIs (44).

In this trial it was also demonstrated that MMs characterized by a high variability in T-cell receptor (TCR) clonality had an increased survival with chemo-immunotherapy (OS>21 months). The authors also showed that an increased immunogenic mutations burden in major histocompatibility complex (MHC) class I and MHC class II was significantly associated with a better response to durvalumab plus chemotherapy (p=0.064 and p=0.023, respectively), especially in the epithelioid subgroup. Moreover, they demonstrated that a higher human leukocyte antigen (HLA)-B locus divergence was linked to an improved radiological response to chemoimmunotherapy, in particular in epithelioid MMs (p=0.06 and p=0.003, respectively) (44). This evidence is in line with HLA class I allele divergence hypothesis, suggesting a better tumor immune response when there is a high HLA class I functional variability. HLA loss of heterozygosity (LOH), *via* immunoediting, reduces antigen presentation by the MHC, thus consenting tumor escape from CD8-T cells immune response. HLA LOH is a late event in MPM clonal evolution. C5 cluster MPMs are the most frequently interested by HLA LOH, another potential explanation of a *de novo* or acquired ICIs resistance in MM (48, 51).

Forde et al., in the PrE0505 study, showed that MMs responding to chemo-immunotherapy had a higher frequency of non-synonymous missense mutations and clonal mutations than those not responding (p=0.086 and p=0.072), in particular in the epithelioid subgroup (p=0.051 and p=0.025, respectively). In line with these data, the authors demonstrated a strong correlation between APOBEC mutational signature, underpinning subclonal mutagenesis, and non-responsive epithelioid MMs (p=0.031). They hypothesized that a high subclonal mutation burden, in part caused by an altered function of the APOBEC enzymes, could permit tumor immune evasion (44).

Inflammatory gene signature scores have demonstrated a positive predictive role to immunotherapy in other cancer types (melanoma, gastroesophageal cancer and advanced hepatocellular carcinoma) (52–54). In the Checkmate-743 exploratory analysis, the expression of CD8A, STAT1, LAG3, and CD274 (PD-L1) was quantified using RNA sequencing. This analysis demonstrated that a high four-gene inflammatory signature score was associated with an OS benefit in the nivolumab plus ipilimumab arm (mOS 21.8 months versus 16.8

months in patients with low score). In the chemotherapy arm no correlation between inflammatory gene signature score and response was identified. Inflammatory signature score, could, thus, be considered a positive predictive biomarker of response to immunotherapy (7).

Tumor immune microenvironment

The TIME consists mainly of tumor associated macrophages (TAM), myeloid-derived suppressor cells (MDSC), CD4- CD8- T cells, B lymphocytes, NK cells, DCs, stromal and endothelial cells. TAM are the most represented immune cell type in TIME of MM (~20–40% of the immune infiltrate). Among TAM, M2 macrophages are predominant, indicating therefore an immunosuppressive phenotype (35, 46). Ollila et al. in a study evaluating immune cells infiltrating the tumor microenvironment of MM and their relationship with survival, demonstrated that M2 macrophages, mediators of tissue remodelling (CD163+ pSTAT1− HLA-DRA1−), are associated with low OS whereas proinflammatory M1 macrophages (CD68+ pSTAT1+ HLA-DRA1+) have a positive correlation with survival (55). The M2 macrophages seems to have a role in stimulating tumor proliferation and invasiveness. Moreover, the M2 macrophages are potent cytotoxic T lymphocyte (CTL) suppressors, and often express PD-L1, thus favouring tumor immune escape (35). Creaney et al. demonstrated a high expression of CCL2, TGFβ1, MMP14 and MMP2 (MMP: Matrix metalloproteases) chemokines in the MM's TIME. These chemokines, seemingly secreted by tumor cells, were correlated with M2 macrophages infiltration, suggesting that they may contribute to an immune suppressive environment. Transforming growth factor beta (TGFβ1) is involved in M2-like macrophage differentiation, and its expression correlates with disease stage, tumor volume and shorter survival (46, 49). Monocyte chemoattractant protein-1 (CCL2) is an important TAM-associated chemokine, responsible for T cells, macrophages, and dendritic cells infiltration in the tumor microenvironment. Moreover, it has been noted that CCL2 levels are related to tumor stage, suggesting that macrophages play an important role in cancer progression (49).

Various studies evaluated the role of TAMs as negative predictive biomarker of response to immunotherapy. Indeed, TAMs can bind the Fc-domain glicans of anti-PD-1 antibodies on PD-1+ T cells with TAM's Fcγ-receptor, thus reducing T cells exposure to anti-PD-1 antibodies (56–59). TAM predictive role in neoplastic patients treated with ICI has been shown in various cancer types, as NSCLC, melanoma, glioblastoma and urothelial carcinoma (60–64). Further studies should be conducted to demonstrate a predictive role of TAMs also in MM.

In MM T-lymphocytes represent ~30% of the TIME, comprising CD4+ T cells and CD4+/FOXP3+ Tregs (1–50%) and CD8+ CTLs (5–15%) (65). Mankor et al. conducted a retrospective immune-monitoring analysis on peripheral blood samples of MM patients treated with either nivolumab (NivoMes trial) or nivolumab plus ipilimumab (INITIATE trial), to assess the predictive role of tumor infiltrating lymphocytes (14, 18, 66). The authors demonstrated, in patients treated with aPD-1/aCTLA-4 combination, a relationship between response and a low rate of naive CD8 T cells (CD45RA+ CCR7+), a high rate of pre-treatment "terminally differentiated effector memory T cells" (TEMRA; CD8 T cells CD45RA+ CCR7+) and high frequency of pre-treatment TEMRA expressed Granzyme-B and Interferon-γ cytokines. Moreover, in patients treated with the combination immunotherapy, increased memory T-cells proliferation and CD4- CD8- T cells activation were shown. These proliferation and activation were not related to response, suggesting that nivolumab plus ipilimumab induced a non-tumor specific T cells response. Only patients with pre-ipilimumab plus nivolumab high TEMRA rate had a benefit from treatment, indicating that TEMRAs mediate a tumor specific response. In nivolumab monotherapy patients these correlations were not found indicating that only an anti-CTLA4/anti-PD-1 treatment can reactivate TEMRAs. To conclude peripheral blood TEMRAs could be used as a predictive biomarker of response to combination immunotherapy (66).

Identifying the relations existing between MM immune cells and prognosis may be the first step towards the identification of predictive therapeutic biomarkers in this setting.

In 2017 Chee et al. (67) evaluated the prognostic role of infiltrating T-cells (CD8+, FOXP3+, CD4+, CD45RO+, CD3+), B-cells (CD20+), neutrophils (NP57+), NK cells (CD56+) and macrophages (CD68+) in MM's patients. The authors observed that FOXP3+ CD4+ Tregs are related to a worse survival, in line with their inhibitory activity on effector and helper T-cells. FOXP3+CD4+ Treg cells account for 2.8% of the total CD4+ lymphocytes in MM (68). Further, in epithelioid MMs, a CD4+/CD8+ ratio >1 and a high frequency of CD4+ T cells were associated with an improved survival, consistent with CD4+ T lymphocytes' role in the stimulation of CD8+ TILS and B-cells against cancer cells. This study demonstrated that a high CD8+ T-cells infiltration in MPM's TIME was not associated with an improved survival, as confirmed in a recent RNA-seq analysis of TIME by Creaney et al. (46).

The B cells represent 4% of TIME and have a central role in the immune crosstalk, acting as both positive and negative regulators of cancer. Their role as positive tumor regulators has been associated with B cells that express "signal transducer and activator of transcription 3" (STAT3), that contributes to a proangiogenic environment thus promoting tumor growth (67, 69). Tumor-associated B-cells' role as negative regulator could be explained by their ability to act as antigen presenting cells inducing CD4+ T cells activation, differentiation, and polarization in Th1 and Th2 subtypes. A high density of CD20+ B lymphocytes in the TIME is associated with an increased survival in patients affected by epithelioid MM (49, 69). This evidence is notable considering that a high B cell infiltrate was found in approximately 50% of MMs in Patil et al.'s retrospective analysis (70).

B cells play also a role in the formation of tertiary lymphoid structures (TLS). TLS are organized ectopic lymphoid aggregates that arise in chronically inflamed environments like autoimmune diseases, chronic infection, and cancer (69, 71). TLSs have been identified in different cancer types and have been associated with a better prognosis and response to immunotherapy. So not only immune cell infiltrating the TME, but also their organisation in TLS is important for anti-tumor immune response (71–75).

TLSs are associated with the local immune response, the ability of germinal centres formation and the lymphocytes' recruitment. Tumors harbouring TLSs in their microenvironment are

characterized by an increased immune infiltration. TLSs do not have a capsule, so immune cells resident in them could be directly exposed to macromolecules from the TME, thus driving intratumoral immune response. B cells in TLS can produce antibodies that tie antigen expressing tumor cells inducing subsequent opsonisation, complement-dependent lysis, or antibody mediated cytotoxicity. Moreover, tumors harbouring TLSs and an important CD8+ T cells infiltration have a better prognosis than those characterized only by CD8+ T cells infiltration, suggesting a better immune response quality in tumors with the TLSs. Immunotherapy promotes TLS formation and activity and this can explain the possible role of TLS and B cells infiltration as positive predictive biomarker of response to ICIs in different cancer types (69, 71, 76, 77).

Based on these evidence Mannarino et al. conducted a retrospective multicenter cohort study of MPM patients never treated with chemotherapy in order to identify TIME features potentially predictive of patients' outcome. The authors demonstrated that epithelioid MM patients with long OS (>36 months) were characterized by an inflammatory background with a higher expression of B-cells (CD20+) and prevalence of TLS formations compared to epithelioid MM patients with short OS (<12 months), which showed a higher frequency of neutrophils and M2 macrophages ($p = 0.025$) (69). Therefore, B cells showed a negative impact in cancer development in this study. As said before, a possible explanation is B cells' role in antigen presentation and cytotoxic antitumor T cells activation. In particular MM, even if characterized by a low TMB, is often interested by chromothripsis, and, thus, tumor junction burden with the potential of neoantigens formation. These neoantigenes could be at the origin of B-cells mediated antitumor immunity (69).

Chee et al. demonstrated that a low rate of NP57+ neutrophils in the TIME of epithelioid MPM was associated with better OS. This finding is consistent with the hypothesis that tumor-associated neutrophils can have a facilitating role in tumorigenesis by promoting angiogenesis and facilitating the development of pro-invasive and pro-metastatic TIME (67).

Ollila et al. studied the correlation between tumor infiltrating immune cells and MM's prognosis thanks to TIME high-resolution deep profiling (55). This analysis demonstrated that granzyme B/CD11c positivity was significantly associated with a better OS. Myeloid-derived cells express CD11c. Thanks to immunohistochemistry the authors identified these prognostic favourable CD11c cells to be DCs. DCs have a fundamental role in antigen presentation and consequently in immune activation in TIME of various cancers. Granzyme B is produced by various immune cells, including DC. In conclusion granzyme B and CD11c could be used as prognostic biomarkers and further studies should be conducted to evaluate their role in predicting immunotherapy response in MPM patients.

Ollila et al. also demonstrated that myeloid derived suppressor cells (MDSCs) in the TME are related with a shorter OS (55). The MDSC are abnormal granulocytes that develop in pathological conditions. They have a prevalence of less than 10% in the TIME. The MDSCs favour tumorigenesis and cancer progression *via* inhibition of Tcells activation and proliferation, and promoting TIME reshaping, epithelial to mesenchymal transition and angiogenesis (49).

Lung immune prognostic index (LIPI) score is a prognostic factor in different cancer types, including non-small cells lung cancer (78, 79). It evaluates the presence of a neutrophils/leukocytes minus neutrophils ratio greater than 3 and a lactate dehydrogenase (LDH) level greater than upper limit of normal, thus identifying 3 groups (good, 0 factors; intermediate, 1 factor; poor, 2 factors). In an exploratory analysis of possible ICIs' predictive biomarkers in the Checkmate-743 phase 3 trial, LIPI score seemed to have a prognostic role with an improved OS in patients with a good score than in those with an intermediate or poor score across both treatment arms. LIPI score didn't have a predictive role for response to immunotherapy in CheckMate-743 trial (7).

Considering the central role that immunotherapy is gaining in MM, other immune checkpoint molecules besides PD-1/PD-L1, especially "lymphocyte activation gene-3" (LAG-3), "T-cell immunoglobulin and mucin containing protein 3" (TIM-3) and "V-domain Ig suppressor of T cell activation" (VISTA) represent a new interesting field of study.

VISTA is a negative checkpoint regulator that inhibits T cells proliferation and activation. It is expressed on the surface of myeloid cells, in particular on TAM. As PD-L1, VISTA can induce differentiation of naïve T cells to FoxP3+ regulatory T cells. VISTA can also play its inhibitory role on T cells both as receptor on T cells and as ligand on antigen presenting cells (47, 49, 80).

Hmeljak et al., conducting a comprehensive integrated genomic analysis of MPM samples, demonstrated high levels of VISTA mRNA in MPM, higher than in other solid tumors analysed in TCGA (47). Among MMs samples, VISTA expression reached the highest levels in the epithelioid subgroup. High VISTA expression levels have been related to an improved OS (47, 49). Considering that physiological mesothelium harbours APC properties that could be maintained in cancer, Hmeljak et al. performed an immunohistochemistry analysis of epithelioid MPM samples, normal and reactive mesothelium, in order to identify differences in VISTA expression. VISTA protein was demonstrated on infiltrating immune cells, in epithelioid MPM cells, in normal and reactive mesothelium. This evidence suggests that epithelioid MPMs, the more differentiated MPM subtype, retain APC properties, frequently lost in the other less differentiated subtypes. Another hypothesis is that VISTA expression in MPM is positively selected by immune pressure (47). In conclusion, VISTA should be further investigated as a possible predictive biomarker of response to ICIs.

TIM-3 is another immunosuppressive molecule, expressed on immune cells (CD8 and CD4 T cells, NKs, macrophages, DCs), that inhibits Th1 response and stimulates Tregs activation. TIM-3 ligand is Galectin-9. TIM-3 and Galectin-9 are frequently found in PD-L1 positive MMs (49, 80). TIM-3 is expressed on MPM cells and TILs of MPM, and particularly on NK cells (less on CD4+ and CD8+ T-cells) (81). Sottile et al. demonstrated an association between low levels of TIM-3 and improved OS in MPM patients treated with anti-CTLA4 (82). So, TIM-3 could have a role as predictive biomarker to immunotherapies in MPM.

LAG-3 is an immune checkpoint receptor, with the ability to suppress T-cells activation and expansion. It is expressed on activated T cells and has been found in pleural effusion of MPM patients and on TILs in pleural effusions. Its role on response to ICIs in MPM has still to be clarified (80, 81).

The T cell immunoglobulin and ITIM domain (TIGIT), an inhibitory immunoreceptor, recently emerged as a novel potential

target for immunotherapy. As this novel immune checkpoint is largely unexplored in MM, the TIGIT blockade should be evaluated as an alternative therapeutic approach also for MM (93).

Discussion

Recent years have witnessed significant improvements in our understanding of mesothelioma's biology and innovative strategies are changing the range of therapeutic options. The main breakthrough has been made in the field of immunotherapy. In fact, the immunotherapy revolution has improved the survival outcomes of patients with a several types of cancers, and mesothelioma is now at the forefront. Recently, the FDA and the EMA approved the combination of ipilimumab and nivolumab as new standard of care for unselected patients with unresectable MM in the first-line setting (6). Despite these exciting results, it is still unclear which mesothelioma patients actually benefit from immunotherapy and which do not. In the Checkmate-743 trial, 28% of responsive patients to the combination ipilimumab-nivolumab, still remained responsive after 36 months. On the other hand, 18% of patients treated with immunotherapy resulted primary refractories compared to 5% of patients treated with chemotherapy. The occurrence of early progression or even hyper-progressive disease in MM patients treated with ICIs have been reported also in other studies (94). Moreover, the combination of ipilimumab and nivolumab in first line setting mainly benefits non-epithelioid patients, in part due to the fact that chemotherapy is ineffective for this histotype, whereas the same level of benefit was not observed in epitheliod patients. In second-third line of therapy, PD-1 inhibitors as monotherapy have been found to be superior to placebo in terms of OS and PFS in the CONFIRM trial, but not superior to chemotherapy (vinorelbine or gemcitabine) in the PROMISE-meso trial (8, 13). Both CONFIRM and the PROMISE-meso trials reported responses with ICIs in epithelioid patients. In particular, in the PROMISE-meso trial the ORR was 22% in the epithelioid patients treated with pembrolizumab compared to 6% in patients treated with chemotherapy. Therefore, considering these incoherent results and discrepancies with the use of ICIs for the therapeutic strategy of mesothelioma, it is crucial to identify predictive biomarkers, especially for epithelioid patients where benefit with immunotherapy is less definite.

In general, several efforts are underway to identify predictive biomarkers of response to ICIs. Unlike other cancers, the predictive value of response to ICIs of PD-L1 and TMB in patients with MPM still remains weak and uncertain. Probably, this is due to the extensive tumoral genomic heterogeneity among patients and histological differences typical of mesothelioma (12, 13).

The genomic research and the study of the TIME are testing several new potential predictive biomarkers. In particular, the inclusion of genomic approaches able to detect structural variants, and transcriptomics to evaluate antigen processing and presentation, could improve the selection of patients to immunotherapy. In an exploratory analysis of Checkmate-743 trial, the expression of CD8A, STAT1, LAG3, and CD274 (PD-L1) was quantified using RNA sequencing. A high four-gene inflammatory signature score was associated with an OS benefit in the nivolumab plus ipilimumab arm (mOS 21.8 months versus 16.8 months in patients with low score), suggesting his potential positive predictive role. However, these data require prospective validation.

The TIME of mesothelioma is very complex. Cancer-associated fibroblasts, T-cells, TAMs, and MDSC have immunosuppressive roles in mesothelioma (95). Interestingly, Mannarino and collegues demonstrated that epithelioid MM patients with long OS (>36 months) were characterized by an inflammatory background with a higher expression of B-cells (CD20+) and prevalence of TLS formations compared to epithelioid MM patients with short OS (<12 months), which showed a higher frequency of neutrophils and M2 macrophages ($p = 0.025$). TLSs have been identified in different cancer types and have been associated with a better response to immunotherapy. Moreover, immunotherapy seems to promote TLS formation and activity and this can explain the possible role of TLS and B cells infiltration as positive predictive biomarker of response to ICIs in different cancer types (69, 71, 76, 77).

Lastly, other immune checkpoint molecules besides PD-1/PD-L1, especially LAG-3, TIM-3 and VISTA, represent new interesting biomarkers. In particular, VISTA is expressed on the surface of myeloid cells, especially on TAM, and it is a negative checkpoint regulator that inhibits T cells proliferation and activation. Interestingly, pleural mesothelioma displays the highest expression levels of VISTA among all the cancers studied, particularly in the epithelioid subgroup. Therefore, VISTA is under investigation as a potential predictive biomarker of response to ICIs in mesothelioma and it could become one of the potential targets for overcoming immunotherapy resistance and a molecular target to improve the immune downregulation (96–98).

In conclusion, despite the recent therapeutic progress in mesothelioma, our knowledge of the factors that underpin response to ICIs is limited. The interpatient genomic heterogeneity and the evidences suggested by the immune-modulating therapies are supporting the need of biomarkers able to guide the selection of patients benefiting from specific and personalized therapeutic strategies. In fact, a deep understanding of the mechanisms associated with primary and secondary resistance to ICIs will further improve the outcomes of patients with mesothelioma.

Author contributions

All authors listed have made a substantial, direct, and intellectual contribution to the work and approved it for publication.

Conflict of interest

PZ reports outside the submitted work personal fees for advisory role, speaker engagements and travel and accommodation expenses from Merck Sharp & Dohme MSD, Astellas, Janssen, Sanofi, Ipsen, Pfizer, Novartis, Bristol Meyer Squibb, Amgen, AstraZeneca, Roche, and Bayer. AS reports outside the submitted work personal fees for consultant or advisory role for SArqule, Sanofi, BMS, Servier, Gilead, Pfizer, Eisai, Bayer, Merck Sharp & Dohme MSD.

The remaining authors declare that the research was conducted in the absence of any commercial or financial relationships that could be construed as a potential conflict of interest.

Publisher's note

References

1. Zucali PA, De Vincenzo F, Perrino M, Digiacomo N, Cordua N, D'Antonio F, et al. Advances in drug treatments for mesothelioma. *Expert Opin Pharmacother* (2022) 23 (8):929–46. doi: 10.1080/14656566.2022.2072211

2. Brims F. Epidemiology and clinical aspects of malignant pleural mesothelioma. *Cancers (Basel)* (2021) 13(16):4194. doi: 10.3390/cancers13164194

3. Lettieri S, Bortolotto C, Agustoni F, Lococo F, Lancia A, Comoli P, et al. The evolving landscape of the molecular epidemiology of malignant pleural mesothelioma. *J Clin Med* (2021) 10(5):1034. doi: 10.3390/jcm10051034

4. Tsai YC, Chen HL, Lee TH, Chang HM, Wu KL, Chuang CH, et al. Salvage therapy for relapsed malignant pleural mesothelioma: A systematic review and network meta-analysis. *Cancers (Basel)* (2021) 14(1):182. doi: 10.3390/cancers14010182

5. Vogelzang NJ, Rusthoven JJ, Symanowski J, Denham C, Kaukel E, Ruffie P, et al. Phase III study of pemetrexed in combination with cisplatin versus cisplatin alone in patients with malignant pleural mesothelioma. *J Clin Oncol* (2003) 21(14):2636–44. doi: 10.1200/JCO.2003.11.136

6. Baas P, Scherpereel A, Nowak AK, Fujimoto N, Peters S, Tsao AS, et al. First-line nivolumab plus ipilimumab in unresectable malignant pleural mesothelioma (CheckMate 743): a multicentre, randomised, open-label, phase 3 trial. *Lancet* (2021) 397(10272):375–86. doi: 10.1016/S0140-6736(20)32714-8

7. Peters S, Scherpereel A, Cornelissen R, Oulkhouir Y, Greillier L, Kaplan MA, et al. First-line nivolumab plus ipilimumab versus chemotherapy in patients with unresectable malignant pleural mesothelioma: 3-year outcomes from CheckMate 743. *Ann Oncol* (2022) 33(5):488–99. doi: 10.1016/j.annonc.2022.01.074

8. Fennell DA, Ewings S, Ottensmeier C, Califano R, Hanna GG, Hill K, et al. Nivolumab versus placebo in patients with relapsed malignant mesothelioma (CONFIRM): A multicentre, double-blind, randomised, phase 3 trial. *Lancet Oncol* (2021) 22(11):1530–40. doi: 10.1016/S1470-2045(21)00471-X

9. Calabrò L, Morra A, Fonsatti E, Cutaia O, Amato G, Giannarelli D, et al. Tremelimumab for patients with chemotherapy-resistant advanced malignant mesothelioma: An open-label, single-arm, phase 2 trial. *Lancet Oncol* (2013) 14 (11):1104–11. doi: 10.1016/S1470-2045(13)70381-4

10. Maio M, Scherpereel A, Calabrò L, Aerts J, Perez SC, Bearz A, et al. Tremelimumab as second-line or third-line treatment in relapsed malignant mesothelioma (DETERMINE): A multicentre, international, randomised, double-blind, placebo-controlled phase 2b trial. *Lancet Oncol* (2017) 18(9):1261–73. doi: 10.1016/S1470-2045 (17)30446-1

11. Alley EW, Lopez J, Santoro A, Morosky A, Saraf S, Piperdi B, et al. Clinical safety and activity of pembrolizumab in patients with malignant pleural mesothelioma (KEYNOTE-028): Preliminary results from a non-randomised, open-label, phase 1b trial. *Lancet Oncol* (2017) 18(5):623–30. doi: 10.1016/S1470-2045(17)30169-9

12. Yap TA, Nakagawa K, Fujimoto N, Kuribayashi K, Guren TK, Calabrò L, et al. Efficacy and safety of pembrolizumab in patients with advanced mesothelioma in the open-label, single-arm, phase 2 KEYNOTE-158 study. *Lancet Respir Med* (2021) 9 (6):613–21. doi: 10.1016/S2213-2600(20)30515-4

13. Popat S, Curioni-Fontecedro A, Dafni U, Shah R, O'Brien M, Pope A, et al. A multicentre randomised phase III trial comparing pembrolizumab versus single-agent chemotherapy for advanced pre-treated malignant pleural mesothelioma: The European thoracic oncology platform (ETOP 9-15) PROMISE-meso trial. *Ann Oncol* (2020) 31 (12):1734–45. doi: 10.1016/j.annonc.2020.09.009

14. Quispel-Janssen J, van der Noort V, De Vries JF, Zimmerman M, Lalezari F, Thunnissen E, et al. Programmed death 1 blockade with nivolumab in patients with recurrent malignant pleural mesothelioma. *J Thorac Oncol* (2018) 13(10):1569–76. doi: 10.1016/j.jtho.2018.05.038

15. Okada M, Kijima T, Aoe K, Kato T, Fujimoto N, Nakagawa K, et al. Clinical efficacy and safety of nivolumab: Results of a multicenter, open-label, single-arm, Japanese phase II study in malignant pleural mesothelioma (MERIT). *Clin Cancer Res* (2019) 25 (18):5485–92. doi: 10.1158/1078-0432.CCR-19-0103

16. Hassan R, Thomas A, Nemunaitis JJ, Patel MR, Bennouna J, Chen FL, et al. Efficacy and safety of avelumab treatment in patients with advanced unresectable mesothelioma: Phase 1b results from the JAVELIN solid tumor trial. *JAMA Oncol* (2019) 5(3):351–7. doi: 10.1001/jamaoncol.2018.5428

17. Calabrò L, Morra A, Giannarelli D, Amato G, D'Incecco A, Covre A, et al. Tremelimumab combined with durvalumab in patients with mesothelioma (NIBIT-MESO-1): an open-label, non-randomised, phase 2 study. *Lancet Respir Med* (2018) 6 (6):451–60. doi: 10.1016/S2213-2600(18)30151-6

18. Disselhorst MJ, Quispel-Janssen J, Lalezari F, Monkhorst K, de Vries JF, van der Noort V, et al. Ipilimumab and nivolumab in the treatment of recurrent malignant pleural mesothelioma (INITIATE): Results of a prospective, single-arm, phase 2 trial. *Lancet Respir Med* (2019) 7(3):260–70. doi: 10.1016/S2213-2600(18)30420-X

19. Scherpereel A, Mazieres J, Greillier L, Lantuejoul S, Dô P, Bylicki O, et al. Nivolumab or nivolumab plus ipilimumab in patients with relapsed malignant pleural mesothelioma (IFCT-1501 MAPS2): A multicentre, open-label, randomised, non-comparative, phase 2 trial. *Lancet Oncol* (2019) 20(2):239–53. doi: 10.1016/S1470-2045 (18)30765-4

20. Nowak AK, Lesterhuis WJ, Kok PS, Brown C, Hughes BG, Karikios DJ, et al. Durvalumab with first-line chemotherapy in previously untreated malignant pleural mesothelioma (DREAM): A multicentre, single-arm, phase 2 trial with a safety run-in. *Lancet Oncol* (2020) 21(9):1213–23. doi: 10.1016/S1470-2045(20)30462-9

21. Forde PM, Sun Z, Anagnostou V, Kindler HL, Purcell WT, Goulart BHL, et al. PrE0505: phase II multicenter study of anti-PD-L1, durvalumab, in combination with cisplatin and pemetrexed for the first-line treatment of unresectable malignant pleural mesothelioma (MPM) — a PrECOG LLC study. *J Clin Oncol* (2020) 38(suppl 15):9003. doi: 10.1200/JCO.2020.38.15_suppl.9003

22. Curran D, Sahmoud T, Therasse P, van Meerbeeck J, Postmus PE, Giaccone G. Prognostic factors in patients with pleural mesothelioma: The European organization for research and treatment of cancer experience. *J Clin Oncol* (1998) 16(1):145–52. doi: 10.1200/JCO.1998.16.1.145

23. Herndon JE, Green MR, Chahinian AP, Corson JM, Suzuki Y, Vogelzang NJ. Factors predictive of survival among 337 patients with mesothelioma treated between 1984 and 1994 by the cancer and leukemia group b. *Chest* (1998) 113(3):723–31. doi: 10.1378/chest.113.3.723

24. Verma V, Ahern CA, Berlind CG, Lindsay WD, Shabason J, Sharma S, et al. Survival by histologic subtype of malignant pleural mesothelioma and the impact of surgical resection on overall survival. *Clin Lung Cancer* (2018) 19(6):e901–12. doi: 10.1016/j.cllc.2018.08.007

25. Billé A, Krug LM, Woo KM, Rusch VW, Zauderer MG. Contemporary analysis of prognostic factors in patients with unresectable malignant pleural mesothelioma. *J Thorac Oncol* (2016) 11(2):249–55. doi: 10.1016/j.jtho.2015.10.003

26. Cedres S, Assaf JD, Iranzo P, Callejo A, Pardo N, Navarro A, et al. Efficacy of chemotherapy for malignant pleural mesothelioma according to histology in a real-world cohort. *Sci Rep* (2021) 11:21357. doi: 10.1038/s41598-021-00831-4

27. Vigneswaran WT, Kircheva DY, Ananthanarayanan V, Watson S, Arif Q, Celauro AD, et al. Amount of epithelioid differentiation is a predictor of survival in malignant pleural mesothelioma. *Ann Thorac Surg* (2017) 103(3):962–66. doi: 10.1016/j.athoracsur.2016.08.063

28. Mansfield AS, Roden AC, Peikert T, Sheinin YM, Harrington SM, Krco CJ, et al. B7-H1 expression in malignant pleural mesothelioma is associated with sarcomatoid histology and poor prognosis. *J Thorac Oncol* (2014) 9(7):1036–40. doi: 10.1097/JTO.0000000000000177

29. Cedrés S, Ponce-Aix S, Pardo-Aranda N, Navarro-Mendivil A, Martinez-Marti A, Zugazagoitia J, et al. Analysis of expression of PTEN/PI3K pathway and programmed cell death ligand 1 (PD-L1) in malignant pleural mesothelioma (MPM). *Lung Cancer* (2016) 96:1–6. doi: 10.1016/j.lungcan.2016.03.001

30. Chapel DB, Stewart R, Furtado LV, Husain AN, Krausz T, Deftereos G. Tumor PD-L1 expression in malignant pleural and peritoneal mesothelioma by dako PD-L1 22C3 pharmDx and dako PD-L1 28-8 pharmDx assays. *Hum Pathol* (2019) 87:11–7. doi: 10.1016/j.humpath.2019.02.001

31. White MG, Schulte JJ, Xue L, Berger Y, Schuitevoerder D, Vining CC, et al. Heterogeneity in PD-L1 expression in malignant peritoneal mesothelioma with systemic or intraperitoneal chemotherapy. *Br J Cancer* (2021) 124:564–66. doi: 10.1038/s41416-020-01130-x

32. Gray SG. Emerging avenues in immunotherapy for the management of malignant pleural mesothelioma. *BMC Pulm Med* (2021) 21:148. doi: 10.1186/s12890-021-01513-7

33. De Gooijer CJ, Borm FJ, Scherpereel A, Baas P. Immunotherapy in malignant pleural mesothelioma. *Front Oncol* (2020) 10:187. doi: 10.3389/fonc.2020.00187

34. Nowak AK, Chin WL, Keam S, Cook A. Immune checkpoint inhibitor therapy for malignant pleural mesothelioma. *Lung Cancer* (2021) 162:162–68. doi: 10.1016/j.lungcan.2021.11.006

35. Fennell DA, Dulloo S, Harber J. Immunotherapy approaches for malignant pleural mesothelioma. *Nat Rev Clin Oncol* (2022) 19:573–84. doi: 10.1038/s41571-022-00649-7

36. Alexandrov LB, Nik-Zainal S, Wedge DC, Aparicio SA, Behjati S, Biankin AV, et al. Signatures of mutational processes in human cancer. *Nature* (2013) 500(7463):415–21. doi: 10.1038/nature12477

37. Campesato LF, Barroso-Sousa R, Jimenez L, Correa BR, Sabbaga J, Hoff PM, et al. Comprehensive cancer-gene panels can be used to estimate mutational load and predict clinical benefit to PD-1 blockade in clinical practice. *Oncotarget* (2015) 6(33):34221–7. doi: 10.18632/oncotarget.5950

38. Johnson DB, Frampton GM, Rioth MJ, Yusko E, Xu Y, Guo X, et al. Targeted next generation sequencing identifies markers of response to PD-1 blockade. *Cancer Immunol Res* (2016) 4(11):959–67. doi: 10.1158/2326-6066.CIR-16-0143

39. Bueno R, Stawiski EW, Goldstein LD, Durinck S, De Rienzo A, Modrusan Z, et al. Comprehensive genomic analysis of malignant pleural mesothelioma identifies recurrent mutations, gene fusions and splicing alterations. *Nat Genet* (2016) 48(4):407–16. doi: 10.1038/ng.3520

40. Mansfield AS, Peikert T, Smadbeck JB, Udell JBM, Garcia-Rivera E, Elsbernd L, et al. Neoantigenic potential of complex chromosomal rearrangements in mesothelioma. *J Thorac Oncol* (2019) 14(2):276–87. doi: 10.1016/j.jtho.2018.10.001

41. Uprety D. CheckMate 743: A glimmer of hope for malignant pleural mesothelioma. *Clin Lung Cancer* (2021) 22(2):71–3. doi: 10.1016/j.cllc.2020.11.009

42. Kosari F, Disselhorst M, Yin J, Peikert T, Udell J, Johnson S, et al. Tumor junction burden and antigen presentation as predictors of survival in mesothelioma treated with immune checkpoint inhibitors. *J Thorac Oncol* (2022) 17(3):446–54. doi: 10.1016/j.jtho.2021.10.022

43. Tsao AS, Pass HI, Rimner A, Mansfield AS. New era for malignant pleural mesothelioma: Updates on therapeutic options. *J Clin Oncol* (2022) 40(6):681–92. doi: 10.1200/JCO.21.01567

44. Forde PM, Anagnostou V, Sun Z, Dahlberg SE, Kindler HL, Niknafs N, et al. Durvalumab with platinum-pemetrexed for unresectable pleural mesothelioma: Survival, genomic and immunologic analyses from the phase 2 PrE0505 trial. *Nat Med* (2021) 27 (11):1910–20. doi: 10.1038/s41591-021-01541-0

45. Nastase A, Mandal A, Lu SK, Anbunathan H, Morris-Rosendahl D, Zhang YZ, et al. Integrated genomics point to immune vulnerabilities in pleural mesothelioma. *Sci Rep* (2021) 11(1):19138. doi: 10.1038/s41598-021-98414-w

46. Creaney J, Patch AM, Addala V, Sneddon SA, Nones K, Dick IM, et al. Comprehensive genomic and tumor immune profiling reveals potential therapeutic targets in malignant pleural mesothelioma. *Genome Med* (2022) 14(1):58. doi: 10.1186/s13073-022-01060-8

47. Hmeljak J, Sanchez-Vega F, Hoadley KA, Shih J, Stewart C, Heiman D, et al. Integrative molecular characterization of malignant pleural mesothelioma. *Cancer Discovery* (2018) 8(12):1548–65. doi: 10.1158/2159-8290.CD-18-0804

48. Zhang M, Luo JL, Sun Q, Harber J, Dawson AG, Nakas A, et al. Clonal architecture in mesothelioma is prognostic and shapes the tumor microenvironment. *Nat Commun* (2021) 12(1):1751. doi: 10.1038/s41467-021-21798-w

49. Hiltbrunner S, Mannarino L, Kirschner MB, Opitz I, Rigutto A, Laure A, et al. Tumor immune microenvironment and genetic alterations in mesothelioma. *Front Oncol* (2021) 11:660039. doi: 10.3389/fonc.2021.660039

50. Han G, Yang G, Hao D, Lu Y, Thein K, Simpson BS, et al. 9p21 loss confers a cold tumor immune microenvironment and primary resistance to immune checkpoint therapy. *Nat Commun* (2021) 12(1):5606. doi: 10.1038/s41467-021-25894-9

51. Zauderer MG. The therapeutic implications of the genomic analysis of malignant pleural mesothelioma. *Nat Commun* (2021) 12(1):1819. doi: 10.1038/s41467-021-22142-y

52. Hodi FS, Wolchok JD, Schadendorf D, Larkin J, Long GV, Qian X, et al. TMB and inflammatory gene expression associated with clinical outcomes following immunotherapy in advanced melanoma. *Cancer Immunol Res* (2021) 9(10):1202–13. doi: 10.1158/2326-6066.CIR-20-0983

53. Lei M, Siemers NO, Pandya D, Chang H, Sanchez T, Harbison C, et al. Analyses of PD-L1 and inflammatory gene expression association with efficacy of nivolumab ± ipilimumab in gastric Cancer/Gastroesophageal junction cancer. *Clin Cancer Res* (2021) 27(14):3926–35. doi: 10.1158/1078-0432.CCR-20-2790

54. Sangro B, Melero I, Wadhawan S, Finn RS, Abou-Alfa GK, Cheng AL, et al. Association of inflammatory biomarkers with clinical outcomes in nivolumabtreated patients with advanced hepatocellular carcinoma. *J Hepatol* (2020) 73(6):1460–9. doi: 10.1016/j.jhep.2020.07.026

55. Ollila H, Mäyränpää MI, Paavolainen L, Paajanen J, Välimäki K, Sutinen E, et al. Prognostic role of tumor immune microenvironment in pleural epithelioid mesothelioma. *Front Oncol* (2022) 12:870352. doi: 10.3389/fonc.2022.870352

56. Pittet MJ, Michielin O, Migliorini D. Clinical relevance of tumor-associated macrophages. *Nat Rev Clin Oncol* (2022) 19(6):402–21. doi: 10.1038/s41571-022-00620-6

57. Engblom C, Pfirschke C, Pittet MJ. The role of myeloid cells in cancer therapies. *Nat Rev Cancer* (2016) 16(7):447–62. doi: 10.1038/nrc.2016.54

58. Arlauckas SP, Garris CS, Kohler RH, Kitaoka M, Cuccarese MF, Yang KS, et al. *In vivo* imaging reveals a tumor-associated macrophage-mediated resistance pathway in anti-PD-1 therapy. *Sci Transl Med* (2017) 9(389):eaal3604. doi: 10.1126/scitranslmed.aal3604

59. Mantovani A, Marchesi F, Malesci A, Laghi L, Allavena P. Tumor-associated macrophages as treatment targets in oncology. *Nat Rev Clin Oncol* (2017) 14(7):399–416. doi: 10.1038/nrclinonc.2016.217

60. Duruisseaux M, Martínez-Cardús A, Calleja-Cervantes ME, Moran S, Castro de Moura M, Davalos V, et al. Epigenetic prediction of response to anti-PD-1 treatment in non-small-cell lung cancer: A multicentre, retrospective analysis. *Lancet Respir Med* (2018) 6(10):771–81. doi: 10.1016/S2213-2600(18)30284

61. Hugo W, Zaretsky JM, Sun L, Song C, Moreno BH, Hu-Lieskovan S, et al. Genomic and transcriptomic features of response to anti-PD-1 therapy in metastatic melanoma. *Cell* (2016) 165(1):35–44. doi: 10.1016/j.cell.2016.02.065

62. Jiang P, Gu S, Pan D, Fu J, Sahu A, Hu X, et al. Signatures of T cell dysfunction and exclusion predict cancer immunotherapy response. *Nat Med* (2018) 24(10):1550–8. doi: 10.1038/s41591-018-0136-1

63. Goswami S, Walle T, Cornish AE, Basu S, Anandhan S, Fernandez I, et al. Immune profiling of human tumors identifies CD73 as a combinatorial target in glioblastoma. *Nat Med* (2020) 26(1):39–46. doi: 10.1038/s41591-019-0694-x

64. Yoshida T, Ohe C, Ito K, Takada H, Saito R, Kita Y, et al. Clinical and molecular correlates of response to immune checkpoint blockade in urothelial carcinoma with liver metastasis. *Cancer Immunol Immunother* (2022) 71(11):2815–28. doi: 10.1007/s00262-022-03204-6

65. Fusco N, Vaira V, Righi I, Sajjadi E, Venetis K, Lopez G, et al. Characterization of the immune microenvironment in malignant pleural mesothelioma reveals prognostic subgroups of patients. *Lung Cancer* (2020) 150:53–61. doi: 10.1016/j.lungcan.2020.09.026

66. Mankor JM, Disselhorst MJ, Poncin M, Baas P, Aerts JGJV, Vroman H. Efficacy of nivolumab and ipilimumab in patients with malignant pleural mesothelioma is related to a subtype of effector memory cytotoxic T cells: Translational evidence from two clinical trials. *EBioMedicine* (2020) 62:103040. doi: 10.1016/j.ebiom.2020.103040

67. Chee SJ, Lopez M, Mellows T, Gankande S, Moutasim KA, Harris S, et al. Evaluating the effect of immune cells on the outcome of patients with mesothelioma. *Br J Cancer* (2017) 117(9):1341–8. doi: 10.1038/bjc.2017.269

68. Klampatsa A, O'Brien SM, Thompson JC, Rao AS, Stadanlick JE, Martinez MC, et al. Phenotypic and functional analysis of malignant mesothelioma tumor-infiltrating lymphocytes. *Oncoimmunology* (2019) 8(9):e1638211. doi: 10.1080/2162402X.2019.1638211

69. Mannarino L, Paracchini L, Pezzuto F, Olteanu GE, Moracci L, Vedovelli L, et al. Epithelioid pleural mesothelioma is characterized by tertiary lymphoid structures in long survivors: Results from the MATCH study. *Int J Mol Sci* (2022) 23(10):5786. doi: 10.3390/ijms23105786

70. Patil NS, Righi L, Koeppen H, Zou W, Izzo S, Grosso F, et al. Molecular and histopathological characterization of the tumor immune microenvironment in advanced stage of malignant pleural mesothelioma. *J Thorac Oncol* (2018) 13(1):124–33. doi: 10.1016/j.jtho.2017.09.1968

71. Schumacher TN, Thommen DS. Tertiary lymphoid structures in cancer. *Science* (2022) 375(6576):eabf9419. doi: 10.1126/science.abf9419

72. Vanhersecke L, Brunet M, Guégan JP, Rey C, Bougouin A, Cousin S, et al. Mature tertiary lymphoid structures predict immune checkpoint inhibitor efficacy in solid tumors independently of PD-L1 expression. *Nat Cancer* (2021) 2(8):794–802. doi: 10.1038/s43018-021-00232-6

73. Petitprez F, de Reyniès A, Keung EZ, Chen TW, Sun CM, Calderaro J, et al. B cells are associated with survival and immunotherapy response in sarcoma. *Nature* (2020) 577 (7791):556–60. doi: 10.1038/s41586-019-1906-8

74. Di Caro G, Bergomas F, Grizzi F, Doni A, Bianchi P, Malesci A, et al. Occurrence of tertiary lymphoid tissue is associated with T-cell infiltration and predicts better prognosis in early-stage colorectal cancers. *Clin Cancer Res* (2014) 20(8):2147–58. doi: 10.1158/1078-0432.CCR-13-2590

75. Griss J, Bauer W, Wagner C, Simon M, Chen M, Grabmeier-Pfistershammer K, et al. B cells sustain inflammation and predict response to immune checkpoint blockade in human melanoma. *Nat Commun* (2019) 10(1):4186. doi: 10.1038/s41467-019-12160-2

76. Helmink BA, Reddy SM, Gao J, Zhang S, Basar R, Thakur R, et al. B cells and tertiary lymphoid structures promote immunotherapy response. *Nature* (2020) 577 (7791):549–55. doi: 10.1038/s41586-019-1922-8

77. Cabrita R, Lauss M, Sanna A, Donia M, Skaarup Larsen M, Mitra S. Tertiary lymphoid structures improve immunotherapy and survival in melanoma. *Nature* (2020) 577(7791):561–5. doi: 10.1038/s41586-019-1914-8

78. Kazandjian D, Gong Y, Keegan P, Pazdur R, Blumenthal GM. Prognostic value of the lung immune prognostic index for patients treated for metastatic non-small cell lung cancer. *JAMA Oncol* (2019) 5(10):1481–5. doi: 10.1001/jamaoncol.2019.1747

79. Mezquita L, Auclin E, Ferrara R, Charrier M, Remon J, Planchard D, et al. Association of the lung immune prognostic index with immune checkpoint inhibitor outcomes in patients with advanced non-small cell lung cancer. *JAMA Oncol* (2018) 4 (3):351–7. doi: 10.1001/jamaoncol.2017.4771

80. Kuryk L, Rodella G, Staniszewska M, Pancer KW, Wieczorek M, Salmaso S, et al. Novel insights into mesothelioma therapy: Emerging avenues and future prospects. *Front Oncol* (2022) 12:916839. doi: 10.3389/fonc.2022.916839

81. Désage AL, Karpathiou G, Peoc'h M, Froudarakis ME. The immune microenvironment of malignant pleural mesothelioma: A literature review. *Cancers (Basel)* (2021) 13(13):3205. doi: 10.3390/cancers13133205

82. Sottile R, Tannazi M, Johansson MH, Cristiani CM, Calabroí L, Ventura V, et al. NK- and T-cell subsets in malignant mesothelioma patients: Baseline pattern and changes in the context of anti-CTLA-4 therapy. *Int J Cancer* (2019) 145(8):2238–48. doi: 10.1002/ijc.32363

83. Keir ME, Butte MJ, Freeman GJ, Sharpe AH. PD-1 and its ligands in tolerance and immunity. *Annu Rev Immunol* (2008) 26:677–704. doi: 10.1146/annurev.immunol.26.021607.090331

84. Dong H, Strome SE, Salomao DR, Tamura H, Hirano F, Flies DB, et al. Tumor-associated B7-H1 promotes T-cell apoptosis: A potential mechanism of immune evasion. *Nat Med* (2002) 8(8):793–800. doi: 10.1038/nm730

85. Thompson RH, Kuntz SM, Leibovich BC, Dong H, Lohse CM, Webster WS, et al. Tumor B7-H1 is associated with poor prognosis in renal cell carcinoma patients with long-term follow-up. *Cancer Res* (2006) 66(7):3381–85. doi: 10.1158/0008-5472.CAN-05-4303

86. Wang L, Ma Q, Chen X, Guo K, Li J, Zhang M. Clinical significance of B7-H1 and B7-1 expressions in pancreatic carcinoma. *World J Surg* (2010) 34(5):1059–65. doi: 10.1007/s00268-010-0448-x

87. Nakanishi J, Wada Y, Matsumoto K, Azuma M, Kikuchi K, Ueda S. Overexpression of B7-H1 (PD-L1) significantly associates with tumor grade and postoperative prognosis in human urothelial cancers. *Cancer Immunol Immunother* (2007) 56(8):1173–82. doi: 10.1007/s00262-006-0266-z

88. Desai A, Karrison P, Rose B, Tan Y, Hill B, Pemberton E, et al. Phase II trial of pembrolizumab (NCT02399371) in previously treated malignant mesothelioma: Final analysis. *J Thorac Oncol* (2018) 13(10):S339. doi: 10.1016/j.jtho.2018.08.277

89. Fujimoto N, Okada M, Kijima T, Aoe K, Kato T, Nakagawa K, et al. Clinical efficacy and safety of nivolumab in Japanese patients with malignant pleural mesothelioma: 3-year results of the MERIT study. *JTO Clin Res Rep* (2020) 2 (3):100135. doi: 10.1016/j.jtocrr.2020.100135

90. Addeo A, Friedlaender A, Banna GL, Weiss GJ. TMB or not TMB as a biomarker: That is the question. *Crit Rev Oncol Hematol* (2021) 163:103374. doi: 10.1016/j.critrevonc.2021.103374

91. Marcus L, Fashoyin-Aje LA, Donoghue M, Yuan M, Rodriguez L, Gallagher PS, et al. FDA Approval summary: Pembrolizumab for the treatment of tumor mutational burden-high solid tumors. *Clin Cancer Res* (2021) 27(17):4685–89. doi: 10.1158/1078-0432.CCR-21-0327

92. Marabelle A, Fakih M, Lopez J, Shah M, Shapira-Frommer R, Nakagawa K, et al. Association of tumor mutational burden with outcomes in patients with advanced solid tumors treated with pembrolizumab: Prospective biomarker analysis of the multicohort, open-label, phase 2 KEYNOTE-158 study. *Lancet Oncol* (2020) 21(10):1353–65. doi: 10.1016/S1470-2045(20)30445-9

93. Rovers S, Janssens A, Raskin J, Pauwels P, van Meerbeck JP, Smits E, et al. Recent advances of immune checkpoint inhibition and potential for (Combined) TIGIT blockade as a new strategy for malignant pleural mesothelioma. *Biomedicines* (2022) 10(3):673. doi: 10.3390/biomedicines10030673

94. Zalcman G, Mazieres J, Greillier L, Brosseau S, Lantuejoul S, Do P, et al. Second or third line nivolumab versus nivolumab plus ipilimumab in malignant pleural mesothelioma patients: Long-term results of the IFCT-1501 MAPS2 randomized phase 2 trial with a focus on hyperprogression. *Ann Oncol* (2019) 30(suppl 5):747. doi: 10.1093/annonc/mdz266

95. Khanna S, Graef S, Mussai F, Thomas A, Wali N, Yenidunya BG, et al. Tumor-derived GM-CSF promotes granulocyte immunosuppression in mesothelioma patients. *Clin Cancer Res* (2018) 24(12):2859–72. doi: 10.1158/1078-0432.CCR-17-3757

96. Muller S, Lai WV, Adusumilli PS, Desmeules P, Frosina D, Jungbluth A, et al. V-Domain ig-containing suppressor of T-cell activation (VISTA), a potentially targetable immune checkpoint molecule, is highly expressed in epithelioid malignant pleural mesothelioma. *Mod Pathol* (2020) 33(2):303–11. doi: 10.1038/s41379-019-0364-z

97. Chung YS, Kim M, Cha YJ, Kim KA, Shim HS. Expression of V-set immunoregulatory receptor in malignant mesothelioma. *Mod Pathol* (2020) 33:263–70. doi: 10.1038/s41379-019-0328-3

98. Van Den Ende T, Van Den Boorn HG, Hoonhout NM, Van Etten-Jamaludin FS, Meijer SL, Derks S, et al. Priming the tumor immune microenvironment with chemo (radio)therapy: A systematic review across tumor types. *Biochim Biophys Acta Rev Cancer* (2020) 1874(1):188386. doi: 10.1016/j.bbcan.2020.188386

frontiers | Frontiers in Immunology

TYPE Clinical Trial
PUBLISHED 16 February 2023
DOI 10.3389/fimmu.2023.1112960

OPEN ACCESS

EDITED BY
Christophe Blanquart,
Centre National de la Recherche Scientifique (CNRS), France

REVIEWED BY
Fonteneau Jean-francois,
UMR1307 Centre de Recherche en Cancérologie et Immunologie Intégré Nantes Angers (CRCI2NA) (INSERM), France
Luciano Castiello,
National Institute of Health (ISS), Italy

*CORRESPONDENCE
Prasad S. Adusumilli
adusumip@mskcc.org

†These authors have contributed equally to this work and share first authorship

SPECIALTY SECTION
This article was submitted to Cancer Immunity and Immunotherapy, a section of the journal Frontiers in Immunology

RECEIVED 30 November 2022
ACCEPTED 06 February 2023
PUBLISHED 16 February 2023

CITATION
Chintala NK, Choe JK, McGee E, Bellis R, Saini JK, Banerjee S, Moreira AL, Zauderer MG, Adusumilli PS and Rusch VW (2023) Correlative analysis from a phase I clinical trial of intrapleural administration of oncolytic vaccinia virus (Olvi-vec) in patients with malignant pleural mesothelioma.
Front. Immunol. 14:1112960.
doi: 10.3389/fimmu.2023.1112960

Correlative analysis from a phase I clinical trial of intrapleural administration of oncolytic vaccinia virus (Olvi-vec) in patients with malignant pleural mesothelioma

Navin K. Chintala[1†], Jennie K. Choe[1†], Erin McGee[1], Rebecca Bellis[1], Jasmeen K. Saini[1], Srijita Banerjee[1], Andre L. Moreira[2], Marjorie G. Zauderer[3], Prasad S. Adusumilli[1,4*] and Valerie W. Rusch[1]

[1]Thoracic Service, Department of Surgery, Memorial Sloan Kettering Cancer Center, New York, NY, United States, [2]Department of Pathology, New York University (NYU) Grossman School of Medicine, New York, NY, United States, [3]Thoracic Oncology Service, Department of Medicine, Memorial Sloan Kettering Cancer Center, New York, NY, United States, [4]Center for Cell Engineering, Memorial Sloan Kettering Cancer Center, New York, NY, United States

Background: The attenuated, genetically engineered vaccinia virus has been shown to be a promising oncolytic virus for the treatment of patients with solid tumors, through both direct cytotoxic and immune-activating effects. Whereas systemically administered oncolytic viruses can be neutralized by pre-existing antibodies, locoregionally administered viruses can infect tumor cells and generate immune responses. We conducted a phase I clinical trial to investigate the safety, feasibility and immune activating effects of intrapleural administration of oncolytic vaccinia virus (NCT01766739).

Methods: Eighteen patients with malignant pleural effusion due to either malignant pleural mesothelioma or metastatic disease (non-small cell lung cancer or breast cancer) underwent intrapleural administration of the oncolytic vaccinia virus using a dose-escalating method, following drainage of malignant pleural effusion. The primary objective of this trial was to determine a recommended dose of attenuated vaccinia virus. The secondary objectives were to assess feasibility, safety and tolerability; evaluate viral presence in the tumor and serum as well as viral shedding in pleural fluid, sputum, and urine; and evaluate anti-vaccinia virus immune response. Correlative analyses were performed on body fluids, peripheral blood, and tumor specimens obtained from pre- and post-treatment timepoints.

Results: Treatment with attenuated vaccinia virus at the dose of 1.00E+07 plaque-forming units (PFU) to 6.00E+09 PFU was feasible and safe, with no treatment-associated mortalities or dose-limiting toxicities. Vaccinia virus was detectable in tumor cells 2-5 days post-treatment, and treatment was associated with a decrease in tumor cell density and an increase in immune cell density as

assessed by a pathologist blinded to the clinical observations. An increase in both effector (CD8+, NK, cytotoxic cells) and suppressor (Tregs) immune cell populations was observed following treatment. Dendritic cell and neutrophil populations were also increased, and immune effector and immune checkpoint proteins (granzyme B, perforin, PD-1, PD-L1, and PD-L2) and cytokines (IFN-γ, TNF-α, TGFβ1 and RANTES) were upregulated.

Conclusion: The intrapleural administration of oncolytic vaccinia viral therapy is safe and feasible and generates regional immune response without overt systemic symptoms.

Clinical trial registration: https://clinicaltrials.gov/ct2/show/NCT01766739, identifier NCT01766739.

KEYWORDS

pleural cancers, oncolytic viral therapy, tumor microenvironment, regional therapy, malignant pleural effusion (MPE)

Introduction

With an estimated annual incidence of at least 150,000 patients in the United States, malignant pleural effusions (MPEs) occur in 15% of all patients with cancer during the course of their disease (1). In addition to causing symptoms that limit quality of life, such as shortness of breath that requires interventions (2), the presence of MPE represents advanced cancer and contributes to poor prognosis (3). Palliative interventions have been the mainstay for symptomatic relief and prevention of MPE recurrence that can interrupt cancer therapy in patients with MPE (2, 4). There has been limited success following systemic immune checkpoint inhibitor agent therapy, chemotherapy or a combination of chemo immunotherapies in patients with MPE (5, 6). Intrapleural biological therapies, such as oncolytic viral therapy and chimeric antigen receptor (CAR) T-cell therapy, have been investigated to promote effector immune responses in patients with MPEs (7–10). However, local immune suppressive mechanisms in MPEs that inhibit the efficacy of effector immune responses have been well described (11, 12). Specifically, macrophages and TGFβ in MPEs have been shown to play a pivotal role in hampering the antitumor immune responses (11, 13). Correlative analysis of pre- and post-treatment MPEs and pleural tumor biopsies to characterize the effector and suppressor immune responses following intrapleural therapies can shed light on changes in the immune microenvironment and aid in developing regimens to further enhance functional efficacy.

Malignant pleural mesothelioma (MPM), metastatic non-small cell lung cancer, and breast cancers are common causes of MPEs. Malignant pleural mesothelioma is a rare cancer with diffuse involvement of the pleural cavity. Immune checkpoint inhibitors have shown promising results in patients with MPM; however, the increase in survival is limited to mostly biphasic and sarcomatoid forms of MPM (14, 15). Epithelioid MPM, the most common form of MPM, is known to have the lowest tumor mutational burden and PD-L1 expression among solid tumors (16), with equivalent survival compared to chemotherapy (15). Regional oncolytic viral therapies that can generate effector immune responses in patients with MPM may provide an opportunity for subsequent immune checkpoint inhibitor agent therapy (17).

Oncolytic viruses, which selectively infect and exert cytopathic effects on tumor cells, are a potential therapeutic option for MPM. As a member of the poxvirus family of the genus orthopoxvirus, the vaccinia virus is one such oncolytic virus that possesses multiple favorable features for use as a therapeutic agent. It exhibits rapid cell-to-cell spread, is cytolytic across a broad range of tumor cell types, has a large insertion capacity for exogenous genes, and is genetically stable with low potential for mutagenesis (18). It is amenable to large-scale manufacture, storage and production, and is safe to administer intravenously (19).

In *in vitro* studies, the vaccinia virus has shown to be efficient in killing multiple cancer cell lines, including breast, lung, thyroid, prostate, pancreas, squamous cell carcinoma, and MPM (20). In *in vivo* studies, the vaccinia virus has caused tumor elimination in mouse models of breast cancer and MPM, as well as tumor growth inhibition in mouse models of lung adenocarcinoma, anaplastic thyroid cancer (21), prostate cancer (22), ovarian cancer, pancreatic cancer, and melanoma (23). Isolated case reports have documented complete remission in a patient with multiple myeloma (24) and a patient with chronic lymphocytic leukemia (25, 26) following vaccinia virus administration. Vaccinia virus has also been used in phase I clinical trials to treat patients with bladder cancer (27), metastatic melanoma (28), and advanced hepatocellular carcinoma (29, 30).

We conducted a single-center phase I clinical trial (NCT01766739) to study the intrapleural administration of attenuated vaccinia virus

(GL-ONC1, Genelux Corporation) in patients with MPEs due to MPM or metastatic disease (non-small cell lung cancer or breast cancer). In 2019, the United States Adopted Names Council (USAN) granted Genelux adoption of the name *Olvimulogene nanivacirepvec* (referred to as Olvi-vec) in place of the name GL-ONC1; henceforth referred to as Olvi-vec throughout the manuscript.

Materials and methods

Trial design and patients

An open-label, dose-escalating, non-randomized, single-center phase I study was conducted to study the intrapleural administration of attenuated vaccinia virus (Olvi-vec) as a bolus. Olvi-vec was administered either as a single dose or as three consecutive daily doses to patients with a histologically or cytologically documented diagnosis of MPE, as detailed in the study protocol (Supplementary Material).

Study oversight

The study protocol and amendments were approved by the Memorial Sloan Kettering Cancer Center Institutional Review Board (IRB# 12-169, NCT01766739). All patients provided written informed consent to participate in the study, and all response and toxicity outcomes were documented. Patients were enrolled in groups of three and individually assessed for safety and dose-limiting toxicity. Inclusion and exclusion criteria are listed in the protocol (Supplementary Material). Patients were treated following the diagnosis of histologically or cytologically documented MPEs (due to primary non-small-cell lung carcinoma, MPM, and other histologies) and had free pleural space (partial or total) that permitted intrapleural drug instillation.

Olvi-vec manufacturing

A genetically engineered vaccinia virus, designated as GLV-1h68, was used in preclinical investigation. GLV-1h68 was derived from the LIVP strain by inserting *RUC-GFP* (a fusion gene of *Renilla* luciferase and green fluorescent protein), *LacZ* (beta-galactosidase), and *gusA* (beta-glucuronidase) expression cassettes into *F14.5L* (located between *F14L* and *F15L*), thymidine kinase (TK), and hemagglutinin loci, respectively. Disruption of these non-essential genes and expression of the foreign gene expression cassettes not only attenuated the virus but also enhanced its tumor-specific targeting. The GMP-derived material of this same virus is called Olvi-vec. Olvi-vec has been used primarily for all safety pharmacology and toxicological experiments, as well as for *in vitro* potency comparisons (in cell cultures) and *in vivo* potency comparisons (in tumorous animals). Details of the virus manufacturing process and analyses are described in the study protocol (Supplementary Material).

Intrapleural treatment

Eligible patients were admitted into the hospital for treatment on protocol. The pleural effusion was drained *via* insertion of a chest tube or pleural catheter (PleurX^{TM} Catheter, Becton, Dickinson and Company, Franklin Lakes, NJ). A chest CT scan was performed to document drainage of the effusion and to assess the extent of pleural disease. Within 72 hours of the CT scan, the virus was instilled as a bolus into the pleural space *via* the chest tube or pleural catheter. Up to 150 ml of additional saline was used to flush the chest tube or pleural catheter to ensure that all the treatment drug was instilled into the pleural space. The chest tube or pleural catheter was left clamped for 4 hours (+/- 1 hour), after which it was reopened and placed to drainage in order to drain the pleural space. As dictated by the patient's clinical status, the chest tube was either left inserted or removed until the surgical procedure (video-assisted thoracoscopic surgery, VATS) was performed 2-7 days after treatment to collect MPE and obtain pleural biopsy.

Study objectives and assessment

The primary objective of this study was to determine a recommended dose of Olvi-vec. The secondary objectives included the assessment of feasibility, safety and tolerability, evaluation of viral presence in the tumor, pleural fluid, serum, sputum, and urine, and evaluation of anti-vaccinia virus immune response. All patients were included in the reporting of adverse events (AEs). The safety of Olvi-vec was assessed by the evaluation of the type, frequency, and severity of AEs, changes in clinical laboratory tests (hematological and chemistry), immunogenicity, and physical examination. All AEs and laboratory toxicities were graded using the Common Terminology Criteria for Adverse Events (National Cancer Institute, version 4.0). Laboratory testing was performed at baseline (i.e., within 14 days before treatment), daily during the first 3 days after treatment, and at termination of study (day 60 ± 5).

Hematoxylin and eosin staining

Hematoxylin and eosin staining was performed on FFPE blocks of tumor biopsies collected before (pre-treatment) and 2-5 days after (post-treatment) Olvi-vec therapy. Semi-quantitative scoring of tumor cell density and immune cell density (0: very low density; 1: low density; 2: moderate density; 3: high density) was performed by a primary and secondary pathologist who were blinded to sample identity.

Multiplex immunofluorescence staining

Multiplex immunofluorescence (mIF) staining was performed on tumor biopsies collected before (pre-treatment) and 2-5 days after (post-treatment) Olvi-vec therapy. Formalin-fixed and

paraffin-embedded (FFPE) blocks were cut into sections of 5 μm thickness. Sections from each biopsy were stained with antibodies (Supplementary Table 1) using the Opal™ 7-Color Kit for Multiplex Immunohistochemistry (Akoya Biosciences, Marlborough, MA). After mIF staining, slides were scanned using the Vectra® 3.0 Automated Quantitative Pathology Imaging System (PerkinElmer Inc., Hopkinton, MA). Quantitative assessment of cell markers was performed using inForm® software (version 2.2.1, PerkinElmer Inc., Hopkinton, MA). Cell segmentation and phenotyping algorithms were reviewed and confirmed by study pathologists.

Viral plaque assay and vaccinia virus neutralization assay

Viral plaque assays were performed on body fluid samples (blood, sputum, urine, pleural fluid) collected from patients immediately before and 24, 48, 72, and 96 hours after Olvi-vec treatment to assess for the presence of viral particles. Post-treatment tumor biopsies collected 2-5 days after treatment also underwent assessment for viral particles using viral plaque assays. In brief, patient samples were plated on confluent layers of CV-1 cells. Evaluation of virus infection was done by visual assessment of viral plaque in wells with both CV-1 cells and patient samples. Additionally, post-treatment serum samples obtained from patients 60 days after Olvi-vec treatment were assessed for the presence of Olvi-vec neutralizing antibodies *via* standard vaccinia virus neutralization assay and compared to corresponding pre-treatment serum samples.

Effusion and pleural biopsy analysis

Pleural fluid and serum samples were obtained from patients both pre-treatment (baseline) and post-treatment (at 24, 48, 72, and 96 hours, and on days 2, 3, and 60). All specimens available were assessed for a panel of effector and suppressive cytokines using a 41-plex MILLIPLEX® MAP Human Cytokine/Chemokine kit (MilliporeSigma, Burlington, MA). The kit was run on a Luminex® 100/200™ System (Luminex Corporation, Austin, TX).

Values represent the mean of the duplicate wells ± standard deviation. These data were analyzed using IS 2.3 software (Luminex Software, Inc., Riverside, CA), Microsoft Excel and GraphPad Prism. Additionally, RNA isolation was performed on FFPE sections of tumor biopsies taken pre- and post-treatment using the RNeasy® FFPE Kit in accordance with the manufacturer's protocol (Qiagen, Germantown, MD). RNA concentration and purity were measured using the NanoDrop™ 2000/2000c Spectrophotometer (Thermo Scientific, Waltham, MA). RNA profiling was performed using the nCounter® PanCancer Immune Profiling Panel by NanoString Technologies, Inc. (Seattle, WA).

Statistical analyses

The sample size was based on a standard dose-escalation design. All statistical tests were two-sided, and statistical significance was defined as $p<0.05$. Data with normal distribution was assessed using paired t-test. Data without normal distribution was assessed using Wilcoxon matched-pairs signed-rank test. Analyses were conducted using R 4.1.2 (R Foundation for Statistical Computing, Vienna, Austria).

Results

Patient characteristics

From February 2013 to April 2015, 18 patients were enrolled who were treated in a dose-escalating fashion (Table 1). Fifteen

TABLE 1 Clinical characteristics of patients treated in the phase I trial.

Patient ID	Age	Sex	Diagnosis	Histologic subtype	Previous regimens	Cohort	Dose (PFU)	# of doses
1	M	78	MPM	Epithelioid	None	1	1.00E+07	1
2	M	59	NSCLC	SCC	Chemotherapy	1	1.00E+07	1
3	M	73	MPM	Epithelioid	None	1	1.00E+07	1
4	M	54	MPM	Epithelioid	None	1	1.00E+07	1
5	M	62	MPM	Epithelioid	None	2	1.00E+08	1
6	M	74	MPM	Epithelioid	None	2	1.00E+08	1
7	M	74	NSCLC	ADC	Chemoradiotherapy	2	1.00E+08	1
8	F	63	MPM	Epithelioid	None	3	1.00E+09	1
9	M	81	MPM	Epithelioid	None	3	1.00E+09	1
10	M	76	MPM	Epithelioid	Chemotherapy	3	1.00E+09	1

(Continued)

TABLE 1 Continued

Patient ID	Age	Sex	Diagnosis	Histologic subtype	Previous regimens	Cohort	Dose (PFU)	# of doses
11	F	51	MPM	Sarcomatoid	None	4	3.00E+09	1
12	F	43	TNBC		Neoadjuvant chemotherapy, surgery, adjuvant hormone therapy	4	3.00E+09	1
13	M	67	MPM	Biphasic	None	4	3.00E+09	1
14	M	74	MPM	Epithelioid	None	4 (expansion)	3.00E+09	1
15	M	70	MPM	Epithelioid	None	5	3.00E+09	3
16	F	67	MPM	Epithelioid	None	5	3.00E+09	3
17	M	79	MPM	Epithelioid	None	5	3.00E+09	3
18	F	47	MPM	Epithelioid	None	6	6.00E+09	3

ADC, adenocarcinoma; MPM, malignant pleural mesothelioma; NSCLC, non-small cell lung cancer; PFU, plaque-forming units; SCC, squamous cell carcinoma; TNBC, triple negative breast cancer.

patients had MPM (13 epithelioid, 1 biphasic, and 1 sarcomatoid), 2 had non-small cell lung cancer (1 adenocarcinoma and 1 squamous cell carcinoma), and 1 had triple negative breast cancer. 5 out of 18 patients were female, and the mean age of all patients was 66 years. All 3 patients with NSCLC or breast cancer and 1 patient with MPM had received previous lines of therapy.

Feasibility and safety

Attenuated vaccinia virus (Olvi-vec) was administered intrapleurally as a bolus through a pleural catheter after complete evacuation of pleural effusion in all patients (Figure 1). The intrapleural administration of vaccinia virus was feasible, and there were no failures in administration of the agent. Table 2 lists the adverse events that occurred at any grade (1–4) in ≥15% of the total cohort (n=18), up to day 60 post-treatment.

There was 1 reversible grade-4 laboratory abnormality (hypocalcemia). The most frequent grade 3 adverse events were lymphopenia (3 patients, 17%), fatigue (2 patients, 11%), and hypophosphatemia (2 patients, 11%). The most frequent grade 2 adverse events were anemia (5 patients, 28%), hyperglycemia (5 patients, 28%), and fever (4 patients, 22%). There were no dose-limiting toxicities, and maximally tolerated dose was not reached. As a result, the primary objective of establishing a recommended dose was not reached.

Vaccinia detection and qualitative assessment of treatment effect in tumor

Resected post-treatment samples from 14 patients were stained by immunohistochemistry with an antibody against Olvi-vec (A27L). Positive cytoplasmic expression was observed in 7 of 14 specimens (representative images shown in Figures 2A, B). When the A27L antibody was tested in a multiplex immunofluorescence panel with anti-mesothelin antibody on pre- and post-treatment specimens from Patient #16, cytoplasmic expression of Olvi-vec was observed in the post-treatment specimen but not the pre-treatment specimen (representative images shown in Figure 2C).

Resected samples from 13 patients were stained by multiplex immunofluorescence with a panel of antibodies against mesothelin (MSLN), CD3, CD4, CD8, and FoxP3. 4 patients had matched pre- and post-treatment specimens, and 9 patients had post-treatment specimens only. The density of MSLN+ tumor cells was qualitatively observed to decrease and the density of CD3+ immune cells was qualitatively observed to increase from pre-treatment to post-treatment specimens (representative images shown in Figure 2D).

Quantitative assessment of treatment effect in tumor

Resected samples from 16 patients were stained with hematoxylin and eosin and independently scored semi-quantitatively for tumor-cell density and immune-cell density by two pathologists (Table 3). Four patients had matched pre- and post-treatment specimens, and 12 patients had post-treatment specimens only. When matched tumor specimens were compared (n=4), tumor cell density score decreased from pre-treatment to post-treatment in all patients (Figure 3). Immune cell density score increased from pre-treatment to post-treatment in 3 of 4 patients. Among all post-treatment tumor specimens (n=16), the average score per high power field (1 mm^2) was lower for tumor cell density compared to immune cell density.

When matched tumor specimens were stained using multiplex immunofluorescence and then compared (n=4), mean CD8+ cells per mm^2 increased in 3 of 4 patients (Figure 4). Mean MSLN+ tumor cells per mm^2 decreased from pre-treatment to post-treatment in all patients. Comparing available pre-treatment specimens to all post-treatment specimens (n=13), mean CD8+ cells increased and mean MSLN+ tumor cells decreased, although neither achieved statistical significance (Figure 5).

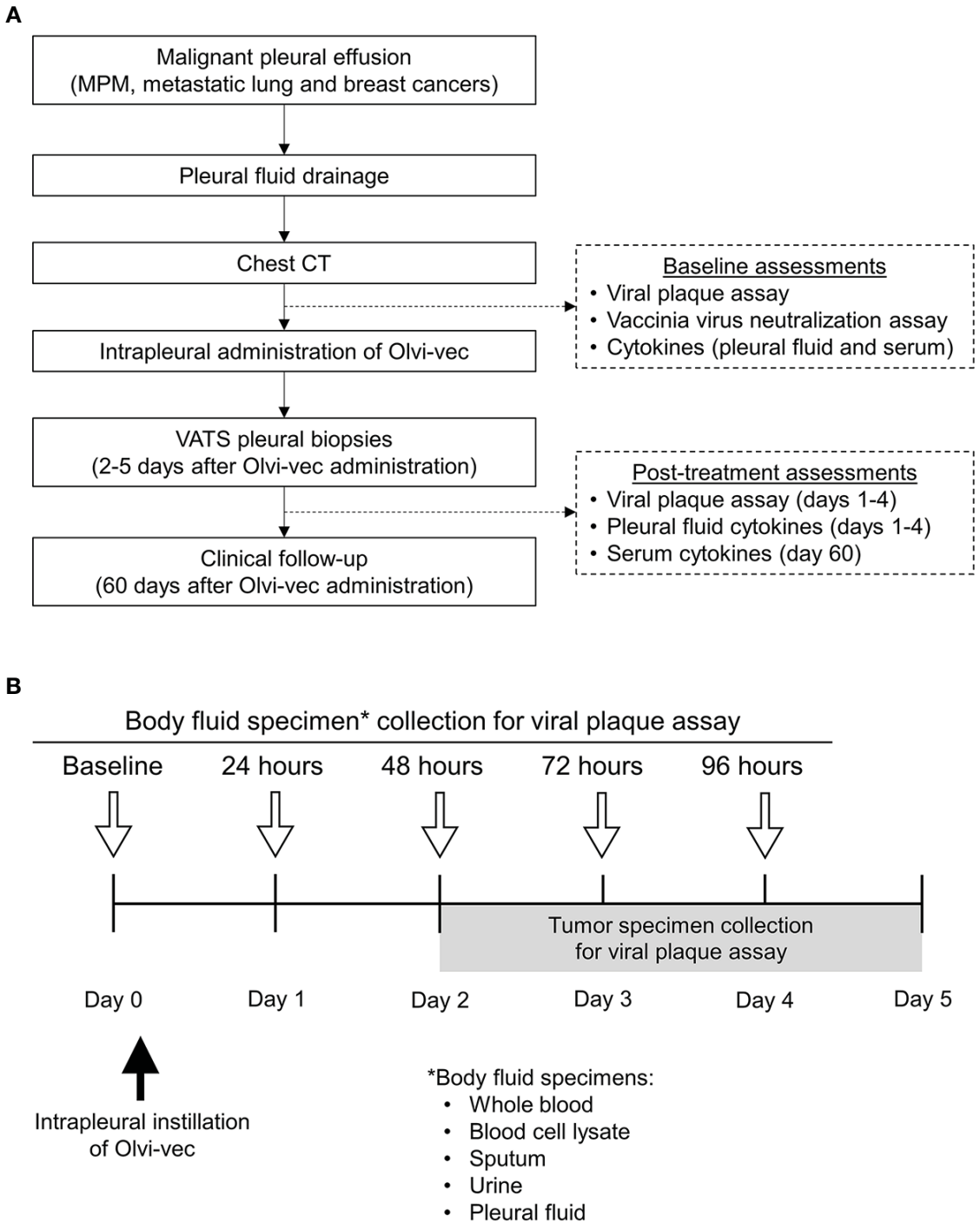

FIGURE 1
Protocol schema **(A)** and specimen collection schema for viral plaque assay **(B)**. *List of specimens collected.

Gene expression analysis of pre- and post-treatment tumor specimens (n=16), using nCounter immune cell type scoring module, revealed increased scores (i.e., change in score by 1 unit, indicating twice the abundance of that cell type) for CD45+, Th1+, Tregs, CD8+, exhausted CD8+, NK+, cytotoxic cells, dendritic cells, macrophage, and neutrophil immune cell populations in post-treatment tumor specimens compared to pre-treatment specimens (Figure 6). Similarly, scoring of individual protein mRNA levels pre- and post-treatment tumor specimens (n=13) revealed increased scores in immune effector proteins (IFN-γ, granzyme B, perforin), immune suppressive proteins (TGFβ, FoxP3), and immune checkpoint regulatory proteins (PD-1, PD-L1, PD-L2) following treatment (Figure 7). The data discussed in this publication have been deposited in NCBI's Gene Expression Omnibus (31) and are accessible through GEO Series accession number GSE223395 (https://www.ncbi.nlm.nih.gov/geo/query/acc.cgi?acc=GSE223395).

10.3389/fimmu.2023.1112960

TABLE 2 Adverse events that occurred during the phase I trial (n=18).

Adverse event*	Any grade (%)	Grade 3 (%)	Grade 4 (%)
Hyperglycemia	18 (100%)	1 (6%)	0 (0%)
Anemia	17 (94%)	1 (6%)	0 (0%)
Hypocalcemia	13 (72%)	0 (0%)	1 (6%)
Hypoalbuminemia	13 (72%)	0 (0%)	0 (0%)
Pain	12 (67%)	0 (0%)	0 (0%)
Fatigue	11 (61%)	2 (11%)	0 (0%)
Fever	8 (44%)	0 (0%)	0 (0%)
Elevated ALT	7 (39%)	1 (6%)	0 (0%)
Nausea	7 (39%)	0 (0%)	0 (0%)
Chills	7 (39%)	0 (0%)	0 (0%)
General disorders and administration site conditions	6 (33%)	0 (0%)	0 (0%)
Hypophosphatemia	5 (28%)	2 (11%)	0 (0%)
Dyspnea	5 (28%)	1 (6%)	0 (0%)
Sinus tachycardia	5 (28%)	0 (0%)	0 (0%)
Hyperkalemia	5 (28%)	0 (0%)	0 (0%)
Elevated alkaline phosphate	5 (28%)	0 (0%)	0 (0%)
Flu-like symptoms	5 (28%)	0 (0%)	0 (0%)
Headache	5 (28%)	0 (0%)	0 (0%)
Elevated AST	4 (22%)	1 (6%)	0 (0%)
Thrombocytopenia	4 (22%)	0 (0%)	0 (0%)
Hyponatremia	4 (22%)	0 (0%)	0 (0%)
Elevated INR	4 (22%)	0 (0%)	0 (0%)
Lymphopenia	3 (17%)	3 (17%)	0 (0%)
Leukopenia	3 (17%)	0 (0%)	0 (0%)
Myalgia	3 (17%)	0 (0%)	0 (0%)
Generalized muscle weakness	3 (17%)	0 (0%)	0 (0%)
Diarrhea	3 (17%)	0 (0%)	0 (0%)

*Shown are adverse events that occurred in 15% or more of the study population up to day 60 post-treatment.
ALT, alanine aminotransferase; AST, aspartate aminotransferase; INR, international normalized ratio.

Vaccinia detection in body fluids and anti-vaccinia immune response

Vaccinia virus was detectable by viral plaque assay in the pleural fluid of 7 patients (Table 4A). Vaccinia was initially detected in pleural fluid at the dose 1.00E8 PFU (Cohort 2) and exhibited dose-dependent increase in PFU/mL in Cohorts 3, 4, 5, and 6. Viral plaque assay was also positive for vaccinia in the post-treatment tumor lysate of 4 patients. There was minimal viral shedding into other compartments, as shown by low positivity in the urine of 2 patients, blood lysate of 1 patient, and sputum of 1 patient (Table 4B). Of note, among patients who received multiple doses of Olvi-vec (Cohorts 5 and 6), significant increase in the number of plaque-forming units was observed in the pleural fluid of 2 patients.

Among 7 patients whose baseline serum was available to perform vaccinia virus neutralization assay, 4 patients had low levels of anti-vaccinia neutralizing antibodies pre-treatment, and 3 had no neutralizing antibodies (Table 5). Five of the patients had high levels of neutralizing antibodies at day 60 post-treatment.

Pleural fluid and serum cytokine analysis

Luminex analysis of pleural fluid specimens from baseline to up to 96 hours following treatment indicated significant increase in the levels of the following cytokines by 48 hours: IFN-γ, TNF-α, VEGF, IL-1ra, IL-1β, and IP-10 (Figure 8). In contrast, analysis of serum specimens showed an increase only in IL-8 levels from baseline to

10.3389/fimmu.2023.1112960

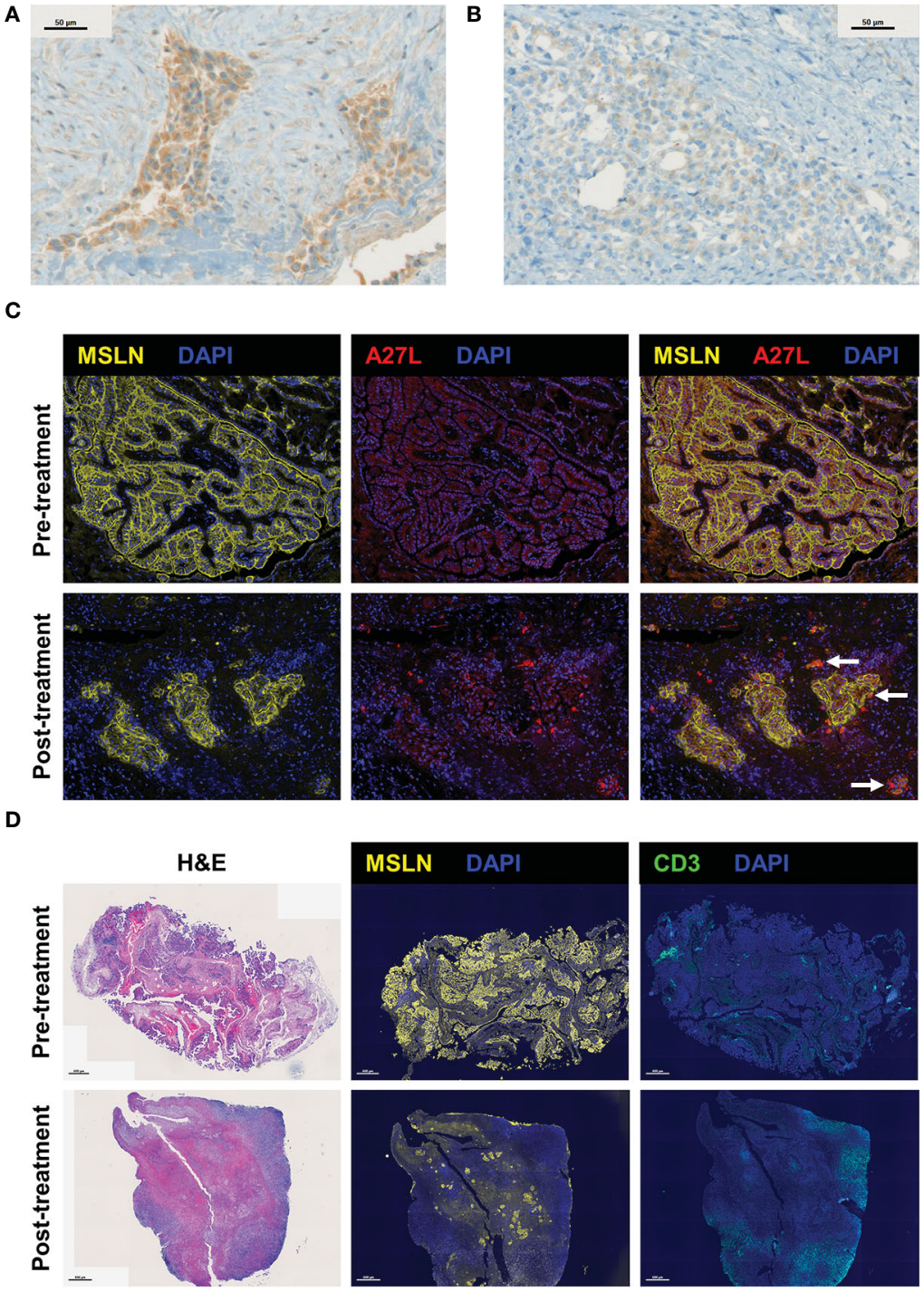

FIGURE 2
Visualization of Olvi-vec within tumor cells and the immune cell infiltrate in malignant pleural mesothelioma (MPM) tumors following Olvi-vec treatment. **(A)** Representative image of an immunohistochemistry (IHC)-stained section of a post-treatment tumor specimen from Patient #1 showing cytoplasmic positivity for Olvi-vec. **(B)** Representative image of an IHC-stained section from Patient #1 nine months later, showing weak/absent Olvi-vec staining. **(C)** Representative multiplex immunofluorescence (mIF) images of pre- and post-treatment tumor specimens from Patient #16, stained with anti-mesothelin and A27L (anti-Olvi-vec) antibodies. Arrows indicate tumor cells with cytoplasmic positivity for Olvi-vec, which are observed in the post-treatment specimen but not the pre-treatment specimen. **(D)** Representative images of pre- and post-treatment tumor specimens from Patient #16 stained with hematoxylin and eosin (H&E) (left panel), anti-mesothelin (MSLN) antibody (middle panel), and anti-CD3 antibody (right panel) in three consecutive cut sections. In the post-treatment specimen compared to pre-treatment, the density of tumor cells positive for MSLN is observed to be lower, and the density of immune cells positive for CD3 is observed to be higher.

10.3389/fimmu.2023.1112960

TABLE 3 Tumor and immune cell scoring of tumor specimens stained with hematoxylin and eosin.

Patient	Pathology	Cohort	Dose (PFU)	# of doses	Pre-treatment specimen		Post-treatment specimen	
					Tumor cells	Immune cells	Tumor cells	Immune cells
1	MPM (epithelioid)	1	1.00E+07	1	–	–	1	3
2	NSCLC (SCC)	1	1.00E+07	1	–	–	1	1
3	MPM (epithelioid)	1	1.00E+07	1	–	–	3	3
4	MPM (epithelioid)	1	1.00E+07	1	–	–	0	3
5	MPM (epithelioid)	2	1.00E+08	1	–	–	2	2
6	MPM (epithelioid)	2	1.00E+08	1	–	–	3	3
7	NSCLC (ADC)	2	1.00E+08	1	–	–	–	–
8	MPM (epithelioid)	3	1.00E+09	1	–	–	–	–
9	MPM (epithelioid)	3	1.00E+09	1	–	–	3	3
10	MPM (epithelioid)	3	1.00E+09	1	–	–	2	3
11	MPM (sarcomatoid)	4	3.00E+09	1	–	–	3	3
12	TNBC	4	3.00E+09	1	–	–	2	0
13	MPM (biphasic)	4	3.00E+09	1	3	2	1	3
14	MPM (epithelioid)	4 (expansion)	3.00E+09	1	2	1	0	0
15	MPM (epithelioid)	5	3.00E+09	3	–	–	3	3
16	MPM (epithelioid)	5	3.00E+09	3	2	1	1	3
17	MPM (epithelioid)	5	3.00E+09	3	–	–	1	3
18	MPM (epithelioid)	6	6.00E+09	3	3	0	2	2

– Insufficient sample
ADC, adenocarcinoma; MPM, malignant pleural mesothelioma; NSCLC, non-small cell lung cancer; PFU, plaque-forming units; SCC, squamous cell carcinoma; TNBC, triple negative breast cancer.

day 3 following treatment (p=0.0065; Figure 8). By day 60, only RANTES (CCL5) was found to be significantly elevated in serum compared to baseline (p=0.0276; Figure 9).

Long-term outcomes

All patients received subsequent other therapies as determined by treating physician following participation in the trial. Among all patients, median overall survival (OS) was 19.5 months. The median OS among patients who had MPM was 22 months (Figure 10). One patient with epithelioid MPM is alive; 87 months after treatment, the patient received other treatments that are standard of care for patients with MPM.

Discussion

Our phase I study of intrapleural oncolytic viral therapy is based on strong rationale developed in preclinical models of malignant pleural mesothelioma (32–34). The strength of our phase I study is the correlative analysis performed on pre- and post-treatment pleural effusions and pleural biopsies along with systemic immune response assessment by cytokine analysis following intrapleural oncolytic viral therapy. Intrapleural administration of Olvi-vec treatment is feasible, safe, and associated with induction of effector immune responses. All patients received treatment with the established dose *via* intrapleural delivery. Olvi-vec was detected using direct and indirect methods in resected tumor specimens and pleural fluid collected post-treatment. The treatment was safe, with one grade 4 laboratory abnormality and no treatment-associated mortalities noted. There were no dose-limiting toxicities or dose de-escalations, and the maximally tolerated dose was not reached. Therefore, a recommended dose was not established. Presence of the vaccinia virus within tumor cells was detectable 2-5 days after treatment and associated with local reduction in tumor cell density and an increase in immune cell density. Specifically, CD8+ T-cell density increased, indicating the generation of treatment-induced immunogenicity. Gene expression analysis showed increases in multiple immune cell populations (including CD8+, CD45+, Th1 +, Tregs, NK cells, macrophages, neutrophils, dendritic cells, and cytotoxic cells), as well as increased concentration of effector proteins, immune checkpoint proteins, and cytokines in post-treatment tumor and pleural fluid samples. Viral shedding outside the pleural compartment was observed in only 4 patients. The number of plaque-forming units in pleural fluid was significantly increased in 2 patients who received multiple doses of Olvi-vec (cohorts 5 and 6). Most importantly, there was minimal systemic

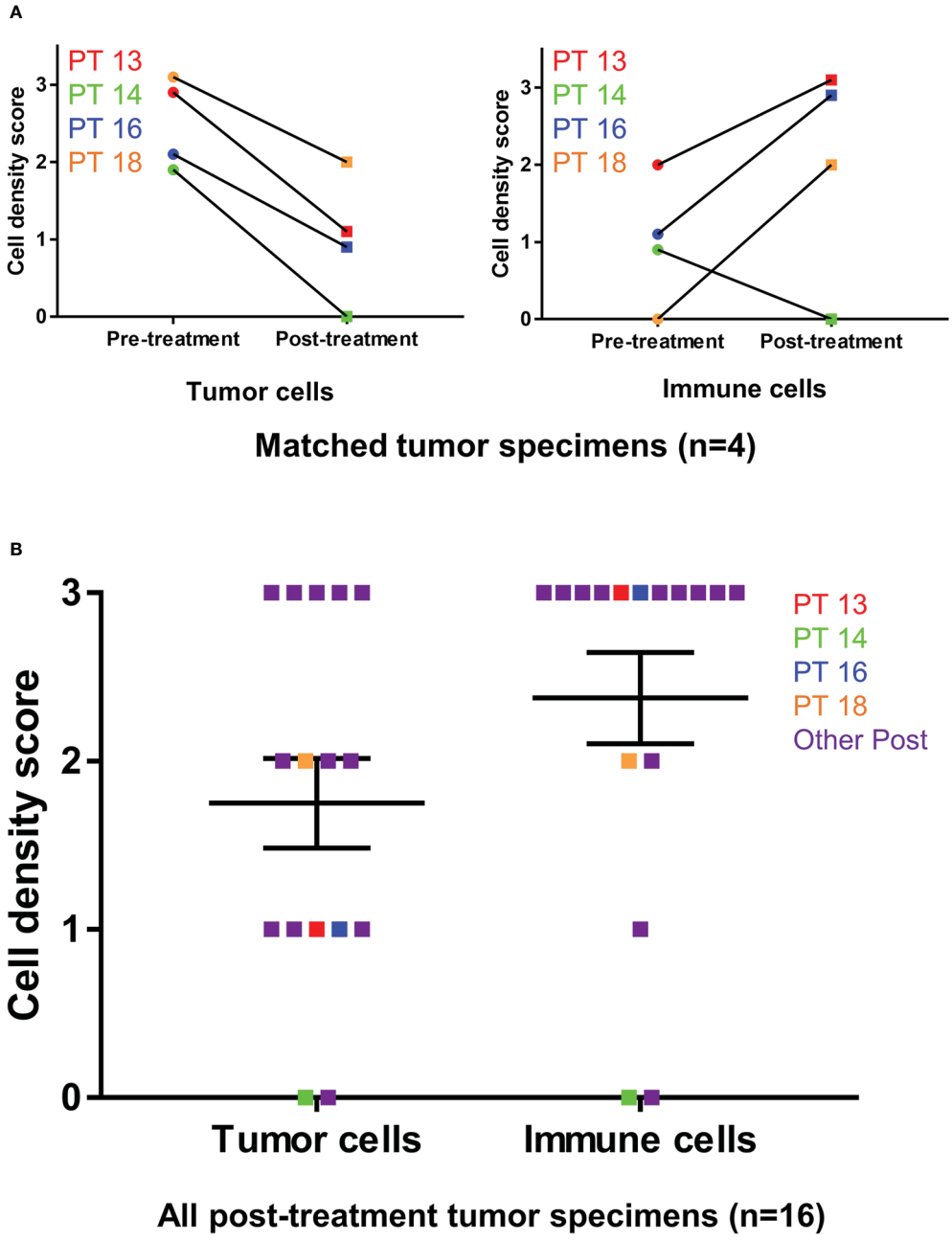

FIGURE 3
Tumor cell and immune cell density scoring before and after Olvi-vec therapy. **(A)** Matched MPM tumor sections obtained before and after Olvi-vec therapy underwent staining with hematoxylin and eosin and were scored for tumor cell density and immune cell density. **(B)** Tumor cell density scores and immune cell density were scored for all post-treatment tumor sections. Bars indicate mean and standard error of the mean (SEM).

immune activation following intrapleural treatment, with only 2 cytokines noted to be elevated in serum. Among trial patients who had MPM, median OS was 22 months following treatment.

Our observations in treating patients with MPE-associated immunosuppressive microenvironment are similar to published studies of vaccinia viral therapy without immunosuppression at the administered site. Administered as systemic therapy in clinical trials, vaccinia viral therapy was associated with a trend toward improved progression-free survival and increased CD4+/Treg ratio in patients with metastatic breast cancer (35). In patients with advanced colorectal liver metastases and metastatic melanoma, vaccinia viral therapy was associated with significant increases in IFN-stimulated and pro-inflammatory cytokines, as well as NK-cell activation and CD8+ proliferation (36). Vaccinia viral therapy had no observed benefit in patients with advanced soft tissue sarcoma (37).

Intrapleural oncolytic viral therapy has been investigated by use of multiple oncolytic viruses. In patients with MPM, intrapleural delivery of adenoviral gene-mediated cytotoxic therapy has been investigated. Adenoviral vectors have been used for gene transfer of

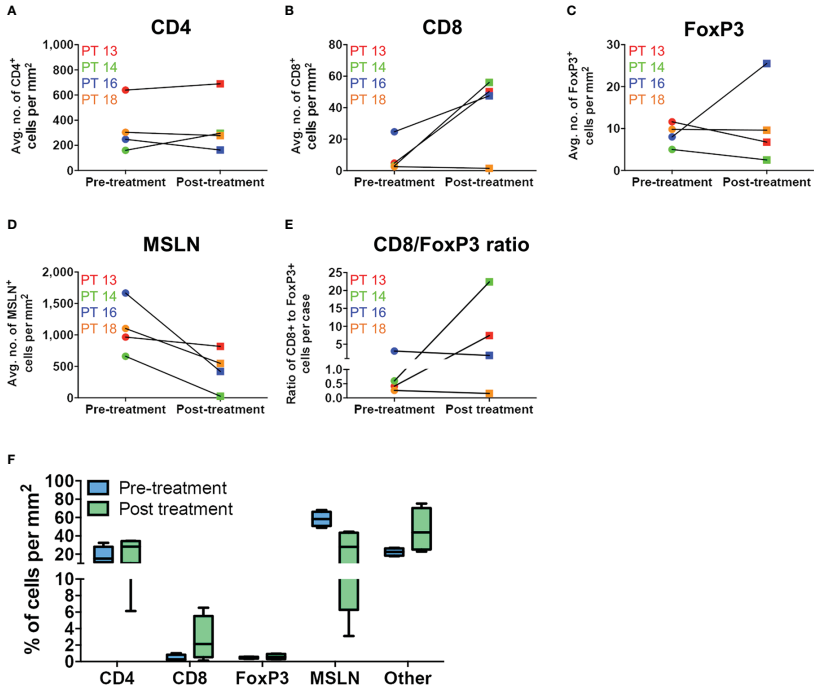

FIGURE 4
Immune cell infiltration in matched MPM tumor specimens before and after Olvi-vec therapy. **(A–D)** Matched MPM tumor sections obtained before and after Olvi-vec therapy underwent mIF staining and quantification of **(A)** CD4+ T cells, **(B)** CD8+ T cells, **(C)** FoxP3+ T cells, and **(D)** mesothelin (MSLN)+ tumor cells. **(E)** The ratio of CD8+ to FoxP3+ T cells in pre- and post-treatment tumor sections was calculated to identify patients with immunogenic (CD8+/FoxP3 + >1) vs. immune suppressive (CD8+/FoxP3+ <1) tumor microenvironments. **(F)** Immune cell populations present in matched pre- and post-treatment tumor sections were expressed as a percentage of total cells per mm^2. "Other" cells are DAPI+ but negative for CD4, CD8, FoxP3, and MSLN—they may be fibroblasts, mesothelial cells, or other classes of immune cells. Bars indicate mean, interquartile range, and SEM.

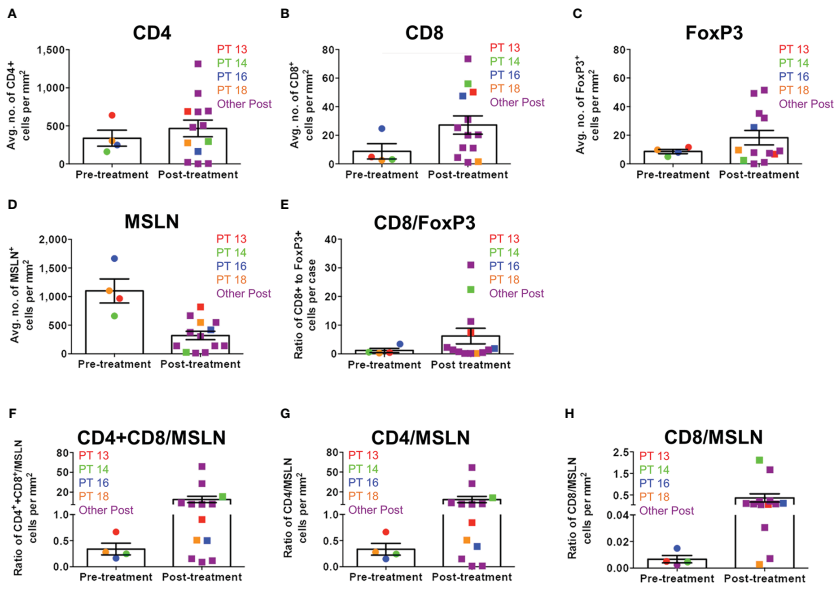

FIGURE 5
Immune cell infiltration ratios in all MPM tumor specimens before and after Olvi-vec therapy. **(A–D)** MPM tumor sections obtained before and after Olvi-vec therapy underwent multiplex immunofluorescence (mIF) staining and quantification of **(A)** CD4+ T cells, **(B)** CD8+ T cells, **(C)** FoxP3+ T cells, and **(D)** mesothelin (MSLN)+ tumor cells. **(E)** The ratio of CD8+ to FoxP3+ T cells (high ratio indicating relative immunogenicity, low ratio indicating relative immune suppression) in pre- and post-treatment tumor sections was calculated. **(F–H)** Ratios of **(F)** total T cells (CD4+ and CD8+) to MSLN+ tumor cells, **(G)** CD4+ T cells to MSLN+ tumor cells, and **(H)** CD8+ T cells to MSLN+ tumor cells were calculated. Bars indicate mean and SEM.

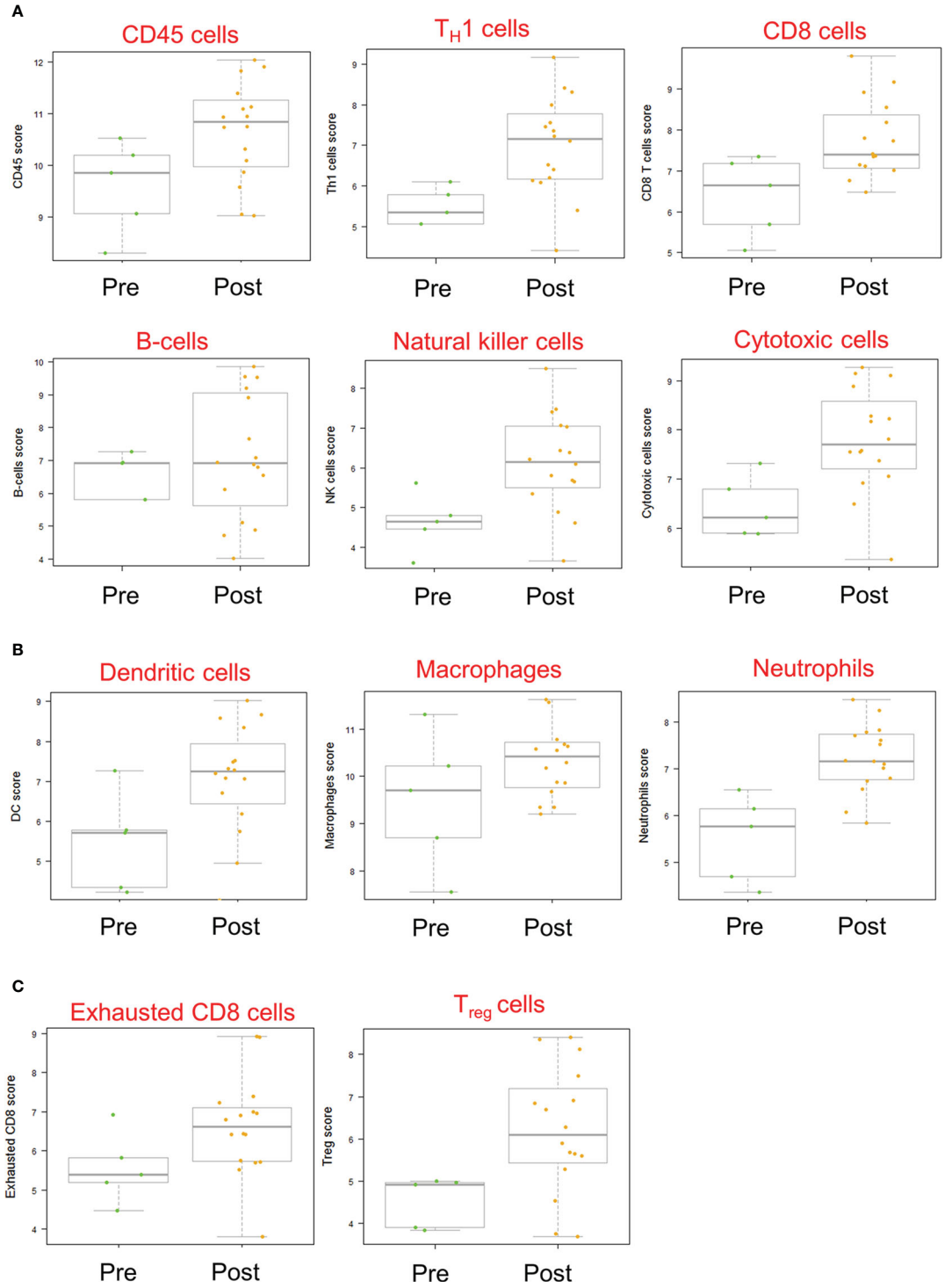

FIGURE 6
Immune cell scores based on mRNA transcript abundance before and after Olvi-vec therapy. **(A–C)** Total RNA was isolated from MPM tumor sections before and after Olvi-vec therapy. The number of mRNA transcripts specific to **(A)** lymphoid, **(B)** myeloid, and **(C)** exhausted and regulatory cell types were quantified. A score increase of one indicates a two-fold increase in cell population abundance in a sample. Bars indicate mean, interquartile range, and range.

cytokines [such as IFN-α (8) and IFN-β (38)] and enzymes (such as TK) that potentiate cytotoxic activity of subsequently administered ganciclovir (39) or valacyclovir (7). These trials reported isolated instances of grade 4 pericardial tamponade (38), grade 4 hypotension (7), and severe flu-like symptoms requiring dose de-escalation (8). We did not observe any dose-limiting or treatment-related grade ≥4 toxicities in our trial. Adenovirus-mediated IFN-β and IFN-α gene transfer were reported to be associated with increases in activated NK-cell populations (8, 40). Our correlative data noted a 2-fold increase in NK cells based on gene expression

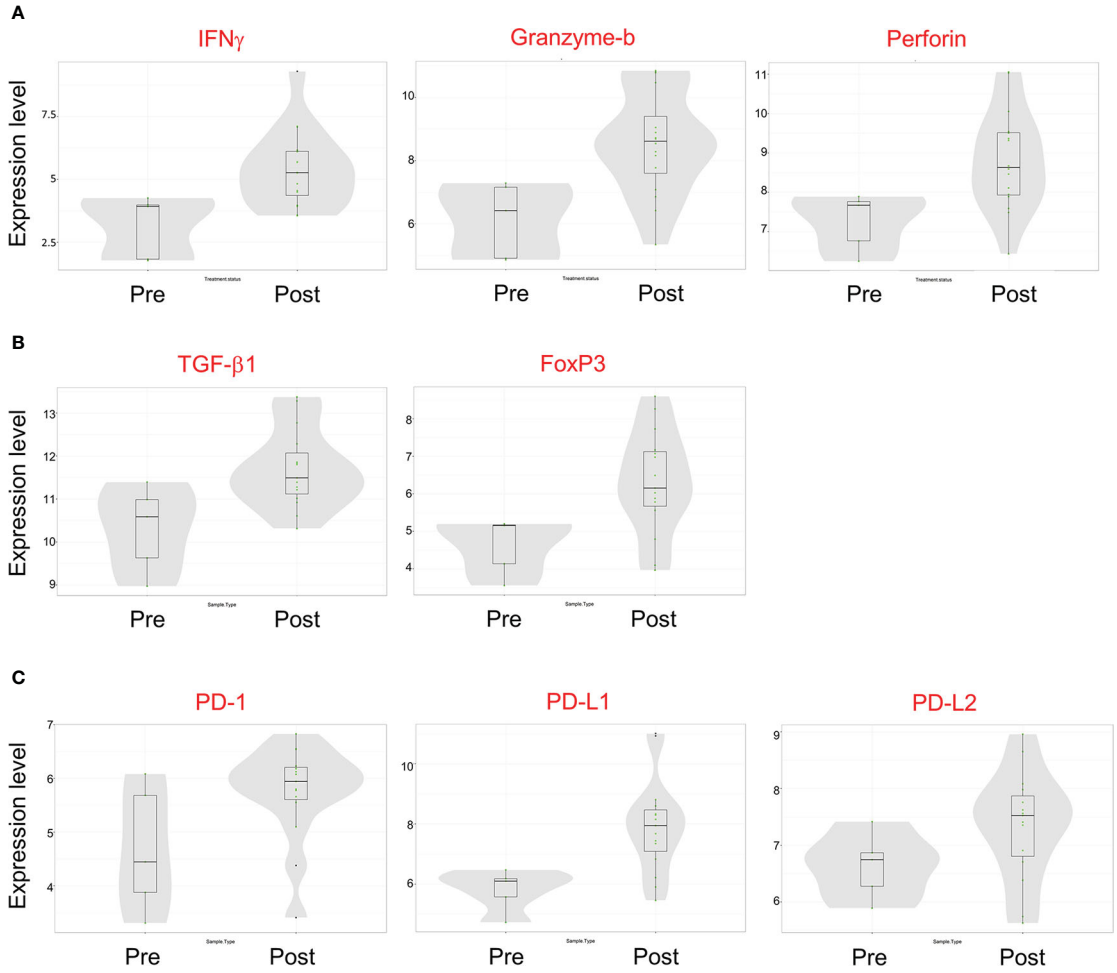

FIGURE 7
mRNA transcript expression of immune-modulatory proteins before and after Olvi-vec therapy. **(A–C)** Total RNA was isolated from MPM tumor sections before and after Olvi-vec therapy. The number of mRNA transcripts for **(A)** immune effector proteins, **(B)** immune suppressive proteins, and **(C)** immune checkpoint regulatory proteins were quantified. Bars indicate mean, interquartile range, and range.

TABLE 4A Results of viral plaque assay (pleural fluid).

Patient	Pathology	Dose (PFU)	# of doses	Olvi-vec plaque-forming units/mL (dilution factor)					
				Pleural fluid					Post-treatment tumor lysate
				Baseline	24 hours	48 hours	72 hours	96 hours	
1	MPM (epithelioid)	1.00E+07	1	0	0	0			4
2	NSCLC (SCC)	1.00E+07	1	0	0	0			0
3	MPM (epithelioid)	1.00E+07	1	0	0	0			0
4	MPM (epithelioid)	1.00E+07	1	0	0	0			0
5	MPM (epithelioid)	1.00E+08	1	0	0	0			0

(Continued)

TABLE 4A Continued

Patient	Pathology	Dose (PFU)	# of doses	Olvi-vec plaque-forming units/mL (dilution factor)					
				Pleural fluid					Post-treatment tumor lysate
				Baseline	24 hours	48 hours	72 hours	96 hours	
6	MPM (epithelioid)	1.00E+08	1	0	–	0			0
7	NSCLC (ADC)	1.00E+08	1	0	0	0	–	7	–
8	MPM (epithelioid)	1.00E+09	1	0	42	60 (10)		51	18 (100)
9	MPM (epithelioid)	1.00E+09	1	–	0	0			0
10	MPM (epithelioid)	1.00E+09	1	0	–	0		0	0
11	MPM (sarcomatoid)	3.00E+09	1	0	44 (100)	126 (10)		221	0
12	TNBC	3.00E+09	1	0	0	0			0
13	MPM (biphasic)	3.00E+09	1	0	0	0			0
14	MPM (epithelioid)	3.00E+09	1	0	5 (10)	0			60
15	MPM (epithelioid)	3.00E+09	3	0	339	129 (10)	399 (10)	48	0
16	MPM (epithelioid)	3.00E+09	3	0	6 (1000)	33 (1000)	72 (1000)	30 (1000)	56 (1000)
17	MPM (epithelioid)	3.00E+09	3	0	0	0	26	0	0
18	MPM (epithelioid)	6.00E+09	3	0	3	4	32	9	0

-Insufficient sample
Not performed
ADC, adenocarcinoma; MPM, malignant pleural mesothelioma; NSCLC, non-small cell lung cancer; PFU, plaque-forming units; SCC, squamous cell carcinoma; TNBC, triple negative breast cancer.

TABLE 4B Results of viral plaque assay (other specimens).

Patient	Pathology	Dose (PFU)	# of doses	Specimen type	Olvi-vec plaque-forming units/mL (dilution factor)				
					Specimen				
					Baseline	24 hours	48 hours	72 hours	96 hours
1	MPM (epithelioid)	1.00E+07	1	Urine	0	0	14		
3	MPM (epithelioid)	1.00E+07	1	Urine	4	0	0		
5	MPM (epithelioid)	1.00E+08	1	Blood lysate	0	2	0		
18	MPM (epithelioid)	6.00E+09	3	Sputum	7	0	0	17	0

Not performed
MPM, malignant pleural mesothelioma; PFU, plaque-forming units.

analysis. Adenovirus-mediated TK and IFN gene transfers were associated with survival greater than 2 years in multiple patients (7, 8, 40, 41), as was observed following vaccinia treatment in our study. However, the survival observed cannot be attributed to the treatment agent due to the phase I nature of the study and limited clinical anti-tumor efficacy observed immediately after the treatment.

Following adenovirus-mediated TK/ganciclovir therapy, gene transfer was observed to be limited to superficial layers of the tumor (39). Yet, radiologic response and persistent clinical response were

TABLE 5 Results of vaccinia virus neutralization assay (serum).

Patient	Pathology	Dose (PFU)	# of doses	Specimen type	Vaccinia Virus Neutralization Assay (dilution factor)	
					Baseline	Day 60
1	MPM (epithelioid)	1.00E+07	1	Serum	–	–
2	NSCLC (SCC)	1.00E+07	1	Serum	–	–
3	MPM (epithelioid)	1.00E+07	1	Serum	–	–
4	MPM (epithelioid)	1.00E+07	1	Serum	–	–
5	MPM (epithelioid)	1.00E+08	1	Serum	–	–
6	MPM (epithelioid)	1.00E+08	1	Serum	–	–
7	NSCLC (ADC)	1.00E+08	1	Serum	–	–
8	MPM (epithelioid)	1.00E+09	1	Serum	–	–
9	MPM (epithelioid)	1.00E+09	1	Serum	–	–
10	MPM (epithelioid)	1.00E+09	1	Serum	–	–
11	MPM (sarcomatoid)	3.00E+09	1	Serum	Negative	–
12	TNBC	3.00E+09	1	Serum	Negative	–
13	MPM (biphasic)	3.00E+09	1	Serum	Positive (20)	Positive (2560)
14	MPM (epithelioid)	3.00E+09	1	Serum	Positive (10)	Positive (640)
15	MPM (epithelioid)	3.00E+09	3	Serum	Positive (10)	Positive (2560)
16	MPM (epithelioid)	3.00E+09	3	Serum	Negative	Positive (1280)
17	MPM (epithelioid)	3.00E+09	3	Serum	Positive (40)	Positive (20480)
18	MPM (epithelioid)	6.00E+09	3	Serum	–	–

–Insufficient sample
ADC, adenocarcinoma; MPM, malignant pleural mesothelioma; NSCLC, non-small cell lung cancer; PFU, plaque-forming units; SCC, squamous cell carcinoma; TNBC, triple negative breast cancer.

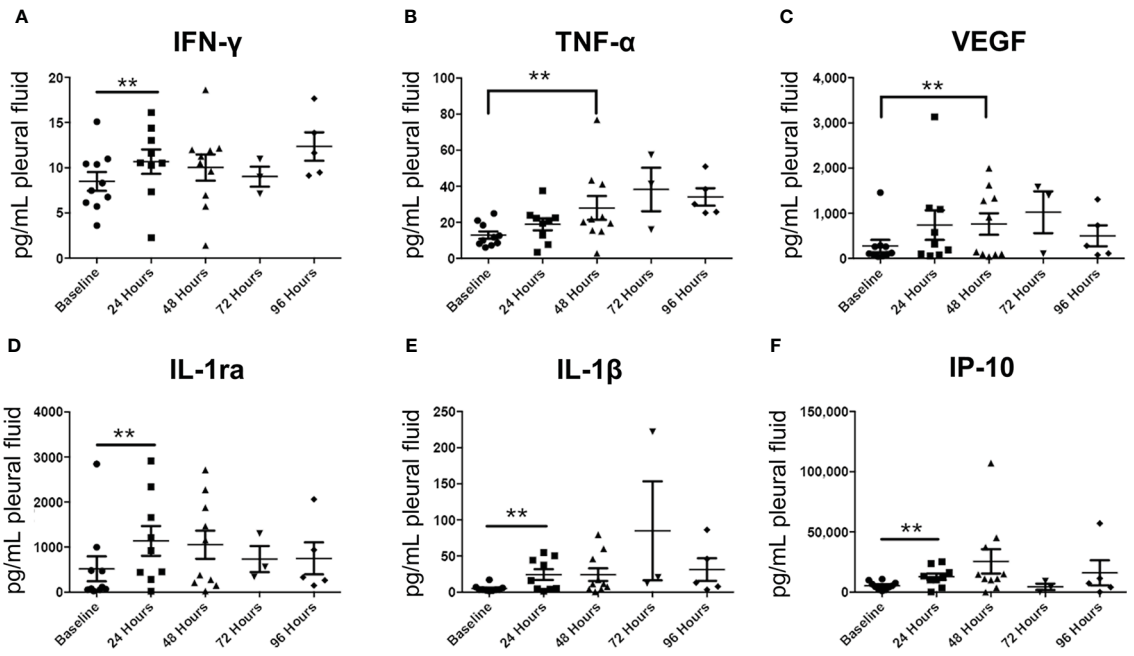

FIGURE 8
Pleural fluid cytokine profiles before and after Olvi-vec therapy. **(A–F)** Pleural fluid sampled before and after Olvi-vec therapy (at 24 hours, 48 hours, 72 hours, and 96 hours post-treatment) was evaluated for concentrations of cytokines. Bars indicate mean and SEM. **p<0.05, paired t-test.

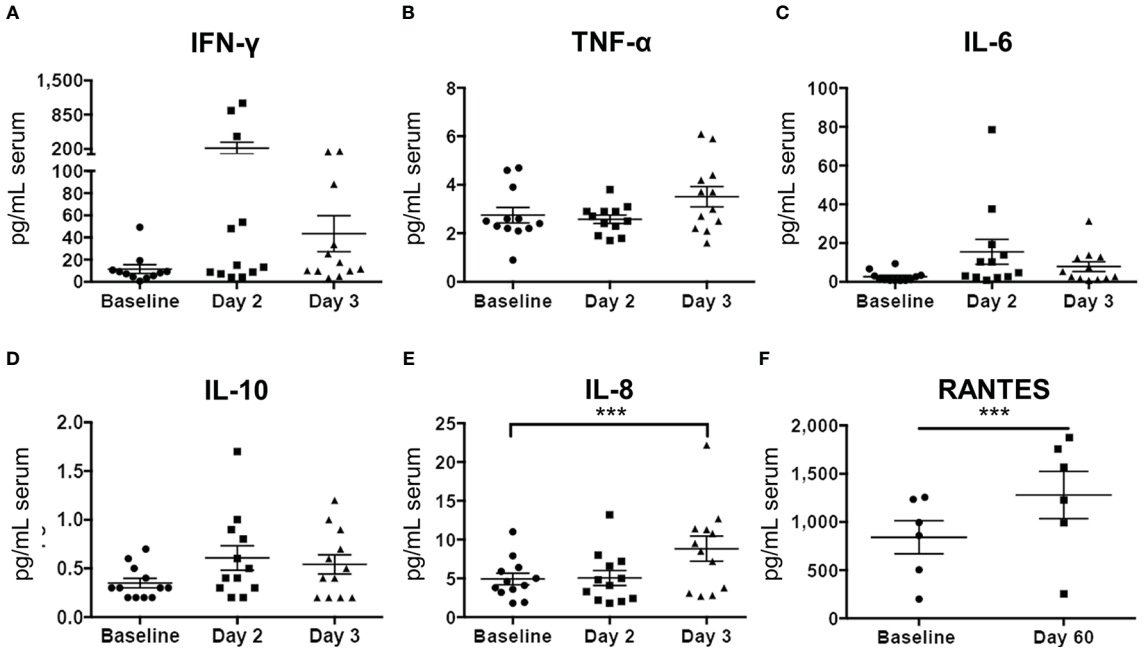

FIGURE 9
Serum cytokine profiles before and after Olvi-vec therapy. **(A–F)** Serum sampled before and after Olvi-vec therapy (at Day 2, Day 3, and Day 60) was evaluated for concentrations of cytokines. Bars indicate mean and SEM. ***p<0.01, paired t-test.

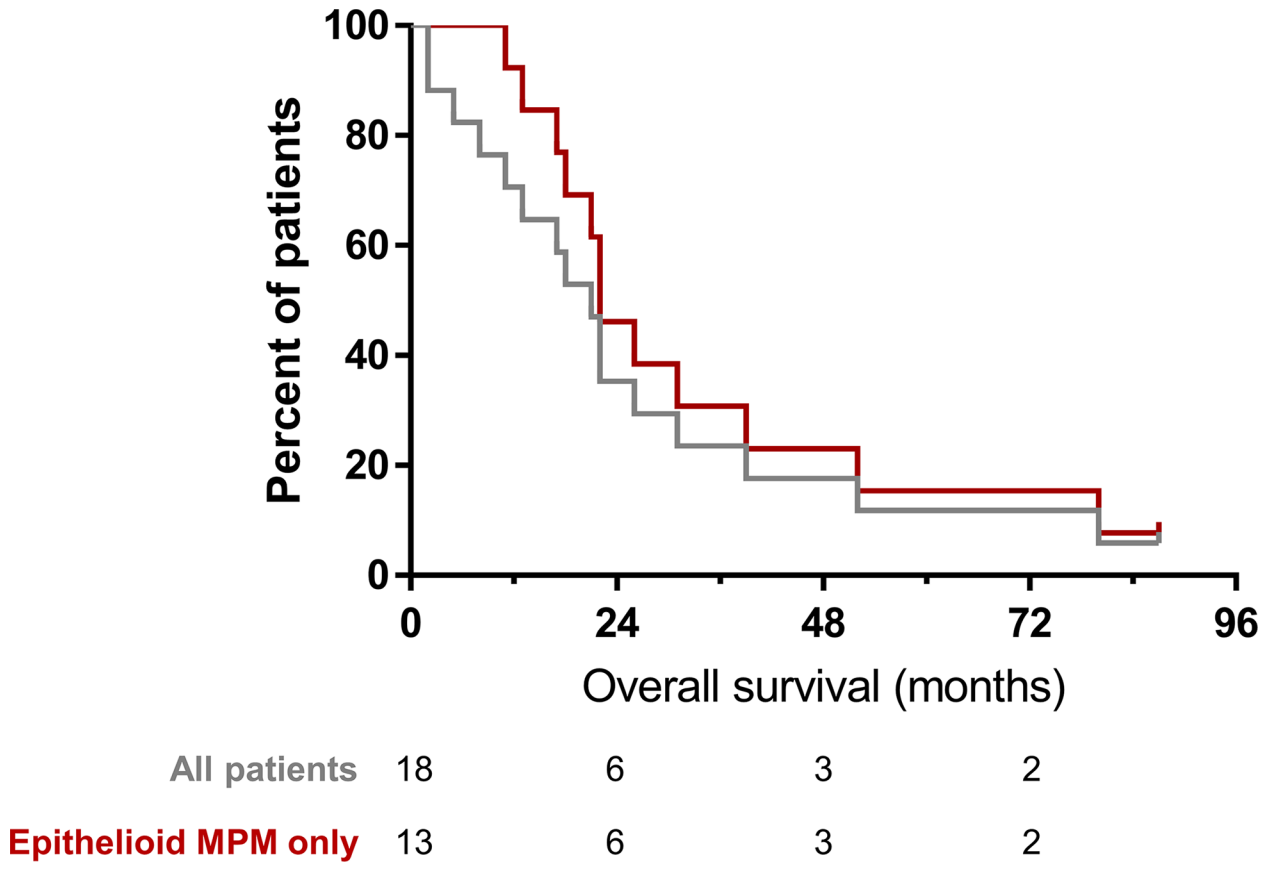

FIGURE 10
Overall survival of patients following Olvi-vec therapy.

observed in 3 patients (41), prompting the authors to hypothesize that the therapy had immune activating effects in addition to direct cytotoxicity. Indeed, administration of adenovirus TK has been shown to increase PD-L1 expression on tumor cells (7). In the current trial we observed increased expression of PD-1, PD-L1, and PD-L2 mRNA transcripts following vaccinia virus treatment. We also observed presence of vaccinia virus in the tumor as identified by multiplex immunofluorescence along with associated immune activation signature by nanostring and cytokine analyses. Oncolytic virus-induced tumor cytotoxicity may potentially shift the balance of the immune microenvironment towards activation through pathogen-associated and damage-associated molecular pattern signaling. These observations provide rationale to the addition of checkpoint blockade to vaccinia virus treatment (42) to enhance immune activation and antitumor efficacy. In preclinical studies, vaccinia virus combined with anti-PD1 therapy caused tumor reduction in glioblastoma (42), and vaccinia virus combined with MEK inhibitory therapy resulted in enhanced cytotoxicity in doxorubicin-resistant ovarian cancer (43).

In addition to effector immune responses (an increase in CD45+, Th1+, CD8+, NK+, cytotoxic T cells, and dendritic cells), we also observed an increase in exhausted CD8+ T cells and macrophages indicating the suppressor immune response. However, it is not certain whether these alterations are limited to tumors with pre-existing immune suppressor responses that are augmented following vaccinia viral therapy. In addition, our clinical trial was limited by the inclusion of a small number of patients from a single institution, who had heterogeneous types and stages of disease. Not all specimens investigated were available from all patients, a limitation inherent in a phase I clinical trial. Nevertheless, our correlative analyses demonstrating immune activation support the potential utility of vaccinia virus as an intrapleural oncolytic treatment for patients with MPM.

Data availability statement

The data discussed in this publication have been deposited in NCBI's Gene Expression Omnibus (31) and are accessible through GEO Series accession number GSE223395 (https://www.ncbi.nlm.nih.gov/geo/query/acc.cgi?acc=GSE223395).

Ethics statement

The studies involving human participants were reviewed and approved by the Memorial Sloan Kettering Cancer Center Institutional Review Board (IRB# 12-169). The patients/participants provided their written informed consent to participate in this study.

Author contributions

NC: Data curation, Formal analysis, Investigation, Methodology, Software, Validation, Visualization, Roles/Writing – original draft, Writing – review & editing; JC: Data curation, Formal analysis, Investigation, Methodology, Software, Validation, Visualization, Roles/Writing – original draft, Writing – review & editing; EM: Data curation, Formal analysis, Investigation, Methodology, Writing – review & editing; RB: Data curation, Investigation, Writing – review & editing; JS: Data curation, Investigation, Writing – review & editing; SB: Data curation, Investigation, Writing – review & editing; AM: Data curation, Investigation, Writing – review & editing; MZ: Data curation, Investigation, Writing – review & editing; PA: Conceptualization, Data curation, Formal analysis, Funding acquisition, Investigation, Methodology, Project Administration, Resources, Software, Supervision, Validation, Visualization, Roles/Writing – original draft, Writing – review & editing; VR: Conceptualization, Data curation, Funding acquisition, Investigation, Resources, Supervision, Writing – review & editing. All authors contributed to the article and approved the submitted version.

Funding

Funding support for this investigator-initiated phase I clinical trial is provided by Genelux Corporation. No employee of Genelux Corporation had any influence on the study analysis, interpretation of data, or manuscript writing. JC is supported, in part, by a grant from the National Institutes of Health (T32CA009501-33). PA's laboratory work is supported by grants from the National Institutes of Health (P30 CA008748, R01 CA236615-01, and R01 CA235667), the U.S. Department of Defense (BC132124, LC160212, CA170630, CA180889 and CA200437), the Batishwa Fellowship, the Comedy vs Cancer Award, the DallePezze Foundation, the Derfner Foundation, the Esophageal Cancer Education Fund, the Geoffrey Beene foundation, the Memorial Sloan Kettering Technology Development Fund, the Miner Fund for Mesothelioma Research, the Mr. William H. Goodwin and Alice Goodwin, the Commonwealth Foundation for Cancer Research, and the Experimental Therapeutics Center of Memorial Sloan Kettering Cancer Center. PA's laboratory received research support from the ATARA Biotherapeutics. The research support for all authors was not involved in the study design; in the collection, analysis, and interpretation of data; in the writing of the report; and in the decision to submit the article for publication.

Acknowledgments

We acknowledge excellent editorial assistance from Summer Koop of the MSK Thoracic Surgery Service.

Conflict of interest

In the last 3 years, MZ has received consulting fees from Curis, Ikena, Takeda, GlaxoSmithKline, Aldeyra Therapeutics, and Novocure and honoraria for CME content from PER, Medscape, Research to

Practice, Medical Learning Institute and OncLive. Memorial Sloan Kettering receives research funding from the Department of Defense, the National Institutes of Health, Precog, GlaxoSmithKline, Epizyme, Polaris, Sellas Life Sciences, Bristol Myers Squibb, Millenium/Takeda, Curis, and Atara for research conducted by MZ. MZ serves as Chair of the Board of Directors of the Mesothelioma Applied Research Foundation, uncompensated. PA declares research funding from ATARA Biotherapeutics; Scientific Advisory Board Member and Consultant for Abound Bio, ATARA Biotherapeutics, Bayer, Bio4T2, Carisma Therapeutics, Imugene, ImmPactBio, Johnson&Johnson, Orion Pharma, Outpace Bio, Pleuri-tech, Putnam associates; Patents, royalties and intellectual property on mesothelin-targeted CAR and other T-cell therapies licensed to ATARA Biotherapeutics, issued patent method for detection of cancer cells using virus, and pending patent applications on PD-1 dominant negative receptor, wireless pulse-oximetry device, and on an ex vivo malignant pleural effusion culture system. Memorial Sloan Kettering Cancer Center MSK has licensed intellectual property related to mesothelin-targeted CARs and T-cell therapies to ATARA Biotherapeutics, and has associated financial interests.

The remaining authors declare that the research was conducted in the absence of any commercial or financial relationships that could be construed as a potential conflict of interest.

Publisher's note

All claims expressed in this article are solely those of the authors and do not necessarily represent those of their affiliated organizations, or those of the publisher, the editors and the reviewers. Any product that may be evaluated in this article, or claim that may be made by its manufacturer, is not guaranteed or endorsed by the publisher.

Supplementary material

The Supplementary Material for this article can be found online at: https://www.frontiersin.org/articles/10.3389/fimmu.2023.1112960/full#supplementary-material

References

1. American Thoracic Society. Management of malignant pleural effusions. *Am J Respir Crit Care Med* (2000) 162(5):1987–2001. doi: 10.1164/ajrccm.162.5.ats8-00

2. Dipper A, Jones HE, Bhatnagar R, Preston NJ, Maskell N, Clive A. Interventions for the management of malignant pleural effusions: An updated network meta-analysis. *Eur Respir Rev* (2021) 30(160):210025. doi: 10.1183/16000617.0025-2021

3. Yang Y, Du J, Wang YS, Kang HY, Zhai K, Shi HZ. Prognostic impact of pleural effusion in patients with malignancy: A systematic review and meta-analysis. *Clin Transl Sci* (2022) 15(6):1340–54. doi: 10.1111/cts.13260

4. Suzuki K, Servais EL, Rizk NP, Solomon SB, Sima CS, Park BJ, et al. Palliation and pleurodesis in malignant pleural effusion: The role for tunneled pleural catheters. *J Thorac Oncol* (2011) 6(4):762–7. doi: 10.1097/JTO.0b013e31820d614f

5. Ghanim B, Rosenmayr A, Stockhammer P, Vogl M, Celik A, Bas A, et al. Tumour cell pd-L1 expression is prognostic in patients with malignant pleural effusion: The impact of c-reactive protein and immune-checkpoint inhibition. *Sci Rep* (2020) 10 (1):5784. doi: 10.1038/s41598-020-62813-2

6. Kawachi H, Tamiya M, Taniguchi Y, Yokoyama T, Yokoe S, Oya Y, et al. Efficacy of immune checkpoint inhibitor with or without chemotherapy for nonsquamous nsclc with malignant pleural effusion: A retrospective multicenter cohort study. *JTO Clin Res Rep* (2022) 3(7):100355. doi: 10.1016/j.jtocrr.2022.100355

7. Aggarwal C, Haas AR, Metzger S, Aguilar LK, Aguilar-Cordova E, Manzanera AG, et al. Phase I study of intrapleural gene-mediated cytotoxic immunotherapy in patients with malignant pleural effusion. *Mol Ther* (2018) 26(5):1198–205. doi: 10.1016/j.ymthe.2018.02.015

8. Sterman DH, Haas A, Moon E, Recio A, Schwed D, Vachani A, et al. A trial of intrapleural adenoviral-mediated interferon-Alpha2b gene transfer for malignant pleural mesothelioma. *Am J Respir Crit Care Med* (2011) 184(12):1395–9. doi: 10.1164/rccm.201103-0554CR

9. Adusumilli PS, Zauderer MG, Riviere I, Solomon SB, Rusch VW, O'Cearbhaill RE, et al. A phase I trial of regional mesothelin-targeted car T-cell therapy in patients with malignant pleural disease, in combination with the anti-Pd-1 agent pembrolizumab. *Cancer Discovery* (2021) 11(11):2748–63. doi: 10.1158/2159-8290.CD-21-0407

10. Ghosn M, Cheema W, Zhu A, Livschitz J, Maybody M, Boas FE, et al. Image-guided interventional radiological delivery of chimeric antigen receptor (Car) T cells for pleural malignancies in a phase I/Ii clinical trial. *Lung Cancer* (2022) 165:1–9. doi: 10.1016/j.lungcan.2022.01.003

11. Lievense LA, Cornelissen R, Bezemer K, Kaijen-Lambers ME, Hegmans JP, Aerts JG. Pleural effusion of patients with malignant mesothelioma induces macrophage-mediated T cell suppression. *J Thorac Oncol* (2016) 11(10):1755–64. doi: 10.1016/j.jtho.2016.06.021

12. Lievense LA, Bezemer K, Cornelissen R, Kaijen-Lambers ME, Hegmans JP, Aerts JG. Precision immunotherapy; dynamics in the cellular profile of pleural effusions in malignant mesothelioma patients. *Lung Cancer* (2017) 107:36–40. doi: 10.1016/j.lungcan.2016.04.015

13. Kosti CN, Vaitsi PC, Pappas AG, Iliopoulou MP, Psarra KK, Magkouta SF, et al. Csf1/Csf1r signaling mediates malignant pleural effusion formation. *JCI Insight* (2022) 7(6):e155300. doi: 10.1172/jci.insight.155300

14. Baas P, Scherpereel A, Nowak AK, Fujimoto N, Peters S, Tsao AS, et al. First-line nivolumab plus ipilimumab in unresectable malignant pleural mesothelioma (Checkmate 743): A multicentre, randomised, open-label, phase 3 trial. *Lancet* (2021) 397(10272):375–86. doi: 10.1016/S0140-6736(20)32714-8

15. Offin M, Rusch VW, Rimner A, Adusumilli PS, Zauderer MG. Evolving landscape of initial treatments for patients with malignant pleural mesotheliomas: Clinical trials to clinical practice. *Oncologist* (2022) 27(8):610–4. doi: 10.1093/oncolo/oyac113

16. Yarchoan M, Albacker LA, Hopkins AC, Montesion M, Murugesan K, Vithayathil TT, et al. Pd-L1 expression and tumor mutational burden are independent biomarkers in most cancers. *JCI Insight* (2019) 4(6):e126908. doi: 10.1172/jci.insight.126908

17. Mankor JM, Disselhorst MJ, Poncin M, Baas P, Aerts J, Vroman H. Efficacy of nivolumab and ipilimumab in patients with malignant pleural mesothelioma is related to a subtype of effector memory cytotoxic T cells: Translational evidence from two clinical trials. *EBioMedicine* (2020) 62:103040. doi: 10.1016/j.ebiom.2020.103040

18. Liu X, Zhao J, Li X, Lao F, Fang M. Design strategies and precautions for using vaccinia virus in tumor virotherapy. *Vaccines (Basel)* (2022) 10(9):1552. doi: 10.3390/vaccines10091552

19. Mastrangelo MJ, Lattime EC. Virotherapy clinical trials for regional disease: *In situ* immune modulation using recombinant poxvirus vectors. *Cancer Gene Ther* (2002) 9(12):1013–21. doi: 10.1038/sj.cgt.7700538

20. Kelly KJ, Woo Y, Brader P, Yu Z, Riedl C, Lin SF, et al. Novel oncolytic agent glv-1h68 is effective against malignant pleural mesothelioma. *Hum Gene Ther* (2008) 19 (8):774–82. doi: 10.1089/hum.2008.036

21. Lin SF, Price DL, Chen CH, Brader P, Li S, Gonzalez L, et al. Oncolytic vaccinia virotherapy of anaplastic thyroid cancer in vivo. *J Clin Endocrinol Metab* (2008) 93 (11):4403–7. doi: 10.1210/jc.2008-0316

22. Donat U, Weibel S, Hess M, Stritzker J, Hartl B, Sturm JB, et al. Preferential colonization of metastases by oncolytic vaccinia virus strain glv-1h68 in a human pc-3 prostate cancer model in nude mice. *PloS One* (2012) 7(9):e45942. doi: 10.1371/journal.pone.0045942

23. Mastrangelo MJ, Maguire HC, Lattime EC. Intralesional Vaccinia/Gm-csf recombinant virus in the treatment of metastatic melanoma. *Adv Exp Med Biol* (2000) 465:391–400. doi: 10.1007/0-306-46817-4_34

24. Kawa A, Arakawa S. The effect of attenuated vaccinia virus as strain on multiple myeloma; a case report. *Jpn J Exp Med* (1987) 57(1):79–81.

25. Hansen RM, Libnoch JA. Remission of chronic lymphocytic leukemia after smallpox vaccination. *Arch Intern Med* (1978) 138(7):1137–8. doi: 10.1001/archinte.1978.03630320073024

26. Yettra M. Remission of chronic lymphocytic leukemia after smallpox vaccination. *Arch Intern Med* (1979) 139(5):603.

27. Gomella LG, Mastrangelo MJ, McCue PA, Maguire HJ, Mulholland SG, Lattime EC. Phase I study of intravesical vaccinia virus as a vector for gene therapy of bladder cancer. *J Urol* (2001) 166(4):1291–5. doi: 10.1016/S0022-5347(05)65755-2

28. Mastrangelo MJ, Maguire HCJr., Eisenlohr LC, Laughlin CE, Monken CE, McCue PA, et al. Intratumoral recombinant gm-Csf-Encoding virus as gene therapy in patients with cutaneous melanoma. *Cancer Gene Ther* (1999) 6(5):409–22. doi: 10.1038/sj.cgt.7700066

29. Liu TC, Hwang T, Park BH, Bell J, Kirn DH. The targeted oncolytic poxvirus jx-594 demonstrates antitumoral, antivascular, and anti-hbv activities in patients with hepatocellular carcinoma. *Mol Ther* (2008) 16(9):1637–42. doi: 10.1038/mt.2008.143

30. Park BH, Hwang T, Liu TC, Sze DY, Kim JS, Kwon HC, et al. Use of a targeted oncolytic poxvirus, jx-594, in patients with refractory primary or metastatic liver cancer: A phase I trial. *Lancet Oncol* (2008) 9(6):533–42. doi: 10.1016/S1470-2045(08)70107-4

31. Edgar R, Domrachev M, Lash AE. Gene expression omnibus: NCBI gene expression and hybridization array data repository. *Nucleic Acids Res* (2002) 30 (1):207–10. doi: 10.1093/nar/30.1.207

32. Adusumilli PS, Stiles BM, Chan M, Mullerad M, Eisenberg DP, Ben-Porat L, et al. Imaging and therapy of malignant pleural mesothelioma using replication-competent herpes simplex viruses. *J Gene Med* (2006) 8(5):603–15. doi: 10.1002/jgm.877

33. Adusumilli PS, Stiles BM, Chan M, Eisenberg DP, Yu Z, Stanziale SF, et al. Real-time diagnostic imaging of tumors and metastases by use of a replication-competent herpes vector to facilitate minimally invasive oncological surgery. *FASEB J* (2006) 20 (6):726–8. doi: 10.1096/fj.05-5316fje

34. Adusumilli PS, Chan M, Hezel M, Yu Z, Stiles BM, Chou T, et al. Radiation-induced cellular DNA damage repair response enhances viral gene therapy efficacy in the treatment of malignant pleural mesothelioma. *Ann Surg Oncol* (2007) 14(1):258–69. doi: 10.1245/s10434-006-9127-4

35. Heery CR, Ibrahim NK, Arlen PM, Mohebtash M, Murray JL, Koenig K, et al. Docetaxel alone or in combination with a therapeutic cancer vaccine (Panvac) in patients with metastatic breast cancer: A randomized clinical trial. *JAMA Oncol* (2015) 1(8):1087–95. doi: 10.1001/jamaoncol.2015.2736

36. Samson A, West EJ, Carmichael J, Scott KJ, Turnbull S, Kuszlewicz B, et al. Neoadjuvant intravenous oncolytic vaccinia virus therapy promotes anticancer immunity in patients. *Cancer Immunol Res* (2022) 10(6):745–56. doi: 10.1158/2326-6066.CIR-21-0171

37. Toulmonde M, Cousin S, Kind M, Guegan JP, Bessede A, Le Loarer F, et al. Randomized phase 2 trial of intravenous oncolytic virus jx-594 combined with low-dose cyclophosphamide in patients with advanced soft-tissue sarcoma. *J Hematol Oncol* (2022) 15(1):149. doi: 10.1186/s13045-022-01370-9

38. Sterman DH, Recio A, Haas AR, Vachani A, Katz SI, Gillespie CT, et al. A phase I trial of repeated intrapleural adenoviral-mediated interferon-beta gene transfer for mesothelioma and metastatic pleural effusions. *Mol Ther* (2010) 18(4):852–60. doi: 10.1038/mt.2009.309

39. Sterman DH, Molnar-Kimber K, Iyengar T, Chang M, Lanuti M, Amin KM, et al. A pilot study of systemic corticosteroid administration in conjunctionwith intrapleural adenoviral vector administration in patients with malignant pleural mesothelioma. *Cancer Gene Ther* (2000) 7(12):1511–8. doi: 10.1038/sj.cgt.7700269

40. Sterman DH, Recio A, Carroll RG, Gillespie CT, Haas A, Vachani A, et al. A phase I clinical trial of single-dose intrapleural ifn-beta gene transfer for malignant pleural mesothelioma and metastatic pleural effusions: High rate of antitumor immune responses. *Clin Cancer Res* (2007) 13(15 Pt 1):4456–66. doi: 10.1158/1078-0432.CCR-07-0403

41. Sterman DH, Recio A, Vachani A, Sun J, Cheung L, DeLong P, et al. Long-term follow-up of patients with malignant pleural mesothelioma receiving high-dose adenovirus herpes simplex thymidine Kinase/Ganciclovir suicide gene therapy. *Clin Cancer Res* (2005) 11(20):7444–53. doi: 10.1158/1078-0432.CCR-05-0405

42. Sun Y, Zhang Z, Zhang C, Zhang N, Wang P, Chu Y, et al. An effective therapeutic regime for treatment of glioma using oncolytic vaccinia virus expressing il-21 in combination with immune checkpoint inhibition. *Mol Ther Oncolytics* (2022) 26:105–19. doi: 10.1016/j.omto.2022.05.008

43. Lee S, Yang W, Kim DK, Kim H, Shin M, Choi KU, et al. Inhibition of mek-erk pathway enhances oncolytic vaccinia virus replication in doxorubicin-resistant ovarian cancer. *Mol Ther Oncolytics* (2022) 25:211–24. doi: 10.1016/j.omto.2022.04.006

frontiers | Frontiers in Immunology

TYPE Original Research
PUBLISHED 14 March 2023
DOI 10.3389/fimmu.2023.1129513

OPEN ACCESS

EDITED BY
Chiara Porta,
University of Eastern Piedmont, Italy

REVIEWED BY
Christophe Blanquart,
Centre National de la Recherche Scientifique (CNRS), France
Emanuele Giurisato,
University of Siena, Italy

*CORRESPONDENCE
Luciano Mutti
luciano.mutti@univaq.it;
luciano.mutti@temple.edu
Emyr Yosef Bakker
ebakker@uclan.ac.uk

†Authors contributed equally

SPECIALTY SECTION
This article was submitted to Cancer Immunity and Immunotherapy, a section of the journal Frontiers in Immunology

RECEIVED 22 December 2022
ACCEPTED 28 February 2023
PUBLISHED 14 March 2023

CITATION
Pentimalli F, Krstic-Demonacos M, Costa C, Mutti L and Bakker EY (2023) Intratumor microbiota as a novel potential prognostic indicator in mesothelioma. *Front. Immunol.* 14:1129513. doi: 10.3389/fimmu.2023.1129513

Intratumor microbiota as a novel potential prognostic indicator in mesothelioma

Francesca Pentimalli[1†], Marija Krstic-Demonacos[2], Caterina Costa[3†], Luciano Mutti[4,5*] and Emyr Yosef Bakker[6*]

[1]Department of Medicine and Surgery, LUM University "Giuseppe DeGennaro", Bari, Italy, [2]Biomedical Research Centre, School of Science, Engineering and Environment, University of Salford, Salford, United Kingdom, [3]Cell Biology and Biotherapy Unit, Istituto Nazionale Tumori-Scientific Institute for Research and Care (IRCCS)-Fondazione G. Pascale, Napoli, Italy, [4]Center for Biotechnology, Sbarro Institute for Cancer Research and Molecular Medicine, College of Science and Technology, Temple University, Philadelphia, PA, United States, [5]Department of Biotechnological and Applied Clinical Sciences, University of Aquila, L'Aquila, Italy, [6]School of Medicine, University of Central Lancashire, Preston, United Kingdom

Introduction: Despite increased attention on immunotherapy, primarily immune checkpoint blockade, as a therapeutic approach for mesothelioma (MMe), its efficacy and tolerability remain questioned. One potential explanation for different responses to immunotherapy is the gut and intratumor microbiota; however, these remain an underexplored facet of MMe. This article highlights the cancer intratumor microbiota as a novel potential prognostic indicator in MMe.

Methods: TCGA data on 86 MMe patients from cBioPortal underwent bespoke analysis. Median overall survival was used to divide patients into "Low Survivors" and "High Survivors". Comparison of these groups generated Kaplan-Meier survival analysis, differentially expressed genes (DEGs), and identification of differentially abundant microbiome signatures. Decontamination analysis refined the list of signatures, which were validated as an independent prognostic indicator through multiple linear regression modelling and Cox proportional hazards modelling. Finally, functional annotation analysis on the list of DEGs was performed to link the data together.

Results: 107 genera signatures were significantly associated with patient survival (positively or negatively), whilst clinical characteristic comparison between the two groups demonstrated that epithelioid histology was more common in "High Survivors" versus biphasic in "Low Survivors". Of the 107 genera, 27 had published articles related to cancer, whilst only one (Klebsiella) had MMe-related published articles. Functional annotation analysis of the DEGs between the two groups highlighted fatty acid metabolism as the most enriched term in "High Survivors", whilst for "Low Survivors" the enriched terms primarily related to cell cycle/division. Linking these ideas and findings together is that the microbiome influences, and is influenced by, lipid metabolism. Finally, to validate the independent prognostic value of the microbiome, multiple linear regression modelling as well as Cox proportional hazards modelling were employed, with both approaches demonstrating that the microbiome was a better prognostic indicator than patient age or stage of the cancer.

10.3389/fimmu.2023.1129513

Discussion: The findings presented herein, alongside the very limited literature from scoping searches to validate the genera, highlight the microbiome and microbiota as a potentially rich source of fundamental analysis and prognostic value. Further in vitro studies are needed to elucidate the molecular mechanisms and functional links that may lead to altered survival.

KEYWORDS

mesothelioma, microbiota, microbiome, bioinformatics, Kaplan-Meier, DEG (differentially expressed gene) analysis, functional annotation analysis, Cox proportional hazards modelling

Introduction

MMe is a rare cancer that may arise in the pleura, peritoneum, pericardium, or tunica vaginalis, with most cases affecting the pleura (1). MMe has historically been characterized by an exceptionally poor prognosis with limited treatment options that largely consisted of first-line anti-folates in combination with platinum-based therapy. Immunotherapy, particularly immune checkpoint blockade, has been investigated in the context of MMe. Although first-line combination of the immune checkpoint inhibitors (ICIs) nivolumab (anti-PD-1) and ipilimumab (anti-CTLA-4), based on the CheckMate 743 trial (2) has been approved for MMe, its efficacy has been questioned, with two comparative studies that have shown no survival benefit in the CheckMate 743 trial relative to trials studying cisplatin + pemetrexed + bevacizumab against cisplatin + pemetrexed (3, 4). One of these studies also casts a doubt on the combination of durvalumab and chemotherapy (4). Moreover ICIs have shown no significant superiority on standard treatment, either from real-world analysis (5) or in second-line settings (6). Thus, there is a need to investigate immunotherapy at a molecular level in mesothelioma, to further elucidate potential mechanisms and improve outcomes (7).

One potential reason for the varying efficacies of immune checkpoint blockade is the gut microbiome (8–10). Microbiome and microbiota are often used interchangeably, but the difference between the terms is that microbiome refers to "the collective genomes of microorganisms in a particular environment", whilst microbiota refers to "the community of microorganisms themselves" (11).

The microbiota consists of a vast collection of commensal archaea, bacteria, fungi and viruses that shows significant intrapopulation variation (9). When the microbiota is in balance with the host, a condition of eubiosis, it contributes to body homeostasis and to a healthy immune system, whereas microbial dysbiosis—the imbalance of microbiota with harmful species outcompeting benign (12)—contributes to the pathogenesis of many diseases including cancer. Indeed, beyond the well-recognized role of the gut microbiota in health and disease, in the past decade many studies have demonstrated the presence of a live and active intratumor microbiota which can affect disease progression and the therapeutic response (13, 14). Despite the rising recognition of the importance of gut and intratumor microbiota in cancer, their presence and impact in MMe remain significantly understudied. As of 15th December 2022, there were only ten peer-reviewed publications in PubMed for the search terms "((microbiota OR microbiome) AND mesothelioma)". Of these, only four actually contained clear and pertinent information on MMe and the microbiota/microbiome (15–18), with the rest as text-mining artefacts.

It is noteworthy that none of these studies have explored a link between the microbiota/microbiome and clinical characteristics in patients with MMe. Therefore, given the very limited literature related to the microbiome in MMe and the potential role it may play in the response to ICIs, there is evidently a need to investigate this further. To address this, herein TCGA intratumor microbiome data from MMe patients has been investigated in association with patients' clinical characteristics. We find that, upon dividing the patients into "Low Survivors" and "High Survivors", the only clinical characteristic that significantly differs between them was histological subtype, with epithelioid being more common in "High Survivors" versus biphasic in "Low Survivors". Additionally, we identify 107 genera signatures that are significantly associated with survival, with only 27 genera returning published papers following a scoping search for each genus and cancer, and only 1 genus (*Klebsiella*) returning a published result for mesothelioma. Tying the intratumor microbiome data with the cancer cell data is that fatty acid metabolism was the most enriched functional annotation in the "High Survivors" group (based on differential gene expression analysis between the two groups), a process that is known to have two-way interplay with the microbiome.

Methods

Overall workflow

Further detail is provided in subsequent headings, but the overall workflow for this study can be seen in Figure 1.

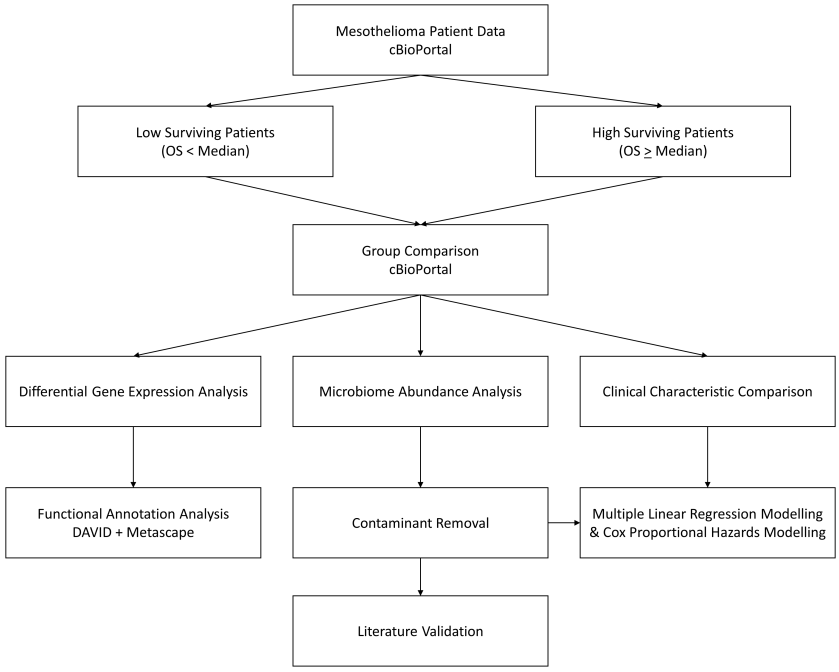

FIGURE 1
Workflow diagram. cBioPortal represents the starting point, where MMe patient data is accessed and patients are divided by the median overall survival. These two groups are then compared to assess differences in clinical characteristics, identify differentially expressed genes, and identify differential abundance in microbiome signatures, which is taken forward for contaminant removal, literature validation, and survival modelling.

Study selection and patient grouping

The cBioPortal database (19, 20) was utilized to interrogate MMe patient data (date of access 05 April 2022). The "Mesothelioma (TCGA, PanCancer Atlas)" study was selected because it included the highest number of patients together with the pertinent intratumor microbiome signatures and survival data required for the study. The other study with the same number of patients ("Mesothelioma (TCGA, Firehose Legacy)") lacked usable survival data (21), whilst the third study ("Pleural Mesothelioma (NYU, Cancer Res 2015)") had only 22 patients and did not have microbiota/microbiome data available (19, 20, 22).

After selecting the "Mesothelioma (TCGA, PanCancer Atlas)" study and choosing "Explore Selected Studies", patient IDs and survival lengths were downloaded to be analysed outside of the cBioPortal platform. After discarding the individual patient whose OS_MONTHS (overall survival in months) value was "N/A", the median OS_MONTHS value was calculated from the remaining patients (n=86). Patients were then divided into "Low Survivors" (OS_MONTHS less than the median) or "High Survivors" (OS_MONTHS greater than or equal to the median).

Identifying microbiome differences

After identifying the patient subgroups described above, the cBioPortal database was accessed once more with the "Mesothelioma (TCGA, PanCancer Atlas)" study. The subgroups were regenerated on the cBioPortal platform *via* the "Custom Selection" (based on Patient ID) and "Groups" functions. After regenerating the subgroups, they were analysed using the "Compare" cBioPortal function under the Groups setting.

This analysis automatically generated the Kaplan-Meier survival curve between the two groups, alongside the microbiome signatures comparison. In order to calculate a more precise p-value alongside the hazard ratio for the survival data, the resultant raw Kaplan-Meier data was downloaded and input to KMPlot using the upload function (23, 24). The microbiome signatures data were originally added to cBioPortal for a number of cancers by another study (25). Clinical parameters were also obtained *via* the Compare analysis, as were the differentially expressed genes.

Whilst exploratory studies such as the analysis contained herein are not strictly required to perform multiple comparison corrections (26, 27), microbiome signatures were only taken further if they were significant based on q-value ($q<0.05$). This permitted a greater focus on those genera that were more likely to have links to patient survival. The same was true for the identification of differentially expressed genes.

Functional annotation analysis

In order to interrogate the differentially expressed genes identified above and how they may relate to survival, the DAVID (28, 29) and Metascape (30) tools were employed. Gene lists that were highly expressed in both the low surviving and high surviving patient groups were in turn entered into each tool to identify clusters of functional annotations and enriched annotations.

Contaminant removal

Due to the recognized issue of contaminants (i.e., tumor sample contamination by external microbes during data collection and processing) when considering microbiome data (25), a decontamination analysis was performed on the list of genera that were statistically significantly associated (based on q-value) with patient survival.

In order to remove potential contaminants, Tables S6-S8 of the paper describing the microbiome analysis of TCGA data were accessed (25). The list of genera retrieved from the previous step above were compared to the genera obtained from Tables S6-S8 to identify potential contaminants, which were then removed from the list.

Literature scoping of genera

The final list of genera identified in the previous step were collated into a table after which searches were conducted to assess the breadth of literature pertaining to each genus. Searches were performed on PubMed (date of access 25th April 2022 – 7th July 2022) using the Boolean operator AND in the below format:

[Genus Name] AND Mesothelioma

[Genus Name] AND cancer

For the genera that had "Candidatus" in their name, searches were performed with and without the "Candidatus_" prefix to ensure searches were as exhaustive as possible. The literature scoping allowed for the identification of the breadth of knowledge related to each genus in both MMe and cancer in general.

Multiple linear regression modelling of putative prognostic factors

To determine the independent prognostic value of the microbiota identified in the previous step, multiple linear regression modelling was employed. To begin, the full microbiome abundance values (per patient, in log RNA Seq CPM) for all 1406 genera was downloaded from cBioPortal, alongside known clinical parameters such as overall survival (months), age, stage, and tumor histology (19, 20). This microbiome data was then filtered to include only the genera identified in the previous step, which were then subdivided into "good genera"—those identified to be more abundant in High Survivors than Low Survivors—and "bad genera"—those identified to be more abundant in Low Survivors than High Survivors.

It is known that inclusion of too many covariates on a multiple regression model can lead to overfitting, where the model on the surface appears to predict the outcome variable well, but in fact is responding only to noise (31–33). To avoid this problem, the log RNA Seq CPM values for all "good genera" were summed to an individual value per patient ("Positive Microbiome Value"), with the same step performed for the "bad genera" ("Negative Microbiome Value").

Other parameters commonly thought to influence prognosis—namely age, stage, and tumor histology—were also considered. The age values for each patient were taken as-is, whilst the staging information was simplified to include only the numbers (e.g. 1A and 1B under Neoplasm Disease Stage American Joint Committee on Cancer Code both became 1). It should be noted that this simplification applied only to three patients, as the remainder were simply Stage I, Stage II, Stage III, or Stage IV. Tumor histology was converted to a binary dummy variable (34), with 0 being epithelioid histology whilst 1 indicated non-epithelioid histology. The rationale for this division was the clinical reality that epithelioid patients have significantly better outcomes than non-epithelioid patients (35).

The dependent (outcome) variable for the multiple linear regression model was the overall survival of the patients in months. The initial independent variables were age, stage, histology, Positive Microbiome Value and Negative Microbiome Value. The initial multiple linear regression model was then refined through several iterations (e.g. removal of independent variables) by examination of the resultant adjusted R^2 values, alongside the p-values for the individual independent variables that were produced at each stage. High p-values were removed on subsequent iterations of the multiple linear regression model.

Cox proportional hazards modelling

To further validate the potential of the microbiome as a prognostic indicator using an independent method, Cox proportional hazard modelling was employed (36). The same data (age, stage, histology, Positive Microbiome Value, and Negative Microbiome Value) was used for this as in the multiple linear regression model above. Overall Survival Status (i.e. 0 (living) and 1 (deceased)) was also extracted from cBioPortal for each patient (19, 20). These data were input to SPSS, with overall survival (in months) used as the "Time" variable and overall survival status used as the "Status" variable. 1 (deceased) was used as the event for Status. As explained above, age, stage, histology, positive microbiome and negative microbiome were all used as covariates.

Results

Validation of survival difference

After generating the "Low Survivors" and "High Survivors" groups described in the Methods above, the survival difference was analysed *via* a Kaplan-Meier curve to validate the grouping approach and ensure the integrity of downstream analysis (Figure 2).

Figure 2 clearly highlights the survival difference between the two groups ($p < 10^{-16}$ and hazard ratio of zero). Whilst clearly an expected result, the significance of the survival difference validates the downstream comparison.

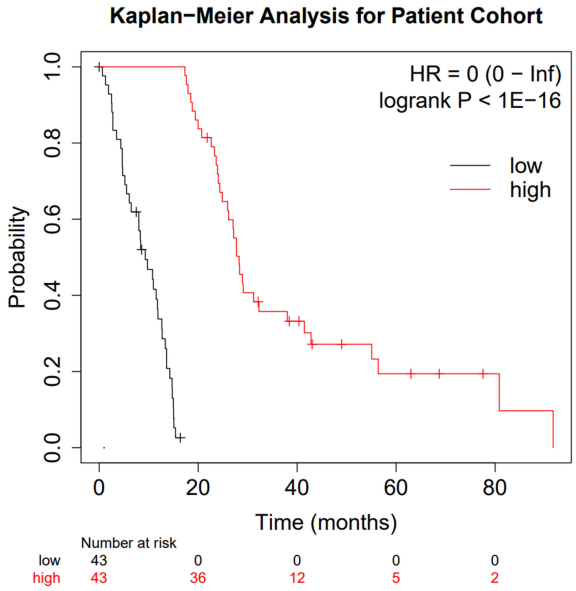

FIGURE 2
Kaplan-Meier curve comparing the two patient subgroups. Low surviving patients are shown in black whilst high-surviving patients are shown in red.

Although the diagnosis age, cancer stage, gender, and histological subtype are of known importance for MMe, there was no statistically significant difference for any of these parameters (based on p- and q-values; see Supplementary Figures 1–7) except the histological subtype, with biphasic MMe being more common in the "Low Survivors" group as opposed to the "High Survivors" group alongside epithelioid histology being less common in the "Low Survivors" group (Supplementary Figure 7). It should be noted that there was the presence of the 9050/3 (Mesothelioma, malignant, NOS) group. This group contains mesothelioma patients who were diagnosed with mesothelioma but with no further information on their histology (NOS = Not Otherwise Specified) (37), but there was not a difference between "Low Survivors" and "High Survivors" for this subtype designation (Supplementary Figure 7). Epithelioid histology being less common in "Low Survivors" whilst biphasic was more common is consistent with known literature that epithelioid histology has the best prognosis of the different histological types of mesothelioma (35).

Microbiome analysis

Following the process described in the Methods, 175 microbiome signatures (genera) were initially identified to be differentially abundant between the "Low Survivors" and "High Survivors" groups ($q < 0.05$). After decontamination analysis, this number was reduced to 107, of which four genera were more abundant in low survivors and 103 were more abundant in high survivors. Literature scoping highlighted that only one genus (*Klebsiella*) returned an article in association with mesothelioma, whilst even a broader general cancer search still yielded very few results (Supplementary Table 1). Figure 3 below demonstrates the frequency distribution of the number of results returned in PubMed for the genera and cancer in general:

The relative scarcity of literature for the genera and cancer, and especially so for the genera and mesothelioma, highlights the significant infancy of this field, and warrants further investigation. As highlighted, only one genus (*Klebsiella*) returned papers for MMe. Conversely,

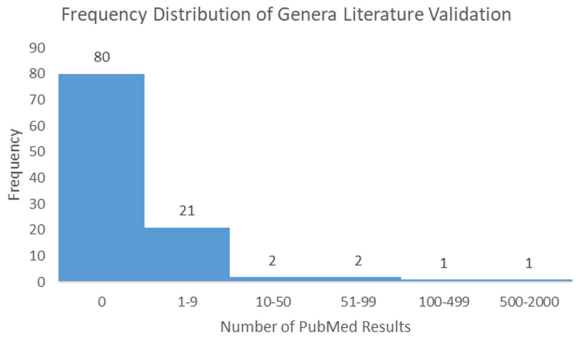

FIGURE 3
Frequency distribution of PubMed results for genera and cancer.

10.3389/fimmu.2023.1129513

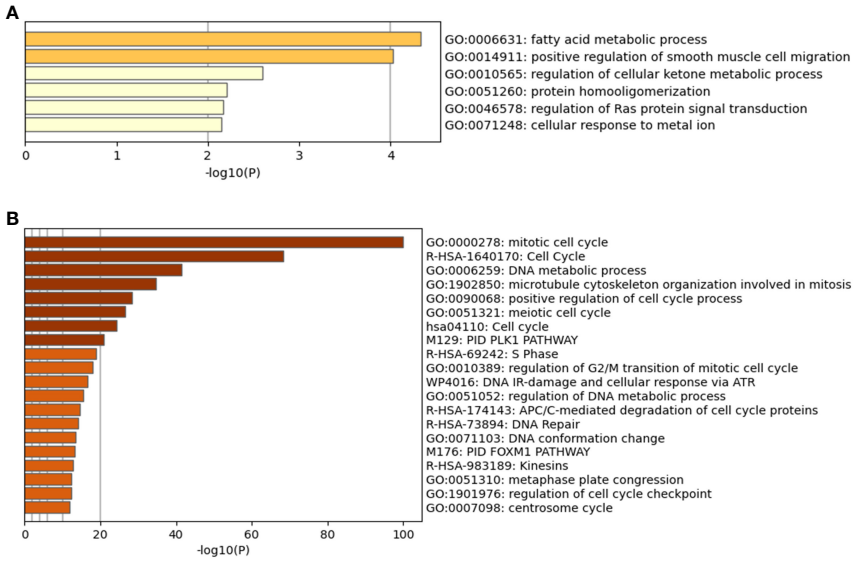

FIGURE 4
Metascape analysis for differentially expressed genes. **(A)** is the High Survivors group, whilst **(B)** is the Low Survivors group.

when searching for cancer in general, 27 genera returned papers. Ranked in order from most to least papers, these were *Klebsiella, Lambdalikevirus, Cyclobacterium, Achromobacter, Yatapoxvirus, Leeia, Magnetococcus, Leptonema, Pragia, Candidatus_Arthromitus, Closterovirus, Vagococcus, Microchaete, Cetobacterium, Chelativorans, Sulfuricurvum, Actinopolymorpha, Cycloclasticus, Beggiatoa, Thalassospira, Pleurocapsa, Anaerofustis, Dichelobacter, Yokenella, Crinivirus, Thioalkalimicrobium*, and *Gemmata*.

Differential gene expression and functional annotation analysis

Following the approach described in the Methods and based on q<0.05, a total of 60 genes were identified to be significantly more expressed in the "High Survivors" group whilst 274 were significantly more expressed in the "Low Survivors" group, listed in Supplementary File 1. To assess the functional relevance of these

TABLE 1 Multiple linear regression model and iterations.

Model Number	Independent Variables Included	P-Values for Independent Variables (*≤0.05)	Adjusted R^2 Value for Model	Independent Variables Removed for Subsequent Model & Why
Model 1	Age	0.506623975	0.170160087	Negative Microbiome Value – with only four genera adding to its value, it was unlikely to show significant differences
	Stage	0.701255523		
	Histology	0.067083872		
	Positive Microbiome Value	0.003256009*		
	Negative Microbiome Value	0.368887571		
Model 2	Age	0.567797635	0.17203895	Age and Stage—as p-values remained high despite previous refinement (in fact, they increased)
	Stage	0.764346949		
	Histology	0.017645789*		
	Positive Microbiome Value	0.000343888*		
Model 3	Histology	0.0064759*	0.188463827	N/A
	Positive Microbiome Value	0.000318305*		

Model number, independent variables included alongside their p-values are provided, as well as the adjusted R^2 value for the model. All models used overall survival (in months) as the dependent (outcome) variable. Raw data behind the models can be seen in Supplementary File 2.

10.3389/fimmu.2023.1129513

genes, the DAVID (28, 29) and Metascape (30) tools were accessed, with the latter shown in Figure 4.

In addition to the figures generated by Metascape, DAVID analysis identified 64 clusters of annotations for the genes upregulated in the Low Survivors group, with the top three containing terms related to cell division and DNA repair (Supplementary File 1). Comparatively, DAVID identified ten clusters of annotations for genes upregulated in the High Survivors group, with the most enriched cluster containing lipid metabolism (Supplementary File 1). Thus, the DAVID analysis complements the Metascape analysis, highlighting the distinct biological processes that are overrepresented in each group.

Multiple linear regression modelling

As described in the Methods, multiple linear regression modelling was performed to identify the independent prognostic value of the microbiome in mesothelioma. The first iteration of the model—"Model 1"—incorporated the patients' age, stage, tumor histology, Positive Microbiome Value (the sum abundance of the 103 identified to be significantly more abundant in High Survivors), and Negative Microbiome Value (sum abundance of the 4 genera identified to be significantly more abundant in Low Survivors). Table 1 below summarizes the iterations (refinement) of the model, the independent variables they include, alongside the adjusted R^2 values and independent variable p-values.

As highlighted above in Table 1, despite the low adjusted R^2 indicating that the independent variables explain at most 18.8% of the variation in overall survival, it remains clear that—at least for this patient cohort—the Positive Microbiome Value was the best predictor for overall survival (based on p-value). This was true against known prognostic factors, including age, stage, and tumor histology.

Cox proportional hazards modelling

To independently validate the prognostic value of the microbiome further using an additional method, Cox proportional hazards modelling (also known as Cox regression) (36) was employed. The same data as for the multiple linear regression model above was used, with the only additional input being the overall survival status (0=alive; 1=deceased) for each patient. The p-value for the Cox proportional hazards model when compared to a null model was <0.001, indicating significant predictive utility. Table 2 below summarizes the coefficients, p-values, hazard ratios, and 95% confidence intervals for each input variable:

Consistent with the multiple linear regression model, only Positive Microbiome Value and Histology were significantly associated with survival in this patient cohort. Positive microbiome had a negative coefficient and a hazard ratio significantly below 1 (based on the 95% confidence interval), emphasizing the protective role of these genera. Comparatively, histology (which was a dummy variable with zero for epithelioid and one for non-epithelioid) had a positive coefficient and a hazard ratio significantly above 1 (based on the 95% confidence interval). Thus, it is again demonstrated that non-epithelioid histology is a negative prognostic factor, consistent with previous literature (35).

Discussion

This study interrogated existing and publicly available patient data with a novel analytical approach to identify genera that were associated with patient survival. It is clear, despite the rising importance of the microbiome in cancer, that the microbiome remains a factor that is highly under-investigated. This is true for cancer in general, with only 27 of the 107 genera identified herein having published literature surrounding them in the context of cancer. The statement of the microbiome being under-investigated is particularly true for MMe, where only one genus out of 107 had literature returned resulting from the search.

Klebsiella, whose signature was more abundant in low survivors, returned only three papers in the context of MMe. However, analysis of these papers further highlights the very limited knowledge that exists around the microbiome in MMe. The first study (38) was a case report highlighting incidence of cerebral air embolism in a patient with chronic hydropneumothorax secondary to epithelioid MMe following pleural catheter insertion. Whilst case reports are naturally limited, the only mention of *Klebsiella* was detailed in the pleural fluid culture, where *Klebsiella oxytoca* and *Enterococcus faecalis* were identified. However, it was not stated if this originated from the pleural fluid or if it was a potential contaminant from the catheter. Thus, it is highly probable that

TABLE 2 Cox proportional hazards modelling.

Variables in the Equation	Coefficient (B)	Sig.	Hazard Ratio (Exp(B))	95.0% CI for Exp(B)	
				Lower	Upper
Positive Microbiome Value	-0.014	**0.001**	0.986	0.978	0.995
Negative Microbiome Value	0.093	0.097	1.097	0.983	1.224
Age	0.011	0.467	1.011	0.981	1.042
Stage	-0.087	0.534	0.916	0.696	1.207
Histology	0.577	**0.045**	1.781	1.013	3.131

Coefficients, p-values, hazard ratios, and 95% confidence intervals for each variable are shown. Statistically significant p-values are in bold.

these genera in this instance were not associated with the intratumor microbiome.

The second paper returned from the search for *Klebsiella* and MMe highlighted sputum-obtained *Klebsiella pneumoniae* from a MMe patient (39). However, this detection did not describe the link to the cancer, only that it was detected in the patient, and may in fact have originated from an upper respiratory infection. The third and final paper that was returned described a novel compound that had demonstrated efficacy against both microbes (including *Klebsiella*) and MMe cells cultured *in vitro* (40). However, no link was made between *Klebsiella* and MMe.

It is evident from the above that there is currently no literature explaining why the microbiome signature of *Klebsiella* was more abundant in low-surviving patients. The fact that the remaining 106 genera had zero papers returned from the literature search highlights the degree of under-exploration that the microbiome suffers in MMe.

Interrogation of the wider literature around *Klebsiella* in other types of cancers highlights some findings that may be of note. In the case of lung cancer, from the analysis of the microbiome in 67 patients with adenocarcinoma (AD) and 47 cases with squamous cell cancer (SCC), *Klebsiella*, alongside *Acidovorax, Rhodopherax* and *Anerococcus* were identified. These genera were found to be more significantly present in SCC than in AD. In addition, the bacterial flora of patients with lung cancer consists mainly of *Proteobacteria* (especially *Acinetobacter* and *Acidovorax*) with a reduced presence of the genus *Firmicutes* (such as *Streptococcus*) and *Bacteroidetes* (*Prevotella*); instead they were present in the flora of patients with pulmonary emphysema. This composition is different in smoking patients with lung cancer, thus attributing an important role to smoking in carcinogenesis and microbiome change. Of note, smoking patients not only had these more abundant genera, but TP53 mutations in the tissue of these subjects also correlated with impaired epithelial function in the lung and thus with the change in the microbiome (41–43). Furthermore, polyketide synthase positive strains of *E. coli* and *K. pneumoniae* (this locus codes for the bacterial toxin colibactin) were isolated in samples from patients with colorectal cancer. This expression has been related to *K. pneumoniae* hypervirulence and intestinal mucosal invasion (44). Finally, it should be noted that a retrospective study revealed that adjuvant treatment with gemcitabine improves survival in *K. pneumoniae*-negative pancreatic cancer patients, whereas adjuvant treatment with quinolones (which are bactericidal) was associated with better overall survival (OS). This result suggests that the presence of *K. pneumoniae* may promote chemoresistance to adjuvant gemcitabine in pancreatic cancer (45). Taken together, is evident that the wider literature supports the negative impact *Klebsiella* has on patients, which is consistent with our finding that *Klebsiella* was more abundant in Low Survivors than High Survivors.

The independent prognostic value of the microbiome was validated through the multiple linear regression model (Table 1). It may initially be surprising that neither age nor stage were validated as predictors of overall survival; however, examination of the underlying data (Supplementary File 2) alongside access of the wider literature highlights that this may not be unusual. The 86 patients included within this study were relatively uniform in age; the median age was 64 (mean 63.08) with a standard deviation of 9.78. The more restricted variability in age could help explain the lack of predictive utility for this variable. Similarly, the number of patients at different stages were uneven: ten patients were Stage 1; sixteen patients were Stage 2; forty-four patients were Stage 3; and sixteen patients were Stage 4. This again indicates a skew in the data, potentially explaining the lack of predictive utility for this variable. Whilst the histology dummy variable was still skewed (62 epithelioid to 24 non-epithelioid) it was less so than the other variables explained previously. An extended analysis (Supplementary File 3) divided patients into "more malignant" and "less malignant" using two independent analyses as a proxy: firstly, division by lymph node involvement and secondly (separately) division by metastatic status. No differential abundance in microbiome signatures between the lymph node groups was observed (based on q-value), and only one genus was differentially abundant based on metastatic state (*Bromovirus*); however, this genus was not present on the list of 107 genera linked to survival (Supplementary File 3). As such, it may be that the genera influence survival through mechanisms outside of malignant state (/lymph node involvement/metastasis).

Further to the above, the identification that epithelioid histology was a significant prognostic indicator compared to other variables has evidence in the literature (46). As Petersen and colleagues published in 2021, epithelioid histology was the only positive independent prognostic factor for treated pleural mesothelioma patients (46). In this patient cohort, neither age nor gender nor stage were significant by univariate analysis for overall survival (OS). It should be noted that another group in the same study (46), those receiving best supportive care (BSC) rather than anti-tumor treatment, did demonstrate, *via* univariate analysis, significant association for gender (female), epithelioid histology, and performance status. However, stage was significant for the BSC group only at the $p<0.1$ level, not $p<0.05$ level, thus indicating general agreement between the results by Petersen (46) and the results presented in this article. It is evident that the potential prognostic value of the microbiome should be explored further.

It is also recognized that tumor-associated macrophages have an impact on mesothelioma prognosis, with the presence of M2-like macrophages leading to worse outcomes (47). As such, given the importance of the microbiome identified herein, it would be interesting to investigate any potential links between M2 macrophages, the microbiome, and mesothelioma. However, as of 17th February 2023, there were zero articles returned on PubMed for a basic Boolean search of this (search terms: (Mesothelioma) AND ((M2-like macrophages) OR (M2 macrophages)) AND (microbiome)). Looking into the wider literature also yielded limited results; only sixteen articles were returned for a search for these terms without mesothelioma on the 17th February 2023 (search terms: (Microbiome[Title/Abstract]) AND ((M2-like macrophages [Title/Abstract]) OR (M2 macrophages[Title/Abstract]))), dropping to nine when "cancer" was added as a search term (without the Title/Abstract] filter). That said, despite the limited literature, some valuable insights are present. Examples of the microbiome affecting M2 macrophages include positive effects of *Lactobacillus murinus* on

the reduction of intestinal injury in mice *via* stimulation of IL-10 release from macrophages (48) and stimulation of tissue remodelling through M2 macrophages in inflammatory bowel disease by *Clostridium innocuum* (a gut bacteria) (49). *Clostridium butyricum*-derived extracellular vesicles affect repolarization of M2 macrophages and protect against colitis (50). In extramammary Paget's disease high levels of *Staphylococcus aureus* were detected that coincided with CD163-positive M2-like macrophages (51), whereas potential association of *Shewanella*, *V. parahaemolyticus*, and *Microbacterium* sp. with prostate cancer has been described, with indications that malignant tissue has higher proportion of M2 microphages (52). High risk colon cancer patients were shown to have increased proportion of M2 macrophages (53), whereas *Fusobacterium nucleatum* is negatively associated with M2 macrophages and positively associated with better outcome in patients with oral squamous cell carcinoma (54). As highlighted, there were no mesothelioma-specific articles returned on this topic, and half of the articles found from the wider search were published in 2020 or later, again indicating this field's relative infancy. The importance of immune infiltration and inflammation lead to a supplementary analysis involving GeneCards (55, 56), where the differentially expressed genes between the Low and High Survivors were compared to the top 5% of genes involved in each process (Supplementary File 4). However, there was minimal overlap between the genes involved in each process and the differentially expressed genes (3/334), indicating that further exploration is required.

Complementing the microbiome analysis was the differential gene expression and functional annotation analyses. Through this, 60 genes were identified to be upregulated in high surviving patients, whilst 274 were upregulated in low surviving patients. The functional annotation analysis also generated insight, with the low surviving group having enriched annotations in terms relating to the cell cycle, cell division, and DNA repair. These processes, if upregulated and deregulated, could potentially explain the poor survival rate of these patients. Comparatively, the most enriched term (according to Metascape) for the high surviving patients was fatty acid metabolic process. Of note is that the high surviving patients had 103 genera signatures more abundant than in the low surviving patients, versus four genera signatures in the reverse direction. This could be interpreted as the high survivors having more abundant microbiome in general, or at least a higher proportion of certain genera in their microbiome composition. Building on this, there are published links between dietary lipids/lipid metabolism and the gut microbiota (57). Fatty acids have the ability to lyse and solubilize bacterial cell membranes (57–59) whilst the gut microbiome may influence lipid metabolism. The links between lipids and gut microbiota have been comprehensively reviewed (57) and although the present study examined the cancer intratumor microbiome rather than the gut microbiome, the fact that "fatty acid metabolic process" was the most enriched term in the group which most genera were increased in demonstrates a potentially direct link between the microbiota/microbiome signatures, the differentially expressed genes and annotations, and the patient survival. Furthermore, it is intriguing that *Klebsiella*, whose signature was more abundant in "Low Survivors", is known to modify its lipopolysaccharide to evade immune surveillance, in the lungs of mice (60). Thus, this demonstrates further potential linkage between the microbiome and cancer, as evading immune detection is a known cancer hallmark (61). Although the association between these genera and fatty acid metabolism in MMe could be correlational rather than causative, we believe it certainly lays the groundwork for further studies to investigate these in more detail.

Although age was not found to be an independent predictor of survival, we observed that the low survivor group tended to have a higher age at diagnosis (median age 66 versus 62, with standard deviations of 11.52 and 7.86 respectively). This, although not statistically significant, may be due to a generally worse clinical status of older patients, but it is interesting to note that ageing affects the microbiota composition and, in turn, the microbiome impacts on organismal ageing and lifespan (62). Indeed, microbiome dysbiosis has been proposed as an additional hallmark and biomarker of aging (62). Ageing is associated with a reduced microbiome diversity and with commensals which favor inflammageing and impair immune functions (63, 64). Compared with the healthy elderly, frail elderly people host more proinflammatory Bacteroidetes commensals and fewer producers of beneficial short-chain fatty acids (65), which is notable given the high surviving group in this study, who could be argued to have 'more' intratumor microbiota due to abundance differences, had fatty acid metabolism as the most enriched biological function. A recent study performed on the duodenal microbiome of elderly patients showed that beyond chronological age, also the number of concomitant diseases and the number of medications affected the microbiome composition with the latter increasing the presence of *Klebsiella* (65). Taken together, such evidence seems consistent with the scenario that we unveiled analyzing the tumor microbiome in mesothelioma patients, which deserves further investigation.

A key limitation of this article is that only pleural mesothelioma has been explored. Indeed, it is recognized that the different subtypes of mesothelioma—pleural, pericardial, peritoneal and testicular—may have different underlying development mechanisms and response to stimuli e.g. a difference in the response to asbestos was noted between peritoneal and pleural mesothelioma (66). Regrettably, cBioPortal (19, 20) had no available information on peritoneal mesothelioma patients. As such, a key area for further exploration would be the investigation in this mesothelioma subtype.

In summary, this article has identified 107 cancer microbiome genera that are pertinent to MMe patient survival, which opens avenues for a new research area in this under-researched cancer. Furthermore, the microbiome was validated in this article as being important for survival through two separate approaches (multiple linear regression modelling and Cox proportional hazards modelling), both of which recognized it as more statistically significant than patient age, tumor stage and even histology (though the effect size of histology remained greater due to its hazard ratio). Laboratory analyses, for example *in vitro* co-culture methods, could be used to start generating solid mechanistic insight at the preclinical level. This foundation will improve understanding of how the microbiome is relevant in MMe and may lead to improved patient outcomes.

Data availability statement

The original contributions presented in the study are included in the article/Supplementary Material. Further inquiries can be directed to the corresponding authors.

Author contributions

Conceptualization: EB; Data curation: FP, MK-D, CC, LM, and EB; Funding Acquisition: LM; Investigation: FP, MK-D, CC, LM, and EB; Project Administration: LM and EB; Validation: FP, MK-D, CC, LM, and EB; Writing: FP, MK-D, CC, LM, and EB. All authors contributed to the article and approved the submitted version.

Acknowledgments

We acknowledge the Italian Ministry of Health "ricerca corrente L3/5" project to CC and FP, LM. We would also like to acknowledge Gruppo Italiano Mesothelioma; G.I.Me.

Conflict of interest

The authors declare that the research was conducted in the absence of any commercial or financial relationships that could be construed as a potential conflict of interest.

Publisher's note

All claims expressed in this article are solely those of the authors and do not necessarily represent those of their affiliated organizations, or those of the publisher, the editors and the reviewers. Any product that may be evaluated in this article, or claim that may be made by its manufacturer, is not guaranteed or endorsed by the publisher.

Supplementary material

The Supplementary Material for this article can be found online at: https://www.frontiersin.org/articles/10.3389/fimmu.2023.1129513/full#supplementary-material

SUPPLEMENTARY FIGURE 1
Comparison of age between "High Survivors" and "Low Survivors"

SUPPLEMENTARY FIGURE 2
Comparison of metastatic state (TNM value) between "High Survivors" and "Low Survivors"

SUPPLEMENTARY FIGURE 3
Comparison of tumor size (TNM value) between "High Survivors" and "Low Survivors"

SUPPLEMENTARY FIGURE 4
Comparison of lymph node involvement (TNM value) between "High Survivors" and "Low Survivors"

SUPPLEMENTARY FIGURE 5
Comparison of cancer stage (number staging system) between "High Survivors" and "Low Survivors"

SUPPLEMENTARY FIGURE 6
Comparison of biological sex between "High Survivors" and "Low Survivors"

SUPPLEMENTARY FIGURE 7
Comparison of histological subtype between "High Survivors" and "Low Survivors". Note that per the World Health Organization (https://apps.who.int/iris/bitstream/handle/10665/96612/9789241548496_eng.pdf), 9050/3 refers to "Mesothelioma, malignant, NOS", 9052/3 to "Epithelioid mesothelioma, malignant, NOS", and 9053/3 to "Mesothelioma, biphasic, malignant, NOS".

SUPPLEMENTARY FILE 1
Excel file of DEGs and DAVID analysis.

SUPPLEMENTARY FILE 2
Excel file of multiple linear regression inputs and iterations, as well as clinical data for the patients.

SUPPLEMENTARY FILE 3
Excel file of microbiome abundance analysis based on patient subdivision by malignancy

SUPPLEMENTARY FILE 4
Excel file of differentially expressed genes mapped to genes involved in either immune infiltration and inflammation (per GeneCards (55, 56)).

References

1. Bakker E, Guazzelli A, Ashtiani F, Demonacos C, Krstic-Demonacos M, Mutti L. Immunotherapy advances for mesothelioma treatment. *Expert Rev Anticancer Ther* (2017) 17(9):799–814. doi: 10.1080/14737140.2017.1358091

2. Baas P, Scherpereel A, Nowak AK, Fujimoto N, Peters S, Tsao AS, et al. First-line nivolumab plus ipilimumab in unresectable malignant pleural mesothelioma (CheckMate 743): a multicentre, randomised, open-label, phase 3 trial. *Lancet* (2021) 397(10272):375–86. doi: 10.1016/S0140-6736(20)32714-8

3. Meirson T, Pentimalli F, Cerza F, Baglio G, Gray SG, Correale P, et al. Comparison of 3 randomized clinical trials of frontline therapies for malignant pleural mesothelioma. *JAMA Netw Open* (2022) 5(3):e221490. doi: 10.1001/jamanetworkopen.2022.1490

4. Messori A, Trippoli S. Current treatments for inoperable mesothelioma: indirect comparisons based on individual patient data reconstructed retrospectively from 4 trials. *J Chemother* (2022), 1–5. doi: 10.1080/1120009X.2022.2061183

5. Kerrigan K, Jo Y, Chipman J, Haaland B, Puri S, Akerley W, et al. A real-world analysis of the use of systemic therapy in malignant pleural mesothelioma and the differential impacts on overall survival by practice pattern. *JTO Clin Res Rep* (2022) 3 (3):100280. doi: 10.1016/j.jtocrr.2022.100280

6. Correale P, Pentimalli F, Nardone V, Giordano A, Mutti L. CONFIRM trial: what is the real efficacy of second-line immunotherapy in mesothelioma? *Lancet Oncol* (2022) 23(1):e13. doi: 10.1016/S1470-2045(21)00702-6

7. O'Connor GM, Bakker EY. Patient-level omics data analysis identifies gene-specific survival associations for a PD-1/PD-L1 network in pleural mesothelioma. *BioMedInformatics* (2022) 2(4):580–92. doi: 10.3390/biomedinformatics2040037

8. Sivan A, Corrales L, Hubert N, Williams JB, Aquino-Michaels K, Earley ZM, et al. Commensal bifidobacterium promotes antitumor immunity and facilitates anti-PD-L1 efficacy. *Science* (2015) 350(6264):1084–9. doi: 10.1126/science.aac4255

9. Liu L, Shah K. The potential of the gut microbiome to reshape the cancer therapy paradigm: A review. *JAMA Oncol* (2022) 8(7):1059–67. doi: 10.1001/jamaoncol.2022.0494

10. Araji G, Maamari J, Ahmad FA, Zareef R, Chaftari P, Yeung SJ. The emerging role of the gut microbiome in the cancer response to immune checkpoint inhibitors: A

narrative review. *J Immunother Precis Oncol* (2022) 5(1):13–25. doi: 10.36401/JIPO-21-10

11. Valdes AM, Walter J, Segal E, Spector TD. Role of the gut microbiota in nutrition and health. *BMJ* (2018) 361:k2179. doi: 10.1136/bmj.k2179

12. Chen J, Douglass J, Prasath V, Neace M, Atrchian S, Manjili MH, et al. The microbiome and breast cancer: a review. *Breast Cancer Res Treat* (2019) 178(3):493–6. doi: 10.1007/s10549-019-05407-5

13. Nejman D, Livyatan I, Fuks G, Gavert N, Zwang Y, Geller LT, et al. The human tumor microbiome is composed of tumor type-specific intracellular bacteria. *Science* (2020) 368(6494):973–80. doi: 10.1126/science.aay9189

14. Helmink BA, Khan MAW, Hermann A, Gopalakrishnan V, Wargo JA. The microbiome, cancer, and cancer therapy. *Nat Med* (2019) 25(3):377–88. doi: 10.1038/s41591-019-0377-7

15. Higuchi R, Goto T, Hirotsu Y, Otake S, Oyama T, Amemiya K, et al. Streptococcus australis and ralstonia pickettii as major microbiota in mesotheliomas. *J Pers Med* (2021) 11(4):297. doi: 10.3390/jpm11040297

16. Carr NJ. New insights in the pathology of peritoneal surface malignancy. *J Gastrointest Oncol* (2021) 12(Suppl 1):S216–s229. doi: 10.21037/jgo-2020-01

17. Magouliotis DE, Tasiopoulou VS, Molyvdas PA, Gourgoulianis KI, Hatzoglou C, Zarogiannis SG. Airways microbiota: Hidden trojan horses in asbestos exposed individuals? *Med Hypotheses* (2014) 83(5):537–40. doi: 10.1016/j.mehy.2014.09.006

18. Setlai BP, Mkhize-Kwitshana ZL, Mehrotra R, Mulaudzi TV, Dlamini Z. Microbiomes, epigenomics, immune response, and splicing signatures interplay: Potential use of combination of regulatory pathways as targets for malignant mesothelioma. *Int J Mol Sci* (2022) 23(16):8991. doi: 10.3390/ijms23168991

19. Cerami E, Gao J, Dogrusoz U, Gross BE, Sumer SO, Aksoy BA, et al. The cBio cancer genomics portal: an open platform for exploring multidimensional cancer genomics data. *Cancer Discovery* (2012) 2(5):401–4. doi: 10.1158/2159-8290.CD-12-0095

20. Gao J, Aksoy BA, Dogrusoz U, Dresdner G, Gross B, Sumer SO, et al. Integrative analysis of complex cancer genomics and clinical profiles using the cBioPortal. *Sci Signal* (2013) 6(269):pl1. doi: 10.1126/scisignal.2004088

21. Kannan S, O'Connor GM, Bakker EY. Molecular mechanisms of PD-1 and PD-L1 activity on a pan-cancer basis: A bioinformatic exploratory study. *Int J Mol Sci* (2021) 22(11):5478. doi: 10.3390/ijms22115478

22. Guo G, Chmielecki J, Goparaju C, Heguy A, Dolgalev I, Carbone M, et al. Whole-exome sequencing reveals frequent genetic alterations in BAP1, NF2, CDKN2A, and CUL1 in malignant pleural mesothelioma. *Cancer Res* (2015) 75(2):264–9. doi: 10.1158/0008-5472.CAN-14-1008

23. Lánczky A, Győrffy B. Web-based survival analysis tool tailored for medical research (KMplot): Development and implementation. *J Med Internet Res* (2021) 23(7):e27633. doi: 10.2196/27633

24. Győrffy B, Lanczky A, Eklund AC, Denkert C, Budczies J, Li Q, et al. An online survival analysis tool to rapidly assess the effect of 22,277 genes on breast cancer prognosis using microarray data of 1,809 patients. *Breast Cancer Res Treat* (2010) 123(3):725–31. doi: 10.1007/s10549-009-0674-9

25. Poore GD, Kopylova E, Zhu Q, Carpenter C, Fraraccio S, Wandro S, et al. Microbiome analyses of blood and tissues suggest cancer diagnostic approach. *Nature* (2020) 579(7800):567–74. doi: 10.1038/s41586-020-2095-1

26. Althouse AD. Adjust for multiple comparisons? it's not that simple. *Ann Thorac Surg* (2016) 101(5):1644–5. doi: 10.1016/j.athoracsur.2015.11.024

27. Rothman KJ. No adjustments are needed for multiple comparisons. *Epidemiology* (1990) 1(1):43–6. doi: 10.1097/00001648-199001000-00010

28. Sherman BT, Hao M, Qiu J, Jiao X, Baseler MW, Lane HC, et al. DAVID: a web server for functional enrichment analysis and functional annotation of gene lists (2021 update). *Nucleic Acids Res* (2022) 50(W1):W216–21. doi: 10.1093/nar/gkac194

29. Huang da W, Sherman BT, Lempicki RA. Systematic and integrative analysis of large gene lists using DAVID bioinformatics resources. *Nat Protoc* (2009) 4(1):44–57. doi: 10.1038/nprot.2008.211

30. Zhou Y, Zhou B, Pache L, Chang M, Khodabakhshi AH, Tanaseichuk O, et al. Metascape provides a biologist-oriented resource for the analysis of systems-level datasets. *Nat Commun* (2019) 10(1):1523. doi: 10.1038/s41467-019-09234-6

31. Zhang Z. Too much covariates in a multivariable model may cause the problem of overfitting. *J Thorac Dis* (2014) 6(9):E196–7. doi: 10.3978/j.issn.2072-1439.2014.08.33

32. Harrell FEJr., Lee KL, Matchar DB, Reichert TA. Regression models for prognostic prediction: advantages, problems, and suggested solutions. *Cancer Treat Rep* (1985) 69(10):1071–77.

33. Lever J, Krzywinski M, Altman N. Model selection and overfitting. *Nat Methods* (2016) 13(9):703–4. doi: 10.1038/nmeth.3968

34. Schneider A, Hommel G, Blettner M. Linear regression analysis: part 14 of a series on evaluation of scientific publications. *Dtsch Arztebl Int* (2010) 107(44):776–82. doi: 10.3238/arztebl.2010.0776

35. Tischoff I, Neid M, Neumann V, Tannapfel A. Pathohistological diagnosis and differential diagnosis. *Recent Results Cancer Res* (2011) 189:57–78. doi: 10.1007/978-3-642-10862-4_5

36. Crichton N. Cox proportional hazards model. *J Clin Nurs* (2002) 11(6):723. doi: 10.1046/j.1365-2702.2002.00714.x

37. Brustugun OT, Nilssen Y, Eide IJZ. Epidemiology and outcome of peritoneal and pleural mesothelioma subtypes in norway. a 20 year nation-wide study. *Acta Oncol* (2021) 60(10):1250–6. doi: 10.1080/0284186X.2021.1955971

38. Jayawardena DMC, Panchal RK, Agrawal S, Das I. Cerebral air embolism after indwelling pleural catheter insertion in a chronic hydropneumothorax secondary to epithelioid mesothelioma. *BMJ Case Rep* (2021) 14(7):e244006. doi: 10.1136/bcr-2021-244006

39. Moland ES, Hong SG, Thomson KS, Larone DH, Hanson ND. Klebsiella pneumoniae isolate producing at least eight different beta-lactamases, including AmpC and KPC beta-lactamases. *Antimicrob Agents Chemother* (2007) 51(2):800–1. doi: 10.1128/AAC.01143-06

40. Başkan C, Ertürk AG, Aydın B, Sırıken B. 3-imino derivative-sulfahydantoins: Synthesis, *in vitro* antibacterial and cytotoxic activities and their DNA interactions. *Bioorg Chem* (2022) 119:105517. doi: 10.1016/j.bioorg.2021.105517

41. Goto T. Microbiota and lung cancer. *Semin Cancer Biol* (2022) 86(Pt 3):1–10. doi: 10.1016/j.semcancer.2022.07.006

42. Liu Y, O'Brien JL, Ajami NJ, Scheurer ME, Amirian ES, Armstrong G, et al. Lung tissue microbial profile in lung cancer is distinct from emphysema. *Am J Cancer Res* (2018) 8(9):1775–87.

43. Greathouse KL, White JR, Vargas AJ, Bliskovsky VV, Beck JA, von Muhlinen N, et al. Interaction between the microbiome and TP53 in human lung cancer. *Genome Biol* (2018) 19(1):123. doi: 10.1186/s13059-018-1501-6

44. Strakova N, Korena K, Karpiskova R. Klebsiella pneumoniae producing bacterial toxin colibactin as a risk of colorectal cancer development - a systematic review. *Toxicon* (2021) 197:126–35. doi: 10.1016/j.toxicon.2021.04.007

45. Weniger M, Hank T, Qadan M, Ciprani D, Michelakos T, Niess H, et al. Influence of klebsiella pneumoniae and quinolone treatment on prognosis in patients with pancreatic cancer. *Br J Surg* (2021) 108(6):709–16. doi: 10.1002/bjs.12003

46. Ringgaard Petersen T, Panou V, Meristoudis C, Weinreich UM, Røe OD. Clinical prognostic factors in pleural mesothelioma: best supportive care and anti-tumor treatments in a real-life setting. *Acta Oncol* (2021) 60(4):521–7. doi: 10.1080/0284186X.2021.1876246

47. Cersosimo F, Barbarino M, Lonardi S, Vermi W, Giordano A, Bellan C, et al. Mesothelioma malignancy and the microenvironment: Molecular mechanisms. *Cancers (Basel)* (2021) 13(22):5664. doi: 10.3390/cancers13225664

48. Hu J, Deng F, Zhao B, Lin Z, Sun Q, Yang X, et al. Lactobacillus murinus alleviate intestinal ischemia/reperfusion injury through promoting the release of interleukin-10 from M2 macrophages *via* toll-like receptor 2 signaling. *Microbiome* (2022) 10(1):38. doi: 10.1186/s40168-022-01227-w

49. Ha CWY, Martin A, Sepich-Poore GD, Shi B, Wang Y, Gouin K, et al. Translocation of viable gut microbiota to mesenteric adipose drives formation of creeping fat in humans. *Cell* (2020) 183(3):666–683.e17. doi: 10.1016/j.cell.2020.09.009

50. Liang L, Yang C, Liu L, Mai G, Li H, Wu L, et al. Commensal bacteria-derived extracellular vesicles suppress ulcerative colitis through regulating the macrophages polarization and remodeling the gut microbiota. *Microb Cell Fact* (2022) 21(1):88. doi: 10.1186/s12934-022-01812-6

51. Sakamoto R, Kajihara I, Mijiddorj T, Otsuka-Maeda S, Sawamura S, Nishimura Y, et al. Existence of staphylococcus aureus correlates with the progression of extramammary paget's disease: potential involvement of interleukin-17 and M2-like macrophage polarization. *Eur J Dermatol* (2021) 31(1):48–54. doi: 10.1684/ejd.2021.3972

52. Salachan PV, Rasmussen M, Fredsøe J, Ulhøi B, Borre M, Sørensen KD. Microbiota of the prostate tumor environment investigated by whole-transcriptome profiling. *Genome Med* (2022) 14(1):9. doi: 10.1186/s13073-022-01011-3

53. Yu J, Nong C, Zhao J, Meng L, Song J. An integrative bioinformatic analysis of microbiome and transcriptome for predicting the risk of colon adenocarcinoma. *Dis Markers* (2022) 2022:7994074. doi: 10.1155/2022/7994074

54. Neuzillet C, Marchais M, Vacher S, Hilmi M, Schnitzler A, Meseure D, et al. Prognostic value of intratumoral fusobacterium nucleatum and association with immune-related gene expression in oral squamous cell carcinoma patients. *Sci Rep* (2021) 11(1):7870. doi: 10.1038/s41598-021-86816-9

55. Stelzer G, Rosen N, Plaschkes I, Zimmerman S, Twik M, Fishilevich S, et al. The GeneCards suite: From gene data mining to disease genome sequence analyses. *Curr Protoc Bioinf* (2016) 54(1):1.30.1–1.30.33. doi: 10.1002/cpbi.5

56. Safran M, Rosen N, Twik M, BarShir R, Stein TI, Dahary D, et al. *The GeneCards suite, in practical guide to life science databases*. Abugessaisa I, Kasukawa T, editors. Singapore: Springer Nature Singapore (2021) p. 27–56.

57. Schoeler M, Caesar R. Dietary lipids, gut microbiota and lipid metabolism. *Rev Endocr Metab Disord* (2019) 20(4):461–72. doi: 10.1007/s11154-019-09512-0

58. Jackman JA, Yoon BK, Li D, Cho NJ. Nanotechnology formulations for antibacterial free fatty acids and monoglycerides. *Molecules* (2016) 21(3):305. doi: 10.3390/molecules21030305

59. Shilling M, Matt L, Rubin E, Visitacion MP, Haller NA, Grey SF, et al. Antimicrobial effects of virgin coconut oil and its medium-chain fatty acids on clostridium difficile. *J Med Food* (2013) 16(12):1079–85. doi: 10.1089/jmf.2012.0303

60. Llobet E, Martínez-Moliner V, Moranta D, Dahlström KM, Regueiro V, Tomás A, et al. Deciphering tissue-induced klebsiella pneumoniae lipid a structure. *Proc Natl Acad Sci* (2015) 112(46):E6369–78. doi: 10.1073/pnas.1508820112

61. Hanahan D. Hallmarks of cancer: New dimensions. *Cancer Discovery* (2022) 12 (1):31–46. doi: 10.1158/2159-8290.CD-21-1059

62. Bana B, Cabreiro F. The microbiome and aging. *Annu Rev Genet* (2019) 53:239–61. doi: 10.1146/annurev-genet-112618-043650

63. Conway J, Duggal, NA. Ageing of the gut microbiome: Potential influences on immune senescence and inflammageing. *Ageing Res Rev* (2021) 68:101323. doi: 10.1016/j.arr.2021.101323

64. Spakowicz D, Bibi A, Muniak M, Williams NF, Hoyd R, Presley CJ. The aging microbiome and response to immunotherapy: Considerations for the treatment of older adults with cancer. *J Geriatr Oncol* (2021) 12(6):985–9. doi: 10.1016/j.jgo.2021.02.001

65. Leite G, Pimentel M, Barlow GM, Chang C, Hosseini A, Wang J, et al. Age and the aging process significantly alter the small bowel microbiome. *Cell Rep* (2021) 36 (13):109765. doi: 10.1016/j.celrep.2021.109765

66. Dragon J, Thompson J, MacPherson M, Shukla A. Differential susceptibility of human pleural and peritoneal mesothelial cells to asbestos exposure. *J Cell Biochem* (2015) 116(8):1540–52. doi: 10.1002/jcb.25095

frontiers | Frontiers in Immunology

TYPE Original Research
PUBLISHED 21 March 2023
DOI 10.3389/fimmu.2023.1148798

OPEN ACCESS

EDITED BY
Chiara Porta,
University of Eastern Piedmont, Italy

REVIEWED BY
Paolo Andrea Zucali,
Humanitas University, Italy
Elisa Giovannetti,
VU Medical Center, Netherlands

*CORRESPONDENCE
Luc Willems
luc.willems@uliege.be

†These authors have contributed equally to this work and share last authorship

SPECIALTY SECTION
This article was submitted to Cancer Immunity and Immunotherapy, a section of the journal Frontiers in Immunology

RECEIVED 20 January 2023
ACCEPTED 20 February 2023
PUBLISHED 21 March 2023

CITATION
Willems M, Scherpereel A, Wasielewski E, Raskin J, Brossel H, Fontaine A, Grégoire M, Halkin L, Jamakhani M, Heinen V, Louis R, Duysinx B, Hamaidia M and Willems L (2023) Excess of blood eosinophils prior to therapy correlates with worse prognosis in mesothelioma. *Front. Immunol.* 14:1148798. doi: 10.3389/fimmu.2023.1148798

Excess of blood eosinophils prior to therapy correlates with worse prognosis in mesothelioma

Mégane Willems[1], Arnaud Scherpereel[2], Eric Wasielewski[2], Jo Raskin[3], Hélène Brossel[1], Alexis Fontaine[1], Mélanie Grégoire[1], Louise Halkin[1], Majeed Jamakhani[1], Vincent Heinen[4], Renaud Louis[4], Bernard Duysinx[4], Malik Hamaidia[1†] and Luc Willems[1*†]

[1]Laboratory of Molecular and Cellular Epigenetics (GIGA at University of Liege), Sart-Tilman, Molecular Biology, Teaching and Research Centre (TERRA), Gembloux, Belgium, [2]Department of Pneumology and Thoracic Oncology, (CHU Lille) and INSERM (ONCOTHAI), Lille, France, [3]Department of Pulmonology and Thoracic Oncology, Antwerp University Hospital, Edegem, Belgium, [4]Department of Pneumology, University Hospital of Liege, Liege, Belgium

Background: Only a fraction of patients with malignant pleural mesothelioma (MPM) will respond to chemo- or immunotherapy. For the majority, the condition will irremediably relapse after 13 to 18 months. In this study, we hypothesized that patients' outcome could be correlated to their immune cell profile. Focus was given to peripheral blood eosinophils that, paradoxically, can both promote or inhibit tumor growth depending on the cancer type.

Methods: The characteristics of 242 patients with histologically proven MPM were retrospectively collected in three centers. Characteristics included overall survival (OS), progression-free survival (PFS), overall response rate (ORR) and disease control rate (DCR). The mean absolute eosinophil counts (AEC) were determined by averaging AEC data sets of the last month preceding the administration of chemo- or immunotherapy.

Results: An optimal cutoff of 220 eosinophils/µL of blood segregated the cohort into two groups with significantly different median OS after chemotherapy (14 and 29 months above and below the threshold, $p = 0.0001$). The corresponding two-year OS rates were 28% and 55% in the AEC ≥ 220/µL and AEC < 220/µL groups, respectively. Based on shorter median PFS (8 *vs* 17 months, $p < 0.0001$) and reduced DCR (55.9% vs 35.2% at 6 months), the response to standard chemotherapy was significantly affected in the AEC ≥ 220/µL subset. Similar conclusions were also drawn from data sets of patients receiving immune checkpoint-based immunotherapy.

Conclusion: In conclusion, baseline AEC ≥ 220/µL preceding therapy is associated with worse outcome and quicker relapse in MPM.

KEYWORDS

malignant pleural mesothelioma, eosinophils, chemotherapy, cisplatin, pemetrexed

Introduction

Malignant pleural mesothelioma (MPM) is a cancer associated with very poor prognosis mainly induced by occupational exposure to asbestos fibers (1). Despite the ban or limitation of asbestos use (2), incidence of MPM is still increasing worldwide (3) due to the long latency time between exposure and neoplasm development. There are 3 main histological subtypes of MPM: epithelioid (60–80% of cases), sarcomatoid (< 10%) and biphasic/mixed (10–15%) (4, 5). Therapeutic standard options include conventional treatments (surgery, radiotherapy, chemotherapy) and, more recently, immunotherapy (6–8). Thus, since 2003 the first-line standard-of-care for unresectable MPM has been chemotherapy based on the combination of a DNA cross-linking agent (cisplatin or carboplatin) and an antifolate (pemetrexed) (6). The median overall survival (mOS) obtained with this regimen ranges between 13 and 16 months (6, 9). Addition of an anti-VEGF antibody (bevacizumab) to cisplatin/pemetrexed improved mOS up to 18.8 months compared to 16.0 months in the control arm (9). As many MPM patients have a weakened immune system, chemotherapy initially seemed to be a better option than immunotherapy (10). However, the recent first-line dual immunotherapy by immune checkpoint inhibitors (ICIs) (nivolumab and ipilimumab, targeting PD-1 and CTLA-4, respectively) extended mOS from 14.1 months with standard chemotherapy to 18.1 months (11). Immunotherapy has only a limited benefit for the epithelioid subtype but is particularly effective for non-epithelioid MPM (12). Compared with chemotherapy, ICIs clearly provide much better OS rates at 4 years in non-epithelioid MPM (i.e., 14% *vs* 1%, respectively).

Despite these recent improvements, the prognosis of MPM remains globally poor. The biological mechanisms that drive the effectiveness of available therapies are still not well understood. However, the recent breakthroughs of ICIs indicate that the tumor microenvironment (TME) is a major parameter in cancer development and response to therapy. Even though mesothelioma was initially considered as a "cold" tumor (*i.e.*, absence of T cells within or at the edges of the tumor), the paradigm has recently been revisited (10). In the mesothelioma TME, tumor-associated macrophages (TAMs) are the most abundant immune infiltrating cells (13–18). The phenotype of these TAMs is shaped by mediators expressed by tumor cells. Therefore, the ability of TAMs to orchestrate the innate immune response and to modulate activation of effector T-cells is impaired in MPM. Among immune cells that regulate macrophage polarization, eosinophils favor the M1 phenotype through the production of IFN-γ and TNF-α. However, eosinophil-derived IL-4 and IL-13 can also promote suppressive TAMs and shape the TME (19, 20). The balance between Th1- and Th2-related cytokines modulates the migration and activation of $CD8^+$ T-cells and affects the local anti-tumor response. Among their pleiotropic activities, eosinophils also promote angiogenesis and tissue healing *via* VEGF, FGF and PDGF production. Besides their ability to shape the TME through the expression of cytokines, eosinophils display cytotoxic effects by secreting granule proteins and granzyme A.

Altogether, this evidence thus indicates that eosinophils exert both pro- and anti-tumorigenic activities. The final outcome will depend on a variety of parameters that include the cytokine balance, the interaction of eosinophils with other immune cells and the resulting cytotoxicity against the tumor. In this context, we investigated the correlation of blood eosinophil counts with mOS, progression-free survival (PFS) and duration of response in patients undergoing chemo- or immunotherapy.

Materials and methods

Patients' selection and data collection

Two hundred and forty-two eligible MPM patients were included in this study. Between January 2009 and December 2021, these patients were given chemo- or immunotherapy in 3 hospitals: 68 at the University Hospital of Liege (Belgium), 61 at the University Hospital of Antwerp (Belgium) and 101 at the University Hospital of Lille (France). According to standard guidelines, 230 patients received cisplatin or carboplatin and pemetrexed as first-line chemotherapy (4, 21). Among these, 32 patients also received 2^{nd} or 3^{rd} line immunotherapy with nivolumab and ipilimumab. Twelve patients were given ICIs in first-line therapy.

Exclusion criteria included autoimmune disease, congenital or acquired immunodeficiency including HIV, asthma, and active parasitic infection at diagnosis, requiring systemic treatment. Patients diagnosed less than a year before the study was initiated or who did not complete a full treatment plan were also excluded as the follow-up period was too short.

All data were collected for medical purposes and obtained retrospectively. The following data were collected from hospital databases: date of birth; date of diagnosis; sex; histological subtype; BAP-1 deletion; date and type of treatment; response to treatment at 3 months, 6 months and 1 year; hematological lab tests before, during and after treatment; smoking status; diabetes status; asbestos exposure information; comorbidity information; date of death if applicable. Clinical staging was not available for most patients.

This study was performed in compliance with the Helsinki Declaration and was approved by the local Ethics Committee with the reference 2020/45 (University Hospital of Liege) and 2022/1844 (University Hospital of Antwerp) and declared to the local Data Protection Officer (DPO), per General Data Protection Regulation (University Hospital of Lille). As this was a retrospective and non-interventional study, informed consent was not required. Medical records were analyzed pseudonymously.

Outcomes and statistical analysis

Absolute eosinophil counts (AEC) are routinely determined from hemograms collected at presentation. They were retrieved from the available medical records. Optimal AEC cutoff was determined with the X-tile 3.6.1 software (Yale University, New Heaven, CT) and validated by the receiver operating characteristics (ROC) curve. The analysis was based on the mean AEC, averaged during the last month preceding the administration of chemo- or immunotherapy.

The primary studied endpoint was mOS, defined as the time from the diagnosis to the date of death due to any cause. Secondary endpoints included PFS, response rate, duration of response and disease control rate. The response was assessed with radiographic tumor assessment according to the modified Response Criteria (mRECIST) [version 1.1] (4, 22). PFS was defined as the time between diagnosis and first-documented tumor progression or death due to any cause, whichever came first. Response rate was defined as the best overall response of complete response (CR) or partial response (PR). Duration of response was defined as the time from the first response to the first documented tumor progression or death due to any cause, whichever occurred first. Disease control rate was defined as the best overall response of CR, PR, or stable disease (SD).

Hazard ratios (HRs) and confidence intervals (CIs) of 95% were assessed using an unstratified Cox proportional hazards regression model. Survival curves and rates were estimated with the Kaplan-Meier method and Log-Rank test. Patients with missing values were excluded from the analysis. For statistical purposes, age was categorized as less than 65 years and more or equal to 65 years, whereas subtype was classified as epithelioid and non-epithelioid (i.e., sarcomatoid, biphasic or desmoplastic).

Statistical analysis and graphs were performed by using Prism GraphPad 8 or RStudio 2022.07.1 + 554.

Results

A threshold of AEC at 220/µL splits the cohort into two groups with different overall survival

The X-tile software was used to identify the optimal AEC cutoff associated with survival in the cohort of 230 MPM patients receiving first-line chemotherapy. This bioinformatic tool is a graphical method for biomarker assessment and outcome-based cut-point optimization (23). The program provides the optimal division of the data by selecting significant uncorrected p-value and the highest Chi-square. An average AEC was calculated for each patient using the counts of the last month preceding the first administration of chemotherapy. The optimal AEC cutoff determined with the X-tile software was 220 eosinophils/µL of blood (Chi-square = 10.5992, uncorrected p = 0.00113, Figure 1A). This threshold divided the cohort into two groups of 169 (72.40%) and 61 (27.60%) subjects with AEC < 220/µL (in grey) and AEC ≥ 220/µL (in blue), respectively (Figure 1B). These settings optimally segregated the Kaplan-Meier survival curves of the two subsets (Figure 1C). The relative risk was estimated by dividing the death incidence corresponding to each AEC by that of the population (Figure 1D). The AEC 220/µL cutoff classified the patients into two populations with highly significant different distributions (p = 0.0005, Figure 1E). The ROC curve illustrating the true (sensitivity) and false (1-specificity) positive rates validated the cutoff of 220 eosinophils/µL of blood (AUC = 0.6475, p = 0.0006, Figure 1F).

To verify that the measured AEC levels did not result from an increase of all white blood cells, the average absolute counts of other leukocytes were calculated. In populations with AEC < 220/µL and AEC ≥ 220/µL, the absolute counts of lymphocytes, monocytes and neutrophils were similar (Figure 1G). Since the absolute counts of eosinophils differed significantly (p < 0.0001), it was concluded that high levels of AEC did not result from a general increase of all leukocyte subsets. Furthermore, X-tiles analysis of neutrophils, lymphocytes, monocytes and neutrophil-to-lymphocyte ratio (NLR) did not highlight any threshold or correlation with mOS.

This cut-point selection analysis thus indicated that a threshold of AEC ≥ 220/µL within the last month preceding the first administration of chemotherapy optimally divided the total population into two subsets displaying statistically significant different overall survival times.

Study population

Among the 230 eligible patients treated by chemotherapy, 53 males and 8 females' cases were above the threshold of AEC ≥ 220/µL (Table 1). The median age at the time of diagnosis of the patients with AEC < 220/µL and AEC ≥ 220/µL was similar (67 +/- 10.4 *vs* 67 +/- 10.9 years, respectively). In both categories, most patients were male (74.0% and 86.9%) and presented an epithelioid subtype of MPM (87.0% and 77.0%). These characteristics were thus representative of typical gender and histologic distributions of MPM (4).

Due to limitations of a retrospective study, only partial information was available for asbestos exposure, Eastern Cooperative Oncology Group (ECOG) performance status prior to chemotherapy, smoking status, diabetes, and BAP-1 expression (Table 1). Prior exposure to asbestos was confirmed in 28.4% and 34.4% of patients with AEC < and ≥ 220/µL, respectively. The proportions of patients presenting different ECOG performance status were similar. OS and AEC/µL were not statistically different in patients with ECOG status 0, 1 and 2 (Supplementary Figure 1). Both active tobacco consumption and diabetes affected a minority of patients. Loss of BAP-1 expression determined by immunohistochemistry was validated in 24.9% of AEC < 220/µL and 18.0% of AEC ≥ 220/µL subsets.

It thus appeared that the two populations split by the AEC 220/µL cutoff shared similar characteristics of age, gender and histological subtype.

AEC ≥ 220/µL is correlated with shorter overall survival

Kaplan-Meier analysis showed that patients characterized by AEC ≥ 220/µL during the month preceding their chemotherapy had a highly significant shorter OS compared to subjects with AEC < 220/µL (Figure 2A). The mOS of the 230 individuals enrolled in this study were 14 months and 29 months for AEC above or equal to and below 220/µL, respectively (p = 0.0001, HR of 2.063 [95% CI

A

% Total	AEC Range (/µL)	Chi square	Uncorrected P
72.40 %	0 to 219	10.5992	0.00113
27.60 %	220 to 1,020		

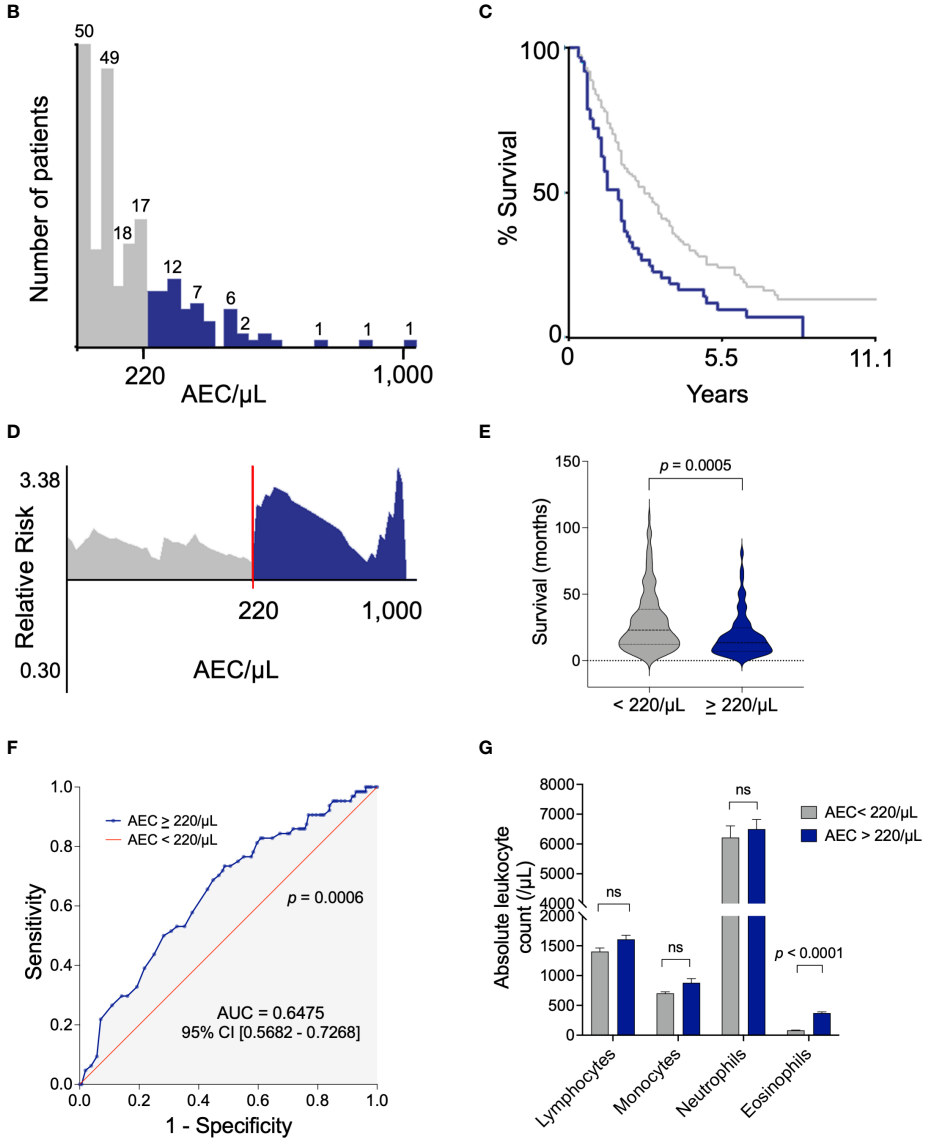

FIGURE 1
Determination of the AEC cutoff that optimally segregates the cohort according to OS. **(A)** An average AEC was calculated for each patient using the counts of the last month preceding the first administration of chemotherapy. The X-tile 3.6.1 software divided the data set into two populations by selecting significative uncorrected p-value and the highest Chi square. **(B)** Distribution of patients according to their AEC (below 219 per µl of blood in grey and 220-1,020 in blue). **(C)** Kaplan-Meier survival curve according to the AEC < 220/µL and AEC ≥ 220/µL. **(D)** The relative risk estimated by dividing the death incidence at each AEC by the death incidence of the population. **(E)** Median survival (in months) of the populations according to the AEC threshold. Normality of the populations was analyzed by the Shapiro-Wilk test and distributions were compared by Mann-Whitney test. **(F)** The ROC analysis of the true (sensitivity) and false (1-specificity) positive rates. **(G)** Absolute leucocyte counts (mean +/- standard deviation) in patients with AEC < 220/µL and AEC ≥ 220/µL. Statistical significance was calculated with the unpaired t-test. AEC, absolute eosinophil count; ROC, receiver operating characteristics; AUC, area under the curve.

1.420 – 2.998]). At 1 year, the OS rates were 58% [44.8 – 68.4] in subjects with AEC ≥ 220/µL compared to 79% [72.1 – 84.9] in the AEC < 220/µL group. The difference between the two categories was more pronounced at 2 years (28% [17.4 – 39.0] *vs* 55% [46.6 – 62.6]) corresponding to a 2.0-fold improvement in mOS when AEC < 220/µL. The lower mOS in the AEC ≥ 220/µL subset was observed independently of the histologic subtype (Figures 2B, C).

Although the proportion of patients with AEC ≥ 220/µL differed in the 3 hospitals (i.e., 17.8% in Lille, 32.35% in Liege and 34.4% in Antwerp; Supplementary Table 1), the mOS was significantly

10.3389/fimmu.2023.1148798

TABLE 1 Baseline characteristics of all patients receiving chemotherapy, segregated by the AEC cutoff of 220/µL.

	AEC < 220/µL		AEC ≥ 220/µL	
	N of patients (total 169)	% of patients	*N* of patients (total 61)	% of patients
Age at diagnosis:	67 ± 10.4 years		67 ± 10.9 years	
Sex				
Male	125	74.0%	53	86.9%
Female	44	26.0%	8	13.1%
Histological subtype				
Epithelioid	147	87.0%	47	77.0%
Sarcomatoid	10	5.9%	7	11.5%
Biphasic	6	3.6%	5	8.2%
Desmoplastic	3	1.8%	1	1.6%
Unknown	3	1.8%	1	1.6%
Known asbestos exposure				
Yes	48	28.4%	21	34.4%
No	91	53.8%	25	41.0%
Unknown	36	21.3%	15	24.6%
ECOG status prior to chemotherapy				
0	28	16.6%	8	13.1%
1	84	49.7%	26	42.6%
2	6	3.6%	2	3.3%
Unknown	57	33.7%	25	41.0%
Smoking status				
Smoking	25	14.8%	11	18.0%
Detoxed	56	33.1%	14	23.0%
No	78	46.2%	35	52.5%
Unknown	10	5.9%	4	6.6%
Diabetes				
Insulin-dependent	13	7.7%	5	8.2%
Non-insulin-dependent	19	11.2%	3	4.9%
No	128	75.7%	51	83.6%
Unknown	9	5.3%	2	3.3%
BAP-1 loss of expression				
Yes	42	24.9%	11	18.0%
No	17	10.1%	4	6.6%
Unknown	110	65.1%	46	75.4%

reduced from 36 to 17 months (p = 0.0062 for CHU of Lille) and from 29 to 16 months (p = 0.0184 for UZ Antwerp) (Supplementary Figure 2). However, there was no statistical difference in patients from the Liege CHU (17 vs 15 months, p = 0.4610) which may indicate a center bias. Furthermore, OS was shorter for patients with AEC ≥ 220/µL in predefined subgroups (Supplementary Figure 3).

Altogether, this retrospective observational study thus indicated that MPM patients with AEC ≥ 220/µL had a shorter mOS.

10.3389/fimmu.2023.1148798

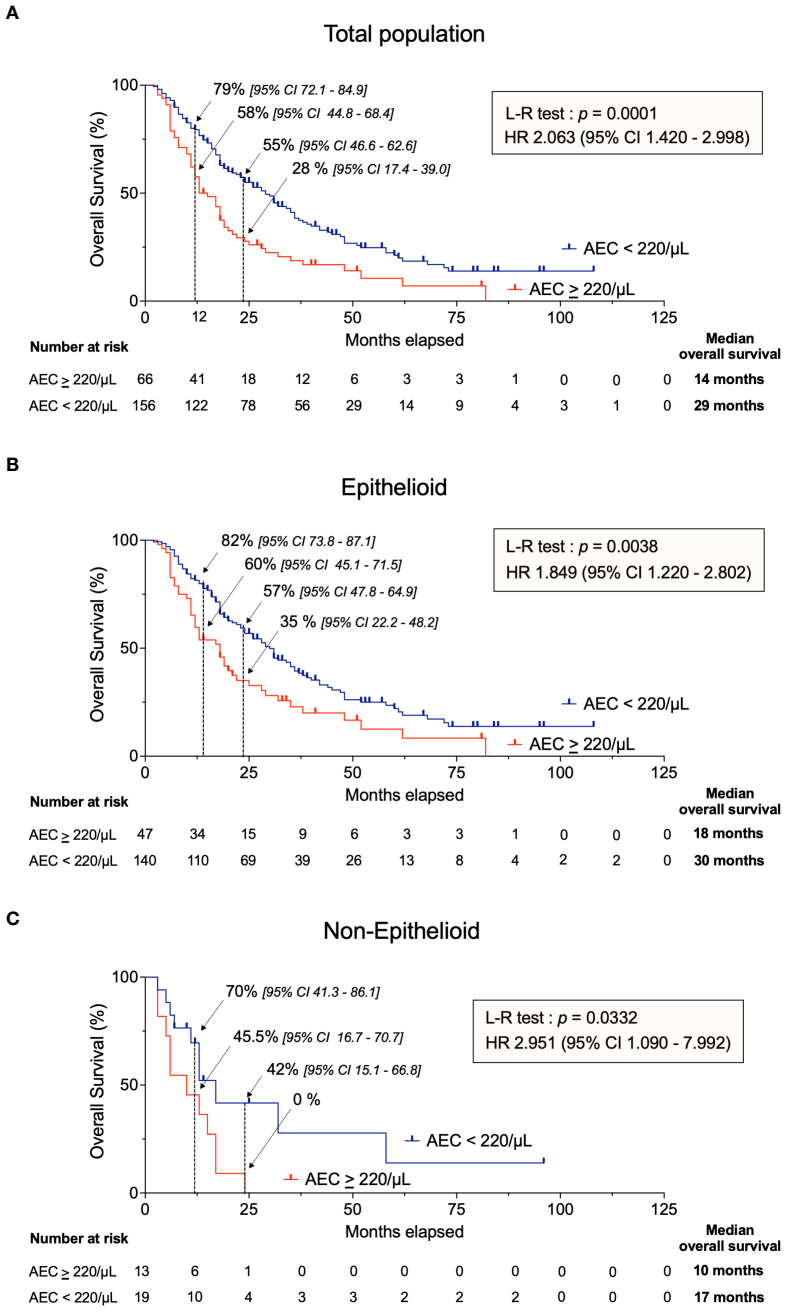

FIGURE 2
Kaplan-Meier analysis of OS in chemotherapy-treated patients with AEC ≥ 220/µL (in red) and AEC < 220/µL (in blue). **(A)** All patients of the cohort, **(B)** epithelioid MPM and **(C)** non-epithelioid MPM. AEC, absolute eosinophil count; OS, overall survival; L-R test; Log-Rank test; HR, hazard ratio; CI, confidence interval.

AEC superior or equal to 220/µL is associated with earlier relapse

The median PFS after chemotherapy was significantly lower in the AEC ≥ 220/µL group compared to the AEC < 220/µL subset (8 months *vs* 17 months; $p < 0.0001$, HR 2.589 [1.606 – 4.173]) (Figure 3A). Notably, PFS at 2 years was 13% [4.6 – 25.4] *vs* 42% [33.5 – 51.1] in patients with AEC ≥ 220/µL and AEC < 220/µL, respectively. Furthermore, the median time until progression or relapse differed significantly (7 months when AEC ≥ 220/µL *vs* 16 months when AEC < 220/µL; $p = 0.0011$, HR 1.950 [1.307 – 2.908]) (Figure 3B). Analysis of this retrospective dataset thus indicated that relapse after chemotherapy occurred more rapidly when AEC ≥ 220/µL.

Partial information on response to treatment was available in the retrospective data set (145 and 45 patients in the AEC < 220/µL and AEC ≥ 220/µL groups, respectively (Table 2). Information on response to treatment was missing in 31 patients. A single CR was

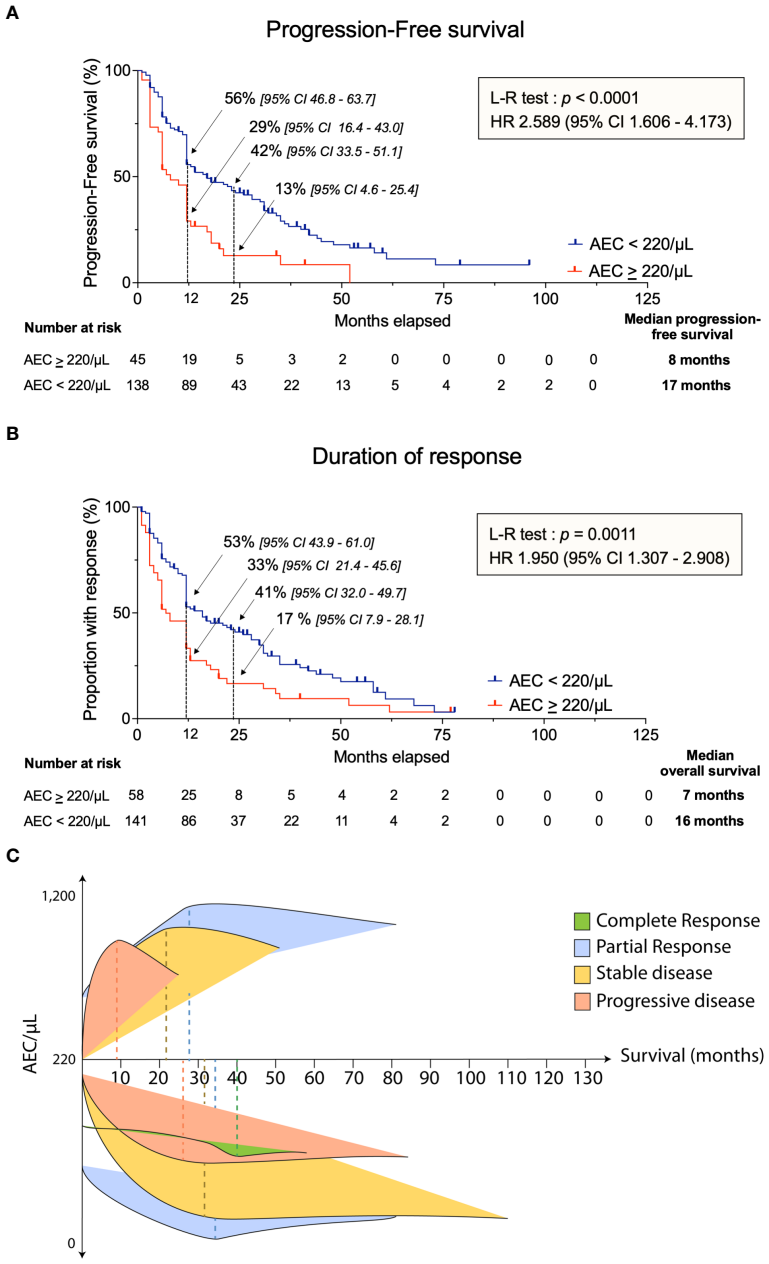

FIGURE 3
Response to chemotherapy according to AEC cutoff. **(A)** Progression-free survival in all randomized patients. **(B)** Duration of response in confirmed responders segregated by the AEC cutoff of 220/µL. **(C)** Schematic representation of response to chemotherapy, survival distribution and AEC. Dashed lines are the median survival (in months) corresponding to the type of response. L-R test, Log-Rank test; HR, hazard ratio; AEC, absolute eosinophil count.

observed in each category, consistently with other MPM trials (11, 24, 25). The objective response rate (ORR) combining CR and PR was similar in the 2 subsets (15.9% *vs* 20.4% at 3 months and 9.0% *vs* 9.3% at 6 months). In contrast, SD was significantly more common in patients with AEC < 220/µL (56.6%) than in those with AEC ≥ 220/µL (38.9%). This difference in SD was due to a higher proportion of patients with progressive disease (PD) in the AEC ≥ 220/µL subgroup (33.3%, *vs* 17.2%). Only 33% [21.4 – 45.6] of patients with AEC ≥ 220/µL displayed a disease control, including CR, PR and SD of at least 1 year, compared to 53% [43.9 – 61.0] in subjects with AEC < 220/µL. This difference was still observed after 2 years (17% in AEC ≥ 220/µL *vs* 41% in AEC < 220/µL).

Together, these data showed that the AEC cutoff of 220/µL identified groups of patients with different mOS (Figure 2A) and response to chemotherapy (Figure 3C). The same conclusion was drawn when the study was extended to patients who received immunotherapy (Supplementary Figures 4, 5). Indeed, Kaplan-Meier analysis highlighted that, patients with AEC ≥ 220/µL prior to immunotherapy had a shorter OS (p = 0.0022) and was characterized by a higher proportion of PD (42.9% *vs* 18.9%) compared with the AEC < 220/µL group.

10.3389/fimmu.2023.1148798

TABLE 2 Summary of patient's response in all randomized patients receiving chemotherapy, segregated by the AEC cutoff of 220/µL.

	AEC < 220/µL		AEC ≥ 220/µL	
	N of patients (total 145)	% of patients	*N* of patients (total 54)	% of patients
Best overall response				
Complete response	1	0.7%	1	1.9%
Partial response	37	25.5%	14	25.9%
Stable disease	82	56.6%	21	38.9%
Progressive disease	25	17.2%	18	33.3%
Disease control rate (CR + PR + SD)				
3 months	99	68.3%	29	53.7%
6 months	81	55.9%	19	35.2%
Objective response rate (CR + PR)				
3 months	23	15.9%	11	20.4%
6 months	13	9.0%	5	9.3%
Proportion of patients with a response of at least 1 year				
1 year	53%		33%	
95% CI	43.9 – 61.0		21.4 – 45.6	
2 years	41%		17%	
95% CI	32.0 – 49.7		7.9 – 28.1	

Responses were assessed accordingly to mRECIST v1.1 criteria. CR, complete response; PR, partial response; SD, stable disease; CI, confidence interval.

Discussion

In this report, we showed that patients with an AEC ≥ 220/µL prior to their therapy appear to have a worse outcome and relapse more rapidly. Importantly, we have considered the mean AEC value measured during the month preceding administration of chemo- or immunotherapy. In particular, the disease control rate was improved in chemotherapy-treated patients with AEC < 220/µL and, consistently, the proportion of subjects with a response at two years was increased by 2.4-fold (i.e., 41% *vs* 17%, Table 2). While the proportion of patients with objective response rate (CR + PR) was similar above and below the threshold of AEC 220/µL, there was a statistically significant difference of SD (Table 2; Supplementary Figures 4C and 5C).

It should be mentioned that, in this study, we excluded patients with hypereosinophilia induced by asthma, allergy, parasitic infection, autoimmune disease, and medication (26, 27). Indeed, these conditions require systemic treatments that would have affected the immune system. It should also be noted that, within the "normal" range (0-450 eosinophils/µL of blood), there is no clear mechanism that explains the fluctuations of eosinophil levels.

In this retrospective study, successive CT evaluations and over time distinguishable tumor margins were often missing. It should however be mentioned that multiple radiographic assessments are particularly challenging in MPM (28). Therefore, OS is preferred and considered to be a more objective and reliable endpoint compared to PFS, response rate and duration of response (11). In this perspective, we showed that the AEC 220/µL threshold predicted a significant difference in mOS (14 *vs* 29 months in patients treated with chemotherapy and 25 *vs* 48 months with immunotherapy, Figure 2 and Supplementary Figure 4). The significant association between AEC and OS does not preclude that eosinophilic MPM patients could still respond to chemotherapy or ICIs (29). Consistently, MPM case reports of poor response and fast deterioration have been described in eosinophilic patients (29–31). If validated by prospective and interventional studies, this conclusion could thus be of particular interest for MPM management.

In fact, the association of AEC and OS has been investigated in other cancers, yielding to opposite conclusions. Indeed, excess of eosinophils in the peripheral blood has been correlated with either a better or a worse prognosis depending on the cancer type (20, 32, 33). For example, in non-small cell lung cancer (NSCLC) and melanoma, an AEC equal or superior to 300/µL measured before therapy was associated with a better outcome (34–43). By contrast, the level of peripheral blood eosinophils is an independent prognostic factor for disease progression and disease-specific death in Hodgkin's lymphoma and primary cutaneous T-cell lymphoma (40, 44–46).

Due to the more recent advent of immunotherapy in MPM, the number of first-line immunotherapy-treated patients included in this study was limited. However, the difference of OS in the AEC ≥ 220/µL and AEC < 220/µL groups was nevertheless statistically significant (L-R test $p = 0.0022$; Supplementary Figure 4). This conclusion was valid providing that AECs were determined before, but not during or after, the initiation of therapy. In contrast, increase of peripheral blood eosinophils during treatment with ICIs is associated with better

response and clinical outcome in NSCLC, indicating that the correlation could be dependent on the tumor type (47, 48). Although the biological mechanisms underlying this difference are still not well understood, it is likely that the TME is a central parameter of this cancer specificity. The TME most likely shapes the phenotype of eosinophils into diverse subpopulations with opposite functions, as illustrated in asthma (49–51). In MPM, the interaction of eosinophils with other immune cells such as macrophages, monocytes and neutrophils may direct pro- or anti-tumor functions as well as response to therapy (13–18). Consistently, inflammation markers such as lymphocyte predominance, NLR and absolute monocyte count (AMC) have been correlated with poor survival (52–57). Analysis of the data set of our cohort did not reveal any association of OS with NLR, AMC and monocyte-to-lymphocyte ratios.

Although a causal link still needs to be demonstrated, the correlation between AEC and OS possibly opens direct prospects for therapeutic intervention. Indeed, our report suggests that there might be a benefit to decrease the AEC below the 220/μL threshold before initiating the chemo- or immunotherapy. For example, glucocorticoids (e.g., methylprednisolone) used to prevent pemetrexed-associated rash, emesis and inflammation (58–60) are able to induce apoptosis of eosinophils (61). In our study, a single dose of methylprednisolone at 48mg effectively reduced inflammation but did not reduce myeloid cell counts as numbers remained approximately constant before and after administration. More specific approaches targeting eosinophils have recently been developed in the treatment of asthma (62). Monoclonal antibodies interacting with cytokines associated with eosinophilia (e.g., IL-5, IL-33) are currently evaluated in clinical trials to treat eosinophilic COPD patients: Mepolizumab (anti-IL-5; NCT04075331), MEDI3506 (anti-IL-33; NCT04570657), REGN3500 (anti-IL-33; NCT04701983 and NCT04751487) and Astegolimab (anti-ST2; NCT03615040). Whether these targeted approaches are effective as add-on therapy in MPM could thus merit further evaluation.

Conclusion

In summary, this retrospective study shows that an AEC threshold of 220/μL measured prior to therapy identifies populations with distinct outcomes in mesothelioma, supporting further prospective analysis and possibly interventional trials.

Data availability statement

The original contributions presented in the study are included in the article/Supplementary Material. Further inquiries can be directed to the corresponding author.

Ethics statement

The studies involving human participants were reviewed and approved by University Hospital of Liège Ethical Committee, reference 2020/45 University Hospital of Antwerp Ethical Committee, reference 2022/1844. Written informed consent for participation was not required for this study in accordance with the national legislation and the institutional requirements.

Author contributions

MW, AS and EW collected the dataset in Lille CHU. JR collected the dataset in Antwerp CHU. MW, AF and MH collected the dataset in Liege CHU. AF, AS, EW, HB, JR, MG, LH, MJ, VH, RL participated in data interpretation and manuscript reviewing. MW, LW and MH designed the study. MW and LW drafted the manuscript. All authors contributed to the article and approved the submitted version.

Funding

This work was supported by the Belgian Foundation against Cancer, the Fonds National de la Recherche Scientifique (FNRS), the Télévie, and the Fondation Léon Fredericq.

Acknowledgments

The authors thank the GIGA Platforms (ULiège, Belgium) for support, help and advice. We gratefully acknowledge Ramatou Sare (Gembloux Agro Bio-Tech) for the collection of data in Lille CHU. We also thank Jan Van Meerbeeck for making this study possible.

Conflict of interest

Beyond the scope of this study, AS participated to clinical trials and expert boards with Amphera, AstraZeneca, BMS, MSD, Regeneron/Sanofi, Roche and Trizell. VH declares consultancy fees from AstraZeneca and Chiesi.

The remaining authors declare that the research was conducted in the absence of any commercial or financial relationships that could be construed as a potential conflict of interest.

Publisher's note

Supplementary material

The Supplementary Material for this article can be found online at: https://www.frontiersin.org/articles/10.3389/fimmu.2023.1148798/full#supplementary-material

References

1. Asciak R, George V, Rahman NM. Update on biology and management of mesothelioma. *Eur Respir Rev* (2021) 30:1–13. doi: 10.1183/16000617.0226-2020

2. Kazan-Allen L. *Current asbestos bans* (2022). Available at: http://www.ibasecretariat.org/alpha_ban_list.php (Accessed September 14, 2022).

3. Bray F, Ferlay J, Soerjomataram I, Siegel RL, Torre LA, Jemal A. Global cancer statistics 2018: GLOBOCAN estimates of incidence and mortality worldwide for 36 cancers in 185 countries. *CA Cancer J Clin* (2018) 68:394–424. doi: 10.3322/caac.21492

4. Popat S, Baas P, Faivre-Finn C, Girard N, Nicholson AG, Nowak AK, et al. Malignant pleural mesothelioma: ESMO clinical practice guidelines for diagnosis, treatment and follow-up. *Ann Oncol* (2022) 33:129–42. doi: 10.1016/j.annonc.2021.11.005

5. Alì G, Bruno R, Fontanini G. The pathological and molecular diagnosis of malignant pleural mesothelioma: A literature review. *J Thorac Dis* (2018) 10:S276–84. doi: 10.21037/jtd.2017.10.125

6. Vogelzang NJ, Rusthoven JJ, Symanowski J, Denham C, Kaukel E, Ruffie P, et al. Phase III study of pemetrexed in combination with cisplatin versus cisplatin alone in patients with malignant pleural mesothelioma. *J Clin Oncol* (2003) 21:2636–44. doi: 10.1200/JCO.2003.11.136

7. Fennell DA, Ewings S, Ottensmeier C, Califano R, Hanna GG, Hill K, et al. Nivolumab versus placebo in patients with relapsed malignant mesothelioma (CONFIRM): A multicentre, double-blind, randomised, phase 3 trial. *Lancet Oncol* (2021) 22:1530–40. doi: 10.1016/S1470-2045(21)00471-X

8. Baas P. Nivolumab plus ipilimumab should be the standard of care for first-line unresectable epithelioid mesothelioma. *J Thorac Oncol* (2022) 17:30–3. doi: 10.1016/j.jtho.2021.07.029

9. Zalcman G, Mazieres J, Margery J, Greillier L, Audigier-Valette C, Moro-Sibilot D, et al. Bevacizumab for newly diagnosed pleural mesothelioma in the mesothelioma avastin cisplatin pemetrexed study (MAPS): A randomised, controlled, open-label, phase 3 trial. *Lancet* (2016) 387:1405–14. doi: 10.1016/S0140-6736(15)01238-6

10. Désage AL, Karpathiou G, Peoc'h M, Froudarakis ME. The immune microenvironment of malignant pleural mesothelioma: A literature review. *Cancers (Basel)* (2021) 13:1–31. doi: 10.3390/cancers13133205

11. Baas P, Scherpereel A, Nowak AK, Fujimoto N, Peters S, Tsao AS, et al. First-line nivolumab plus ipilimumab in unresectable malignant pleural mesothelioma (CheckMate 743): a multicentre, randomised, open-label, phase 3 trial. *Lancet* (2021) 397:375–86. doi: 10.1016/S0140-6736(20)32714-8

12. Fennell DA, Dulloo S. Chemotherapy with or without bevacizumab should be the standard of care for first-line unresectable epithelioid mesothelioma. *J Thorac Oncol* (2022) 17:34–7. doi: 10.1016/j.jtho.2021.08.004

13. Chéné AL, D'Almeida S, Blondy T, Tabiasco J, Deshayes S, Fonteneau JF, et al. Pleural effusions from patients with mesothelioma induce recruitment of monocytes and their differentiation into M2 macrophages. *J Thorac Oncol* (2016) 11:1765–73. doi: 10.1016/j.jtho.2016.06.022

14. Lievense LA, Cornelissen R, Bezemer K, Kaijen-Lambers MEH, Hegmans JPJJ, Aerts JGJV. Pleural effusion of patients with malignant mesothelioma induces macrophage-mediated T cell suppression. *J Thorac Oncol* (2016) 11:1755–64. doi: 10.1016/j.jtho.2016.06.021

15. Hamaidia M, Gazon H, Hoyos C, Hoffmann GB, Louis R, Duysinx B, et al. Inhibition of EZH2 methyltransferase decreases immunoediting of mesothelioma cells by autologous macrophages through a PD-1-dependent mechanism. *JCI Insight* (2019) 4:1–17. doi: 10.1172/jci.insight.128474

16. Gauttier V, Pengam S, Durand J, Biteau K, Mary C, Morello A, et al. Selective SIRPα blockade reverses tumor T cell exclusion and overcomes cancer immunotherapy resistance. *J Clin Invest* (2020) 130:6109–23. doi: 10.1172/JCI135528

17. Mola S, Pinton G, Erreni M, Corazzari M, De Andrea M, Grolla AA, et al. Inhibition of the histone methyltransferase EZH2 enhances protumor monocyte recruitment in human mesothelioma spheroids. *Int J Mol Sci* (2021) 22:1–25. doi: 10.3390/ijms22094391

18. Hoyos C, Fontaine A, Jacques JR, Heinen V, Louis R, Duysinx B, et al. HDAC inhibition with valproate improves direct cytotoxicity of monocytes against mesothelioma tumor cells. *Cancers (Basel)* (2022) 14:1–19. doi: 10.3390/cancers14092164

19. Reichman H, Karo-atar D, Munitz A. Emerging roles for eosinophils in the tumor microenvironment. *Trends Cancer* (2016) 2:664–75. doi: 10.1016/j.trecan.2016.10.002

20. Varricchi G, Galdiero MR, Loffredo S, Lucarini V, Marone G, Mattei F, et al. Eosinophils: The unsung heroes in cancer? *Oncoimmunology* (2018) 7:1–14. doi: 10.1080/2162402X.2017.1393134

21. Scherpereel A, Opitz I, Berghmans T, Psallidas I, Glatzer M, Rigau D, et al. ERS/ESTS/EACTS/ESTRO guidelines for the management of malignant pleural mesothelioma. *Eur Respir J* (2020) 55:1–31. doi: 10.1183/13993003.00953-2019

22. Byrne MJ, Nowak AK. Modified RECIST criteria for assessment of response in malignant pleural mesothelioma. *Ann Oncol* (2004) 15:257–60. doi: 10.1093/annonc/mdh059

23. Camp RL, Dolled-Filhart M, Rimm DL. X-Tile: A new bio-informatics tool for biomarker assessment and outcome-based cut-point optimization. *Clin Cancer Res* (2004) 10:7252–9. doi: 10.1158/1078-0432.CCR-04-0713

24. Santoro A, O'Brien ME, Stahel RA, Nackaerts K, Baas P, Karthaus M, et al. Pemetrexed plus cisplatin or pemetrexed plus carboplatin for chemonaïve patients with malignant pleural mesothelioma: Results of the international expanded access program. *J Thorac Oncol* (2008) 3:756–63. doi: 10.1097/JTO.0b013e31817c73d6

25. Van Meerbeeck JP, Gaafar R, Manegold C, Van Klaveren RJ, Van Marck EA, Vincent M, et al. Randomized phase III study of cisplatin with or without raltitrexed in patients with malignant pleural mesothelioma: An intergroup study of the European organisation for research and treatment of cancer lung cancer group and the national cancer institute. *J Clin Oncol* (2005) 23:6881–9. doi: 10.1200/JCO.20005.14.589

26. Kovalszki A, Weller PF. Eosiniophilia. *Prim Care* (2016) 43:607–17. doi: 10.1016/j.pop.2016.07.010.Eosinophilia

27. Kovalszki A, Weller PF. "Eosinophils and eosinophilia", In: Rich RR, Fleisher TA, Shearer WT, Schroeder HW, Frew A, Weyand CM, editors. *Clinical Immunology Principles and Practices (Fifth Edition)* (2019), p. 349–61. doi: 10.1016/B978-0-7020-6896-6.00024-7

28. U.S. Food and Drug Administration. *Clinical trial endpoints for the approval of cancer drugs and biologics: Guidance for industry* (Rockville: U.S. Food and Drug Administration) (2018). pp. 1–16.

29. Yamazoe M, Ozasa H, Kim YH. Effectiveness of nivolumab on sarcomatoid malignant pleural mesothelioma with eosinophilia and eosinophilic pleural effusion. *J Thorac Oncol* (2019) 14:e251–3. doi: 10.1016/j.jtho.2019.06.007

30. Takeuchi E, Takahashi N, Morizumi S, Tamiya H, Matsuoka H, Kuroda N, et al. Interleukin-5-producing malignant pleural mesothelioma with eosinophilic pleural effusion. *Thorac Cancer* (2020) 11:3043–6. doi: 10.1111/1759-7714.13652

31. Yamazaki M, Ohwada A, Miyaji A, Yamazaki H, Nara T, Hirai S, et al. Pulmonary paragonimiasis with coincidental malignant mesothelioma. *Intern Med* (2008) 47:1027–31. doi: 10.2169/internalmedicine.47.0852

32. Grisaru-Tal S, Itan M, Klion AD, Munitz A. A new dawn for eosinophils in the tumour microenvironment. *Nat Rev Cancer* (2020) 20:594–607. doi: 10.1038/s41568-020-0283-9

33. Simon SCS, Utikal J, Umansky V. Opposing roles of eosinophils in cancer. *Cancer Immunol Immunother* (2019) 68:823–33. doi: 10.1007/s00262-018-2255-4

34. Wu HX, Zhuo KQ, Cheng DY. Peripheral blood eosinophil as a biomarker in outcomes of acute exacerbation of chronic obstructive pulmonary disease. *Int J COPD* (2019) 14:3003–15. doi: 10.2147/COPD.S226783

35. Zhang Y, Liang LR, Zhang S, Lu Y, Chen YY, Shi HZ, et al. Blood eosinophilia and its stability in hospitalized COPD exacerbations are associated with lower risk of all-cause mortality. *Int J COPD* (2020) 15:1123–34. doi: 10.2147/COPD.S245056

36. Reichman H, Itan M, Rozenberg P, Yarmolovski T, Brazowski E, Varol C, et al. Activated eosinophils exert antitumorigenic activities in colorectal cancer. *Cancer Immunol Res* (2019) 7:388–400. doi: 10.1158/2326-6066.CIR-18-0494

37. Onesti CE, Josse C, Boulet D, Thiry J, Beaumecker B, Bours V, et al. Blood eosinophilic relative count is prognostic for breast cancer and associated with the presence of tumor at diagnosis and at time of relapse. *Oncoimmunology* (2020) 9:1–11. doi: 10.1080/2162402X.2020.1761176

38. Günduz S, Göksu SS, Arslan D, Tatli AM, Uysal M, Gündüz UR, et al. Factors affecting disease-free survival in patients with human epidermal growth factor receptor 2-positive breast cancer who receive adjuvant trastuzumab. *Mol Clin Oncol* (2015) 3:1109–12. doi: 10.3892/mco.2015.610

39. Steel JL, Kim KH, Dew MA, Unruh ML, Antoni MH, Olek MC, et al. Cancer-related symptom clusters, eosinophils, and survival in hepatobiliary cancer: An exploratory study. *J Pain Symptom Manag* (2010) 39:859–71. doi: 10.1016/j.jpainsymman.2009.09.019

40. Davis BP, Rothenberg ME. Eosinophils and cancer. *Cancer Immunol Res* (2014) 2:1–9. doi: 10.1158/2326-6066.CIR-13-0196

41. Simon SCS, Hu X, Panten J, Grees M, Renders S, Thomas D, et al. Eosinophil accumulation predicts response to melanoma treatment with immune checkpoint inhibitors. *Oncoimmunology* (2020) 9:1–12. doi: 10.1080/2162402X.2020.1727116

42. Moreira A, Leisgang W, Schuler G, Heinzerling L. Eosinophilic count as a biomarker for prognosis of melanoma patients and its importance in the response to immunotherapy. *Immunotherapy* (2017) 9:115–21. doi: 10.2217/imt-2016-0138

43. Wei Y, Zhang X, Wang G, Zhou Y, Luo M, Wang S, et al. The impacts of pretreatment circulating eosinophils and basophils on prognosis of stage I–III colorectal cancer. *Asia Pac J Clin Oncol* (2018) 14:e243–51. doi: 10.1111/ajco.12871

44. Tancrède-Bohin E, Ionescu MA, de la Salmonière P, Dupuy A, Rivet J, Rybojad M, et al. Prognostic value of blood eosinophilia in primary cutaneous T-cell lymphomas. *Arch Dermatol* (2004) 140:1057–61. doi: 10.1001/archderm.140.9.1057

45. Utsunomiya A, Ishida T, Inagaki A, Ishii T, Yano H, Komatsu H, et al. Clinical significance of a blood eosinophilia in adult T-cell leukemia/lymphoma: A blood eosinophilia is a significant unfavorable prognostic factor. *Leuk Res* (2007) 31:915–20. doi: 10.1016/j.leukres.2006.10.017

46. Bishara S, Griffin M, Cargill A, Bali A, Gore ME, Kaye SB, et al. Pre-treatment white blood cell subtypes as prognostic indicators in ovarian cancer. *Eur J Obstet Gynecol Reprod Biol* (2008) 138:71–5. doi: 10.1016/j.ejogrb.2007.05.012

47. Okauchi S, Shiozawa T, Miyazaki K, Nishino K, Sasatani Y, Ohara G, et al. Association between peripheral eosinophils and clinical outcomes in patients with non-small cell lung cancer treated with immune checkpoint inhibitors. *Polish Arch Intern Med* (2021) 131:152–60. doi: 10.20452/pamw.15776

48. Alves A, Dias M, Campainha S, Barroso A. Peripheral blood eosinophilia may be a prognostic biomarker in non-small cell lung cancer patients treated with immunotherapy. *J Thorac Dis* (2021) 13:2716–27. doi: 10.21037/jtd-20-3525

49. Januskevicius A, Jurkeviciute E, Janulaityte I, Kalinauskaite-Zukauske V, Miliauskas S, Malakauskas K. Blood eosinophils subtypes and their survivability in asthma patients. *Cells* (2020) 9:1–17. doi: 10.3390/cells9051248

50. Mesnil C, Raulier S, Paulissen G, Xiao X, Birrell MA, Pirottin D, et al. Lung-resident eosinophils represent a distinct regulatory eosinophil subset. *J Clin Invest* (2016) 126:3279–95. doi: 10.1172/JCI85664

51. Percopo CM, Brenner TA, Ma M, Kraemer LS, Hakeem RMA, Lee JJ, et al. SiglecF + Gr1 hi eosinophils are a distinct subpopulation within the lungs of allergen-challenged mice. *J Leukoc Biol* (2017) 101:321–8. doi: 10.1189/jlb.3a0416-166r

52. Gutierrez-Sainz L, Cruz P, Martinez-Recio S, Higuera O, Esteban-Rodriguez MI, Arias-Lotto F, et al. Malignant pleural mesothelioma: clinical experience and prognostic value of derived neutrophil-to-lymphocyte ratio and PD-L1 expression. *Clin Transl Oncol* (2021) 23:2030–5. doi: 10.1007/s12094-021-02605-w

53. Urso L, Silic-Benussi M, Boscolo A, Lorenzi M, Bonanno L, Lunardi F, et al. Detection of circulating immunosuppressive cytokines in malignant pleural mesothelioma patients for prognostic stratification. *Cytokine* (2021) 146:155622. doi: 10.1016/j.cyto.2021.155622

54. De Fonseka D, Arnold DT, Morley AJ, Brett M, Bhatt N, Edey A, et al. Lymphocyte predominance in blood, pleural fluid, and tumour stroma; a prognostic marker in pleural mesothelioma. *BMC Pulm Med* (2022) 22:1–6. doi: 10.1186/s12890-022-01968-2

55. Cimen F, Agackiran Y, Düzgün S, Aloglu M, Senturk A, Atikcan S. Factors affecting the life expectancy in malignant pleural mesothelioma: Our 10 years of studies and experience. *Med (Baltimore)* (2022) 101:e30711. doi: 10.1097/md.0000000000030711

56. Okita R, Okada M, Inokawa H, Murakami T, Ikeda E. Prognostic values of preoperative c-reactive protein, albumin, and neutrophil ratios in patients with malignant pleural mesothelioma who underwent extrapleural pneumonectomy. *Surg Oncol* (2022) 43:101813. doi: 10.1016/j.suronc.2022.101813

57. Fournel L, Charrier T, Huriet M, Iaffaldano A, Lupo A, Damotte D, et al. Prognostic impact of inflammation in malignant pleural mesothelioma: A large-scale analysis of consecutive patients. *Lung Cancer* (2022) 166:221–7. doi: 10.1016/j.lungcan.2022.03.014

58. Hazarika M, White RM, Booth BP, Wang Y, Ham DYL, Liang CY, et al. Pemetrexed in malignant pleural mesothelioma. *Clin Cancer Res* (2005) 11:982–92. doi: 10.1158/1078-0432.982.11.3

59. Sakurada T, Kakiuchi S, Tajima S, Horinouchi Y, Konaka K, Okada N, et al. Pemetrexed-induced rash may be prevented by supplementary corticosteroids. *Biol Pharm Bull* (2015) 38:1752–6. doi: 10.1248/bpb.b15-00435

60. Sakurada T, Nokihara H, Koga T, Zamami Y, Goda M, Yagi K, et al. Prevention of pemetrexed-induced rash using low-dose corticosteroids: A phase II study. *Oncologist* (2022) 27:e554–60. doi: 10.1093/oncolo/oyab077

61. Cook AM, McDonnell AM, Lake RA, Nowak AK. Dexamethasone co-medication in cancer patients undergoing chemotherapy causes substantial immunomodulatory effects with implications for chemo-immunotherapy strategies. *Oncoimmunology* (2016) 5:1–11. doi: 10.1080/2162402X.2015.1066062

62. Cusack RP, Whetstone CE, Xie Y, Ranjbar M, Gauvreau GM. Regulation of eosinophilia in asthma–new therapeutic approaches for asthma treatment. *Cells* (2021) 10:1–23. doi: 10.3390/cells10040817

frontiers | Frontiers in Immunology

TYPE Original Research
PUBLISHED 24 March 2023
DOI 10.3389/fimmu.2023.1104560

OPEN ACCESS

EDITED BY
Chiara Porta,
University of Eastern Piedmont, Italy

REVIEWED BY
Rebecca Kesselring,
University of Freiburg Medical Center, Germany
Sabahattin Cömertpay,
Kahramanmaras Sütçü Imam University, Türkiye
Paul Baas,
The Netherlands Cancer Institute (NKI), Netherlands

*CORRESPONDENCE
Jie Wang
zlhuxi@163.com

SPECIALTY SECTION
This article was submitted to Cancer Immunity and Immunotherapy, a section of the journal Frontiers in Immunology

RECEIVED 21 November 2022
ACCEPTED 10 March 2023
PUBLISHED 24 March 2023

CITATION
Liu Z, Wan R, Bai H and Wang J (2023) Damage-associated molecular patterns and sensing receptors based molecular subtypes in malignant pleural mesothelioma and implications for immunotherapy.
Front. Immunol. 14:1104560.
doi: 10.3389/fimmu.2023.1104560

Damage-associated molecular patterns and sensing receptors based molecular subtypes in malignant pleural mesothelioma and implications for immunotherapy

Zheng Liu, Rui Wan, Hua Bai and Jie Wang*

State Key Laboratory of Molecular Oncology, Department of Medical Oncology, National Cancer Center/National Clinical Research Center for Cancer/Cancer Hospital, Chinese Academy of Medical Sciences and Peking Union Medical College, Beijing, China

Objectives: Malignant pleural mesothelioma (MPM) is characterized as an incredibly aggressive form of cancer with a dismal diagnosis and a dearth of specific biomarkers and therapeutic options. For MPM patients, the effectiveness of immunotherapy may be influenced by damage-associated molecular pattern (DAMP)-induced immunogenic cell death (ICD).The objective of this work is to create a molecular profile associated with DAMPs to categorize MPM patients and predict their prognosis and response to immunotherapy.

Methods: The RNA-seq of 397 patients (263 patients with clinical data, 57.2% male, 73.0% over 60 yrs.) were gathered from eight public datasets as a training cohort to identify the DAMPs-associated subgroups of MPMs using K-means analysis. Three validation cohorts of patients or murine were established from TCGA and GEO databases. Comparisons were made across each subtype's immune status, gene mutations, survival prognosis, and predicted response to therapy.

Results: Based on the DAMPs gene expression, MPMs were categorized into two subtypes: the nuclear DAMPs subtype, which is classified by the upregulation of immune-suppressed pathways, and the inflammatory DAMPs subtype, which is distinguished by the enrichment of proinflammatory cytokine signaling. The inflammatory DAMPs subgroup had a better prognosis, while the nuclear DAMPs subgroup exhibited a worse outcome. In validation cohorts, the subtyping system was effectively verified. We further identified the genetic differences between the two DAMPs subtypes. It was projected that the inflammatory DAMPs subtype will respond to immunotherapy more favorably, suggesting that the developed clustering method may be implemented to predict the effectiveness of immunotherapy.

Conclusion: We constructed a subtyping model based on ICD-associated DAMPs in MPM, which might serve as a signature to gauge the outcomes of immune checkpoint blockades. Our research may aid in the development of innovative immunomodulators as well as the advancement of precision immunotherapy for MPM.

KEYWORDS

malignant mesothelioma, damage-associated molecular patterns, immunogenic cell death, immunotherapy, tumor microenvironment

1 Introduction

Mesothelioma is an unusual malignancy that originates from the mesothelial cells of the pleural or other regions. About 81% of the tumors originate from the pleura. The prevalence of malignant mesothelioma is increasing, but the mortality remains unchanged. In China, the incidence rate of malignant mesothelioma was only $1.50/10^6$ whereas the fatality rate was $1.22/10^6$ (1). MPM is mainly seen in older men exposed to asbestos. Compared with European and American countries, the onset age of mesothelioma is younger in China. The prevalence and fatality of malignant mesothelioma in China increase rapidly after the age of 35 or 40, reaching a peak at the age of 80 or 85 (1). Malignant pleural mesothelioma (MPM) is difficult to treat and has a dismal prognosis because most patients are at advanced stages when first diagnosed and are with early onset of evident clinical manifestations. Due to its resistance to conventional therapies and the absence of effective alternative regimens, MPM presents a highly difficult challenge. Despite the prompt advancement of immunotherapy and the fairly encouraging outcomes of ICIs in treating MPM, it remains high mortality on a global scale. The 5-year survival rate is around 10%, and the median overall survival is roughly one year.

Based on multiple studies conducted in MPM with immunotherapy alone or combined applied, the median PFS of 4~7 months does not seem particularly impressive. However, the increased median OS is mainly driven by a small portion of patients with long-lasting responses and deserves more explorations (2). CheckMate-743, a phase 3 randomized controlled trial, recently showed that MPM could benefit from PD-1 inhibitors combined with CTLA-4 inhibitors (3). Subgroup analyses revealed that the response rate to ICIs in MPM is somewhat but not entirely related to histology. Coupled with the fact that ICIs are more expensive and not covered by health insurance, it will result in a low cost-benefit ratio if the treatment is not effective. Therefore, there is an urgent need for identifying the subtypes of MPM patients who would potentially benefit from immunotherapy (4).

Immunogenic cell death (ICD) is a form of regulated cell death (RCD), acting as a major initiator of adaptive immune response in the context of malignant neoplasms (5). The promotion of ICD sensitizes MPM to ICIs treatments, as demonstrated by *in-vitro* experiments, preclinical models, and preliminary trials (6–11). which raises the possibility that ICD-associated biomarkers could serve as prospective predictive indicators for immunotherapy. An increased amount of work has discovered that induction of adaptive immune responses by cancer cells undergoing ICD is dependent on the emission and detection of a particular panel of DAMPs, including cell surface-exposed calreticulin (CALR), high mobility group box 1 (HMGB1) and extracellular adenosine triphosphate (ATP) (12, 13). In addition, previous studies also have demonstrated that ICD-associated DAMPs produced by chemotherapy or radiotherapy activate the cytotoxic CD8+ T cell and alleviate the immunosuppressive tumor microenvironment (TME), thus suggesting an essential role of DAMPs in immunotherapy (10). Pattern recognition receptors (PRRs) bound by DAMPs present adjuvanticity by activating transcription factors, eliciting APC cell activation, differentiation, and maturation, promoting the release of type 1 interferons and chemokines, resulting in the recruitment of APCs and T cells, and ultimately modulating intrinsic and adaptive immunity (14). Whether there is a pre-existing anti-tumor immune response is essential for effective immune checkpoint blockade. Effector T cells release interferon-γ (IFN-γ) by recognizing tumor neoantigens, which activates the Janus kinase (JAK)– signal transducer and activator of transcription (STAT) signaling pathway. The expression of programmed cell death ligand 1 (PD-L1) on the surface of tumor cells is mediated by the subsequent stimulation of the transcription factor interferon regulatory factor 1 (IRF1), which negatively regulates the effector T cell response in turn (15, 16). Immune checkpoint inhibitors (ICIs) disrupt this negative feedback loop as one of the primary mechanisms to restore anti-tumor immunity and exert anti-tumor efficiency. Hence, sensitizing tumors to ICIs by maneuvering ICD-associated DAMPs hinges on the inflammatory tumor immune microenvironment of MPM. Thus, we plan to assess the distinctive TiME to analyze the immune profiles of distinct MPM subtypes, which is crucial to interpret varied prognoses and efficacy of immunotherapy.

Despite the fact that an increasing amount of predictive models related to immunotherapy have been constructed to elaborate subtypes of MPM, ICD-associated DAMPs and their receptors were barely based upon to construct a predictive classification model. In this research, we performed consensus clustering analysis based on the ICD-associated DAMPs gene set and investigated the impact of DAMPs and their sensing receptors on the immune status from a variety of perspectives and on the survival

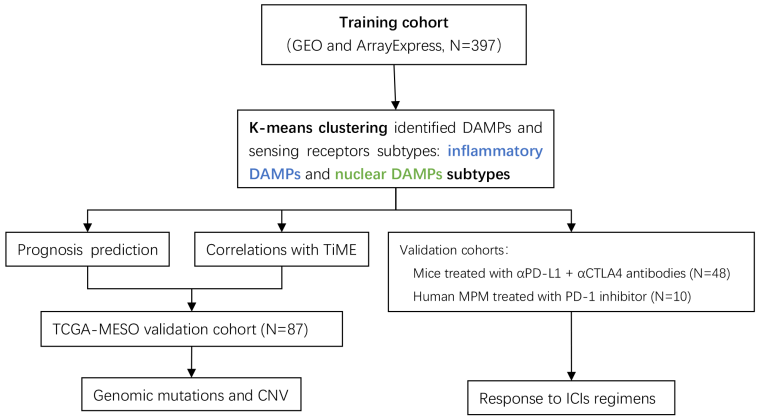

FIGURE 1
Flow chart of the data analysis process. The DAMPs-associated subtypes were established based on 397 TNBCs from the training cohort and validated in the TCGA cohort. DAMPs, damage-associated molecular patterns; TCGA, The Cancer Genome Atlas.

expectancy of MPM patients. Additionally, the DAMPs-based classification we established was assessed for its predictive value of immune checkpoint inhibitors (ICIs) applied to mesothelioma (the flow chart of analysis is demonstrated in Figure 1). Our research offers novel information to discover the potential molecular mechanisms in different subtypes of MPM, which may fulfill the demand for precision immunotherapy of MPM.

2 Materials and methods

2.1 Data collection

Normalized microarray gene expression data and clinical information of GSE42977, GSE2549, GSE12345, GSE51024, GSE163720, GSE163721, GSE29354, and GSE99070 were obtained from the GEO database (https://www.ncbi.nlm.nih.gov/geo/). Raw microarray gene expression data and follow-up data were downloaded from the ArrayExpress repository under accession code E-MTAB-6877 (https://www.ebi.ac.uk/biostudies/arrayexpress). TCGA sequencing data (including mRNA and genomic data) and clinical data of MPM patients were collected from Genomic Data Commons Data Portal (https://portal.gdc.cancer.gov/). Raw Next-Generation Sequencing (NGS) data of GSE117358 and GSE153941 were obtained from GEO database (https://www.ncbi.nlm.nih.gov/geo/).

Our study established one training cohort from malignant pleural mesothelioma patients from GEO and ArrayExpress datasets, including GSE42977, GSE2549, GSE12345, GSE51024, GSE163720, GSE163721, GSE29354 and E-MTAB-6877 (a total of 397 MPM patients, 57.2% male, 63 patients with overall survival data) and three validation cohorts consist of the TCGA-MESO datasets (a total of 86 MPM patients with CNV and WES data, 82.5% male, 86 patients with overall survival data), two murine GEO datasets (including GSE117358 and GSE153941), and one GEO dataset(GSE99070), respectively.

The raw data were normalized by using the RMA algorithm provided by "limma" package of R software (http://bioconductor.org/packages/limma/). Furthermore, the batch effect across datasets was subtracted using the "removeBatchEffect" function implemented in the "limma" package.

The demographic information and clinical characteristics of the training cohort are displayed in Table 1.

TABLE 1 Correlation between clinical characteristics and pathological features and DAMPs associated subtypes.

Features	Number of patients	DAMPs associated subtypes	
		Inflammatory DAMPs	Nuclear DAMPs
Total	397	230	167
Age			*P*=0.193
>60 years	46	27	19
≤60 years	17	13	4
Gender			*P*=0.719
Male	111	71	40

(Continued)

TABLE 1 Continued

Features	Number of patients	DAMPs associated subtypes	
		Inflammatory DAMPs	Nuclear DAMPs
Female	83	51	32
Stage			*P*=0.982
I	2	2	0
II	7	4	3
III	25	14	11
IV	17	11	6
Histology			*P*>0.05
Epithelial	88	51	37
Biphasic	17	10	7
Sarcomatoid	10	6	4
DMM	1	0	1
Asbestos exposure			*P*>0.05
Exposed	44	28	16
Not exposed	13	7	6
Probably exposed	3	2	1

2.2 Identification of DAMPs subgroups by K-means analysis

32 DAMPs-related genes were collected according to previous research (5, 17, 18). 25 DAMPs-related genes were contained in the training and validation cohorts and their information is shown in Table 2.

R package "ConsensusClusterPlus" based on the DAMPs-related gene list expressed in cohorts were employed to conduct unsupervised clustering. K-means clustering (the "kmeans"

TABLE 2 DAMPs-associated genes.

Gene	Protein	Molecular type	Function (s)
TLR4	Toll-like receptor 4	PRRs (TLRs)	Tumor Antigen processing and presentation
TLR2	Toll-like receptor 2	PRRs (TLRs)	NLRP3 inflammasome activation
CLEC4E	C-type lectin domain family 4 member E	PRRs (CLRs)	Activates innate immune receptors on monocytes, macrophages, and immature dendritic cells
CLEC7A	C-type lectin domain family 7 member A(Dectin-1)	PRRs (CLRs)	Recognize a variety of glucans to activate innate immune response
NLRP3	NOD-like receptor thermal protein domain associated protein 3 (cryopyrin)	PRRs (NLRs)	Regulates inflammation, the immune response, and apoptosis
FPR1	Formyl peptide receptor 1	PRRs (GPCRs)	Guide phagocytic leukocytes to regions of inflammation (19)
AIM2	Absent in melanoma 2	PRRs (ALRs)	Initiates inflammasome assembly in response to DNA damage (20, 21)
IFIH1	Interferon induced with helicase c domain 1	PRRs (RLRs)	Promotes the production of IFN-I and cytokines
DDX58	Retinoic acid-inducible gene I protein	PRRs (RLRs)	Trigger a transduction cascade
FPR2	Formyl peptide receptor 2	PRRs (GPCRs)	Regulates monocyte chemotaxis
TLR7	Toll-like receptor 7	PRRs (TLRs)	Stimulates autoreactive B cells (22, 23)
TLR3	Toll-like receptor 3	PRRs (TLRs)	Promotes type I IFN secretion; initiates CXCL10 release (24–26)

(Continued)

TABLE 2 Continued

Gene	Protein	Molecular type	Function (s)
IL33	Interleukin 33	DAMPs	Involves the activation of natural killer cells (27–29)
TREM1	Triggering receptor expressed on myeloid cells 1	PRRs (TREMs)	Triggers pro-inflammatory cytokine and chemokine secretion; enhanced inflammatory responses (30–32)
BCL2	Apoptosis regulator Bcl-2	DAMPs	Blocks the apoptotic death of lymphocytes (33)
CASR	Extracellular calcium-sensing receptor	PRRs (GPCRs)	Promotes NLRP3 activation
AGER	Advanced glycosylation end product-specific receptor	PRRs	Elevates pro-inflammatory genes expression
IL1A	Interleukin-1 alpha	DAMPs	Cell activation, cytokine release
CALR	Calreticulin	DAMPs	Promotes the uptake of dying cells and type I IFN secretion by APCs (34–36)
ROCK1	Rho-associated protein kinase 1	DAMPs	Regulates focal adhesions of fibroblasts and gathering of lymphocytes (37)
HSP90AA1	Heat shock protein HSP 90-alpha	DAMPs	Assists the proper folding of specific proteins through ATPase activity (38, 39)
PANX1	Pannexin-1	DAMPs	Mediates 'find-me' signal release during apoptosis (40, 41)
PPIA	Peptidyl-prolyl cis-trans isomerase A	DAMPs	Assists to activate the tyrosine kinase Jak2 (42)
HMGN1	Non-histone chromosomal protein HMG-14	DAMPs	Promotes B cell proliferation (43–45)
HSPA4	Heat shock 70 kDa protein 4	DAMPs	Enable ATP binding activity (46)

algorithm in R) was performed to define stable DAMPs-associated subtypes of MPM.

2.3 Signaling pathways analyses

Differentially expressed genes (DEGs) between two groups were defined as genes whose false discovery rate (FDR) value was < 0.05 and |Log2 (Fold Change (FC))|> 1.

Metascape database was used for Gene Ontology (GO) and Kyoto Encyclopedia of Genes and Genomes (KEGG) enrichment analysis (47).

Furthermore, gene set enrichment analysis (GSEA) and gene set variation analysis (GSVA) were employed in two subtypes to exploit the differences in mechanisms (48–50). An adjusted P-value < 0.05 was deemed as statistically significant.

The gene sets utilized for GSEA and GSVA were downloaded from the MSigDB database.

2.4 Immune status analyses

CIBERSORT was applied to characterize immune infiltrating cell type proportions in expression profiles using a validated leukocyte gene signature matrix (LM22) (51).

The R package "estimate" contains the Estimation of Stromal and Immune cells in Malignant Tumor tissues using Expression data (ESTIMATE) program that derived the immune score (52).

2.5 Genomic analyses

Copy number variations (CNV) and genomic mutations were analyzed using GISTIC2.0 in TCGA-MESO cohort (53). We depicted the variances in gene amplification or deletion events and genomic mutations between DAMPs-associated MPM subtypes.

The "ComplexHeatmap" package in R was implemented to visualize the waterfall plot of CNV and genomic mutation data (54).

2.6 Statistical analyses

Statistical analyses were conducted by R (version 4.1.1, https://www.r-project.org).

The Kaplan–Meier algorithm included in the "survival" R package was used to perform the survival analysis.

For the comparison of the two groups, one-way analysis of variance (ANOVA), Chi-square test, or Fisher exact test was performed.

Mantel-Haenszel test was used to analyze the rates of occurrence of death over time.

A $P<0.05$ was deemed statistically significant.

3 Results

3.1 Consensus clustering identified two DAMPs-associated subtypes

We included malignant pleural mesothelioma samples (n=397) from GEO and ArrayExpress datasets as the training cohort. Based

on the gene expression related to DAMPs, they were divided into two subtypes *via* K-means clustering selecting 2 as the ideal and meaningful value of K (Figures 2A–C).

Of the 397 MPM patients included in the training cohort, 167 patients were classified into the nuclear DAMPs subgroup, and 230 were clustered in the inflammatory DAMPs subgroup. The heatmap reveals significant differences between the two subtypes in normalized enrichment scores of genes associated with DAMPs (Figure 2D). Cluster I is classified as the inflammatory DAMPs subtype distinguished by increased expression of PRRs regulating activities of inflammasome or immune cells, such as *TLRs, FPR1, CLEC4E, NLRP3*, etc. Cluster II is defined as the nuclear DAMPs subtype, with nuclear-associated DAMPs, such as *HSP90AA1, HSPA4, CALR* and *high-mobility group nucleosome binding protein 1 (HMGN1)* generally overexpressed, but the receptors being expressed at low levels. According to Kaplan–Meier survival analysis revealed that MPM patients enjoyed a better overall survival (OS) in the inflammatory DAMPs subtype, whereas patients in the nuclear DAMPs subtype had a worse prognosis (median overall survival 23.0months vs. 14.0months, P=0.021; Figure 2E).

3.2 Identification of differentially expressed genes and enrichment of signal pathways in different DAMPs-associated subtypes

We detected DEGs between tumor tissues belonging to two subtypes and normal pleural tissues respectively and then conducted GSEA analysis to investigate their putative signaling pathways. A total of 327 DEGs were identified, among which 311 were belonged to the nuclear DAMPs subtype, and 219 were resided in the inflammatory DAMPs subtype.

For the inflammatory DAMPs subtype, pro-inflammatory pathways were primarily enriched. As shown by KEGG

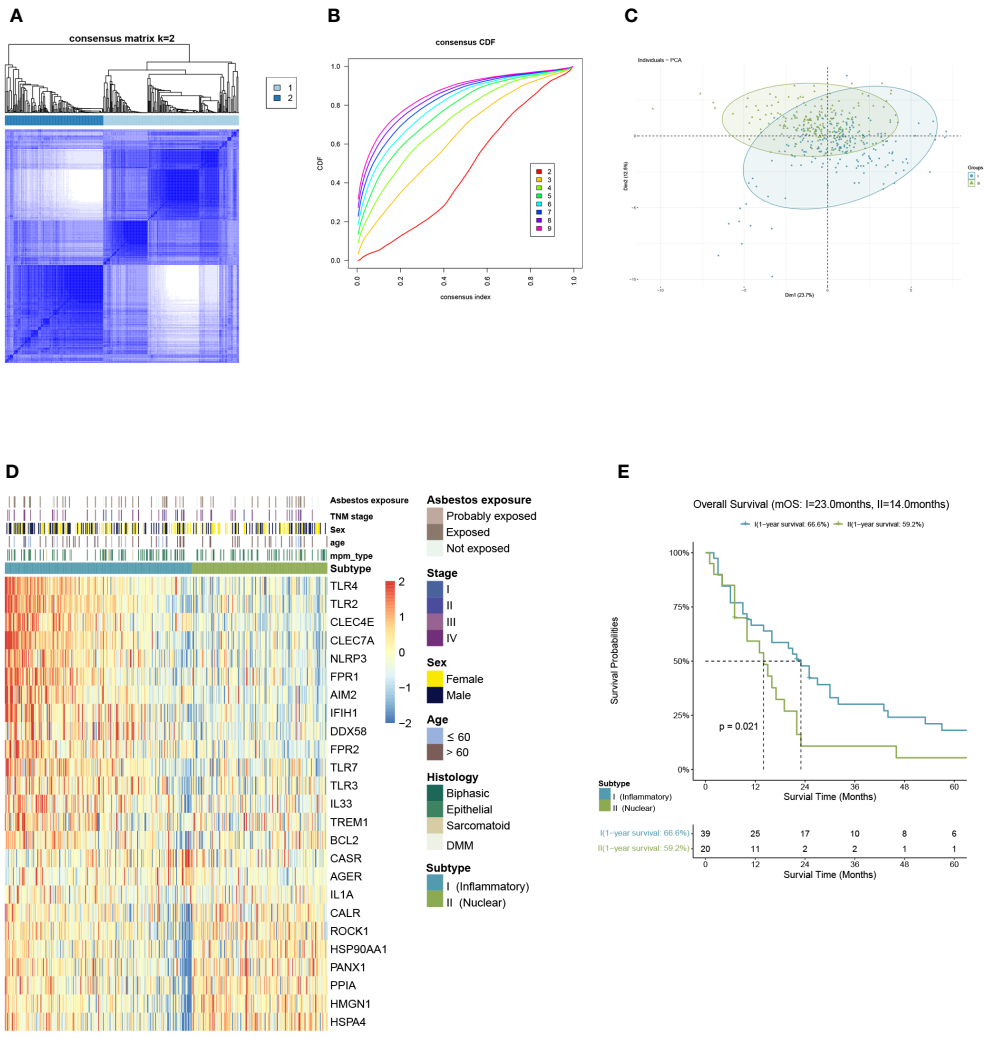

FIGURE 2
Identification of DAMPs-associated subtypes by K-means analysis. **(A–C)** K=2 was identified as the optimum value for consensus clustering. **(D)** DAMPs-associated subtyping of MPM patients (n = 397) from the training cohort. Heatmap displays normalized enrichment scores of the two subtypes. **(E)** Kaplan-Meier curves of overall survival (OS) between the two subtypes in the training cohort.

enrichment analysis, the DEGs were intensely enriched in the toll-like receptor (TLR) signaling pathway. The DEGs were observed to be enriched in immune-related signaling pathways by GO enrichment analysis, including MHC protein binding, tumor necrosis factor receptor (TNFR) binding, and regulation of type I interferon-mediated signaling. GSEA similarly revealed that the subtype of inflammatory DAMPs exhibited strong upregulation of the ATM pathway, TNFR1 pathway, FGF pathway, inflammatory response pathway, CD28-dependent PI3K-AKT signaling pathway, and integrin-A4B1 pathway (Figure 3A).

Based on GSEA enrichment analysis, on the other hand, the DEGs were comparatively elevated in heat shock protein (HSP)-related signaling and immune-suppressed pathways for the nuclear DAMPs subtype, including proteasome pathway, unfolded protein

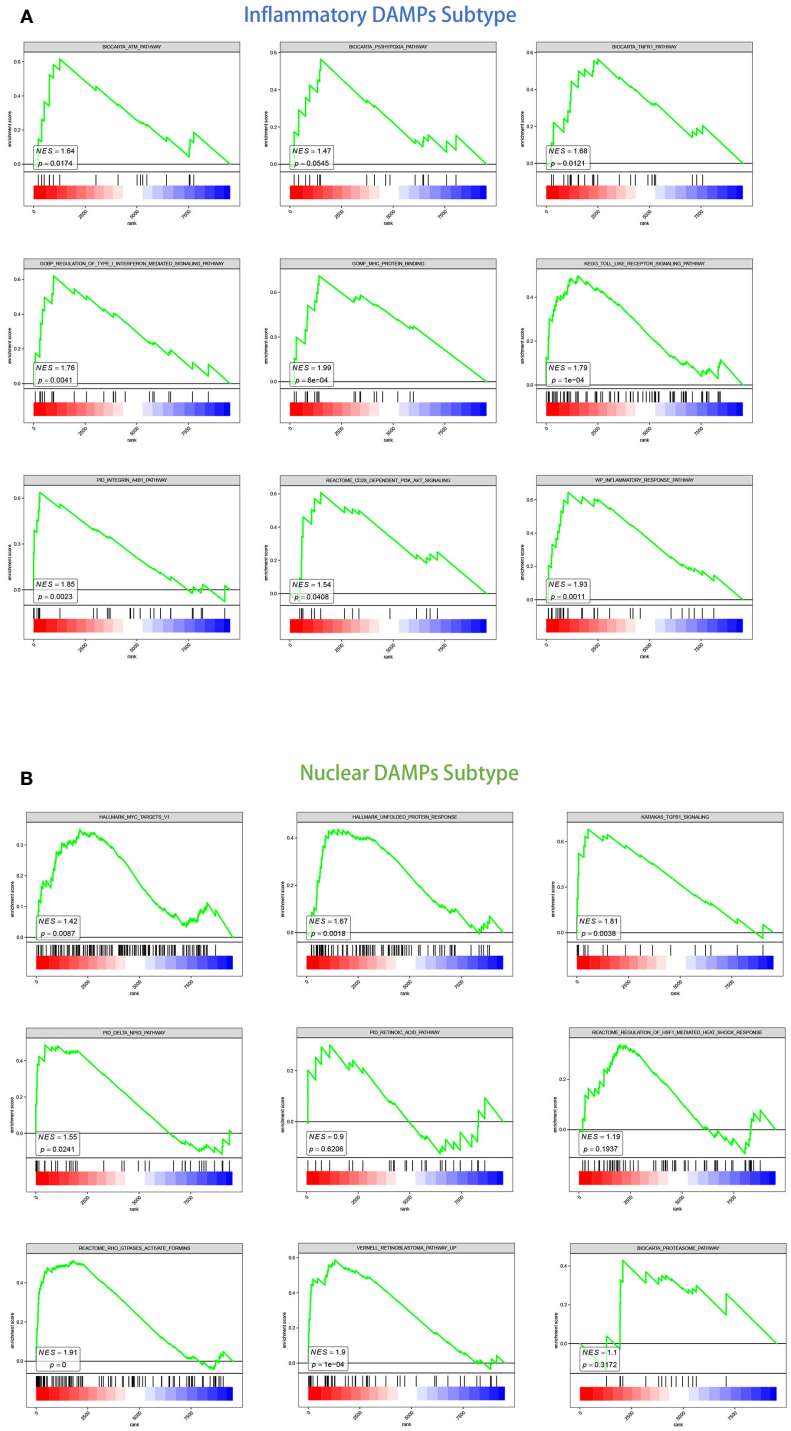

FIGURE 3
GSEA analysis of DEGs in two subtypes. **(A)** GSEA analysis of canonical pathways, gene ontology, hallmark gene sets for patients in the inflammatory DAMPs subtype. **(B)** GSEA analysis of canonical pathways, gene ontology, hallmark gene sets for patients in the nuclear DAMPs subtype.

response (UPR), TGFB1 signaling, Rho GTPases activate formins and regulation of HSF1-mediated heat shock response. The retinoblastoma pathway, delta NP63 pathway, MYC targets, defective intrinsic pathway for apoptosis, and retinoic acid pathway were also enriched significantly indicating that the nuclear DAMPs subtype proliferates fiercely (Figure 3B).

We then identified DEGs between two subtypes, and GSVA was performed to compare the significantly differential pathway (Figures 4A–C). GSVA analysis of cancer hallmarks, canonical pathways, and gene ontology revealed that natural killer T cell (NKT), DC, and T cell activation, complement, inflammatory response, adaptive immune response, antigen binding, cytokine receptor, IL-2 family, IL-12, IFN-γ, TNF superfamily, TLR, chemokine signaling, IL6-JAK-STAT signaling pathways were triggered in the inflammatory DAMPs subtype. In contrast, the DAMPs in the nuclear DAMPs subtype triggered cancer hallmark MYC targets, NOTCH signaling, TGF-β signaling, unfolded protein response (UPR), MTORC1 signaling, and IL-8 production.

3.3 Immune statuses of the patients in the two molecular subtypes varied

The immune variances between the two subtypes were investigated by immune analysis. The infiltration ratio of 22 immune cell types was analyzed in the training cohort using CIBERSORT and compared between the two groups. As demonstrated in Figure 5, the predominant infiltrating immune cells in the inflammatory DAMPs subtype were memory CD4+ T cells, while M1-like macrophages and activated DCs had a tendency to infiltration more, whereas Treg cells increased significantly with M2-like macrophages showed a tendency of higher infiltration in the nuclear DAMPs subtype (Figure 5A). Moreover, ESTIMATE indicated that patients within the inflammatory DAMPs subtype had considerably greater stromal, immune, and ESTIMATE scores compared to the others (Figures 5B–D). Additionally, the expression of CD8A (P=0.0000), PD-1 (P=0.0000), PD-L1 (P= 0.0010), and CTLA4 (P=0.0000) in the inflammatory DAMPs subtype were also notably greater than in the nuclear DAMPs subtype (Figure 5E), implying that PD-1/PD-L1 and CTLA4 may be the biomarkers of immune checkpoint inhibitors efficacy in MPM.

3.4 Solid validation of the immune characteristics in the TCGA-MESO cohort

Patients of MPM were selected from the TCGA dataset as a validation cohort and they were segregated into two DAMPs-associated subgroups based on the processed algorithm in order to further test whether the features we outlined in the two subtypes of the training cohort could be generalized. By applying CIBERSORT as above, we inferred that M2-like macrophages in the nuclear DAMPs subtype infiltrated substantially and that activated memory CD4+ T cells, M1-like macrophages, and activated DCs infiltrated in the inflammatory DAMPs subtype increased significantly (Figure 6A). These findings are comparable to those of the training cohort. Additionally, patients of the inflammatory DAMPs subtype also exhibited better immune, stromal, and ESTIMATE scores (Figures 6C–E).

In terms of survival analysis, patients of the inflammatory DAMPs subtype exhibited a superior OS than those in the nuclear DAMPs subtype (median overall survival 20.7months vs. 15.1months, P=0.019; Figure 6B). Additionally, the expression of CD8A (P=0.0024) and CTLA-4(P=0.0014) was notably higher in the inflammatory DAMPs subtype than in the nuclear DAMPs subtypes of TCGA cohort, while no statistical significance was found in terms of PDCD1 (PD-1) and CD274 (PD-L1) (Figure 6F), indicating that PD-L1 is possibly not the optimal indicators for ICIs effectiveness in MPM.

3.5 Contrast of genomic variations in two subgroups in the TCGA-MESO cohort

We employed waterfall plots in order to detect genomic mutations and copy number variations between the two subgroups in the TCGA (Figures 7A, B). Although *TTN* mutations were more frequently detected in the inflammatory DAMPs subtype with genetic alterations (21.6% vs 14.3%, P=0.73; Figure 7C) and *TP53* mutations in nuclear DAMPs subtypes (21.6% vs 28.6%, P=0.55; Figure 7C), it did not achieve statistical significance, which may still be a hint to the significant prolonged OS of inflammatory DAMPs subtypes.

Moreover, the ratio of patients which have a copy number deletion in the nuclear DAMPs subtype was greater than in the inflammatory DAMPs subtype (P<0.001; Figure 7D) while the frequency of amplification between the two subtypes has no significant difference (P>0.05; Figure 7E). Deletions in genes were more frequently observed in the nuclear DAMPs subtype than in the inflammatory DAMPs subtype significantly, among which copy number loss in NF2 presented at the highest frequency (Figure 7F). Deletion was observed in MTAP, FOCAD, MLLT3 and type I IFN (e.g., IFNA1/2/4-10/13/14/16/17/21, IFNB1, IFNE, IFNK, IFNW1, and etc.) but at lower frequencies. Deletions on other genes were also analyzed as displayed in Figure 7F.

3.6 Prediction of immunotherapy efficacy in two subtypes

Furthermore, we evaluated the predictive value of immunotherapy efficacy between two subtypes. The expression of major histocompatibility complex (MHC), and cytokines and their receptors in two subtypes exhibited by heatmap (Figures 8A, B). It notably demonstrated that MHC molecules, immunostimulatory and immunoinhibitory molecules, and cytokines and their receptors are unevenly expressed in distinct subtypes, with the higher expressions, especially of CXCL10 and its receptor CXCR3, in the inflammatory DAMPs subtype, both in the training cohort and the validation cohort of TCGA. In the contrast, the expression of TGFB and TGFBR elevated in the nuclear DAMPs subtype, consistent with the GSEA and GSVA results.

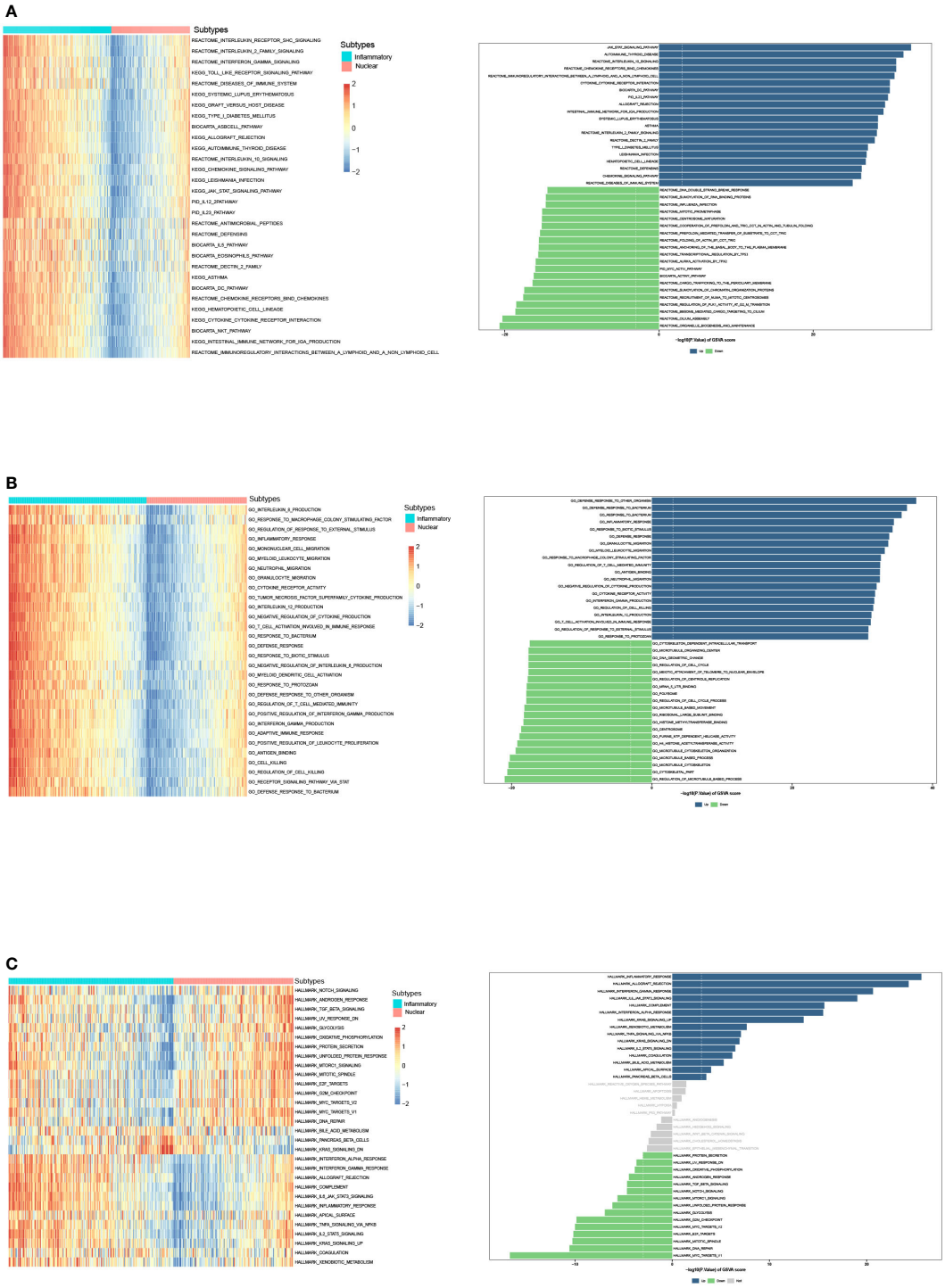

FIGURE 4
GSVA analysis of DEGs in the inflammatory DAMPs and nuclear DAMPs subtype. **(A)** GSVA analysis of canonical pathways (BIOCARTA, KEGG, PID, REACTOME and WIKIPATHWAYS) for patients in the inflammatory DAMPs and nuclear DAMPs subtype. **(B)** GSVA analysis of gene ontology (GO) for patients in the inflammatory DAMPs and nuclear DAMPs subtype. **(C)** GSVA analysis of hallmark gene sets for patients in the inflammatory DAMPs and nuclear DAMPs subtype.

Then the efficacy of ICIs treatment was validated in a murine cohort and a MPM patient cohort treated with ICIs. The inflammatory DAMPs subtype showed a greater response rate than the nuclear DAMPs subtype in the validation cohort of 48 MPM mice receiving PD-L1 inhibitor combined with CTLA-4 inhibitor (100% vs. 7.7%, $P<0.001$; Figure 9A). The response rate of the two subtypes from the validation cohort of 10 MPM patients receiving PD-1 inhibitor as a single agent suggested a similar trend to the results of the murine cohort but failed to achieve statistical significance (57.1% vs. 0%, $P=0.2$; Figure 9B), while the disease

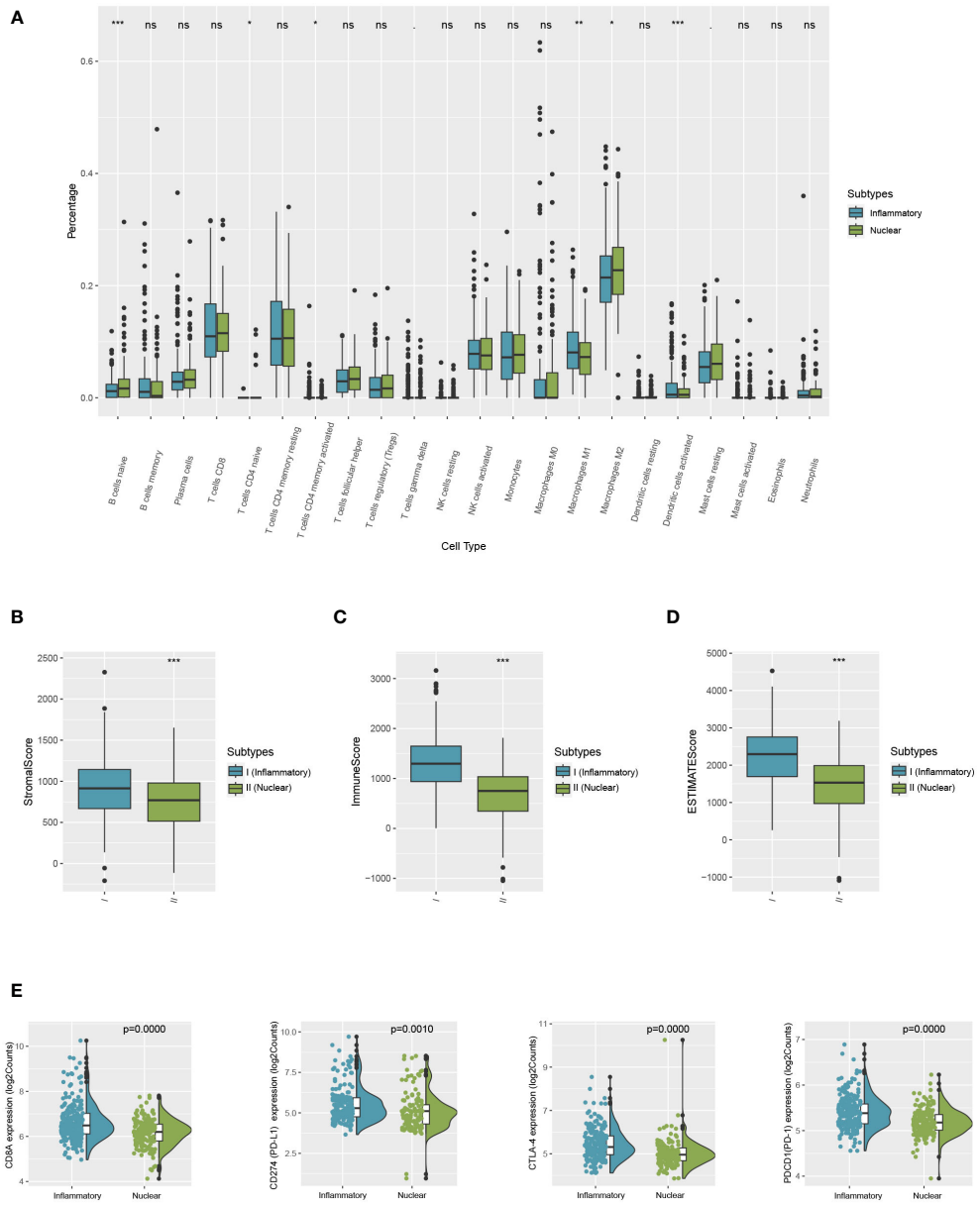

FIGURE 5
Comparison of differences between two subtypes in immune microenvironment status and immune signature expression levels. **(A)** The differential estimated proportion of 22 CIBERSORT immune cell types in DAMPs-associated subtypes. The central line represents the median value. The bottom and top of the boxes are the 25th and 75th percentiles (interquartile range). **(B)** Stromal score in DAMPs-associated subtypes. **(C)** Immune score in DAMPs-associated subtypes. **(D)** ESTIMATE score difference between the two subtypes in the training cohort. **(E)** Expression differences in CD8A, PD-1, PD-L1 and CTLA4 between two subtypes. *P < 0.05; **P < 0.01; ***P < 0.001; ns, not significant.

control rate of the two subtypes was deemed to be statistically significant (85.7% vs. 0%, *P*=0.033; Figure 9C). These findings indicated that the developed DAMPs-associated clustering is capable of forecasting the efficacy of ICBs in MPM.

4 Discussion

Our study categorized MPM patients into two subgroups based on DAMPs and PRRs. In the nuclear DAMPs subtype, nuclear-associated HSP90AA1, HSPA4, CALR and HMGN1 were strongly expressed in the nuclear DAMPs subtype, whereas PRRs modulating activities of inflammasome or immune cells, such as TLRs, AIM2 and NLRP3, were primarily expressed in the inflammatory DAMPs subtype.

HMGN1(also known as alarmin), as a member of the high-mobility group protein family, is activated in undifferentiated cells which proliferate continuously. Extracellular HMGN1 functions as an innate danger-associated inflammatory mediator directly inducing the generation of cytokine and DC maturation. Upon translocation to the cytoplasm, it binds to PRRs to initiate proinflammatory signaling. Increasing expression

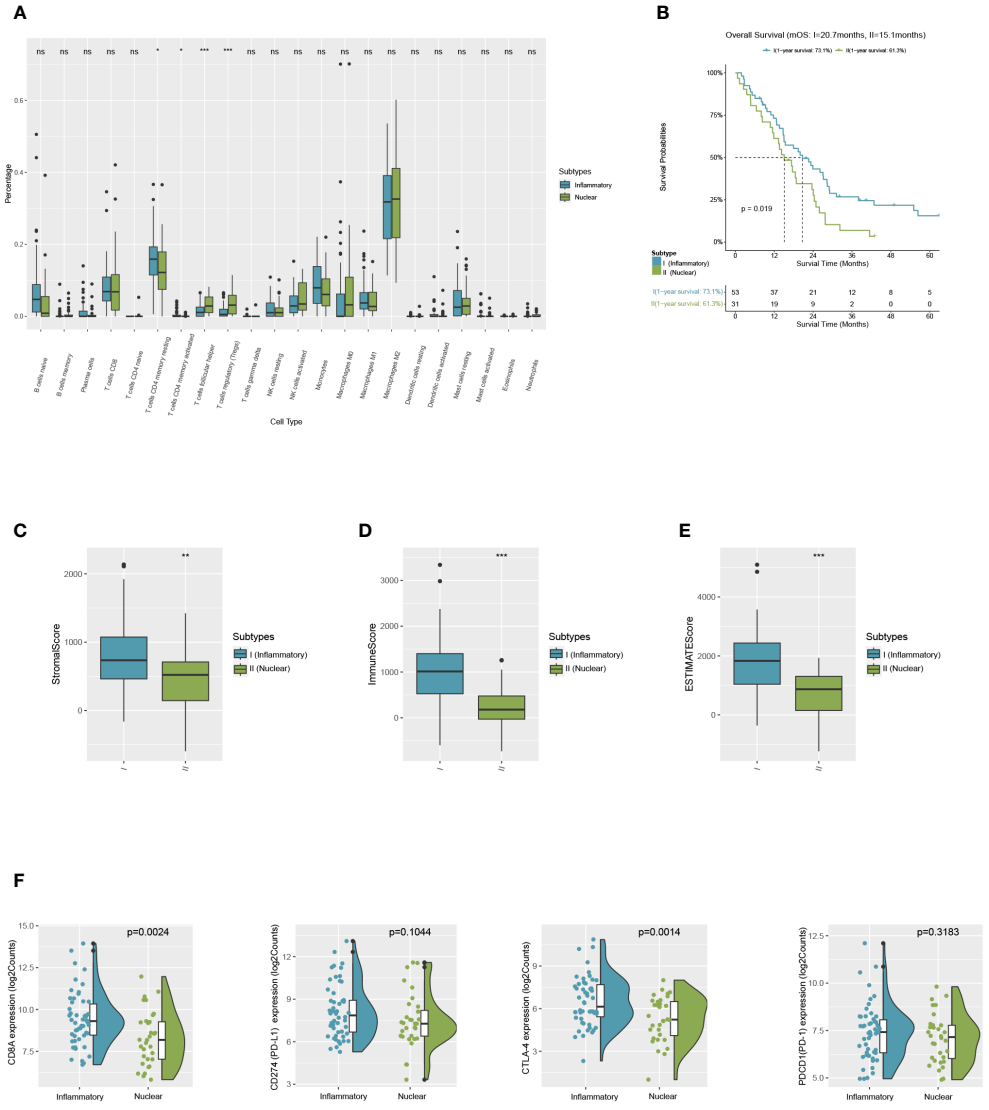

FIGURE 6
Successful validation of DAMPs-associated subtypes in the validation cohort of TCGA. **(A)** The differential estimated proportion of 22 CIBERSORT immune cell types in DAMPs-associated subtypes. The central line represents the median value. The bottom and top of the boxes are the 25th and 75th percentiles (interquartile range). **(B)** Kaplan-Meier curves of overall survival (OS) between the two subtypes in the validation cohort of TCGA. **(C)** Stromal score in DAMPs-associated subtypes. **(D)** Immune score in DAMPs-associated subtypes. **(E)** ESTIMATE score difference between the two subtypes in the validation cohort of TCGA. **(F)** Expression differences in CD8A, PD-1, PD-L1 and CTLA4 between two subtypes. *P < 0.05; **P < 0.01; ***P < 0.001; ns, not significant.

of HMGN1 might provoke chronic inflammation contributing to carcinogenesis and indicating a poorer prognosis (55). The intracellular functions of CALR as a crucial regulator of Ca2+ homeostasis and the integrin-dependent signaling is probably required for tumor progression (56) which therefore implies that CALR expression is robustly related to prompt tumor progression and poor prognosis (57, 58) in the nuclear DAMPs subtype. HSPs in cells are essential in protein folding. The enriched Notch signaling positively regulate the activity of the mTOR pathway (59), and mTOR complex 1 (mTORC1) activates MYC-induced protein synthesis (60). Extreme endoplasmic reticulum (ER) stress and UPR are triggered by the uncontrolled buildup of misfolded proteins in the ER, which induce biological effects *via* upregulation of molecular chaperones such as HSP (e.g., HSP90AA1 and HSPA4). Elevated expression of HSPA4 and HSP90AA1 is related with poor clinical outcomes in cancer patients (61).

However, DAMPs alone are insufficient to elicit an ICD, and a corresponding receptor is required to generate biological effects. Toll-like receptors (TLRs), an evolutionarily conserved transmembrane protein expressed in epithelial cells and immune cells, serve as an important receptor to identify the DAMPs. TLRs bind with ligands such as HMGN1, CALR, HSPA4 and HSP90 to generate the affiliated biological effects *via* activation of MyD88-dependent and independent pathways. AIM2 and NLRP3 are sensors of DNA released from necrotic cells or increased Ca2+ release that initiate the inflammasome assembly (62, 63). Interleukin (IL)-1β and IL-18 are the inflammasome effector cytokines released as a result of

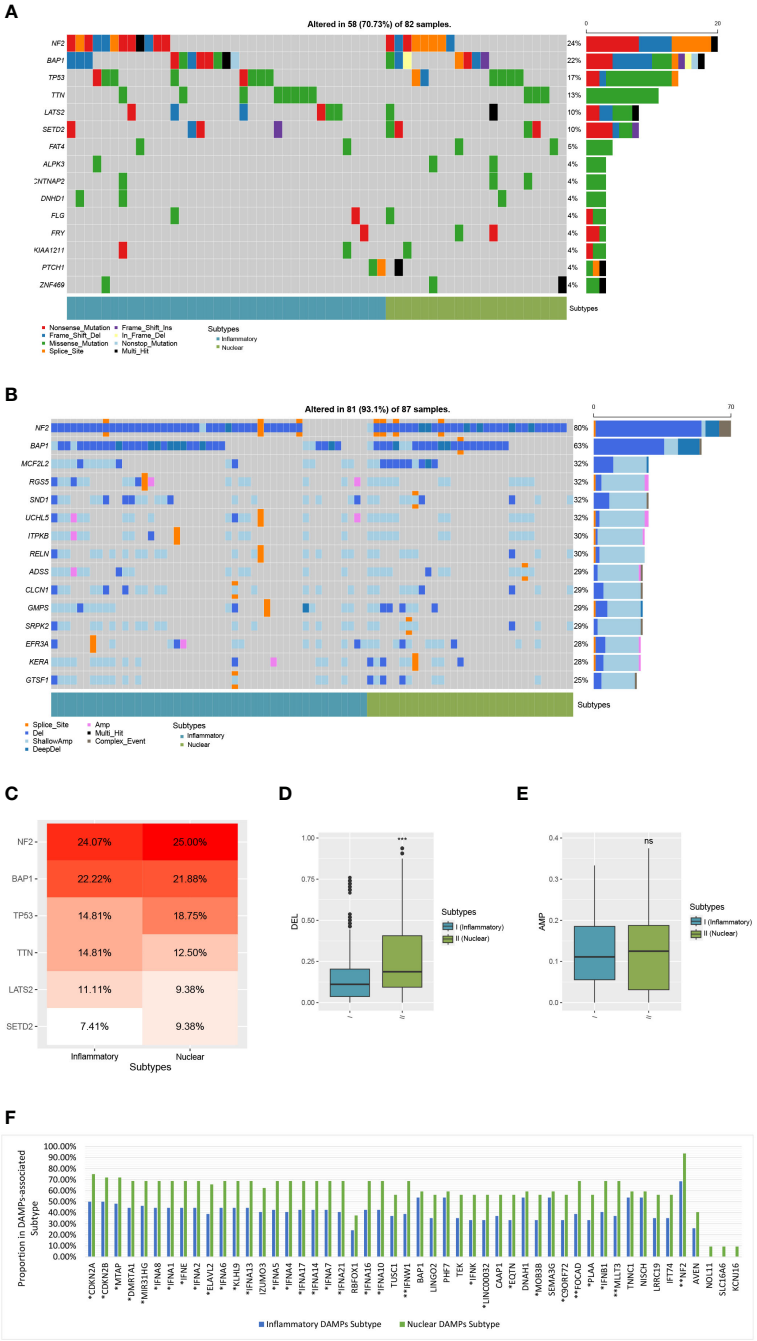

FIGURE 7
Comparison of genomic alterations of DAMPs-associated subtypes in the validation cohort of TCGA. **(A)** Differential somatic mutation analysis between the two subgroups. **(B)** Differential CNV analysis between the two subgroups. **(C)** Somatic mutation percentage of mostly mutated genes. **(D)** Arm-level copy number deletion in DAMPs-associated subtypes. **(E)** Arm-level copy number amplification in DAMPs-associated subtypes. **(F)** Comparison of Genes with copy number deletion in DAMPs-associated subtypes. *P < 0.05; **P < 0.01; ***P<0.001; ns, not significant.

signaling pathways that are regulated by inflammasomes. These cytokines assure an optimum inflammatory immune response against cancer cells (64). Therefore, MPM belonging to nuclear DAMPs subtype with higher expression of nuclear-associated DAMPs genes and lower corresponding PRRs expression are more likely to exhibit more aggressive biological behaviors. Nuclear-associated DAMPs are needed to regulate the progression of nuclear DAMPs subtype of MPM, which in consequence leads to poor outcomes. Under the circumstances of PRRs deficiency, the downstream signaling pathway cannot be activated, even with the presence or overexpression of DAMPs, causing effector cells suppressed and adapted immunity muted, which probably accounts for the suppressed immune microenvironment of the nuclear DAMPs subtype and primary resistance to immunotherapy, consistent with the predicted results of our survival analysis and exploration of immune status and ICIs efficacy.

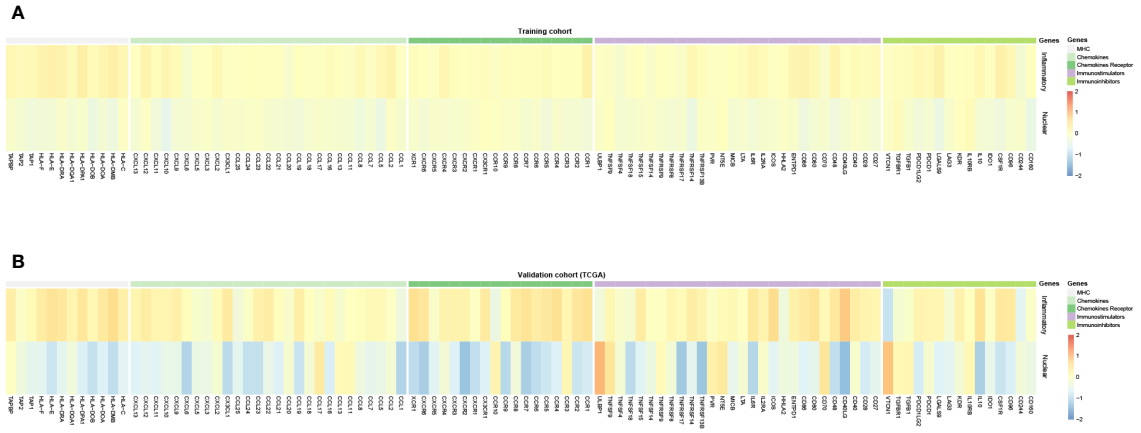

FIGURE 8
(A) Expression of MHC, chemokines and receptors, and immunomodulatory molecules for DAMPs-associated subtypes in the training cohort. **(B)** Expression of MHC, chemokines and receptors, and immunomodulatory molecules for DAMPs-associated subtypes in the TCGA cohort.

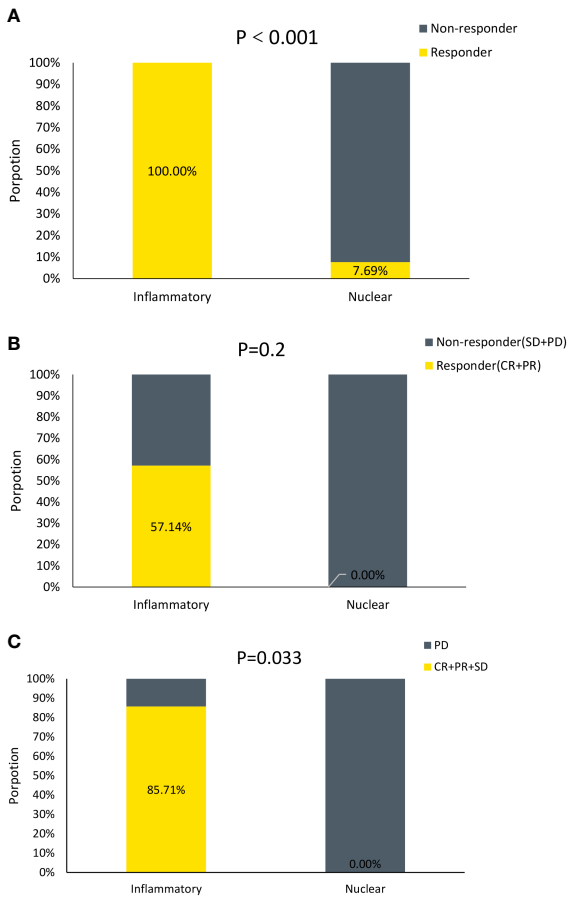

FIGURE 9
DAMPs-associated clusters can predict immunotherapy outcome. **(A)** Proportion of Responder and Non-responder to ICIs in mice. **(B)** Proportion of Responder and Non–responder to ICIs in MPM patients. **(C)** Proportion of Disease Control (CR+PR+SD) and Disease Progression (PD) to ICIs in MPM patients.

The underlying biological pathways were then explored with functional analyses. Based on the DEGs, GSEA and GSVA identified inflammatory DAMPs subtype considerably enriched in the pro-inflammatory pathways that enhance adaptive immune responses. Apart from the toll-like receptor signaling pathway in line with higher expression of TLRs, TNFR binding and regulation of type I interferon-mediated signaling generates the antiproliferative effects of type I IFNs and TNFs (65) *via* activating the proinflammatory NF-κb pathway (66). Cytokine/chemokines pathways (such as IL-2 family, IL-12, IFN-γ, TNF superfamily, chemokine signaling, and IL6-JAK-STAT signaling) and effector immune cell pathways (such as NKT, DC, and T cell activation) were also significantly overexpressed. Upregulated IFN-γ signaling amplifies the antitumor response by mediating induced effects of IL-12 (67) and produces chemokines that attract immune effector cells, effectively changing the TME (68). The release of IFN-γ also leads to increasing antigen presentation of cancer and noncancer cells. Inflammatory chemokines induce recruitment of monocytes and help to support and regulate activated T cells (69). IL-2 mainly produced by CD4+ T cells activates effector T cells and innate lymphoid cells (ILCs) (70). The cytokines aforementioned regulate pro-inflammatory immunity by linking intrinsic and adaptive immune responses. Furthermore, ATM pathway, integrin A4B1 pathway and FGF pathway are enriched in this subtype. ATM (Ataxia-telangiectasia mutated proteins) is a key regulator of the DNA damage response (DDR) and contributes to cell cycle checkpoint maintenance, DNA damage repair and telomere maintenance in DNA double-strand breaks (DSB). The ATM pathway also regulates the suppression of anti-tumor immune cancer-associated fibroblasts (CAFs) differentiation (71). Advanced desmoplasia and stromal changes caused by CAFs have been identified as substantial factors in the progression of MPM (72). Accordingly, inhibition of ATM has the potential to overcome immune resistance in combination with ICIs in a minor subset of MPM patients of inflammatory DAMPs subtype. Fibroblast growth factors (FGFs) and integrin-α4β1 pathways are involved in oncogenic behaviors such as metastasis, angiogenesis, and activation of CAFs (73–75). Thereby, inhibitors targeting FGFs or integrin A4B1, or administrating anti-angiogenic agents may introduce promising directions for the management of this subtype. For the nuclear DAMPs subtype, GSEA revealed that expression of cancer hallmarks of MYC targets, NOTCH signaling, TGF-β signaling, unfolded protein response (UPR), MTORC1 signaling, and IL-8 production was higher in the nuclear DAMPs subtype. MM cells are dependent on Notch signaling, leading to activation of the phosphatidylinositol 3-kinase (PI3K)/Akt/mammalian target of rapamycin (mTOR) signaling pathway (76). NOTCH signaling facilitates immune escape by up-regulating PD-L1 and is associated with the expansion of exhausted CD8+ T cells (76). Expression profiles of malignant mesotheliomas revealed that 46% displayed altered expression of RPTOR (mTORC1 component) that activates the mechanistic target of rapamycin complex 1 (mTORC1) to enhance MM cell growth (77) suggesting the worse outcome of nuclear DAMPs subtype. On the other hand, studies have demonstrated the potential role of IL-8 as a driver of resistance to ICIs and that IL-8 has an essential role in reinforcing the immunosuppressive microenvironment and triggering EMT by determining the types and quantity of myeloid cells infiltrating tumors (78, 79). TGF-β is correlated with suppressing T cell proliferation and activation, impairing DC and NK cell function, encouraging Treg cell differentiation, and boosting CAF activities, ultimately gives rise to resistance to the immunotherapy (80) in the nuclear DAMPs subtype. Thus, targeting the aforementioned pathways is a plausible way to modify the suppressive immune microenvironment and provides new therapeutic options for this subtype.

The components in the tumor immune microenvironment (TiME) provide clues to predict MPM patient outcomes and ICIs responses (81). Activated memory CD4+ T cells, M1-like macrophages, and activated DCs were more prevalent in the inflammatory DAMPs subtype according to the CIBERSORT, while the ESTIMATE revealed that a significantly higher immune score, which have positive relations with better outcomes and more benefits from ICIs. Comparatively, M2-like macrophages of the nuclear DAMPs subtype were massively recruited, which have recently been discovered to participate in promoting resistance to ICIs therapy and predicting a poor outcome (82, 83). Furthermore, the improved OS and response rate to ICIs in the inflammatory DAMPs subtype may be associated with the dramatically elevated expression of CD8A and PD-1. These findings support the previous report that MPM patients with increased expression of CD8A and PD-1 enjoy a favorable prognosis and potentially benefit from ICIs in preceding clinical trials (84) (85). The expression of MHC class I and class II protein, particularly human leukocyte antigen class I (HLA-I) alleles, and proinflammatory chemokines and immunomodulators, especially CXCL10 and CXCR3, is more robust in the inflammatory DAMPs subtypes than the other. MHC expression on tumor cells from treatment-naive patients positively correlates with the clinical outcome and response to anti-CTLA-4, anti-PD-1, or their combination by recognizing tumor-specific antigens (86). In respect of CXCL10 and CXCR3 as downstream adjuvant effectors of type I IFNs, their signaling boosts the efficacy of immunotherapy by increasing immune infiltration of cytotoxic lymphocytes (CTLs), natural killer cells (NKs) and DCs (87). Therefore, upregulated CXCL10 and CXCR3 are positively linked with the efficacy of immunotherapy (88, 89). The above results laid further foundations for our reasonably predicting the better prognosis and response rate of ICIs treatment in the inflammatory DAMPs subtype than the other.

In the TCGA cohort, mutations of *TTN* were found more frequently in the inflammatory DAMPs subtypes and mutations of *TP53* in the nuclear DAMPs subtypes were clinical outcome and efficacy on the trend. Previous studies showed that patients with mutated *TTN* are associated with longer progression-free survival or overall survival (90). TTN expression was favorably associated with the infiltration levels of effector T cells owning an inflammatory TiME and TMB in numerous tumor types, and therefore is linked with susceptibility to immune checkpoint inhibitors (91–93). We can infer that *TTN* may have a connection with clinical outcomes and efficacy of immunotherapy as our model

projected (94). As for TP53 mutation implying a more malignant nature, the nuclear DAMPs subtype is indicated to require more intense management (95).

Copy number deletion in MPM is a characteristic genetic alteration that may result from altered methylation caused by external factors such as asbestos. Copy number deletions of cancer suppressor genes (including CDKN2A/B, FOCAD, NF2, etc.) are always accompanied by adjacent functional genes (including MTAP, MLLT3, etc.) deletion that synergistically contributes to oncogenesis. Studies have shown that copy number deletion is associated with loss of tumor neoantigens and reduced gene expression of immune-related pathways (96), which predicts dismal immune efficacy in this subtype as our subtyping model does (97). Copy number loss of Cyclin-dependent kinase (CDK) inhibitor 2A (CDKN2A) occurs at a significantly higher frequency in the nuclear DAMPs subtype. CDKN2A copy number loss suggests dismal outcomes and predicts immunotherapy resistance (98). CDKN2A encodes p16INK4a which regulates cell-cycle by inhibition of CDK4/6. Emerging clinical data demonstrates selective CDK4/6 inhibitors widely used in clinical practice contribute to PD-L1 up-regulation and immune surveillance enhancement. Hence the combination of ICIs and CDK4/6 inhibitors is a worthwhile strategy for improving outcomes in the immunotherapy-tolerant nuclear DAMPs subtype of MPM. Fifty-seven percent of patients with CDKN2A copy number loss had methylthioadenosine phosphorylase (MTAP) co-deletion in the TCGA validation cohort, since both genes reside in the same cluster of the 9p21 region (99). Co-deletion occurs more frequently indicating poorer prognosis in nuclear DAMPs subtype than the other (72% vs 48%, P=0.032). Studies show that methionine adenosyltransferase 2A (MAT2A) inhibitors induce synthetic lethality of MTAP-deleted cancer, especially in combination with taxanes and gemcitabine (100), which demonstrate a potential to treat MPM of the nuclear DAMPs subtype. Accordingly, distinctive copy number deletion also offers novel approaches to the management of the immune-resistant subtype of MPM.

The antigenicity and adjuvanticity determine the immunogenicity of cell death. Despite MPM is characterized by genetic alterations in tumor suppressor genes (101, 102) suggesting a lack of tumor-associated antigens (TAAs) and a low level of tumor mutation burden (TMB) (103), studies showed that the lowest antigenicity associated with tumorigenesis might be minor but is sufficient to support immunogenicity (12). In this regard, the adjuvanticity of DAMPs and their PRRs in immunogenic cell death may constitute a promising target for activating the immune response, since it is in a superior position to preserve homeostasis of immune microenvironment. Counteracting the inhibition of DAMPs and PRRs (e.g., TLRs stimulators) may suppress tumor growth as well as balance the production of cytokines within the TiME, and further, suppress the immunosuppressive cells while activating the immunostimulatory or effector cells (12), and thus the efficacy of immunotherapy can be enhanced by intervening with the immunomodulatory effects of DAMPs and its downstream signaling. According to the perspectives above, pathways and genomic alterations more peculiar in the nuclear DAMPs subtype of MPM which is primarily resistant to ICIs can be manipulated to modulate the immune status to some extent.

However, there are drawbacks to our study. Firstly, a few genes in the established gene list were excluded due to limitations of expression sequencing by microarray, yet the modified gene set was representative of the concerned genes in the process of ICD. Secondly, there is insufficient sequencing data on patients treated with ICIs since mesothelioma is a rare tumor. Models constructed of mice of the same strain (BALB/c) with identical genetic backgrounds inoculated subcutaneously with the same cell lines (AB1-HA cells) and then treated with anti-CTLA-4 and anti-PD-L1 were selected for additional validation. Moreover, the ORR of PD-1 inhibitors applied to MPM patients of two separate subtypes in the validation cohort did not reach statistical significance, although there was a trend that implied patients belonging to the inflammatory subtype benefit more from ICIs and the DCR, probably on account of small sample size or limited efficacy of ICIs as a single agent in MPM. Additional research is expected to confirm the validity and clinical practicability in larger cohorts or elaborately designed clinical trials.

5 Conclusion

In conclusion, we identified two molecular subtypes *via* K-means analysis based on the expression of ICD-associated DAMPs and their corresponding receptors in MPM. Characteristic signaling pathways and different immune statuses in these two subtypes result in disparate prognoses and efficacy of immune checkpoint inhibitors.

Our research offers a novel method to predict the prognoses and identify the MPM patients with a potential to benefit from ICIs and provides a new perspective to enhance the efficacy of immunotherapy for MPM patients with primary resistance to ICIs. Our work has made a step forward in the process of development of precision therapy in MPM.

Data availability statement

The datasets presented in this study can be found in online repositories. The names of the repository/repositories and accession number(s) can be found within the article/supplementary materials.

Author contributions

ZL: conceptualization, methodology, software, data curation, investigation, validation, visualization, writing- original draft

preparation, writing- reviewing and editing. HB: supervision, funding acquisition. RW: writing- reviewing and editing. JW: conceptualization, supervision, writing- reviewing and editing, funding acquisition. All authors contributed to the article and approved the submitted version.

Funding

This work was supported by grants from the National key R&D program of China (2022YFC2505000); NSFC general program (82272796); CAMS Innovation Fund for Medical Sciences(CIFMS) 2022-I2M-1-009; CAMS Key Laboratory of Translational Research on Lung Cancer (2018PT31035); Aiyou foundation (KY201701).

Conflict of interest

The authors declare that the research was conducted in the absence of any commercial or financial relationships that could be construed as a potential conflict of interest.

Publisher's note

References

1. Zhao J, Zuo T, Zheng R, Zhang S, Zeng H, Xia C, et al. Epidemiology and trend analysis on malignant mesothelioma in China. *Chin J Cancer Res* (2017) 29(4):361–8. doi: 10.21147/j.issn.1000-9604.2017.04.09

2. Fennell DA, Dulloo S, Harber J. Immunotherapy approaches for malignant pleural mesothelioma. *Nat Rev Clin Oncol* (2022) 19(9):573–84. doi: 10.1038/s41571-022-00649-7

3. Peters S, Scherpereel A, Cornelissen R, Oulkhouir Y, Greillier L, Kaplan MA, et al. First-line nivolumab plus ipilimumab versus chemotherapy in patients with unresectable malignant pleural mesothelioma: 3-year outcomes from CheckMate 743. *Ann Oncol* (2022) 33(5):488–99. doi: 10.1016/j.annonc.2022.01.074

4. Quispel-Janssen J, van der Noort V, de Vries JF, Zimmerman M, Lalezari F, Thunnissen E, et al. Programmed death 1 blockade with nivolumab in patients with recurrent malignant pleural mesothelioma. *J Thorac Oncol* (2018) 13(10):1569–76. doi: 10.1016/j.jtho.2018.05.038

5. Galluzzi L, van der Noort V, de Vries JF, Zimmerman M, Lalezari F, Thunnissen E, et al. Consensus guidelines for the definition, detection and interpretation of immunogenic cell death. *J Immunother Cancer* (2020) 8(1):e000337. doi: 10.1136/jitc-2019-000337corr1

6. Di Somma S, Iannuzzi CA, Passaro C, Forte IM, Iannone R, Gigantino V, et al. The oncolytic virus dl922-947 triggers immunogenic cell death in mesothelioma and reduces xenograft growth. *Front Oncol* (2019) 9:564. doi: 10.3389/fonc.2019.00564

7. Riganti C, Lingua MF, Salaroglio IC, Falcomatà C, Righi L, Morena D, et al. Bromodomain inhibition exerts its therapeutic potential in malignant pleural mesothelioma by promoting immunogenic cell death and changing the tumor immune-environment. *Oncoimmunology* (2018) 7(3):e1398874. doi: 10.1080/2162402X.2017.1398874

8. Leclercq S, Gueugnon F, Boutin B, Guillot F, Blanquart C, Rogel A, et al. A 5-aza-2'-deoxycytidine/valproate combination induces cytotoxic T-cell response against mesothelioma. *Eur Respir J* (2011) 38(5):1105–16. doi: 10.1183/09031936.00081310

9. Salas-Benito D, Pérez-Gracia JL, Ponz-Sarvisé M, Rodriguez-Ruiz ME, Martínez-Forero I, Castañón E, et al. Paradigms on immunotherapy combinations with chemotherapy. *Cancer Discovery* (2021) 11(6):1353–67. doi: 10.1158/2159-8290.CD-20-1312

10. Jeong SD, Jung BK, Ahn HM, Lee D, Ha J, Noh I, et al. Immunogenic cell death inducing fluorinated mitochondria-disrupting helical polypeptide synergizes with PD-L1 immune checkpoint blockade. *Adv Sci (Weinh)* (2021) 8(7):2001308. doi: 10.1002/advs.202001308

11. Kroemer G, Galluzzi L, Kepp O, Zitvogel L. Immunogenic cell death in cancer therapy. *Annu Rev Immunol* (2013) 31:51–72. doi: 10.1146/annurev-immunol-032712-100008

12. Galluzzi L, Buqué A, Kepp O, Zitvogel L, Kroemer G. Immunogenic cell death in cancer and infectious disease. *Nat Rev Immunol* (2017) 17(2):97–111. doi: 10.1038/nri.2016.107

13. Krysko O, Løve Aaes T, Bachert C, Vandenabeele P, Krysko DV. Many faces of DAMPs in cancer therapy. *Cell Death Dis* (2013) 4(5):e631. doi: 10.1038/cddis.2013.156

14. Man SM, Jenkins BJ. Context-dependent functions of pattern recognition receptors in cancer. *Nat Rev Cancer* (2022) 22(7):397–413. doi: 10.1038/s41568-022-00462-5

15. Tumeh PC, Harview CL, Yearley JH, Shintaku IP, Taylor EJ, Robert L, et al. PD-1 blockade induces responses by inhibiting adaptive immune resistance. *Nature* (2014) 515(7528):568–71. doi: 10.1038/nature13954

16. Kalbasi A, Ribas A. Tumour-intrinsic resistance to immune checkpoint blockade. *Nat Rev Immunol* (2020) 20(1):25–39. doi: 10.1038/s41577-019-0218-4

17. Gong T, Liu L, Jiang W, Zhou R. DAMP-sensing receptors in sterile inflammation and inflammatory diseases. *Nat Rev Immunol* (2020) 20(2):95–112. doi: 10.1038/s41577-019-0215-7

18. Hernandez C, Huebener P, Schwabe RF. Damage-associated molecular patterns in cancer: a double-edged sword. *Oncogene* (2016) 35(46):5931–41. doi: 10.1038/onc.2016.104

19. Zhang Q, Raoof M, Chen Y, Sumi Y, Sursal T, Junger W, et al. Circulating mitochondrial DAMPs cause inflammatory responses to injury. *Nature* (2010) 464 (7285):104–7. doi: 10.1038/nature08780

20. Komada T, Chung H, Lau A, Platnich JM, Beck PL, Benediktsson H, et al. Macrophage uptake of necrotic cell DNA activates the AIM2 inflammasome to regulate a proinflammatory phenotype in CKD. *J Am Soc Nephrol* (2018) 29(4):1165–81. doi: 10.1681/ASN.2017080863

21. Li T, Chen ZJ. The cGAS-cGAMP-STING pathway connects DNA damage to inflammation, senescence, and cancer. *J Exp Med* (2018) 215(5):1287–99. doi: 10.1084/jem.20180139

22. Viglianti GA, Lau CM, Hanley TM, Miko BA, Shlomchik MJ, Marshak-Rothstein A. Activation of autoreactive b cells by CpG dsDNA. *Immunity* (2003) 19 (6):837–47. doi: 10.1016/S1074-7613(03)00323-6

23. Lau CM, Broughton C, Tabor AS, Akira S, Flavell RA, Mamula MJ, et al. RNA-Associated autoantigens activate b cells by combined b cell antigen receptor/Toll-like receptor 7 engagement. *J Exp Med* (2005) 202(9):1171–7. doi: 10.1084/jem.20050630

24. Sistigu A, Yamazaki T, Vacchelli E, Chaba K, Enot DP, Adam J, et al. Cancer cell-autonomous contribution of type I interferon signaling to the efficacy of chemotherapy. *Nat Med* (2014) 20(11):1301–9. doi: 10.1038/nm.3708

25. Chiba S, Baghdadi M, Akiba H, Yoshiyama H, Kinoshita I, Dosaka-Akita H, et al. Tumor-infiltrating DCs suppress nucleic acid-mediated innate immune responses through interactions between the receptor TIM-3 and the alarmin HMGB1. *Nat Immunol* (2012) 13(9):832–42. doi: 10.1038/ni.2376

26. Cavassani KA, Ishii M, Wen H, Schaller MA, Lincoln PM, Lukacs NW, et al. TLR3 is an endogenous sensor of tissue necrosis during acute inflammatory events. *J Exp Med* (2008) 205(11):2609–21. doi: 10.1084/jem.20081370

27. Chen L, Song Z, Cao X, Fan M, Zhou Y, Zhang G. Interleukin-33 regulates the endoplasmic reticulum stress of human myometrium via an influx of calcium during initiation of labor. *Elife* (2022) 11:e75072. doi: 10.7554/eLife.75072.sa2

28. Vasanthakumar A, Kallies A. Interleukin (IL)-33 and the IL-1 family of cytokines-regulators of inflammation and tissue homeostasis. *Cold Spring Harb Perspect Biol* (2019) 11(3):a028506. doi: 10.1101/cshperspect.a028506

29. Brunner SM, Rubner C, Kesselring R, Martin M, Griesshammer E, Ruemmele P, et al. Tumor-infiltrating, interleukin-33-producing effector-memory CD8(+) T cells in resected hepatocellular carcinoma prolong patient survival. *Hepatology* (2015) 61 (6):1957–67. doi: 10.1002/hep.27728

30. Tammaro A, Derive M, Gibot S, Leemans JC, Florquin S, Dessing MC. TREM-1 and its potential ligands in non-infectious diseases: from biology to clinical perspectives. *Pharmacol Ther* (2017) 177:81–95. doi: 10.1016/j.pharmthera.2017.02.043

31. Bouchon A, Dietrich J, Colonna M. Cutting edge: inflammatory responses can be triggered by TREM-1, a novel receptor expressed on neutrophils and monocytes. *J Immunol* (2000) 164(10):4991–5. doi: 10.4049/jimmunol.164.10.4991

32. Bouchon A, Facchetti F, Weigand MA, Colonna M. TREM-1 amplifies inflammation and is a crucial mediator of septic shock. *Nature* (2001) 410 (6832):1103–7. doi: 10.1038/35074114

33. Iwata A, Morgan-Stevenson V, Schwartz B, Liu L, Tupper J, Zhu X, et al. Extracellular BCL2 proteins are danger-associated molecular patterns that reduce tissue damage in murine models of ischemia-reperfusion injury. *PloS One* (2010) 5(2):e9103. doi: 10.1371/journal.pone.0009103

34. Garg AD, Krysko DV, Verfaillie T, Kaczmarek A, Ferreira GB, Marysael T, et al. A novel pathway combining calreticulin exposure and ATP secretion in immunogenic cancer cell death. *EMBO J* (2012) 31(5):1062–79. doi: 10.1038/emboj.2011.497

35. Panaretakis T, Joza N, Modjtahedi N, Tesniere A, Vitale I, Durchschlag M, et al. The co-translocation of ERp57 and calreticulin determines the immunogenicity of cell death. *Cell Death Differ* (2008) 15(9):1499–509. doi: 10.1038/cdd.2008.67

36. Obeid M, Tesniere A, Ghiringhelli F, Fimia GM, Apetoh L, Perfettini JL, et al. Calreticulin exposure dictates the immunogenicity of cancer cell death. *Nat Med* (2007) 13(1):54–61. doi: 10.1038/nm1523

37. Patel RA, Forinash KD, Pireddu R, Sun Y, Sun N, Martin MP, et al. RKI-1447 is a potent inhibitor of the rho-associated ROCK kinases with anti-invasive and antitumor activities in breast cancer. *Cancer Res* (2012) 72(19):5025–34. doi: 10.1158/0008-5472.CAN-12-0954

38. Song KH, Oh SJ, Kim S, Cho H, Lee HJ, Song JS, et al. HSP90A inhibition promotes anti-tumor immunity by reversing multi-modal resistance and stem-like property of immune-refractory tumors. *Nat Commun* (2020) 11(1):562. doi: 10.1038/s41467-019-14259-y

39. Xu Q, Tu J, Dou C, Zhang J, Yang L, Liu X, et al. HSP90 promotes cell glycolysis, proliferation and inhibits apoptosis by regulating PKM2 abundance via thr-328 phosphorylation in hepatocellular carcinoma. *Mol Cancer* (2017) 16(1):178. doi: 10.1186/s12943-017-0748-y

40. Chekeni FB, Elliott MR, Sandilos JK, Walk SF, Kinchen JM, Lazarowski ER, et al. Pannexin 1 channels mediate 'find-me' signal release and membrane permeability during apoptosis. *Nature* (2010) 467(7317):863–7. doi: 10.1038/nature09413

41. Ruan Z, Orozco IJ, Du J, Lü W. Structures of human pannexin 1 reveal ion pathways and mechanism of gating. *Nature* (2020) 584(7822):646–51. doi: 10.1038/s41586-020-2357-y

42. Hakim S, Craig JM, Koblinski JE, Clevenger CV. Inhibition of the activity of cyclophilin a impedes prolactin receptor-mediated signaling, mammary tumorigenesis, and metastases. *iScience* (2020) 23(10):101581. doi: 10.1016/j.isci.2020.101581

43. Lane AA, Chapuy B, Lin CY, Tivey T, Li H, Townsend EC, et al. Triplication of a 21q22 region contributes to b cell transformation through HMGN1 overexpression and loss of histone H3 Lys27 trimethylation. *Nat Genet* (2014) 46(6):618–23. doi: 10.1038/ng.2949

44. Rattner BP, Yusufzai T, Kadonaga JT. HMGN proteins act in opposition to ATP-dependent chromatin remodeling factors to restrict nucleosome mobility. *Mol Cell* (2009) 34(5):620–6. doi: 10.1016/j.molcel.2009.04.014

45. Lim JH, Catez F, Birger Y, West KL, Prymakowska-Bosak M, Postnikov YV, et al. Chromosomal protein HMGN1 modulates histone H3 phosphorylation. *Mol Cell* (2004) 15(4):573–84. doi: 10.1016/j.molcel.2004.08.006

46. Wu HY, Trevino JG, Fang BL, Riner AN, Vudatha V, Zhang GH, et al. Patient-derived pancreatic cancer cells induce C2C12 myotube atrophy by releasing Hsp70 and Hsp90. *Cells* (2022) 11(17):2756. doi: 10.3390/cells11172756

47. Zhou Y, Zhou B, Pache L, Chang M, Khodabakhshi AH, Tanaseichuk O, et al. Metascape provides a biologist-oriented resource for the analysis of systems-level datasets. *Nat Commun* (2019) 10(1):1523. doi: 10.1038/s41467-019-09234-6

48. Mootha VK, Lindgren CM, Eriksson K-F, Subramanian A, Sihag S, Lehar J, et al. PGC-1α-responsive genes involved in oxidative phosphorylation are coordinately downregulated in human diabetes. *Nat Genet* (2003) 34(3):267–73. doi: 10.1038/ng1180

49. Subramanian A, Tamayo P, Mootha VK, Mukherjee S, Ebert BL, Gillette MA, et al. Gene set enrichment analysis: A knowledge-based approach for interpreting genome-wide expression profiles. *Proc Natl Acad Sci U S A* (2005) 102(43):15545–50. doi: 10.1073/pnas.0506580102

50. Hänzelmann S, Castelo R, Guinney J. GSVA: Gene set variation analysis for microarray and RNA-seq data. *BMC Bioinf* (2013) 14:7. doi: 10.1186/1471-2105-14-7

51. Newman AM, Liu CL, Green MR, Gentles AJ, Feng W, Xu Y, et al. Robust enumeration of cell subsets from tissue expression profiles. *Nat Methods* (2015) 12 (5):453–7. doi: 10.1038/nmeth.3337

52. Yoshihara K, Shahmoradgoli M, Martínez E, Vegesna R, Kim H, Torres-Garcia W, et al. Inferring tumour purity and stromal and immune cell admixture from expression data. *Nat Commun* (2013) 4:2612. doi: 10.1038/ncomms3612

53. Mermel CH, Schumacher SE, Hill B, Meyerson ML, Beroukhim R, Getz G. *GISTIC2.0 facilitates sensitive and confident localization of the targets of focal somatic copy-number alteration in human cancers. Genome Biol* (2011) 12(4):R41.

54. Gu Z, Eils R, Schlesner M. Complex heatmaps reveal patterns and correlations in multidimensional genomic data. *Bioinformatics* (2016) 32(18):2847–9. doi: 10.1093/bioinformatics/btw313

55. Wei F, Yang F, Jiang X, Yu W, Ren X. High-mobility group nucleosome-binding protein 1 is a novel clinical biomarker in non-small cell lung cancer. *Tumor Biol* (2015) 36(12):9405–10. doi: 10.1007/s13277-015-3693-7

56. Fucikova J, Spisek R, Kroemer G, Galluzzi L. Calreticulin and cancer. *Cell Res* (2021) 31(1):5–16. doi: 10.1038/s41422-020-0383-9

57. Lwin ZM, Guo C, Salim A, Yip GW, Chew FT, Nan J, et al. Clinicopathological significance of calreticulin in breast invasive ductal carcinoma. *Mod Pathol* (2010) 23 (12):1559–66. doi: 10.1038/modpathol.2010.173

58. Chen CN, Chang CC, Su TE, Hsu WM, Jeng YM, Ho MC, et al. Identification of calreticulin as a prognosis marker and angiogenic regulator in human gastric cancer. *Ann Surg Oncol* (2009) 16(2):524–33. doi: 10.1245/s10434-008-0243-1

59. Chan SM, Weng AP, Tibshirani R, Aster JC, Utz PJ. Notch signals positively regulate activity of the mTOR pathway in T-cell acute lymphoblastic leukemia. *Blood* (2007) 110(1):278–86. doi: 10.1182/blood-2006-08-039883

60. Mossmann D, Park S, Hall MN. mTOR signalling and cellular metabolism are mutual determinants in cancer. *Nat Rev Cancer* (2018) 18(12):744–57. doi: 10.1038/s41568-018-0074-8

61. Düzgün MB, Theofilatos K, Georgakilas AG, Pavlopoulou A. A bioinformatic approach for the identification of molecular determinants of Resistance/Sensitivity to cancer thermotherapy. *Oxid Med Cell Longev 2019* (2019) p:4606219.

62. Lian Q, Xu J, Yan S, Huang M, Ding H, Sun X, et al. Chemotherapy-induced intestinal inflammatory responses are mediated by exosome secretion of double-strand DNA via AIM2 inflammasome activation. *Cell Res* (2017) 27(6):784–800. doi: 10.1038/cr.2017.54

63. Mangan MSJ, Olhava EJ, Roush WR, Seidel HM, Glick GD, Latz E. Targeting the NLRP3 inflammasome in inflammatory diseases. *Nat Rev Drug Discovery* (2018) 17 (8):588–606. doi: 10.1038/nrd.2018.97

64. Sharma BR, Kanneganti TD. Inflammasome signaling in colorectal cancer. *Transl Res* (2022) 252:45–52. doi: 10.1016/j.trsl.2022.09.002

65. MacEwan DJ. TNF ligands and receptors–a matter of life and death. *Br J Pharmacol* (2002) 135(4):855–75. doi: 10.1038/sj.bjp.0704549

66. Dostert C, Grusdat M, Letellier E, Brenner D. The TNF family of ligands and receptors: Communication modules in the immune system and beyond. *Physiol Rev* (2019) 99(1):115–60. doi: 10.1152/physrev.00045.2017

67. Tugues S, Burkhard SH, Ohs I, Vrohlings M, Nussbaum K, Vom Berg J, et al. New insights into IL-12-mediated tumor suppression. *Cell Death Differ* (2015) 22 (2):237–46. doi: 10.1038/cdd.2014.134

68. Ribas A, Haining WN, Schumacher TNM. When cancer cells become the enablers of an antitumor immune response. *Cancer Discovery* (2022) 12(10):2244–8. doi: 10.1158/2159-8290.CD-22-0706

69. Palomino DC, Marti LC. Chemokines and immunity. *Einstein (Sao Paulo)* (2015) 13(3):469–73. doi: 10.1590/S1679-45082015RB3438

70. Raeber ME, Sahin D, Boyman O. Interleukin-2-based therapies in cancer. *Sci Transl Med* (2022) 14(670):eabo5409. doi: 10.1126/scitranslmed.abo5409

71. Mellone M, Piotrowska K, Venturi G, James L, Bzura A, Lopez MA, et al. ATM Regulates differentiation of myofibroblastic cancer-associated fibroblasts and can be targeted to overcome immunotherapy resistance. *Cancer Res* (2022) 82(24):4571–85. doi: 10.1158/0008-5472.CAN-22-0435

72. Mathilakathu A, Wessolly M, Mairinger E, Uebner H, Kreidt D, Brcic L, et al. Cancer-associated fibroblasts regulate kinase activity in mesothelioma cell lines via paracrine signaling and thereby dictate cell faith and behavior. *Int J Mol Sci* (2022) 23 (6):3278. doi: 10.3390/ijms23063278

73. Bordignon P, Bottoni G, Xu X, Popescu AS, Truan Z, Guenova E, et al. Dualism of FGF and TGF-β signaling in heterogeneous cancer-associated fibroblast activation with ETV1 as a critical determinant. *Cell Rep* (2019) 28(9):2358–2372.e6. doi: 10.1016/j.celrep.2019.07.092

74. Turner N, Grose R. Fibroblast growth factor signalling: From development to cancer. *Nat Rev Cancer* (2010) 10(2):116–29. doi: 10.1038/nrc2780

75. Baiula M, Spampinato S, Gentilucci L, Tolomelli A. Novel ligands targeting α(4)β(1) integrin: Therapeutic applications and perspectives. *Front Chem* (2019) 7:489. doi: 10.3389/fchem.2019.00489

76. Graziani I, Eliasz S, De Marco MA, Chen Y, Pass HI, De May RM, et al. Opposite effects of notch-1 and notch-2 on mesothelioma cell survival under hypoxia are exerted through the akt pathway. *Cancer Res* (2008) 68(23):9678–85. doi: 10.1158/0008-5472.CAN-08-0969

77. Sato T, Mukai S, Ikeda H, Mishiro-Sato E, Akao K, Kobayashi T, et al. Silencing of SmgGDS, a novel mTORC1 inducer that binds to RHEBs, inhibits malignant mesothelioma cell proliferation. *Mol Cancer Res* (2021) 19(5):921–31. doi: 10.1158/1541-7786.MCR-20-0637

78. Bakouny Z, Choueiri TK. IL-8 and cancer prognosis on immunotherapy. *Nat Med* (2020) 26(5):650–1. doi: 10.1038/s41591-020-0873-9

79. David JM, Dominguez C, Hamilton DH, Palena C. The IL-8/IL-8R axis: A double agent in tumor immune resistance. *Vaccines (Basel)* (2016) 4(3):22. doi: 10.3390/vaccines4030022

80. Yi M, Niu M, Wu Y, Ge H, Jiao D, Zhu S, et al. Combination of oral STING agonist MSA-2 and anti-TGF-β/PD-L1 bispecific antibody YM101: a novel immune cocktail therapy for non-inflamed tumors. *J Hematol Oncol* (2022) 15(1):142. doi: 10.1186/s13045-022-01363-8

81. Harber J, Kamata T, Pritchard C, Fennell D. Matter of TIME: The tumor-immune microenvironment of mesothelioma and implications for checkpoint blockade efficacy. *J Immunother Cancer* (2021) 9(9):e003032. doi: 10.1136/jitc-2021-003032

82. Zheng X, Weigert A, Reu S, Guenther S, Mansouri S, Bassaly B, et al. Spatial density and distribution of tumor-associated macrophages predict survival in non-

small cell lung carcinoma. *Cancer Res* (2020) 80(20):4414–25. doi: 10.1158/0008-5472.CAN-20-0069

83. Chen SMY, Popolizio V, Woolaver RA, Ge H, Krinsky AL, John J, et al. Differential responses to immune checkpoint inhibitor dictated by pre-existing differential immune profiles in squamous cell carcinomas caused by same initial oncogenic drivers. *J Exp Clin Cancer Res* (2022) 41(1):123. doi: 10.1186/s13046-022-02337-x

84. Alcala N, Mangiante L, Le-Stang N, Gustafson CE, Boyault S, Damiola F, et al. Redefining malignant pleural mesothelioma types as a continuum uncovers immune-vascular interactions. *EBioMedicine* (2019) 48:191–202. doi: 10.1016/j.ebiom.2019.09.003

85. Popat S, Scherpereel A, Antonia S, Oulkhouir Y, Bautista Y, Cornelissen R, et al. First-line nivolumab plus ipilimumab versus chemotherapy in unresectable malignant pleural mesothelioma (MPM) in CheckMate 743. *J Oncol Pharm Pract* (2022) 28(2 SUPPL):5.

86. Rodig SJ, Gusenleitner D, Jackson DG, Gjini E, Giobbie-Hurder A, Jin C, et al. MHC proteins confer differential sensitivity to CTLA-4 and PD-1 blockade in untreated metastatic melanoma. *Sci Transl Med* (2018) 10(450):eaar3342. doi: 10.1126/scitranslmed.aar3342

87. Li X, Lu M, Yuan M, Ye J, Zhang W, Xu L, et al. CXCL10-armed oncolytic adenovirus promotes tumor-infiltrating T-cell chemotaxis to enhance anti-PD-1 therapy. *Oncoimmunology* (2022) 11(1):2118210. doi: 10.1080/2162402X.2022.2118210

88. Shi Z, Shen J, Qiu J, Zhao Q, Hua K, Wang H. CXCL10 potentiates immune checkpoint blockade therapy in homologous recombination-deficient tumors. *Theranostics* (2021) 11(15):7175–87. doi: 10.7150/thno.59056

89. Janji B, Hasmim M, Parpal S, De Milito A, Berchem G, Noman MZ. Lighting up the fire in cold tumors to improve cancer immunotherapy by blocking the activity of the autophagy-related protein PIK3C3/VPS34. *Autophagy* (2020) 16(11):2110–1. doi: 10.1080/15548627.2020.1815439

90. Wang Z, Wang C, Lin S, Yu X. Effect of TTN mutations on immune microenvironment and efficacy of immunotherapy in lung adenocarcinoma patients. *Front Oncol* (2021) 11:725292. doi: 10.3389/fonc.2021.725292

91. Oh J-H, Jang SJ, Kim J, Sohn I, Lee J-Y, Cho EJ, et al. Spontaneous mutations in the single TTN gene represent high tumor mutation burden. *NPJ Genomic Med* (2020) 5(1):33. doi: 10.1038/s41525-019-0107-6

92. Chen J, Wen Y, Su H, Yu X, Hong R, Chen C, et al. Deciphering prognostic value of TTN and its correlation with immune infiltration in lung adenocarcinoma. *Front Oncol* (2022) 12:877878. doi: 10.3389/fonc.2022.877878

93. Jia Q, Wang J, He N, He J, Zhu B. Titin mutation associated with responsiveness to checkpoint blockades in solid tumors. *JCI Insight* (2019) 4(10):e127901. doi: 10.1172/jci.insight.127901

94. Su C, Wang X, Zhou J, Zhao J, Zhou F, Zhao G, et al. Titin mutation in circulatory tumor DNA is associated with efficacy to immune checkpoint blockade in advanced non-small cell lung cancer. *Transl Lung Cancer Res* (2021) 10(3):1256–65. doi: 10.21037/tlcr-20-1118

95. Baslan T, Morris JPT, Zhao Z, Reyes J, Ho YJ, Tsanov KM, et al. Ordered and deterministic cancer genome evolution after p53 loss. *Nature* (2022) 608(7924):795–802. doi: 10.1038/s41586-022-05082-5

96. Jhunjhunwala S, Hammer C, Delamarre L. Antigen presentation in cancer: insights into tumour immunogenicity and immune evasion. *Nat Rev Cancer* (2021) 21(5):298–312. doi: 10.1038/s41568-021-00339-z

97. Roh W, Chen PL, Reuben A, Spencer CN, Prieto PA, Miller JP, et al. Integrated molecular analysis of tumor biopsies on sequential CTLA-4 and PD-1 blockade reveals markers of response and resistance. *Sci Transl Med* (2017) 9(379):eaah3560. doi: 10.1126/scitranslmed.aah3560

98. Gutiontov SI, Turchan WT, Spurr LF, Rouhani SJ, Chervin CS, Steinhardt G, et al. CDKN2A loss-of-function predicts immunotherapy resistance in non-small cell lung cancer. *Sci Rep* (2021) 11(1):20059. doi: 10.1038/s41598-021-99524-1

99. Krasinskas AM, Bartlett DL, Cieply K, Dacic S. CDKN2A and MTAP deletions in peritoneal mesotheliomas are correlated with loss of p16 protein expression and poor survival. *Modern Pathol* (2010) 23(4):531–8. doi: 10.1038/modpathol.2009.186

100. Kalev P, Hyer ML, Gross S, Konteatis Z, Chen CC, Fletcher M, et al. MAT2A inhibition blocks the growth of MTAP-deleted cancer cells by reducing PRMT5-dependent mRNA splicing and inducing DNA damage. *Cancer Cell* (2021) 39(2):209–224.e11. doi: 10.1016/j.ccell.2020.12.010

101. Shao C, Li G, Huang L, Pruitt S, Castellanos E, Frampton G, et al. Prevalence of high tumor mutational burden and association with survival in patients with less common solid tumors. *JAMA Netw Open* (2020) 3(10):e2025109. doi: 10.1001/jamanetworkopen.2020.25109

102. Frampton GM, Fichtenholtz A, Otto GA, Wang K, Downing SR, He J, et al. Development and validation of a clinical cancer genomic profiling test based on massively parallel DNA sequencing. *Nat Biotechnol* (2013) 31(11):1023–31. doi: 10.1038/nbt.2696

103. Chalmers ZR, Connelly CF, Fabrizio D, Gay L, Ali SM, Ennis R, et al. Analysis of 100,000 human cancer genomes reveals the landscape of tumor mutational burden. *Genome Med* (2017) 9(1):34. doi: 10.1186/s13073-017-0424-2

frontiers | Frontiers in Immunology

TYPE Original Research
PUBLISHED 16 June 2023
DOI 10.3389/fimmu.2023.1116430

OPEN ACCESS

EDITED BY
Chiara Porta,
University of Eastern Piedmont, Italy

REVIEWED BY
Massimiliano Mazza,
IRCCS Istituto Romagnolo per lo Studio dei Tumori (IRST) "Dino Amadori", Italy
Annalisa Chiocchetti,
Università del Piemonte Orientale, Italy

*CORRESPONDENCE
Paola Allavena
paola.allavena@humanitasresearch.it
Cristina Belgiovine
cristina.belgiovine@gmail.com

†PRESENT ADDRESS
Cristina Belgiovine,
Department Clinical, Surgical, Diagnostics and Pediatric Sciences, University of Pavia Pediatric Surgery Unit, Fondazione IRCCS Policlinico San Matteo, Pavia, Italy

RECEIVED 05 December 2022
ACCEPTED 29 May 2023
PUBLISHED 16 June 2023

CITATION
Digifico E, Erreni M, Mannarino L, Marchini S, Ummarino A, Anfray C, Bertola L, Recordati C, Pistillo D, Roncalli M, Bossi P, Zucali PA, D'Incalci M, Belgiovine C and Allavena P (2023) Important functional role of the protein osteopontin in the progression of malignant pleural mesothelioma. *Front. Immunol.* 14:1116430. doi: 10.3389/fimmu.2023.1116430

Important functional role of the protein osteopontin in the progression of malignant pleural mesothelioma

Elisabeth Digifico[1], Marco Erreni[2], Laura Mannarino[3,4], Sergio Marchini[3], Aldo Ummarino[1,4], Clément Anfray[1], Luca Bertola[5], Camilla Recordati[5], Daniela Pistillo[6], Massimo Roncalli[7], Paola Bossi[7], Paolo Andrea Zucali[4,8], Maurizio D'Incalci[3,4], Cristina Belgiovine[1*†] and Paola Allavena[1,4*]

[1]Department Immunology, IRCCS Humanitas Research Hospital, Milan, Italy, [2]Unit of Advanced Optical Microscopy, IRCCS Humanitas Research Hospital, Milano, Italy, [3]Lab. Cancer Pharmacology, IRCCS Humanitas Research Hospital, Milano, Italy, [4]Department Biomedical Sciences, Humanitas University, Milano, Italy, [5]Mouse and Animal Pathology Lab., Fondazione Unimi, and Department of Veterinary Medicine and Animal Sciences, University of Milano, Lodi, Italy, [6]Biobank, Humanitas IRCCS Humanitas Research Hospital, Milano, Italy, [7]Department Pathology, IRCCS Humanitas Research Hospital, Milan, Italy, [8]Department Oncology, IRCCS Humanitas Research Hospital, Milano, Italy

Background: Malignant Pleural Mesothelioma (MPM) is an aggressive cancer of the mesothelial lining associated with exposure to airborne non-degradable asbestos fibers. Its poor response to currently available treatments prompted us to explore the biological mechanisms involved in its progression. MPM is characterized by chronic non-resolving inflammation; in this study we investigated which inflammatory mediators are mostly expressed in biological tumor samples from MPM patients, with a focus on inflammatory cytokines, chemokines and matrix components.

Methods: Expression and quantification of Osteopontin (OPN) was detected in tumor and plasma samples of MPM patients by mRNA, immunohistochemistry and ELISA. The functional role of OPN was investigated in mouse MPM cell lines *in vivo* using an orthotopic syngeneic mouse model.

Results: In patients with MPM, the protein OPN was significantly more expressed in tumors than in normal pleural tissues and predominantly produced by mesothelioma cells; plasma levels were elevated in patients and associated with poor prognosis. However, modulation of OPN levels was not significantly different in a series of 18 MPM patients receiving immunotherapy with durvalumab alone or with pembrolizumab in combination with chemotherapy, some of whom achieved a partial clinical response. Two established murine mesothelioma cell lines: AB1 and AB22 of sarcomatoid and epithelioid histology, respectively, spontaneously produced high levels of OPN. Silencing of the OPN gene (*Spp1*) dramatically inhibited tumor growth *in vivo* in an orthotopic model, indicating that OPN has an important promoting role in the proliferation of MPM cells. Treatment of mice with anti-CD44 mAb, blocking a major OPN receptor, significantly reduced tumor growth *in vivo*.

Conclusion: These results demonstrate that OPN is an endogenous growth factor for mesothelial cells and inhibition of its signaling may be helpful to restrain tumor progression *in vivo*. These findings have translational potential to improve the therapeutic response of human MPM.

KEYWORDS

osteopontin (OPN), MPM (malignant pleural mesothelioma), immune system and cancer, immunotherapy, novel therapeutic approach

Introduction

Malignant Pleural Mesothelioma (MPM) is an aggressive cancer of the mesothelial lining that covers the lungs. It is characterized by a non-resolving, long-lasting inflammation, driven by the presence of non-degradable asbestos fibers inhaled from the environment. Although asbestos production has been discontinued in several western countries in the '90s, MPM incidence is still rising, as the latency period for its development is very long (up to 20-40 years) and the peak is estimated around 2025-2030 (1–3). MPM is usually identified at advanced stages because there are no useful biomarkers for an early diagnosis, and radiological diagnostic tools are not effective for its early detection. This cancer has a very poor prognosis with a median survival time from presentation of approximately 9–12 months (2–4). MPM has been classified into three different histotypes: the most common type is the epithelioid (70%), the sarcomatoid (~20%) has the worst prognosis, and an intermediate third histotype, the biphasic, is characterized by a combination of cells with both epithelioid and sarcomatoid morphology (2, 3).

Chronic inflammation triggered by the non-degradable asbestos fibers has been established as the first pathogenic step in the long chain of events that drives the development of MPM. Over several years, chronic inflammation causes DNA damage and accumulation of DNA mutations. Genetic abnormalities have been extensively studied in MPM; a wide range of different mutations was found in several genes, most prominently in the BRCA1-associated protein–1 (BAP1) gene, and in other genes: CDKN2A, Wnt, p16, TP53, SMACB1, NF2, PI3K (5–11). Recently, point mutations or overexpression of KRAS have been reported in a proportion of human MPM (12).

Malignant mesothelioma is a tumor dramatically resistant to chemotherapy. Despite the introduction of modern therapeutic interventions, only modest changes in survival have been observed over time (2–4, 13–16). Immunotherapy based on checkpoint blockade (ICB) is currently under investigation in clinical trials with - so far - disappointing results (17). Recently, clinical studies using a combination of nivolumab plus ipilimumab have reported a significant extension of patient survival, restricted to the sarcomatoid histotype (18). Another treatment modality that gained credit is the use of alternating electric fields, a noninvasive therapeutic approach that can complement chemotherapy in mesothelioma patients. A combination of cisplatin-based therapies with Tumor-Treating Fields (TTF) has shown *in vitro* anti-tumor activity (19) and clinical activity in a phase 2 study (20). Despite these encouraging successes, it is clear that more effective treatments are urgently needed to assist these patients, and for this we need to increase our knowledge on the biology of MPM, especially on the molecular pathways that govern its continuous proliferation and resistance to treatments.

Our group has a long-lasting interest in the mechanisms of the inflammatory cascade that actively support neoplastic transformation (tumor-promoting inflammation), a condition paradigmatically represented in malignant mesothelioma (21–25). In this study, we performed a transcriptomic analysis of genes of the inflammatory response in human mesothelioma tumor samples to identify which molecular pathways are mostly upregulated. Our attention was caught by the high expression of the *Spp1* gene, coding for the protein osteopontin (OPN). OPN is a highly phosphorylated matricellular protein produced by several cell types: macrophages, stromal and epithelial cells. OPN can interact with integrins and with the CD44 receptor and regulates several cell functional pathways, including cell motility, immune responses, cell proliferation and apoptosis (26–28). Furthermore, OPN is abundantly present in inflamed tissues favoring immune cell accumulation, retention of macrophages and activation of cell survival, thus exacerbating the chronic inflammatory response (29, 30). The expression of OPN in MPM is well known: several studies have investigated this protein as a potential diagnostic or prognostic biomarker (31–39); its functional role in malignant mesothelioma, however, has not been elucidated.

In this study, we have done a comprehensive analysis of the expression of OPN in human MPM patients, including patients undergoing checkpoint blockade immunotherapy, and *in vivo* studies using a murine orthotopic model of mesothelioma. Our findings demonstrate that OPN has an important functional role and promotes the progression of malignant mesothelioma.

Materials and methods

Mesothelioma patients

Tumor and plasma samples were obtained from patients with pathologically confirmed malignant mesothelioma admitted at the IRCCS Humanitas Clinical and Research Center (Rozzano, Milano-

Italy). Samples were collected upon the signing of an informed consent and immediately frozen and stored in the Institutional Biobank. Plasma samples were obtained also from 18 MPM patients with epithelial histology treated with checkpoint blockade immunotherapy: 10 patients with durvalumab as single agent in second-line setting, 8 patients with pembrolizumab combined with carboplatin and pemetrexed in first-line setting. Plasma samples were collected also from 61 MPM patients enrolled in the ATREUS study (ClinicalTrials.gov, NCT02194231), a phase II, single arm, multicenter study aimed to explore the activity of trabectedin in second-line setting (40). Plasma samples were collected before start of therapy. All studies were conducted after approval by the Ethic Committee. Written informed consent was obtained from each patient before entering the study. Recommendations of the Declaration of Helsinki were followed.

The human mesothelioma cell lines CD288 and CD484 were derived from tumor samples of patients with diagnosed epithelioid MPM implanted in athymic nude mice, then established *in vitro*, as described (41).

Murine mesothelioma cell lines

The murine mesothelioma cell lines AB1 (sarcomatoid histology) and AB22 (epithelioid histology), were generated in BALB/c mice upon intraperitoneal injection of crocidolite asbestos fibers and deposited in the Australian cell bank (42). Luciferase-expressing AB1 and AB22 cells were kindly provided by Dr. M. Bianchi, San Raffaele Scientific Institute, Milan, Italy (43). Cell lines were cultured in RPMI 1640 (Lonza) supplemented with 10% FBS (Sigma), 2mM L-glutamine, 100 U/mL penicillin and 100 µg/mL streptomycin (Life Technologies Inc.) at 37°C and 5% CO2. To silence the Spp1 gene coding for osteopontin, AB1 and AB22 cells were stably transduced with the lentiviral vector MISSION shRNA (SHCLNG, 10041725MN, SIGMA). Viral particles were generated in HEK293T cells transfected with Lipofectamine2000 (ThermoFisher Scientific) according to manufacturer's instruction. Selection of transduced cells was performed using Puromycin (2 ug/ml for three days after each defrosting). A non-targeting shRNA (scrambled) was used to transduce the control cell lines. All cell types were routinely checked for Mycoplasma contamination.

In vitro colony assay

Proliferation of mesothelioma cell lines in the presence of anti-CD44 mAb or isotype control (BioXcell, BE0039, 5µg/ml) was quantified by staining with Crystal violet after 1 week; colonies were dissolved in pure DMSO and optical density measured by spectrophotomer at 590 nm.

In vivo experiments in mice

Mice were used in compliance with national (D.L. N. 26, G.U. March 4, 2014) and international law and policies (EEC Council Directive 2010/63/EU, OJ L 276/33, 22-09-2010; National Institutes of Health Guide for the Care and Use of Laboratory Animals, (authorization N° 296/2020-PR), and US National Research Council, 2011). BALB/c mice 8 weeks-old were purchased from Charles River. The procedures for the syngeneic orthotopic mouse model have been previously described (44). AB1 and AB22 MPM cells were injected intra-thoracically. Mice were anesthetized with ketamine/xylazine and positioned on left lateral decubitus. The thoracic area was shaved and sterilized with 70% ethanol. An 8-10 mm skin incision was performed on the right thorax (close to the axillary cavity) and $5x10^4$ cells resuspended in 50 ul saline solution were injected between the third and the fourth costal space, with the needle perpendicularly oriented on the rib cage (29-gauge needle of a 500 ul syringe U100, BD Becton, Dickinson). In order to standardize the injection and avoid lung perforation, the needle was overmounted by a 200ul tip, properly cut to expose the needle of 3 mm only. After cell injection, mice were sutured and kept under a heating lamp to recover from the anesthesia. Tumor growth quantification was performed by *in vivo* imaging over time. Mice were i.p. injected with D-Luciferin (XenoLight D-Luciferin-K+ Salt, PerkinElmer; 150 mg Luciferin/kg body weight). Ten minutes after D-Luciferin injection, the bioluminescent signal was acquired using the IVIS Lumina III system (Perkin Elmer). During the acquisition procedure, mice were anesthetized with Isoflurane (XGI-8 Gas anesthesia system, Perkin Elmer). Data were analyzed with Living image 4.3.1 by designing a ROI on the thoracic area of each mouse. To block the CD44 receptor, mice were treated intra-peritoneally with anti-CD44 mAb (BioXcell, BE0039,10 mg/kg), or an irrelevant antibody at days 7, 12, 16, 19 post tumor injection, or otherwise specified in the figure legends.

ELISA quantification of OPN

To quantify the production of human/murine OPN, cell supernatants or plasma samples were tested with commercial ELISA kits (R&D Systems), according to the manufacturer's instructions. Data were analyzed with SoftMax Pro 5.3 software.

Histopathology

Lungs and intra-thoracic masses of mice were fixed in 10% buffered formalin, routinely processed for histopathology, cut at 4 µm thickness, and stained with hematoxylin and eosin. Digital slides were obtained from haematoxylin and eosin-stained sections using the NanoZoomer S60 Digital slide scanner (Hamamatsu, C13210-01) and visualized by NDP.view2 Viewing software (Hamamatsu, U12388-01). For each case, pulmonary nodules were counted and subsequently manually outlined obtaining the area expressed in mm^2.

Immunohistochemistry

4-µm sections of paraffin-embedded human tissues were stained with primary antibodies anti-OPN (MAB14334, R&D System) or anti-CD206 (AF2534,R&D System). For murine tissues, 4-µm sections of paraffin-embedded lungs were stained as

previously described (43). The primary antibodies used were anti-Iba1 (019-19741, Wako Chemicals), anti-CD206 (ab64693, Abcam), anti-CD3e (Sc-1127, Santa Cruz Biotechnology), anti-CD4 (4SM95; 14-9766-82, eBioscience), anti-CD8 (4SM15; 14-0808-82, eBioscience), anti OPN (MAB808, R&D System). Digital slides were obtained from immunostained sections by using the NanoZoomer S60 Digital slide scanner (Hamamatsu, C13210-01) and visualized by NDP.view2 Viewing software (Hamamatsu, U12388-01). For each case, 1 20X hot spot field was taken from the biggest 10 masses for every evaluated marker. Images were then processed in ImageJ software (http://rsb.info.nih.gov/ij/) to calculate the positive area/total area ratio expressed in percentage.

Real-time RT-PCR

PureZOL RNA isolation reagent (BIORAD) was used to extract total RNA from tumor samples; cDNA was then synthesized from 2ug of total RNA with GeneAmp RNA PCR kit (applied Biosystems). Real-Time PCR was run using SYBR Green dye and 7900HT fast Real Time PCR system (Applied Biosystems). Primer Express Software (Applied Biosystems) was used to design the sequence of primer pairs specific for each gene (SIGMA). mRNA was normalized to GAPDH mRNA by subtracting the cycle threshold (Ct) value of GAPDH mRNA from the Ct value of the gene (ΔCt). ΔCt was then multiplied for an arbitrary unit (100 000). The sequences of primers are as follows:

hOPN Forward: 5' AGTTTCGCAGACCTGACATCCAGT 3'

hOPN Reverse: 5' TTCATAACTGTCCTTCCCACGGCT 3'

mOPN Forward: 5' AGCCACAAGTTTCACAGCCACAAGG 3'

mOPN Reverse: 5' TGAGAAATGAGCAGTTAGTATTC CTGC 3'

TaqMan low density array

Four mesothelioma surgical samples and their corresponding normal tissues were used for low-density array (LDA) analysis as previously described (44). The relative amount of each target gene mRNA to the mean of the five housekeeping genes (HPRT, 18S, GAPDH, B2M, and ACTB) was calculated as $2^{-\Delta Ct}$, where $\Delta Ct = Ct - Ct_{mean\ of\ housekeeping\ genes}$. The fold-change of each target gene mRNA to the corresponding normal tissue was calculated as $2^{-\Delta\Delta Ct}$, where $\Delta\Delta Ct = \Delta Ct_{target\ gene\ in\ tumor\ tissue} - \Delta Ct_{target\ gene\ in\ normal\ tissue}$. The threshold cycle Ct was automatically given by the SDS2.2 software package (Applied Biosystems) (45).

RNA seq analysis

Raw data were demultiplexed with bcl2fastq Conversion Software (Illumina). FastQC (46) was used for data quality check. Data analysis bcbio-nextgen (47) pipeline which was configured with hisat2 (48) as aligner using the Mus musculus *mm10* transcriptome and salmon (49) for gene counts assessment. DESeq2 (50) package was used for data post-processing and differential expression analysis. Counts were filtered retained only genes with at least 10 reads. shOPN cells were compared to control cells (CTR) to assess differentially expressed genes (DEGs) (p-adjust less than 0.05, multiple testing correction with False Discovery Rate). Enrichment analysis was used to associated genes with pathways using the *enrichPathway* function of clusterProfiler (51) R package using the Reactome database (52) mouse was set as organism, p-value cut-off was set to 0.05 and normalized gene counts were used as universe). Pheatmap (53) R package was used for DEGs visualization, clustering was done with the Ward method. Pathway barplot was done with the seaborn (54) package.

Statistical analysis

Prism software (v8.0; GraphPad Software, San Diego, CA) was used to conduct appropriate statistical procedures, as specified in figure legends. Outliers were removed using the ROUT method. A p value < 0.05 was considered significant unless noted otherwise. Overall survival time was calculated from the date of surgery to the date of death or last contact. Statistical analyses of the results were performed using Unpaired t test with Welch's correction.

Results

Osteopontin expression and plasma levels in malignant mesothelioma patients

To study the inflammatory environment of malignant pleural mesothelioma tissues, we performed a gene expression analysis using a TaqMan Low Density Array containing 91 genes related to the inflammatory response (45). RNA was extracted from 4 surgically resected tumor samples and from the adjacent un-diseased tissues. Several genes coding for cytokines/chemokines known to activate inflammatory cells (i.e., CCL2, CCL3, CCL7, CCL11, CCL20, CCL26, CXCL8 and CXCL1) were upregulated in MPM tissues, as well as the vascular growth factor VEGFα, PTGS2 coding for COX-2 and Spp1 coding for osteopontin (OPN) (Supplementary Figure 1). Spp1 results were confirmed in real-time PCR analysis performed on 15 MPM samples; mRNA levels were significantly higher in tumor tissues compared to un-diseased tissues (Figure 1A). OPN is a secreted matrix-related protein with multiple functions in healthy and pathological conditions (29). ELISA quantification in plasma was performed in MPM patients (n=99). OPN levels were significantly higher compared with healthy donors (n=101) (Figure 1B). In a series of 61 patients enrolled in a multicenter phase II study (ATREUS, ClinicalTrials.gov, NCT02194231) receiving the drug trabectedin as monotherapy (40), high plasma levels of OPN at baseline were significantly associated with worse overall survival (Figure 1C). To further characterize the expression of OPN in human MPM, we analyzed its immunoreactivity in 28 surgical human MPM tissues.

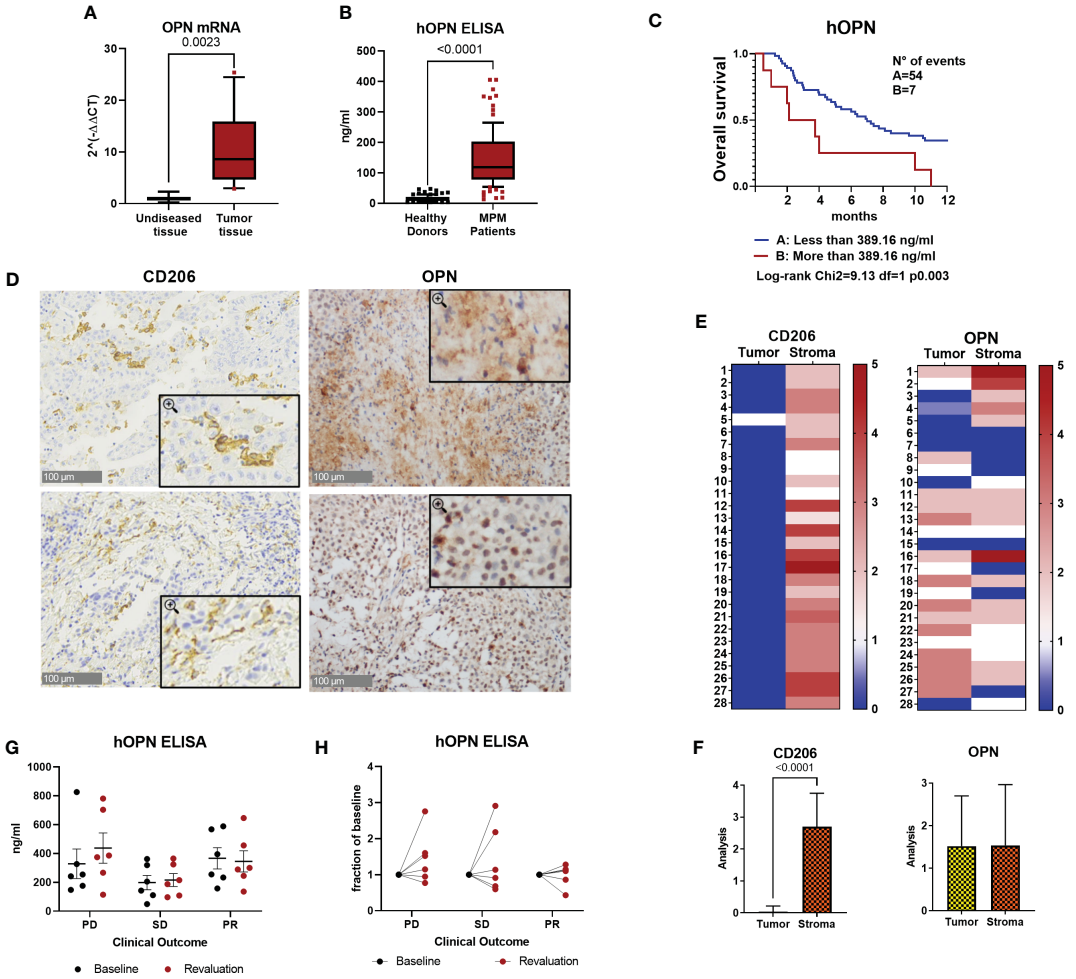

FIGURE 1
Osteopontin is overexpressed in human MPM patients. **(A)** Real Time PCR for the *Spp1* gene (osteopontin, OPN) in surgical human MPM samples. Comparison between tumor and undiseased adjacent tissues. Data are shown as mean ± SEM (Unpaired t test with Welch's correction). **(B)** ELISA quantification of hOPN on plasma samples from 99 MPM patients and 101 healthy subjects. (ROUT, identify outlier and Unpaired t test with Welch's correction). **(C)** Kaplan-Meier curves of overall survival according to OPN levels categorized based on CART analysis cut-off (n=61 MPM patients). **(D–F)** Representative images of immunohistochemistry in MPM tumor tissues stained for OPN or CD206 (40x, insert 100x) and semi-quantitative analysis in 28 cases (0=negative, 1 = 1-25% positivity, 2 = 26-50% positivity, 3= >50% positivity). Data are shown as mean ± SEM. (Unpaired t test with Welch's correction). **(G, H)** ELISA quantification of hOPN on plasma samples from 18 MPM patients treated with immunotherapy. Blood was collected at baseline and after revalutation at 4-6 months. Patients with progressive disease (PD): 6 patients; stable disease (SD): 6 patients; partial response (PR): 6 patients.

Immunostaining for OPN was distinctly localized in the cytoplasm of tumor cells in 75% of the cases, while in other cases a diffuse staining was observed, in line with the secreted soluble form of this protein (Figures 1D–F). As macrophages are known producers of OPN, anti-CD206 immunostaining was also investigated; as expected, macrophage staining was selectively localized in the stroma and in some samples cytoplasmic staining for OPN was also detected in the stroma (Figures 1D–F). Next, we quantified the plasma levels of OPN in a series of 18 MPM patients receiving immunotherapy with Durvalumab alone or with Pembrolizumab in combination with chemotherapy. Baseline levels before treatment in patients with progressive disease (PD) did not differ from those of patients achieving a stable disease (SD) or a transient partial response (PR) (Figure 1G). Modulation of OPN levels after 4-6 months of therapy was similarly heterogeneous among patients; although the low numerosity does not allow to draw conclusions on this point, we noted that while 5/12 patients (PD+SD) showed increased levels compared to baseline values, none of the responding patients had increase of OPN levels at revaluation (Figure 1H).

Collectively, these results confirm the higher expression of OPN in tumor tissues and circulating blood of MPM patients compared to healthy donors and indicate that high OPN may be associated with unfavorable prognosis; however, OPN monitoring during ICB immunotherapy has not been useful to identify patients responding to treatment.

Role of OPN in murine mesothelioma cell proliferation

To test the functional activity of OPN we used two murine mesothelioma cell lines: AB1 cells and AB22 cells with sarcomatoid

and epithelioid histology, respectively. Both cell lines spontaneously produced OPN, quantified by ELISA in cell supernatants. AB1 cells were high producers of OPN and secreted up to 1900 ng/ml (Figure 2A), while AB22 cells produced 220 ng/ml (Figure 2B). Using the lentivirus vector (MISSION shRNA) both AB1 and AB22 cell lines were successfully silenced for the Spp1 gene: 84% and 81%, respectively, (Figures 2A, B), though silencing was not complete in the AB1 cell line producing very high levels of OPN. The *in vitro* characterization of the engineered cells revealed that OPN silencing had no effect on the proliferation of AB1 cells, as AB1shOPN cells did not modify their growth behavior (Figure 2C). On the other hand, gene silencing dramatically reduced the proliferation ability in AB22 shOPN cells, compared with the scrambled-transduced cell line (AB22 sh-scrambled) (Figure 2D). In a colony assay, AB22 shOPN cells formed 47% less colonies than AB22 sh-scrambled cells (Figure 2E). To investigate if the addition of OPN restored their proliferation, silenced cells were treated with 30% conditioned medium from AB22 sh-scrambled cells: after 1 week, AB22 shOPN cells showed 1, 6 fold more colonies (Figure 2E).

To further confirm the involvement of OPN, we investigated the effect of blocking its major receptor CD44. Expression of CD44 by cancer cells was first checked by immunohistochemistry. Murine mesothelioma AB1 and AB22 cells stained strongly positive for CD44 Supplementary Figure 2A, in line with its ubiquitous nature (55). Likewise, two representative samples of human pleural mesothelioma expressed CD44 as shown in Supplementary Figure 2B. To block the receptor, AB22 cells were treated every other day with a blocking anti-CD44 mAb (5 µg/ml). Anti-CD44-treated cells had a significantly lower proliferation rate (Figure 2F); similar results were obtained also using AB22 shOPN cells that were exposed to the conditioned medium containing OPN (Figure 2F). Overall, these results indicate that OPN is an essential endogenous growth factor for the epithelioid AB22 cells. Furthermore, we tested two human MPM cell lines: CD288 and CD484; both cell lines spontaneously produce OPN (Supplementary Figures 3A, B). Also with human MPM cells, addition of anti-CD44 significantly decreased tumor cell proliferation (Supplementary Figures 3C, D).

A Transcriptome Sequencing (RNAseq) was performed on AB22 shOPN cells and results compared with AB22 sh-scrambled control cells. One hundred thirty-two differentially expressed genes (DEGs) were identified (Figure 3A). Reactome enrichment analysis confirmed that top DEGs were involved in biological processes such as immune system, cell proliferation and adhesion, molecular function regulator. The main enriched pathways were: peptide ligand-binding receptor Ga signaling, extracellular matrix organization, activation of MMPs and G-protein-coupled receptor

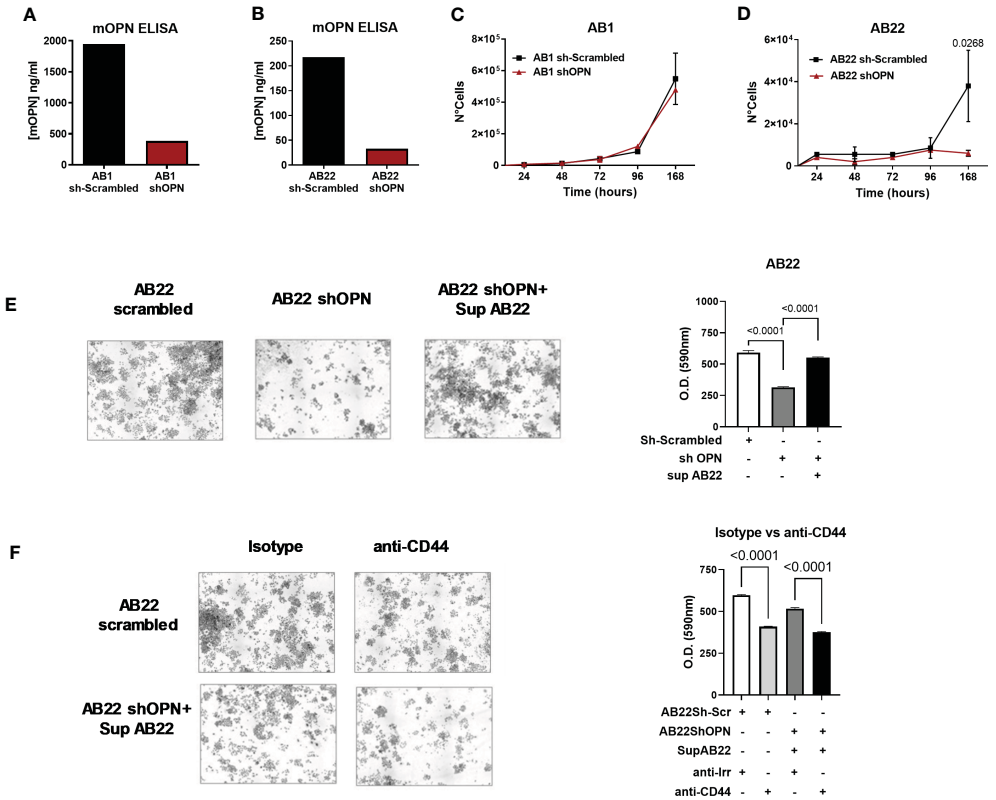

FIGURE 2
In vitro characterization of murine engineered MPM cell lines. **(A, B)** ELISA for mOPN on AB1 sh-scrambled and AB1 shOPN cells **(A)**, and AB22 sh-scrambled and AB22 shOPN cells **(B)**, showing the efficacy of silencing. **(C, D)** cell proliferation assay over time for AB1 **(C)** and AB22 **(D)** sh-scrambled and shOPN cells. Data are shown as mean ± SEM (Two-way ANOVA). **(E)** Representative images of the colony assay and quantification for AB22 scrambled cells, AB22 shOPN cells, also after addition of OPN-containing supernatant from scrambled cells. **(F)** images of the colony assay and quantification in the presence of a blocking anti-CD44 mAb (5 µg/ml). Blockade of CD44 inhibits cell proliferation in AB22 sh-scrambled cells and in AB22 shOPN cells exposed to OPN-containing supernatant. Data are shown as mean +/- SD (One-way ANOVA).

(GPCR) signaling (involved in the downstream signaling of the receptor CD44) (Figure 3B). These findings indicate that loss of OPN has a relevant impact on fundamental biological processes of mesothelioma cells.

Role of OPN in murine mesothelioma cell *in vivo* tumor growth

We next studied the *in vivo* growth of shOPN AB1 and AB22 engineered cells. As described by Digifico et al. (44), we set up an orthotopic model of murine mesothelioma that recapitulates the human MPM. In this model, direct intra-thorax injection of tumor cells was performed with a minimally invasive procedure. As confirmed by histological examinations, tumors developed along the pleura surface, further spreading and colonizing the most peripheral areas of the lungs, without forming any neoplastic mass outside the thoracic cavity. Importantly, acquisition over time of the bioluminescent signal from Luc-transduced cells was totally trustable as it perfectly correlated with the quantification of tumor areas detected with conventional histology (44).

shOPN Luc-expressing AB1 and AB22 cells and their scrambled controls ($5x10^4$ cells) were injected intra-thoracically in syngeneic BALB/c mice and tumor growth was followed by IVIS Lumina III

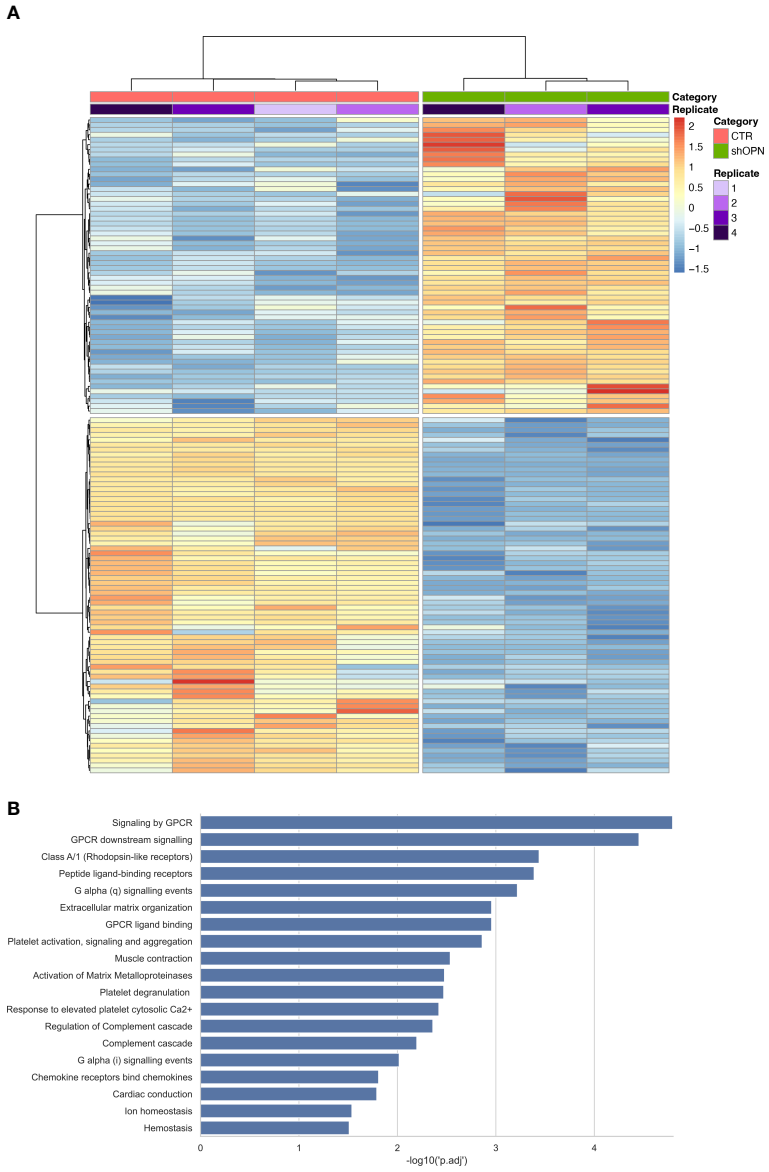

FIGURE 3
Transcriptome Sequencing analysis of AB22 sh-scrambled and AB22 shOPN cells. **(A)** The heatmap shows 132 deregulated gens (DEGs) from shOPN cells and comparison vs sh-scrambled cells (CTR). Supervised clustering shows the CTR samples with a red bar and shOPN samples with a green bar. Replicates are indicated with a violet scale color. Gene expression is shown with false color scale as indicated in the legend: red for positive values, blue for negative values. The darker the color, the higher the expression. **(B)** Pathway analysis software shows the pathways significantly associated with DEGs from the shOPN vs CTR comparison. Pathways are sorted from the most significant to the least, as indicated by the -log10 adjusted p-value on the x-axis.

system up to the day of sacrifice. At day 14 post injection we observed that OPN silencing almost completely abrogated tumor growth *in vivo* of shOPN AB1 cells, as detected by IVIS signal, as well as by histological quantification of total tumor area (Supplementary Figures 4A–C). Immunostaining of explanted tumors evidenced the significantly reduced expression of OPN in silenced tumors (Supplementary Figures 4D, E). A longer experiment confirmed this finding of growth inhibition and revealed that shOPN AB1 cells started growing again by day 33, but only in 2/5 mice (Figures 4A, B). By histological examination, the number of tumor foci at day 33 was still significantly reduced in mice bearing OPN-silenced tumor cells (Figures 4C–E).

With AB22 epithelioid cells, a first *in vivo* experiment demonstrated that OPN silencing strongly reduced tumor growth (Supplementary Figures 5A–C) and OPN expression in tumors (Supplementary Figures 5D, E). In a second *in vivo* experiment with longer time points, mice injected with scrambled cells had to be sacrificed at day 17, while endpoint for mice injected with silenced cells was at days 45-56 (Figures 5A, B). Quantification of tumor foci and tumor area was significantly reduced in shOPN cells at later times, only few masses were visible in 3/5 mice (Figures 5C, D). In the explanted tumors, expression of OPN detected by immunohistochemistry was indeed lower in silenced tumors (Figures 5E, F). Figure 5G shows representative pictures of tumor load around the lungs of mice injected with control AB22 cells or shOPN cells at different time points.

Taken together, these data indicate that OPN in both tumor histotypes is an essential growth factor supporting tumor progression *in vivo*.

Inhibition of OPN signaling through the CD44 receptor reduces tumor growth *in vivo*

Since our *in vivo* experiments revealed a clear role of OPN in promoting *in vivo* proliferation of murine MPM, experiments to block OPN were undertaken. A commercial aptamer, OPN-R3 (56, 57), able to specifically block OPN was first used. Repeated intraperitoneal injections did not affect tumor growth of AB22 cells (Supplementary Figure 6). We then turned to use blocking antibodies against CD44. Mice were treated with anti-CD44 mAb (10 mg/kg) at day 7, 12, 16, 19 post tumor implantation. With the AB1 cell line we did not observe a significant reduction of tumor growth over time (not shown); this finding is likely explained since AB1 cells are very high producer of OPN, secreting 10 times more OPN compared with AB22 cells (Figures 2A, B). We therefore tested the engineered shOPN AB1 cells, where production of OPN was not totally abrogated. Treatment of mice with anti-CD44 antibodies significantly reduced tumor growth of shOPN AB1 cells (Supplementary Figure 7). Next, the sh scrambled AB22 cell line was used for the same type of experiment; growth of AB22 cells (10 mice/group) was substantially reduced (p= 0.0024) in anti-CD44-treated mice compared with mice treated with the irrelevant antibody (Figures 6A–D). By immunohistochemistry, we observed a significantly higher number of CD3+ and CD4+ cells, and a trend to decreased expression of OPN (Figures 6E, F). Instead, the infiltration of CD8+ T cells and that of macrophages (IBA1+ cells) was not changed (Figures 6E, F).

Overall, these data demonstrate that OPN produced by mesothelioma cells sustains the proliferation of cancer cells, and that

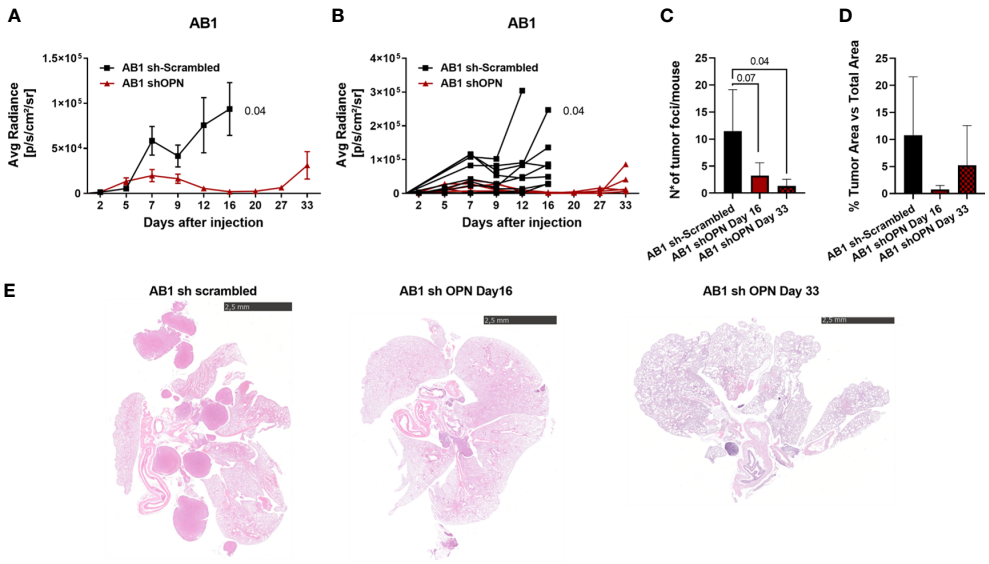

FIGURE 4
Silencing of OPN impairs the growth of AB1 cells *in vivo*. **(A, B)** *In vivo* growth of 5x10^4 AB1 sh- scrambled or AB1 shOPN, injected intra-thoracically in BALB/c mice. **(A)** IVIS *in vivo* imaging luminescence signal, mean+/-SEM values of 9 mice sh-scrambled, 5 for shOPN; **(B)** luminescence signal values of each single mouse. **(C)** Histological quantification of tumor foci, and **(D)** of total tumor area. Data are shown as mean +/- SEM; (**A, B** Two-way ANOVA; **C, D**: One-way ANOVA). **(E)** Representative pictures of explanted lungs from tumor-bearing mice. AB1 sh-scrambled cells (left), AB1 shOPN cells at day 16 (middle) and AB1 shOPN cells at day 33 (right). Bars represent 2.5 mm.

10.3389/fimmu.2023.1116430

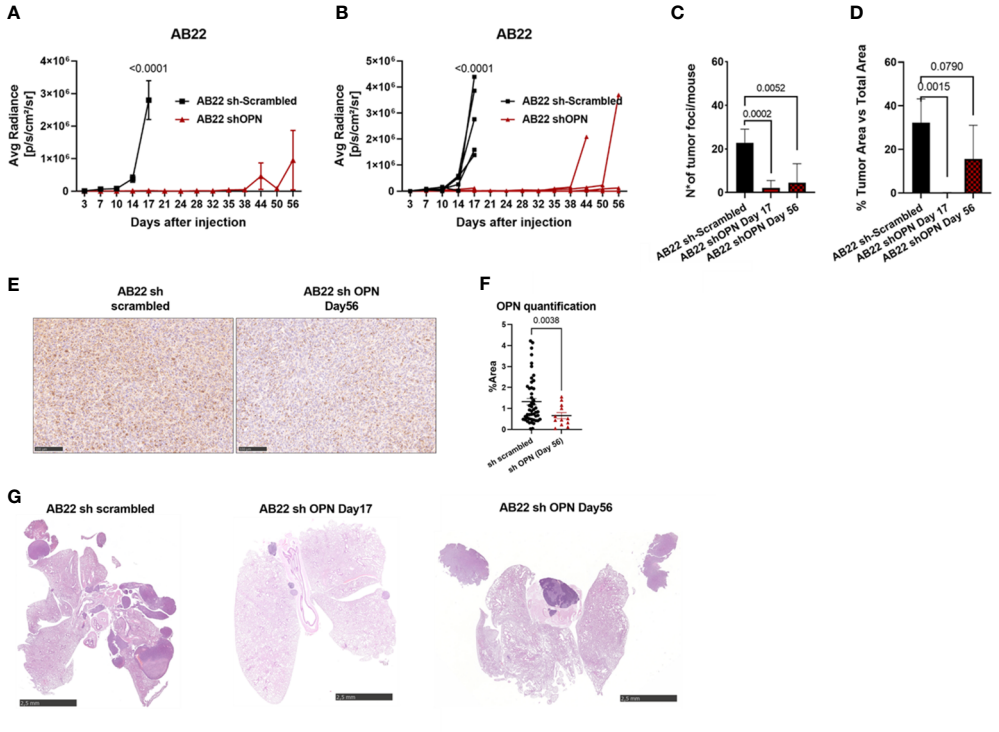

FIGURE 5
Silencing of OPN impairs the growth of AB22 cells *in vivo*. **(A, B)** *In vivo* growth of 5x10^4 AB22 sh- scrambled or AB22 shOPN, injected intra-thoracically in BALB/c mice. **(A)** IVIS *in vivo* imaging luminescence signal, mean+/-SEM values of 5 mice for sh-scrambled, 5 for shOPN; **(B)** luminescence signal values of each single mouse. **(C)** Histological quantification of number of tumor foci, and **(D)** total tumor area. Data are shown as mean +/- SEM; (**A, B** Two-way ANOVA; **C, D**: One-way ANOVA; **E**: Unpaired t test with Welch's correction). **E, F**) immunohistochemistry for OPN in explanted tumors and representative pictures, bars represent 100 μm. **(G)** Representative pictures of explanted lungs from mice bearing control AB22 sh-scrambled cells (left), AB22 shOPN cells at day 17 (middle) and AB22 shOPN cells at day 56 (right). Bars represent 2.5 mm.

inhibition of OPN signaling significantly reduces the pro-tumoral effects of OPN on the progression of malignant mesothelioma.

Discussion

In this paper we studied the expression of OPN in tumor and plasma samples of MPM patients and performed functional studies with murine mesothelioma cell lines using an orthotopic mouse model. Considerable experimental evidence indicates that OPN expression is enhanced in a variety of pathological processes such as chronic inflammation, autoimmune diseases and cancer (26–29, 58, 59). Various studies reported that elevated levels of OPN are detected in different types of malignancies: breast, prostate, colorectal and lung cancer, melanoma and hepatic carcinoma. Most studies agree that OPN plays a key role in cancer progression by enhancing proliferation, motility and invasion of tumor cells and the process of angiogenesis (60–67). These tumor-promoting functions are achieved via different mechanisms: binding to integrins or CD44 receptor increases the integrin-stimulated FAK-Src-Rho pathway, cancer cell adhesion and survival, while activation of MMPs and matrix remodeling enhances tumor cell invasiveness; PI3K/Akt activation promotes tumor angiogenesis, recruitment of endothelial cells and tumor growth (60, 68).

In malignant mesothelioma, OPN has been extensively studied as diagnostic biomarker, frequently in association with another molecule: mesothelin. Using plasma or serum samples from MPM patients, detection of OPN levels by ELISA was found higher in patients in comparison with healthy donors, and even with healthy individuals exposed to asbestos (32, 35, 69). OPN has been investigated also as prognostic biomarker of treatment outcome: elevated OPN levels have been associated with an unfavorable prognosis in a number of studies (35–38, 70).

However, the real clinical utility of OPN as early diagnostic marker has also been questioned, due to its low sensitivity and specificity; for instance, circulating levels of OPN did not discriminate between chronic inflammatory and malignant lung diseases (71, 72).

In this paper we found that OPN in MPM patients is highly expressed both as mRNA and protein in tumor tissues, and as ELISA levels in the peripheral blood. Immunohistochemistry for OPN shows both a cytoplasmic staining in tumor cells as well as a diffused staining, in line with its secreted form. Analysis of the stroma with the macrophage marker CD206 indicates that in some cases macrophages also produce OPN, as already known in the literature (73–75). In a cohort of MPM patients enrolled in the ATREUS study (ClinicalTrials.gov, NCT02194231) (40), those patients with high baseline OPN levels indeed had a lower overall survival. On the other hand, modulation of OPN levels was not

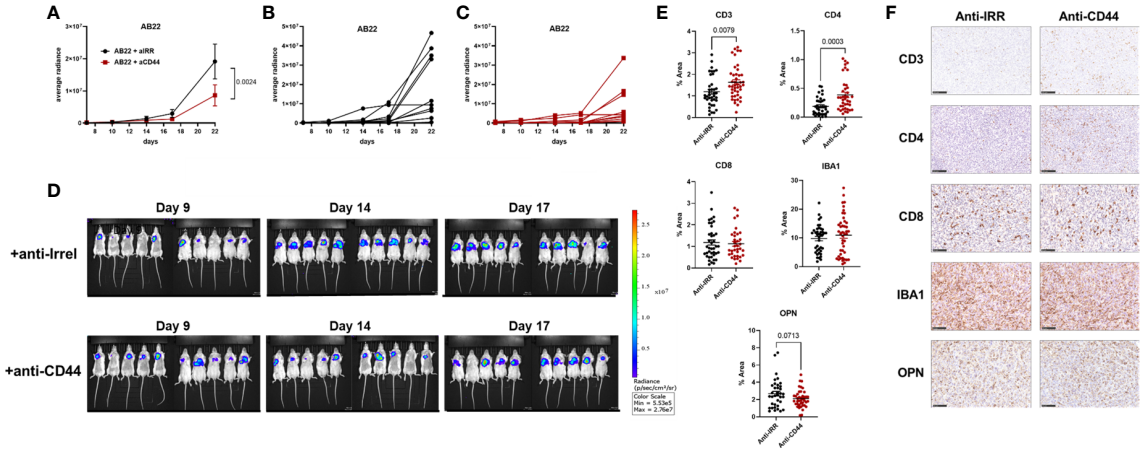

FIGURE 6
Treatment with blocking anti-CD44 mAbs impairs *in vivo* growth of murine mesothelioma cells. **(A–C)** Effect of anti-CD44 mAbs on AB22 tumor cell growth. Mice were treated intra-peritoneally with anti-CD44 (10 mg/kg) or with irrelevant mAbs at day (7, 12, 16, 19) post tumor injection. Data are expressed as average radiance, **(A)** mean+/-SEM values of 10 mice; **(B, C)** values of each single mouse; **(D)** images of IVIS acquisition of LUC signal at different time points. **(E, F)** Representative images of immunohistochemistry of explanted tumors and relative quantification, each dot represents a single ROI. Tumor slices were stained with mAbs against CD3, CD4, CD8, IBA1 (macrophages) and OPN; bars represent 100 μm. Data are shown as mean +/- SEM (Statistical analysis: **(A)**, Two-way ANOVA; **(E)** Unpaired t test with Welch's correction).

significantly different in patients receiving ICB immunotherapy, some of whom achieved a transient partial response. These results are in line with the widespread opinion that OPN is not a robust diagnostic or prognostic biomarker of disease for MPM (4, 71, 72)

While studies on the functional role of OPN in several types of tumors are available (58–65), its biological effects in malignant mesothelioma have not been clarified. To shed light on the functional activities of OPN in this neoplasia, we used two MPM mouse cell lines: AB22 of epithelioid phenotype and AB1 with sarcomatoid phenotype. Both spontaneously produced OPN, the latter up to large amounts. Silencing of OPN caused a strong delay in the proliferation of AB22 *in vitro*. Notably, the addition of cell supernatant containing OPN stimulated proliferation again and this OPN-induced proliferation was substantially reduced by blocking anti-CD44 mAbs. These results confirmed, *in vitro*, the important role of the axis OPN-CD44 in the proliferative expansion of mesothelioma cells. Silenced cells were compared with control cells in a Transcriptome Sequencing; the analysis revealed that the top deregulated genes are involved in receptor signaling pathways, primarily GPCR signaling, chemokines and migration, as well as matrix regulation. Of note, engagement of the receptor CD44 involves downstream signaling via G-protein-coupled receptors, in addition to other signaling pathways (76, 77). These results indicate that loss of OPN impacts on biologically important functions of this molecules through its receptors.

In vivo experiments using a recently optimized orthotopic mouse model of mesothelioma clearly indicated that loss of OPN strongly reduced the proliferation of MPM cells, even in the case of AB1 cells where the gene was only partially switched off. In longer experiments few tumors started to grow again, only in some mice. Macrophages are known to produce OPN, however, silencing in cancer cells was sufficient to give a strong retardation of tumor growth. This finding indicates the importance of OPN as a cell autonomous growth factor for mesothelioma cells, apparently more relevant than the host derived OPN.

Subsequent experiments aimed to provide a proof of principle that pharmacological inhibition of OPN signaling, by targeting the receptor CD44, could indeed decrease mesothelioma cell growth *in vivo*. We found that administration to mice of a blocking anti-CD44 mAb, significantly reduced tumor proliferation of AB22 naïve cells as well as that of shOPN AB1 cells. This finding is remarkable because of the redundancy of receptors used by OPN. This molecule, in fact, binds several integrins in addition to CD44, but our results demonstrate specific inhibition of CD44 was sufficient to have positive therapeutic effects in mice. CD44 receptor has long been considered as a potential therapeutic target in cancer, as it initiates and modulates several signaling networks that are important in tumor progression, metastasis and chemoresistance (78). Being a pleiotropic receptor expressed in multiple tissues, it would not seem a good target for therapeutic purpose. However, CD44 is upregulated in a variety of cancers and alternatively spliced variant isoforms (e.g. CD44v6) are mostly expressed in tumors, particularly in advanced stages. Furthermore, CD44 expression has been associated to the process of Epithelial to Mesenchymal Transition and is a typical receptor of cancer stem cells (79). A number of studies validated the potential of CD44 as a therapeutic target in various tumor types (78). In malignant mesothelioma the expression of CD44, alone or in association with other molecules, has been mainly investigated as marker of disease, not for therapeutic potential (80–83). Our *in vitro* and *in vivo* results suggest that inhibition of OPN signaling might be a possible strategy to restrain mesothelioma cell growth.

Of interest, it has been recently reported that OPN is able to bind to another molecule, the ligand of the Inducible T-cell costimulatory (ICOS-L) (84, 85). ICOS-L, a B7 family member, sustains T cell immunity and the antitumor response by binding to

ICOS, a costimulatory receptor expressed on activated T cells (86). Binding of ICOS-L to OPN, instead promoted tumor metastases in a mouse breast cancer model (85). ICOS-L is expressed also in human malignant mesothelioma (87). Thus, also for this new molecular partner of OPN, interfering with this binding may be explored as a new therapeutic approach.

In conclusion, on the basis of the experimental evidence obtained in this study, our working hypothesis that OPN represents an essential endogenous growth factor for mesothelioma cells, with a relevant role in driving tumor cell survival and proliferation, is confirmed. These results increase our knowledge on the biology of mesothelioma and suggest that therapeutic strategies based on OPN inhibition could have an impact on the management and survival of patients with MPM.

Data availability statement

The original contributions presented in the study are publicly available. This data can be found here: https://www.ebi.ac.uk/ena/ under the accession number PRJEB58309.

Ethics statement

The studies involving human participants were reviewed and approved by Ethical Committee of IRCCS Humanitas Research Institute. The patients/participants provided their written informed consent to participate in this study. The animal study was reviewed and approved by Ministry of Health.

Author contributions

ED, ME, AU, CA, LB, and CB contributed to study design, performed all the experiments, analyzed and interpreted the data. LM and SM performed the experiments of RNAseq. LB, CR, PB, and MR supervised the pathological examinations. PZ and DP took care of patient enrollement, treatment and sample collection. Writing-review & editing: CB, MD'I, and PA. All authors contributed to the article and approved the submitted version.

Funding

This research was partially supported by: Ministry of Health, grant NET-2016-02361632; MATCH study, AFEVA Sezione Casale Monferrato (Asbestos Victims); Fondazione Buzzi Unicem Onlus. The content of this article is the responsibility of the authors and does not reflect the views of these funding bodies.

Acknowledgments

We would like to thank Fondazione Buzzi and AFEVA Sezione Casale Monferrato for their support. We would like to thank all patients that consented to be enrolled in the study.

Conflict of interest

The authors declare that the research was conducted in the absence of any commercial or financial relationships that could be construed as a potential conflict of interest.

The handling editor CP declared a past co-authorship with the author ME.

Publisher's note

Supplementary material

The Supplementary Material for this article can be found online at: https://www.frontiersin.org/articles/10.3389/fimmu.2023.1116430/full#supplementary-material

SUPPLEMENTARY FIGURE 1
Transcriptomic analysis of inflammatory genes in human malignant mesothelioma. Gene expression profiling of four surgical human MPMs samples using TaqMan Low Density Array containing inflammatory 91 genes. Data are shown as fold increase in tumor samples relative to the non-involved pleural tissue from each paired patient. Selected genes are shown for which at least 2 samples showed upregulation over normal tissues.

SUPPLEMENTARY FIGURE 2
Immunohistochemistry of CD44 expression by murine and human mesothelioma. a) murine mesothelioma tumors (AB1 and AB22) grown *in vivo* in mice. b) MPM1 and MPM2 are human mesothelioma surgical samples.

SUPPLEMENTARY FIGURE 3
In vitro characterization of hMPM cell lines. **(A, B)** ELISA for hOPN spontaneously produced by the cell lines CD288 and CD484 (epithelioid phenotype). **(C, D)** Representative images of colony assays and relative quantification: addition of a blocking anti-CD44 mAb (5 mg/ml) inhibits cell proliferation. Data are shown as mean +/- SD (One-way ANOVA).

SUPPLEMENTARY FIGURE 4
Silencing of OPN impairs the growth of murine AB1 mesothelioma cells *in vivo*. a-b-c) *In vivo* growth of $5x10^4$ AB1 sh-scrambled or AB1 shOPN, injected intra-thoracically in BALB/c mice. **(A)** IVIS *in vivo* imaging luminescence signal, mean+/-SEM values of 5 mice; **(B)** Histological quantification of total tumor area. **(C)** Representative images of IVIS acquisition of LUC signal at different time points. **(D, E)** Immunohistochemistry of explanted tumors, relative quantification for the staining of OPN and representative pictures. Data are shown as mean +/- SEM (**A** Two-way ANOVA; **B, D**: Unpaired t-test with Welsh correction).

SUPPLEMENTARY FIGURE 5
Silencing of OPN impairs the growth of murine AB22 mesothelioma cells *in vivo*. **(A–C)** *In vivo* growth of $5x10^4$ AB22 sh-scrambled or AB22 shOPN, injected intra-thoracically in BALB/c mice. **(A)** IVIS *in vivo* imaging luminescence signal, mean+/-SEM values of 5 mice; **(B)** Histological quantification of total tumor area. **(C)** Representative images of IVIS acquisition of LUC signal at different time points. **(D, E)** Immunohistochemistry of explanted tumors, relative quantification for the staining of OPN and representative pictures. Data are

shown as mean +/- SEM (**A** Two-way ANOVA; **B**, **D**: Unpaired t-test with Welsh correction).

SUPPLEMENTARY FIGURE 6
Inhibition of OPN with the aptamer OPN-R3 does not affect the *in vivo* growth of murine AB22 mesothelioma cells. Results of IVIS *in vivo* imaging luminescence signal, mean+/-SEM values of 5 mice per group.

SUPPLEMENTARY FIGURE 7
Treatment with blocking anti-CD44 mAbs impairs *in vivo* growth of murine mesothelioma cells. **(A, C)** Effect of anti-CD44 mAbs on AB1 shOPN tumor growth. Mice were treated intra-peritoneally with anti-CD44 (10 mg/kg) or with irrelevant mAbs at day (4, 7, 12, 16, 19) post tumor injection. Data are expressed as average radiance, **(A)** mean+/-SEM values of 5 mice; **(B)** values of single mice; **(C)** Representative images of IVIS acquisition of LUC signal at different time points.

SUPPLEMENTARY TABLE 1
Single-Cell Transcriptome Sequencing analysis: list of DEGs.

SUPPLEMENTARY TABLE 2
Single-Cell Transcriptome Sequencing analysis: list of pathways.

References

1. Tsao AS, Wistuba I, Roth JA, Kindler HL. Malignant pleural mesothelioma. *J Clin Oncol* (2009) 27(12):2081–90. doi: 10.1200/JCO.2008.19.8523

2. Yap TA, Aerts JG, Popat S, Fennell DA. Novel insights into mesothelioma biology and implications for therapy. *Nat Rev Cancer* (2017) 17(8):475–88. doi: 10.1038/nrc.2017.42

3. Carbone M, Adusumilli PS, Alexander HR, Baas P, Bardelli F, Bononi A, et al. Mesothelioma: scientific clues for prevention, diagnosis, and therapy. *CA Cancer J Clin* (2019) 69(5):402–29. doi: 10.3322/caac.21572

4. Janes SM, Alrifai D, Fennell DA. Perspectives on the treatment of malignant pleural mesothelioma. *N Engl J Med* (2021) 385(13):1207–18. doi: 10.1056/NEJMra1912719

5. Bott M, Brevet M, Taylor BS, Shimizu S, Ito T, Wang L, et al. The nuclear deubiquitinase BAP1 is commonly inactivated by somatic mutations and 3p21.1 losses in malignant pleural mesothelioma. *Nat Genet* (2011) 43(7):668–72. doi: 10.1038/ng.855

6. Bruno F, Baratti D, Martinetti A, Morelli D, Sottotetti E, Bonini C, et al. Mesothelin and osteopontin as circulating markers of diffuse malignant peritoneal mesothelioma: a preliminary study. *Eur J Surg Oncol* (2018) 44(6):792–8. doi: 10.1016/j.ejso.2018.02.010

7. Bueno R, Stawiski EW, Goldstein LD, Durinck S, De Rienzo A, Modrusan Z, et al. Comprehensive genomic analysis of malignant pleural mesothelioma identifies recurrent mutations, gene fusions and splicing alterations. *Nat Genet* (2016) 48(4):407–16. doi: 10.1038/ng.3520

8. Brich S, Bozzi F, Perrone F, Tamborini E, Cabras AD, Deraco M, et al. Fluorescence *in situ* hybridization (FISH) provides estimates of minute and interstitial BAP1, CDKN2A, and NF2 gene deletions in peritoneal mesothelioma. *Mod Pathol* (2020) 33(2):217–27. doi: 10.1038/s41379-019-0371-0

9. Sculco M, La Vecchia M, Aspesi A, Pinton G, Clavenna MG, Casalone E, et al. Malignant pleural mesothelioma: germline variants in DNA repair genes may steer tailored treatment. *Eur J Cancer Oxf Engl 1990* (2022) 163:44–54. doi: 10.1016/j.ejca.2021.12.023

10. Testa JR, Cheung M, Pei J, Below JE, Tan Y, Sementino E, et al. Germline BAP1 mutations predispose to malignant mesothelioma. *Nat Genet* (2011) 43(10):1022–5. doi: 10.1038/ng.912

11. Yoshikawa Y, Emi M, Hashimoto-Tamaoki T, Ohmuraya M, Sato A, Tsujimura T, et al. High-density array-CGH with targeted NGS unmask multiple noncontiguous minute deletions on chromosome 3p21 in mesothelioma. *Proc Natl Acad Sci U S A* (2016) 113(47):13432–7. doi: 10.1073/pnas.1612074113

12. Marazioti A, Krontira AC, Behrend SJ, Giotopoulou GA, Ntaliarda G, Blanquart C, et al. KRAS signaling in malignant pleural mesothelioma. *EMBO Mol Med* (2022) 14(2):e13631. doi: 10.15252/emmm.202013631

13. Zucali PA, De Vincenzo F, Perrino M, Digiacomo N, Cordua N, D'Antonio F, et al. Advances in drug treatments for mesothelioma. *Expert Opin Pharmacother* (2022) 23(8):929–46. doi: 10.1080/14656566.2022.2072211

14. Tsao AS, Pass HI, Rimner A, Mansfield AS. New era for malignant pleural mesothelioma: updates on therapeutic options. *J Clin Oncol* (2022) 40(6):681–92. doi: 10.1200/JCO.21.01567

15. Kindler HL, Novello S, Bearz A, Ceresoli GL, Aerts JGJV, Spicer J, et al. Anetumab ravtansine versus vinorelbine in patients with relapsed, mesothelin-positive malignant pleural mesothelioma (ARCS-m): a randomised, open-label phase 2 trial. *Lancet Oncol* (2022) 23(4):540–52. doi: 10.1016/S1470-2045(22)00061-4

16. Nicolini F, Bocchini M, Bronte G, Delmonte A, Guidoboni M, Crinò L, et al. Malignant pleural mesothelioma: state-of-the-Art on current therapies and promises for the future. *Front Oncol* (2019) 9:1519. doi: 10.3389/fonc.2019.01519

17. Tagliamento M, Bironzo P, Curcio H, De Luca E, Pignataro D, Rapetti SG, et al. A systematic review and meta-analysis of trials assessing PD-1/PD-L1 immune checkpoint inhibitors activity in pre-treated advanced stage malignant mesothelioma. *Crit Rev Oncol Hematol* (2022) 172:103639. doi: 10.1016/j.critrevonc.2022.103639

18. Baas P, Scherpereel A, Nowak AK, Fujimoto N, Peters S, Tsao AS, et al. First-line nivolumab plus ipilimumab in unresectable malignant pleural mesothelioma (CheckMate 743): a multicentre, randomised, open-label, phase 3 trial. *Lancet Lond Engl* (2021) 397(10272):375–86. doi: 10.1016/S0140-6736(20)32714-8

19. Mannarino L, Mirimao F, Panini N, Paracchini L, Marchini S, Beltrame L, et al. Tumor treating fields affect mesothelioma cell proliferation by exerting histotype-dependent cell cycle checkpoint activations and transcriptional modulations. *Cell Death Dis* (2022) 13(7):612. doi: 10.1038/s41419-022-05073-4

20. Ceresoli GL, Aerts JG, Dziadziuszko R, Ramlau R, Cedres S, van Meerbeeck JP, et al. Tumour treating fields in combination with pemetrexed and cisplatin or carboplatin as first-line treatment for unresectable malignant pleural mesothelioma (STELLAR): a multicentre, single-arm phase 2 trial. *Lancet Oncol* (2019) 20(12):1702–9. doi: 10.1016/S1470-2045(19)30532-7

21. Digifico E, Belgiovine C, Mantovani A, Allavena P. Microenvironment and immunology of the human pleural malignant mesothelioma. In: Ceresoli GL, Bombardieri E, D'Incalci M, editors. *Mesothelioma: from research to clinical practice*. Cham: Springer International Publishing (2019). p. 69–84. doi: 10.1007/978-3-030-16884-1_5

22. Mantovani A, Allavena P, Marchesi F, Garlanda C. Macrophages as tools and targets in cancer therapy. *Nat Rev Drug Discovery* (2022) 21(11):799–820. doi: 10.1038/s41573-022-00520-5

23. Germano G, Frapolli R, Belgiovine C, Anselmo A, Pesce S, Liguori M, et al. Role of macrophage targeting in the antitumor activity of trabectedin. *Cancer Cell* (2013) 23(2):249–62. doi: 10.1016/j.ccr.2013.01.008

24. Liguori M, Digifico E, Vacchini A, Avigni R, Colombo FS, Borroni EM, et al. The soluble glycoprotein NMB (GPNMB) produced by macrophages induces cancer stemness and metastasis via CD44 and IL-33. *Cell Mol Immunol* (2021) 18(3):711–22. doi: 10.1038/s41423-020-0501-0

25. Mantovani A, Marchesi F, Malesci A, Laghi L, Allavena P. Tumour-associated macrophages as treatment targets in oncology. *Nat Rev Clin Oncol* (2017) 14(7):399–416. doi: 10.1038/nrclinonc.2016.217

26. Hattori T, Iwasaki-Hozumi H, Bai G, Chagan-Yasutan H, Shete A, Telan EF, et al. Both full-length and protease-cleaved products of osteopontin are elevated in infectious diseases. *Biomed* (2021) 9(8):1006. doi: 10.3390/biomedicines9081006

27. O'Regan AW, Nau GJ, Chupp GL, Berman JS. Osteopontin (Eta-1) in cell-mediated immunity: teaching an old dog new tricks. *Immunol Today* (2000) 21(10):475–8. doi: 10.1016/S0167-5699(00)01715-1

28. Scatena M, Liaw L, Giachelli CM. Osteopontin: a multifunctional molecule regulating chronic inflammation and vascular disease. *Arterioscler Thromb Vasc Biol* (2007) 27(11):2302–9. doi: 10.1161/ATVBAHA.107.144824

29. Denhardt DT, Noda M, O'Regan AW, Pavlin D, Berman JS. Osteopontin as a means to cope with environmental insults: regulation of inflammation, tissue remodeling, and cell survival. *J Clin Invest* (2001) 107(9):1055–61. doi: 10.1172/JCI12980

30. Lund SA, Giachelli CM, Scatena M. The role of osteopontin in inflammatory processes. *J Cell Commun Signal* (2009) 3(3–4):311–22. doi: 10.1007/s12079-009-0068-0

31. Schillebeeckx E, van Meerbeeck JP, Lamote K. Clinical utility of diagnostic biomarkers in malignant pleural mesothelioma: a systematic review and meta-analysis. *Eur Respir Rev Off J Eur Respir Soc* (2021) 30(162):210057. doi: 10.1183/16000617.0057-2021

32. Pass HI, Lott D, Lonardo F, Harbut M, Liu Z, Tang N, et al. Asbestos exposure, pleural mesothelioma, and serum osteopontin levels. *N Engl J Med* (2005) 353(15):1564–73. doi: 10.1056/NEJMoa051185

33. Chen Z, Gaudino G, Pass HI, Carbone M, Yang H. Diagnostic and prognostic biomarkers for malignant mesothelioma: an update. *Transl Lung Cancer Res* (2017) 6(3):259–69. doi: 10.21037/tlcr.2017.05.06

34. Ahmed M, Behera R, Chakraborty G, Jain S, Kumar V, Sharma P, et al. Osteopontin: a potentially important therapeutic target in cancer. *Expert Opin Ther Targets* (2011) 15(9):1113–26. doi: 10.1517/14728222.2011.594438

35. Grigoriu BD, Scherpereel A, Devos P, Chahine B, Letourneux M, Lebailly P, et al. Utility of osteopontin and serum mesothelin in malignant pleural mesothelioma

diagnosis and prognosis assessment. *Clin Cancer Res* (2007) 13(10):2928–35. doi: 10.1158/1078-0432.CCR-06-2144

36. Hollevoet K, Nackaerts K, Gosselin R, De Wever W, Bosquée L, De Vuyst P, et al. Soluble mesothelin, megakaryocyte potentiating factor, and osteopontin as markers of patient response and outcome in mesothelioma. *J Thorac Oncol* (2011) 6 (11):1930–7. doi: 10.1097/JTO.0b013e3182272294

37. Arnold DT, De Fonseka D, Hamilton FW, Rahman NM, Maskell NA. Prognostication and monitoring of mesothelioma using biomarkers: a systematic review. *Br J Cancer* (2017) 116(6):731–41. doi: 10.1038/bjc.2017.22

38. Pass HI, Alimi M, Carbone M, Yang H, Goparaju CM. Mesothelioma biomarkers: a review highlighting contributions from the early detection research network. *Cancer Epidemiol biomark Prev* (2020) 29(12):2524–40. doi: 10.1158/1055-9965.EPI-20-0083

39. Katz SI, Roshkovan L, Berger I, Friedberg JS, Alley EW, Simone CB, et al. Serum soluble mesothelin-related protein (SMRP) and fibulin-3 levels correlate with baseline malignant pleural mesothelioma (MPM) tumor volumes but are not useful as biomarkers of response in an immunotherapy trial. *Lung Cancer Amst Neth* (2021) 154:5–12. doi: 10.1016/j.lungcan.2021.01.011

40. Cortinovis D, Grosso F, Carlucci L, Zucali PA, Pasello G, Tiseo M, et al. Trabectedin in malignant pleural mesothelioma: results from the multicentre, single arm, phase II ATREUS study. *Clin Lung Cancer* (2021) 22(4):361–70. doi: 10.1016/j.cllc.2020.06.028

41. Vázquez R, Licandro SA, Astorgues-Xerri L, Lettera E, Panini N, Romano M, et al. Promising *in vivo* efficacy of the BET bromodomain inhibitor OTX015/MK-8628 in malignant pleural mesothelioma xenografts. *Int J Cancer* (2017) 140(1):197–207. doi: 10.1002/ijc.30412

42. Davis MR, Manning LS, Whitaker D, Garlepp MJ, Robinson BW. Establishment of a murine model of malignant mesothelioma. *Int J Cancer* (1992) 52(6):881–6. doi: 10.1002/ijc.2910520609

43. Mezzapelle R, Rrapaj E, Gatti E, Ceriotti C, Marchis FD, Preti A, et al. Human malignant mesothelioma is recapitulated in immunocompetent BALB/c mice injected with murine AB cells. *Sci Rep* (2016) 6:22850. doi: 10.1038/srep22850

44. Digifico E, Erreni M, Colombo FS, Recordati C, Migliore R, Frapolli R, et al. Optimization of a luciferase-expressing non-invasive intrapleural model of malignant mesothelioma in immunocompetent mice. *Cancers* (2020) 12(8):2136. doi: 10.3390/cancers12082136

45. Erreni M, Bianchi P, Laghi L, Mirolo M, Fabbri M, Locati M, et al. Expression of chemokines and chemokine receptors in human colon cancer. *Methods Enzymol* (2009) 460:105–21. doi: 10.1016/S0076-6879(09)05205-7

46. Babraham Bioinformatics. *FastQC a quality control tool for high throughput sequence data*. Available at: https://www.bioinformatics.babraham.ac.uk/projects/fastqc/.

47. *Contents [[/amp]]mdash; bcbio-nextgen 1.2.9 documentation*. Available at: https://bcbio-nextgen.readthedocs.io/en/latest/.

48. Pertea M, Kim D, Pertea GM, Leek JT, Salzberg SL. Transcript-level expression analysis of RNA-seq experiments with HISAT, StringTie and ballgown. *Nat Protoc* (2016) 11(9):1650–67. doi: 10.1038/nprot.2016.095

49. Patro R, Duggal G, Love MI, Irizarry RA, Kingsford C. Salmon provides fast and bias-aware quantification of transcript expression. *Nat Methods* (2017) 14(4):417–9. doi: 10.1038/nmeth.4197

50. Love MI, Huber W, Anders S. Moderated estimation of fold change and dispersion for RNA-seq data with DESeq2. *Genome Biol* (2014) 15(12):550. doi: 10.1186/s13059-014-0550-8

51. Wu T, Hu E, Xu S, Chen M, Guo P, Dai Z, et al. clusterProfiler 4.0: a universal enrichment tool for interpreting omics data. *Innov Camb Mass* (2021) 2(3):100141. doi: 10.1016/j.xinn.2021.100141

52. Gillespie M, Jassal B, Stephan R, Milacic M, Rothfels K, Senff-Ribeiro A, et al. The reactome pathway knowledgebase 2022. *Nucleic Acids Res* (2022) 50(D1):D687–D692. doi: 10.1093/nar/gkab1028

53. Kolde R. *Pheatmap* (2023). Available at: https://github.com/raivokolde/pheatmap.

54. Waskom ML. Seaborn: statistical data visualization. *J Open Source Software* (2021) 6(60):3021. doi: 10.21105/joss.03021

55. Guo Q, Yang C, Gao F. The state of CD44 activation in cancer progression and therapeutic targeting. *FEBS J* (2022) 289(24):7970–86. doi: 10.1111/febs.16179

56. Mi Z, Guo H, Russell MB, Liu Y, Sullenger BA, Kuo PC. RNA Aptamer blockade of osteopontin inhibits growth and metastasis of MDA-MB231 breast cancer cells. *Mol Ther J Am Soc Gene Ther* (2009) 17(1):153–61. doi: 10.1038/mt.2008.235

57. Talbot LJ, Mi Z, Bhattacharya SD, Kim V, Guo H, Kuo PC. Pharmacokinetic characterization of an RNA aptamer against osteopontin and demonstration of *in vivo* efficacy in reversing growth of human breast cancer cells. *Surgery* (2011) 150(2):224–30. doi: 10.1016/j.surg.2011.05.015

58. Castello LM, Raineri D, Salmi L, Clemente N, Vaschetto R, Quaglia M, et al. Osteopontin at the crossroads of inflammation and tumor progression. *Mediators Inflamm* (2017) 2017:4049098. doi: 10.1155/2017/4049098

59. Hur EM, Youssef S, Haws ME, Zhang SY, Sobel RA, Steinman L. Osteopontin-induced relapse and progression of autoimmune brain disease through enhanced survival of activated T cells. *Nat Immunol* (2007) 8(1):74–83. doi: 10.1038/ni1415

60. Rangaswami H, Bulbule A, Kundu GC. Osteopontin: role in cell signaling and cancer progression. *Trends Cell Biol* (2006) 16(2):79–87. doi: 10.1016/j.tcb.2005.12.005

61. Chambers AF, Wilson SM, Kerkvliet N, O'Malley FP, Harris JF, Casson AG. Osteopontin expression in lung cancer. *Lung Cancer Amst Neth* (1996) 15(3):311–23. doi: 10.1016/0169-5002(95)00595-1

62. Thalmann GN, Sikes RA, Devoll RE, Kiefer JA, Markwalder R, Klima I, et al. Osteopontin: possible role in prostate cancer progression. *Clin Cancer Res* (1999) 5 (8):2271–7.

63. Gotoh M, Sakamoto M, Kanetaka K, Chuuma M, Hirohashi S. Overexpression of osteopontin in hepatocellular carcinoma. *Pathol Int* (2002) 52(1):19–24. doi: 10.1046/j.1440-1827.2002.01316.x

64. Irby RB, McCarthy SM, Yeatman TJ. Osteopontin regulates multiple functions contributing to human colon cancer development and progression. *Clin Exp Metastasis* (2004) 21(6):515–23. doi: 10.1007/s10585-004-2873-4

65. Zhou Y, Dai DL, Martinka M, Su M, Zhang Y, Campos EI, et al. Osteopontin expression correlates with melanoma invasion. *J Invest Dermatol* (2005) 124(5):1044–52. doi: 10.1111/j.0022-202X.2005.23680.x

66. Cook AC, Tuck AB, McCarthy S, Turner JG, Irby RB, Bloom GC, et al. Osteopontin induces multiple changes in gene expression that reflect the six "hallmarks of cancer" in a model of breast cancer progression. *Mol Carcinog* (2005) 43(4):225–36. doi: 10.1002/mc.20105

67. Bandopadhyay M, Bulbule A, Butti R, Chakraborty G, Ghorpade P, Ghosh P, et al. Osteopontin as a therapeutic target for cancer. *Expert Opin Ther Targets* (2014) 18 (8):883–95. doi: 10.1517/14728222.2014.925447

68. Kariya Y, Kariya Y. Osteopontin in cancer: mechanisms and therapeutic targets. *Int J Transl Med* (2022) 2(3):419–47. doi: 10.3390/ijtm2030033

69. Pantazopoulos I, Boura P, Xanthos T, Syrigos K. Effectiveness of mesothelin family proteins and osteopontin for malignant mesothelioma. *Eur Respir J* (2013) 41 (3):706–15. doi: 10.1183/09031936.00226111

70. Cristaudo A, Foddis R, Bonotti A, Simonini S, Vivaldi A, Guglielmi G, et al. Comparison between plasma and serum osteopontin levels: usefulness in diagnosis of epithelial malignant pleural mesothelioma. *Int J Biol Markers* (2010) 25(3):164–70. doi: 10.1177/172460081002500307

71. Paleari L, Rotolo N, Imperatori A, Puzone R, Sessa F, Franzi F, et al. Osteopontin is not a specific marker in malignant pleural mesothelioma. *Int J Biol Markers* (2009) 24 (2):112–7. doi: 10.1177/172460080902400208

72. Lin H, Shen YC, Long HY, Wang H, Luo ZY, Wei ZX, et al. Performance of osteopontin in the diagnosis of malignant pleural mesothelioma: a meta-analysis. *Int J Clin Exp Med* (2014) 7(5):1289–96.

73. Solinas G, Schiarea S, Liguori M, Fabbri M, Pesce S, Zammataro L, et al. Tumor-conditioned macrophages secrete migration-stimulating factor: a new marker for M2-polarization, influencing tumor cell motility. *J Immunol Baltim Md 1950* (2010) 185 (1):642–52. doi: 10.4049/jimmunol.1000413

74. Rittling SR. Osteopontin in macrophage function. *Expert Rev Mol Med* (2011) 13:e15. doi: 10.1017/S1462399411001839

75. Tan Y, Zhao L, Yang YG, Liu W. The role of osteopontin in tumor progression through tumor-associated macrophages. *Front Oncol* (2022) 12:953283. doi: 10.3389/fonc.2022.953283

76. Zhu B, Suzuki K, Goldberg HA, Rittling SR, Denhardt DT, McCulloch CAG, et al. Osteopontin modulates CD44-dependent chemotaxis of peritoneal macrophages through G-protein-coupled receptors: evidence of a role for an intracellular form of osteopontin. *J Cell Physiol* (2004) 198(1):155–67. doi: 10.1002/jcp.10394

77. Rao G, Wang H, Li B, Huang L, Xue D, Wang X, et al. Reciprocal interactions between tumor-associated macrophages and CD44-positive cancer cells via osteopontin/CD44 promote tumorigenicity in colorectal cancer. *Clin Cancer Res Off J Am Assoc Cancer Res* (2013) 19(4):785–97. doi: 10.1158/1078-0432.CCR-12-2788

78. Chen C, Zhao S, Karnad A, Freeman JW. The biology and role of CD44 in cancer progression: therapeutic implications. *J Hematol Oncol J Hematol Oncol* (2018) 11(1):64. doi: 10.1186/s13045-018-0605-5

79. Orian-Rousseau V, Ponta H. Perspectives of CD44 targeting therapies. *Arch Toxicol* (2015) 89(1):3–14. doi: 10.1007/s00204-014-1424-2

80. Cortes-Dericks L, Schmid RA. CD44 and its ligand hyaluronan as potential biomarkers in malignant pleural mesothelioma: evidence and perspectives. *Respir Res* (2017) 18(1):58. doi: 10.1186/s12931-017-0546-5

81. Asplund T, Heldin P. Hyaluronan receptors are expressed on human malignant mesothelioma cells but not on normal mesothelial cells. *Cancer Res* (1994) 54 (16):4516–23.

82. Penno MB, Askin FB, Ma H, Carbone M, Vargas MP, Pass HI. High CD44 expression on human mesotheliomas mediates association with hyaluronan. *Cancer J Sci Am* (1995) 1(3):196–203.

83. Sakurai Y, Kato A, Hida Y, Hamada J, Maishi N, Hida K, et al. Synergistic enhancement of cellular uptake with CD44-expressing malignant pleural mesothelioma by combining cationic liposome and hyaluronic acid-lipid conjugate. *J Pharm Sci* (2019) 108(10):3218–24. doi: 10.1016/j.xphs.2019.06.012

84. Raineri D, Dianzani C, Cappellano G, Maione F, Baldanzi G, Iacobucci I, et al. Osteopontin binds ICOSL promoting tumor metastasis. *Commun Biol* (2020) 3(1):1–15. doi: 10.1038/s42003-020-01333-1

85. Raineri D, Cappellano G, Vilardo B, Maione F, Clemente N, Canciani E, et al. Inducible T-cell costimulator ligand plays a dual role in melanoma metastasis upon binding to osteopontin or inducible T-cell costimulator. *Biomed* (2022) 10(1):51. doi: 10.3390/biomedicines10010051

86. Hutloff A, Dittrich AM, Beier KC, Eljaschewitsch B, Kraft R, Anagnostopoulos I, et al. ICOS is an inducible T-cell co-stimulator structurally and functionally related to CD28. *Nature* (1999) 397(6716):263–6. doi: 10.1038/16717

87. Fontecedro AC, Cecconi V, Bosco EF, Schmitt-Opitz I, Weder W, Stahel RA, et al. Chemotherapy of malignant pleural mesothelioma does not preclude use of check-point blockade. *Ann Oncol* (2015) 26:i48. doi: 10.1093/annonc/mdv052.01

Frontiers in Immunology

Explores novel approaches and diagnoses to treat immune disorders.

The official journal of the International Union of Immunological Societies (IUIS) and the most cited in its field, leading the way for research across basic, translational and clinical immunology.

Discover the latest Research Topics

See more →

Frontiers

Avenue du Tribunal-Fédéral 34
1005 Lausanne, Switzerland
frontiersin.org

Contact us

+41 (0)21 510 17 00
frontiersin.org/about/contact